LOCAL LOADING AND SADDLE SUPPORTS ON CYLINDRICAL VESSELS

(Some analytical and finite element studies of local load and saddle support problems with a special emphasis towards generating improved design methods)

A thesis submitted in fulfilment of the degree of Doctor of Philosophy in Mechanical Engineering.

by

David Hugh Nash BSc., MSc., MIMechE, MemberASME, CEng.

UNIVERSITY OF STRATHCLYDE
Department of Mechanical Engineering

February 1999

ABSTRACT

The study of local loading problems including the support of horizontal vessels on twin saddles was, and continues to be, of considerable interest to pressure vessel designers throughout the world. Whilst design rules are available in codes and standards, the drive is for improved, reliable analysis methods and design procedures by which engineers can produce efficient, commercially competitive, yet structurally reliable components with reasonable ease. The Department of Mechanical Engineering has an international reputation for studies in the field of pressurised systems. This present work continues the work of Emeritus Professor Alwyn S Tooth who commenced an investigation in this area some thirty years ago. The main thrust of this thesis is in two parts. Initially, local load problems are tackled since these are important in their own right. This provides a platform for the other main part, a study on saddle supports.

The present work reviews the background to these classes of problem and considers the main contributions in the literature to solutions for the local loading and saddle support problems. Although a major contribution has been made within the Department of Mechanical Engineering at the University of Strathclyde, other pertinent international works are referenced in Chapter 2. In addition, this chapter details the main aims and objectives of the present work.

The problem of the stress analysis of a cylindrical pressure vessel is tackled by employing Sanders thin shell theory, which is developed in Chapter 3. Governing differential equations are solved by a matrix method to evaluate the displacements of the shell. Thereafter, these are used to establish strains and thus stress resultants and stresses. Externally applied surface loads are described by employing a double Fourier series approach. The solution is then extended to encompass cases where thermal loading is present. Comments on the limitations of the use of Fourier series and rates of convergence are presented.

In Chapter 4, the solution of the governing equations is successfully applied to some difficult local load problems. In this, the interface loading, which is traditionally represented by a radially loaded 'rectangular patch', is extended to circular and elliptical regions. In addition, the more complex loading cases of longitudinal and circumferential moment are also presented. Illustrative examples of the use of the solution are detailed and compared with experimental results obtained from the literature. The solution is also used to examine thermal loading on cylindrical shells with the cases of uniform thermal loading acting over discrete areas of the shell. In addition, the fault condition of a 'hot spot' with a prescribed thermal profile is outlined and a solution detailed. This form of solution may be used to examine, for example, the case of loss of insulation on a reactor wall. Some comments are also made with respect to modelling this class of problem using finite element analysis. Although the use of this mathematical tool is becoming widespread in engineering design and analysis, there are some drawbacks of the technique when examining local

load problems. The important issues pertaining to the use of finite element analysis are examined and some results are thereafter compared with the Fourier series solution. These are fully discussed in this chapter.

The design of cylindrical vessels supported on twin saddles is often driven by the magnitude of the stresses located near the uppermost point of the saddle shell junction. Surcharge pressure loading is generally the main design load for most component parts of a vessel. For the saddle supports, however, it is usually ignored and only the liquid fill load is considered since this is the worst situation and tends to exacerbate these junction stresses. In such cases, the major difficulty is the determination of the interaction forces between the saddle and the shell. This is examined in Chapter 5 by considering the interface pressure distribution between the two components. By discretising the contact area and by considering the compatibility of displacements for two bodies in contact and examining the equilibrium equations, an accurate mathematical solution for the interface pressure and subsequent stress analysis can be derived. A choice of models to describe the interface pressure system is detailed – line load, patch load and line plus patch load model. A brief description is given of the implementation of the computer programs.

The solution of the saddle support problem requires a reasonably powerful computer to solve the equations, and therefore it is preferable to have a simple design method which can either be undertaken by hand calculation or be easily programmed into a simple spreadsheet. Chapter 6 develops a design methodology and parameter study for a typical range of vessel sizes and configurations as defined by the results of an industrial survey. In this, the scope is clearly identified and the range of parameters defined and justified. A 'basic stress' quantity is defined and thereafter modified by the use of a number of factors which describe the influence of the vessel weight, and the leading geometrical factors ~ saddle width, distance to rigid end, saddle interaction, saddle wrapround, and the effect of length change. Some verification and design examples are presented together with a design worksheet and a fatigue example in accordance with British Standard BS 5500. Traditionally, the influence of the stiffness of the vessel end or saddle support have either been ignored or treated in a simplified fashion. Although not included in this section, these topics are covered in Chapters 8 and 9.

The main alternative method to the analytical one described above is the finite element method. Chapter 7 presents an overview of the main factors affecting the solution of saddle support problems using finite element analysis. The complications in modelling the geometry, the selection of element type, the choice and specification of boundary conditions and mesh refinement are examined in detail. Some sample results are given and the general influences of the geometric parameters on the deformations of the vessel are described. In addition, a comparison is made between the finite element analysis stress results and other methods. Some comments are made regarding the nature of the stresses obtained from the finite element analysis.

The flexibility of the vessel dished end closure and the effect of this on the stresses obtained at the saddle shell junction is considered in Chapter 8. The treatment in the British Standard is outlined and compared to a finite element study for the various end closure types ~ rigid, flat, semi-ellipsoidal and hemispherical end closures. Some details are given on the modelling of such components and a parameter study is undertaken examining the main influencing parameters ~ radius, thickness of end and thickness of attached shell section. Some results are presented and an 'end flexibility factor' proposed.

The influence of the saddle flexibility is examined in Chapter 9. This causes major difficulty, not least because of the almost infinite number of possible configurations of support. Obviously, the introduction of a flexible saddle affects the distribution of contact pressure. The first step is to adjust the equations developed in Chapter 5 to accommodate flexibility terms. The interface system for flexible saddles, the compatibility equations and the resulting values of strain and stress are fully detailed. The second step is to develop a mathematical model for the saddle flexibility; a fully parametric finite element model is proposed which works in conjunction with the analytical procedure. Thereafter, several alternative versions of the parametric model are described together with their applications and drawbacks. A new finite element approach using shell, solid and surface elements to introduce surface tractions is proposed and revised finite element models described. Thereafter, results are presented which demonstrate the influence of introducing a more flexible saddle can have great benefit of reducing the stresses in the vessel shell.

Some overall conclusions and final comments are made in Chapter 10, especially with regards to further work and moves towards implementation, standardisation and improved availability via the Internet and adoption by industry.

ACKNOWLEDGEMENTS

The author wishes to principally thank Emeritus Professor Alwyn S Tooth for his supervision, advice and guidance and not least for his fellowship throughout my time in the University.

In addition, gratitude is also given to members of the Department of Mechanical Engineering for their support and advice at different stages especially Professor John Spence, Vice Principal, for advice, encouragement and opportunity as former Head of Department and Professor James Boyle for support in all matters mathematical and computational.

The author would especially like to thank his wife and children for their continuous encouragement and love shown during the writing of this thesis. Their sacrifices, together with those of his parents over the years have, in no small part, contributed to this work. Without their support, this thesis could not have been completed.

'To God be the glory for the things he has done,
Just let me live my life,
Let it be pleasing Lord to Thee,
And should I gain any praise,
Let it go to Calvary'
My Tribute, Andrae Crouch, 1971

David H Nash
February 1999

NOMENCLATURE

A, $A(\phi)_{1,2}$	Distance from vessel end to saddle; Distances defining patch strip size from end of vessel
B, $B(\phi)_{1,2}$	Breadth; Distances defining patch strip size from end of vessel
b	Distance from vessel end to the discrete area centre; Saddle width
C, c	Half saddle, attachment or patch width, Half discrete area width
D	Extensional rigidity = $Et/(1-\nu^2)$
d_x , d_ϕ	Differentiation with respect to x and ϕ; $\partial/\partial x$; $\partial/\partial\phi$
E	Young's modulus of elasticity
H	Height of fluid inside vessel
K	Non dimensional factor = $t^2/(12R^2)$
K_x, K_θ and $K_{x\theta}$	Longitudinal, circumferential and rotational changes of curvature for the cylindrical vessel
L	Length of cylindrical vessel
M, m and Mmax	Numbers of terms in Fourier series in longitudinal direction
M_x, M_θ and $M_{x\theta}$	Longitudinal, circumferential and shear bending stress resultants of the cylindrical vessel
N, n and Nmax	Numbers of terms in Fourier series in circumferential direction
NA	Number of discrete areas into which half saddle angle is divided
NC	Number of discrete areas into which total saddle width is divided
NN	Total number of contact area divisions
N_x, N_θ and $N_{x\theta}$	Longitudinal, circumferential and shear membrane stress resultants of the cylindrical vessel
P	External pressure or applied loading
p	Internal surcharge pressure
P_x, P_θ and $P_{x\theta}$	Longitudinal, circumferential and radial surface loading on the cylindrical vessel
Q_x, and Q_θ	Longitudinal and circumferential shear stress resultants on the cylindrical vessel
R	Mean radius of the circular cylindrical vessel
t	Thickness of shell
T	External tangential surface traction; Temperature
U, V and W	Longitudinal, tangential and radial displacements of the cylindrical vessel

x, χ	Longitudinal cylindrical co-ordinate
α	Angle of fill
β	Half the included angle of the discrete area or patch
θ	Circumferential cylindrical co-ordinate
ϕ	Angle from the vessel nadir to the patch load centre
ρ	Fluid specific weight
ρ_v	Vessel material specific weight
υ	Poisson's ratio
λ	$m\pi R/L$
Δ	Upward rigid body displacement of saddle or attachment with respect to vessel ends

1 INTRODUCTION

Pressurised systems design is governed and regulated by the use of well proved Codes and Standards. These documents have been formulated over the past 100 years or so and have had, as their backbone, two significant contributions. In America, the ASME Boiler and Pressure Vessel code (now with Divisions 1, 2 and 3) has its origins in the Massachusetts Rules of 1911 and in the UK, early rules from the Manchester Boiler Users Association became BS1500, then BS1515 and finally, BS5500, the unfired fusion welded pressure vessel standard. Industry has been keen to adopt such standards and to apply them to a wide range of industries including oil and gas, power generation, petrochemical, nuclear, water and waste management companies, to name but a few. Whilst these industries enjoy the benefits of approved design standards and methods, few companies commit significant resources into research and development to advance and improve design rules for the industry as a whole. Many organisations have in-house rules and computer programs for design but these largely remain exclusive. In the UK, advances in design are largely brought about by willing volunteers, both academic and industrial, who participate in British Standard committees. The fruit of such committees is an improved working environment for all.

The main pressure retaining components are designed using simple formulae and are based on solely satisfying equilibrium. These **'design-by-rule'** procedures often do not require the user to fully understand the origins of the analysis, rather only to follow the rule which in turn will satisfy the specific criteria upon which the procedure is based. This may involve the calculation of a minimum thickness or an allowable pressure, each of which will determine the basis of producing construction data. However, there are certain classes of problems in the pressurised systems field, which do not lend themselves to simple forms of analysis. These include certain cases where nozzles or openings in the vessel are present, situations of local loading onto the shell, support arrangements and other discontinuities, which may result in an increased level of stress in the vessel wall. Such classes of problems can be solved using a **'design-by-analysis'** approach whereby using an appropriate form of analysis, stresses can be

successfully evaluated and thereafter **'categorised'** and assessed against set criterion which prevent the occurrence of known failure mechanisms.

The method of analysis for such procedures is not well defined. Pre-1970, such analyses were often carried out using a **'classical thin shell theory'** approach, which is dealt with in some detail in Chapter 3 of this text. This involves describing the deformations of a doubly curved surface in space by differential equations and thereafter solving in a suitable manner for the specified loading condition. In this, the radii of curvature are large compared with the shell thickness and therefore, the behaviour of the structure through the wall is assumed to be constant across the wall thickness for direct loading and linearly varying across the wall thickness for bending. Using this assumption, it is possible to eliminate second order terms from the analysis. Even with this simplification, such solutions are complex and time-consuming and cannot be readily used for design purposes. Often, design charts or curves have been generated based on a shell theory approach. However, the range of situations for which solutions based on shell analysis are available is somewhat limited.

Since 1970, the **'finite element method'** has been increasingly applied to pressurised systems. By discretising the geometry and thereafter assembling the stiffnesses of each element, the entire solution for a given load case can be evaluated once known boundary conditions and material behaviour have been specified. The benefit of this method of analysis is that complex geometries and loading systems can be undertaken. The drawback of the method is that it still requires the use of a powerful computer, the purchase of suitable finite element software and the skills of an experienced analyst. Such experienced persons are still uncommon in the pressure systems industry and third party consultants are commonly used. These organisations may have the necessary finite element expertise but may not have the required understanding of pressurised systems behaviour or the use of design codes. In addition, there remains the problem of extracting results from the finite element analysis, which can be meaningfully interpreted in the context of 'design-by-analysis' and known failure mechanisms in pressure equipment. To date, no known method of

categorisation has been universally accepted, although much work has been undertaken in addressing the subject. Further discussion of this appears in Chapters 4 and 7.

The present work focuses on two complex problems: the **local loading of cylindrical pressure vessels**, and **the support of cylindrical vessels on twin saddles**. These problems are linked in so much as they are frequently classed as 'design-by-analysis' problems. The twin saddle case is analysed with liquid fill loading only, since surcharge pressure tends to stiffen the shell and hence to alleviate the maximum stress. In addition, the interaction between the load and the vessel shell can be readily expressed by a series of contact areas and therefore, by using equilibrium and compatibility, such problems can be addressed. These two problems are addressed using both of the methods described earlier. The success of any method, which is applied to these problems, lies in having confidence in the stress output data for use in 'categorisation' and subsequent assessment. This data may also be required for use in a fatigue assessment.

The application of the shell analysis to local loading is addressed in Chapter 4 where a number of cases are encompassed including radial, longitudinal and circumferential moment loads and thermal loads applied to square, rectangular, circular and elliptical contact areas. Each case is compared to experimental, design standard and finite element results, where available and appropriate. Chapter 5 describes the application of the shell analysis to the saddle support problem. A full parameter study has been undertaken. A new design methodology is proposed for the results of each influencing parameter and a simple multiplying factor process outlined. Each factor is fully described and the method of application within clearly defined restrictions is presented in Chapter 6.

A feature of the shell analysis approach is that the influence of the vessel end closure and saddle flexibility cannot be readily incorporated in the parameter study (as described). These topics are analysed using finite element analysis in Chapters 8 and 9

respectively. Since there are a limited number of generic head closure shapes, an end flexibility factor has been established which works with the proposed methodology of Chapter 6. The saddle flexibility is also addressed and a procedure for the establishment of an appropriate factor outlined. Some details are presented for a range of saddle types and information is provided to allow saddle flexibilities to be constructed. One complete, fully worked example of the use of saddle flexibility is given in Chapter 9 and comparisons are given with the entirely rigid case.

Chapter 10 concludes the work with some recommendations for exploitation and further work, especially in the context of the proposed new European Pressure Vessel Code.

2 LITERATURE REVIEW

2.1 Introduction

When designing containment pressure vessels, it is necessary to prove the integrity of the component for the required service conditions. In the first instance, primary service loads, such as internal pressure, external pressure and temperature conditions must be considered. After this preliminary stage, the effects of discontinuities such as nozzles and supports and other shell attachments are examined. These must be assessed in conjunction with the primary pressure/temperature loadings.

In those circumstances where horizontal vessels are employed they are usually mounted on twin saddle supports as shown in Figure 2.1. Saddles are also used when building, testing and transporting other vessels which are installed in the vertical position. Although a design method for saddle supported vessels is presently available in the ***British Standard BS5500***[1], based on the original work of ***Leonard P Zick***[2], it has been appreciated for some time that the approach is semi-empirical and only validated experimentally for a few small diameter vessels.

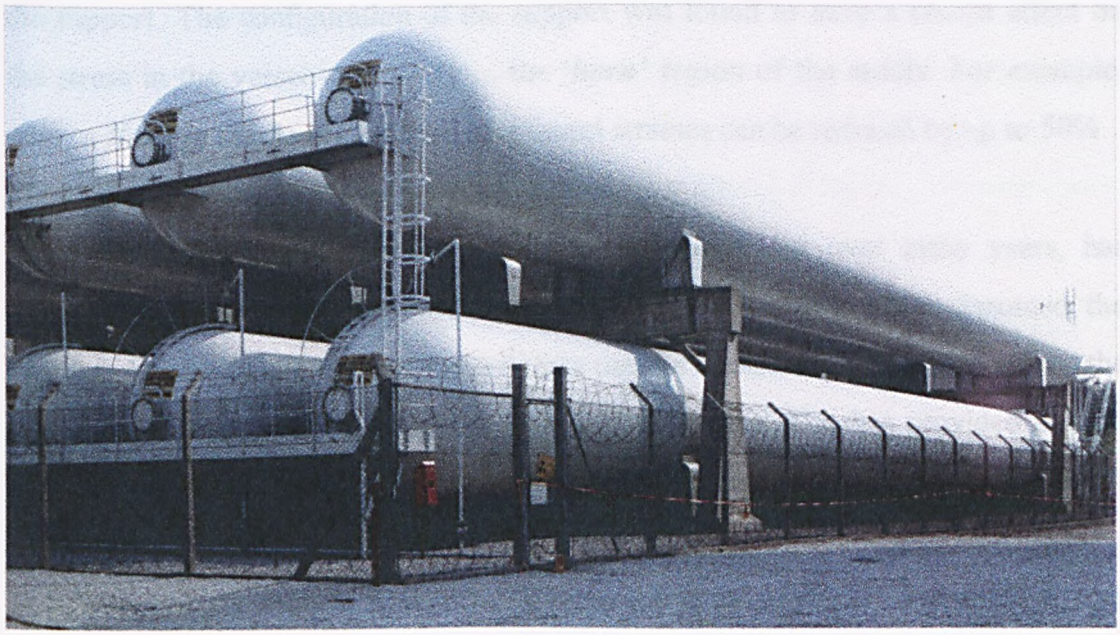

Figure 2.1 Typical horizontal twin saddle supported pressure vessels

Despite this, in the absence of a more fundamental approach, the method has been widely used for many years to design large vessels operating at times in quite rigorous loading conditions. There has been, however, the requirement to provide an accurate stress analysis for use in safety and integrity assessments. This has provided an impetus to develop an analytical approach, which can be applied with confidence to all such vessels under a variety of loading conditions.

Work done in recent years by ***Tooth et al***[3-6] has progressed much of the way to providing such an analytical solution. Advances have been made in understanding the stress system associated with the support regions of these vessels. The analytical technique developed represents the specified loadings, i.e. the vessel self-weight, liquid contents and pressure loadings using double Fourier series. The interaction forces, radial and tangential interface pressures, between the vessel shell and the saddle support, are the major governing unknowns of the problem. These forces are determined using the classical small displacement shell equations for the vessel and by enforcing compatibility and equilibrium at the shell/saddle interface. It has been found that the magnitude of the forces depends on the vessel flexibility and the rigidity of the support. The configuration of the support was found to have a crucial effect on the stress in the vessel - primarily in the '***horn***' region of the saddle. For example, when a ***flexible*** saddle is employed, the vessel stresses can be reduced by up to 50%.

Extensive experimental work on steel vessels, carried out over many years, has indicated that the basic analytical approach, references [3-6], which assumed the vessel to be ideally circular and the interface pressure uniformly distributed across the saddle width, was reasonably valid for the liquid-fill case. This has provided a good platform for the present comprehensive study, which extends and refines the initial work.

Several important aspects have been identified and solutions are presented in this thesis. These include the following specific areas of work:

- *The Tooth model has been updated, enhanced and refined.*

- *A full parameter study isolating the behaviour of each geometric variable in the twin saddle arrangement and the provision of a new design methodology suitable for incorporation into the major pressure vessel codes has been provided.*
- *The influence of the stiffness of the vessel dished end on the overall flexibility of the vessel with respect to support stresses in the horn region has been considered and results derived. This is presently treated in the current Standard by the use of a factor which assumes that the vessel end imparts substantial resistance.*
- *The effects of saddle flexibility are examined and recommendations for the design and implementation of flexible saddles as the optimum support technique given. At present, no governing rules or analyses are available in the standards for the design of flexible saddles.*

In addition to these topics, the problem of local patch loading is also addressed. In this, the work of ***Bijlaard, Hoff et al, Mershon et al, Kitching et al*** and ***Duthie*** and ***Tooth*** is discussed. In this area, a number of new solutions have been derived and are presented in this thesis. The following specific areas of work are addressed:

- *The previous cases of square and rectangular patches have been extended to cover the practical cases of circular and elliptical patches.*
- *Proper consideration has been given to variable loads such as moment loads rather than the approximations inherent in previous work.*
- *A review of the practical application of finite element analysis is presented together with cross comparisons between FEA, the newly derived solutions and experimental results where appropriate.*

2.2 Short Literature Review - The Twin Saddle Support Problem

The consideration of the literature relating to the support of horizontal vessels supported on twin saddle has been presented by a number of researchers in the past. Each of these authors, under the general guidance of ***Professor Alwyn S. Tooth,*** has

presented different aspects of the problem. It is worth noting these contributions at this time.

L S Ong (1985) presented a review of the main contributions relating to the twin saddle support problem. This review contained the work of international researchers including ***Zick, Křupka, Lakis & Dore, Stoneking & Sheth*** and ***Stanley & Mableson.*** A review of the work carried out at the University of Strathclyde was also presented by ***Ong*** and ***Motashar*** (1988), which included the work of ***Forbes, Wilson, Duthie, White,*** and ***Buchanan.***

Work previously undertaken and associated with this problem has been both analytical and experimental using various techniques. However, when considering the **'practical design'** of twin saddle supported pressure vessels, the design rules found in most international pressure vessels codes and rules are based on the work of ***L P Zick*** (1951) who developed a method for analysing cylindrical shells supported on twin saddles. The semi-empirical method in based on a ring and beam analysis. In this, the circumferential effects are addressed by considering the effects of support loading on a local ring whilst the overall longitudinal effects are analysed by considering the horizontal vessel as a beam, Figure 2.2a,b. At the mid-span of the vessel, it was assumed that the whole cylindrical section was available to resist bending, whilst at the saddle position, only a part of the vessel section above the saddle is effective. This treatment allowed the longitudinal overall bending stresses and the tangential shearing to be evaluated correctly, Figure 2.2c-e. In the case of the circumferential bending stresses at the saddle horn, the analysis was based on assuming the vessel profile was an arch. From this, the circumferential bending moment could be obtained at the horn, thus providing the circumferential bending stress at this location. It is interesting to note that this work was only validated using test results from a few relatively small diameter (approx. 6ft dia.) vessels. No details are given of the saddle flexibility or configuration - although from the photograph of the experimental setup used, the saddles appear to be of a flexible design in the horn region.

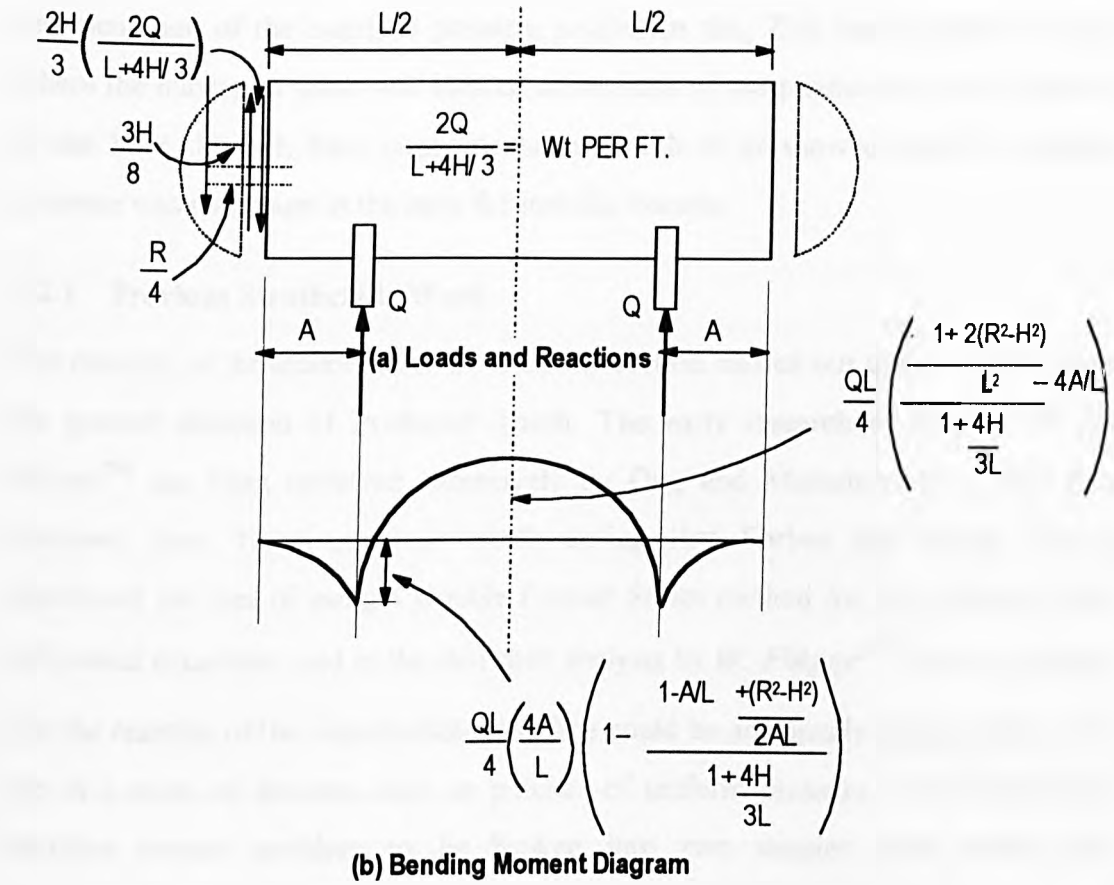

Figure 2.2a,b Zick's approach treating shell as a beam for longitudinal stresses

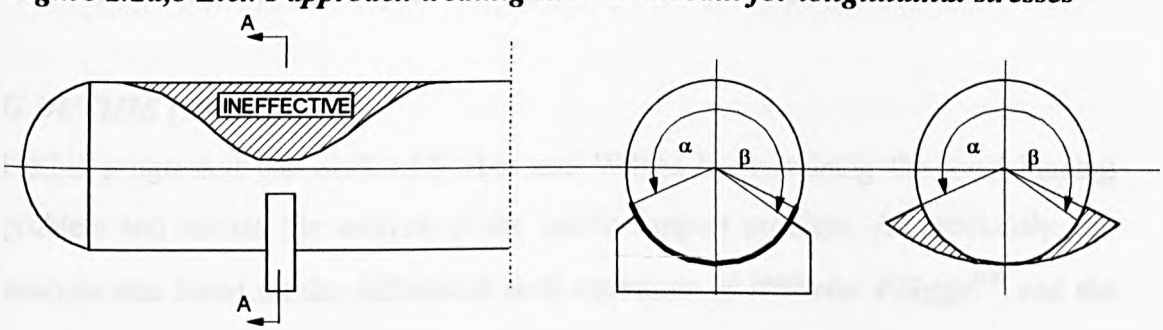

c) Effective portion of shell in longitudinal plane d) Effective portion for shear e) Shear stress distribution

Figure 2.2c-e Zick's approach treating shell as an arch showing effective portion and shear stress distribution in an unstiffened shell

This analysis was incorporated into the British Standard BS1515 in 1965 and ultimately into BS5500 in 1976 with the full derivation being presented in the panel document ***PD6497***[7] in 1982. However Tooth, Duthie and White[8-9] have shown the Zick analysis to be somewhat inadequate. The main problem with the analysis was the

representation of the interface pressure profile. In this, Zick had assumed a profile where the maximum value was located at the base of the saddle and was a minimum at the horn. In fact, later experiments by Tooth *et al* showed that the interface pressure was maximum at the horn for metallic vessels.

2.2.1 Previous Strathclyde Work

The majority of the authors referred to in this section carried out their research under the general direction of Professor Tooth. The early research of Forbes[85,86] and Wilson[88] has been reviewed extensively by Ong and Motashar and is not fully discussed here. However, it is worth noting that Forbes and latterly Wilson introduced the idea of using a Double Fourier Series method for the solution of the differential equations used in the thin shell analysis by ***W. Flügge***[10]. Forbes assumed that the reaction of the vessel/saddle interface could be adequately represented by the use of a series of discrete areas or patches of uniform pressure. This allowed the interface contact problem to be broken into two simpler parts namely the determination of the contact interface pressure and the subsequent application of these to a simply supported cylindrical shell as an external load.

G DUTHIE (1976)[3,4]

Duthie progressed the work of Forbes and Wilson by examining the local loading problem and revised the analysis of the saddle support problem. As previously, the analysis was based on the differential shell equations of ***Wilhelm Flügge***[10] and the same Fourier series expansions used by the previous researchers. The loading components and the middle surface displacements of the cylinder were modelled using the double Fourier series expansions. By examining equilibrium and compatibility of the system, together with the constitutive relationships, three simultaneous equations were derived which were solved using a matrix inversion routine. Ultimately, the solutions for the mid-surface displacements and stress resultants were obtained. This procedure is the core element of the work carried out at Strathclyde by White, Ong, Motashar and by the present author.

In choosing a Fourier series model for the shell displacements, Duthie assumed the vessel to be simply supported at its ends with the end profile of the cylinder remaining wholly circular at the limits. Therefore, as the saddle support is located nearer the end, the stresses and radial displacements tend to zero, the end seemingly providing infinite stiffness. However, Duthie provided a solution for the saddle support problem and compiled a number of solutions for a variety of local load problems including the radial, tangential and longitudinal patch load problems.

The main thrust of Duthie's work was to provide the capability for examining vessels which were either welded to the saddle or were loose by applying equilibrium and enforcing compatibility at the saddle/vessel interface. Using this approach, the effects of initial clearance gaps and flexible saddles could be tackled, the latter requiring the saddle flexibility to be characterised by a simple finite element analysis. It was also noted that much verification work was carried out by Duthie who compared his solutions with experimental results for a number of twin saddle supported vessels. The peak stresses which Duthie obtained on the outside surface of the vessel at the horn of the vessel proved to be much higher than those obtained from the British Standard BS5500 for this location.

This study paved the way forward for other researchers to examine the accuracy of the Duthie solution, the influence of the main geometric parameters and the significance of saddle flexibility, end flexibility, loose saddles and ultimately the development of a design methodology.

G C WHITE (1983)[3-4]

White continued the work by modifying the Duthie analysis to include the saddle flexibility by a more direct manner. Finite element models of different saddles were produced in order to generate a saddle **'flexibility matrix'.** This approach provided good correlation between the modified Duthie analysis and experimental work with the exception of the internal surcharge pressure case.

White also noted that the position of the maximum circumferential stress varies depending upon the geometric flexibility of the saddle and the number of discrete areas chosen to represent the contact surface. As a means of 'smoothing' the results and providing a calculation procedure, White plotted two curves, one for the horn stress and one for the maximum stress obtained. They were extrapolated until the intersection was found and this was deemed the **'improved maximum stress'.** White concluded from his work that:

- *The inclusion of a saddle flexibility model provided a better agreement with experimental and code results*
- *The use of a flexible saddle considerably reduces the maximum stress at the horn*
- *Good agreement is obtained when the vessel is subject to the liquid fill case. However, when surcharge pressure is applied or the pneumatic case is considered, the effects of out-of-roundness are significant.*

J C CARMICHAEL (1982)[4]

To complete the development of the Duthie analysis, Carmichael carried out a series of experiments on two similar 910mm diameter by 7320mm long vessels; one 3.33mm thick, the other 4.67mm. A number of permutations was considered: flexible and semi-rigid saddles, bolted foundations and supported on rollers, out-of-roundness measurements and progressive loading and unloading. Using the Duthie analysis, Carmichael concluded that:

- *The maximum values of stress measured occurs on the outside surface immediately adjacent to the saddle horn,*
- *Maximum saddle stresses are considerably reduced when flexible saddles are used,*
- *The difference in stresses for the liquid fill case is negligible if bolted or roller foundations are used, and*
- *For the liquid fill case, the analytical prediction compared favourably with the experimental results for the semi-rigid saddle case.*

L S ONG (1985)[5,11,21,22,23,28,29]

From the main conclusions, drawn from the above work, it was decided that the effects of out-of-roundness required special consideration. The main thrust of Ong's work[11] was to develop a non-linear theory, based on the shell equations of ***J Lyell Sanders Jr***[12], which was able to take account of out-of-roundness measurements or initial imperfections in the cylinder. This was facilitated by the use of the Haigh theory to represent imperfections in a non-restrained profile.

This new analysis required a complete re-write of the work of Duthie although some of the main logical elements of the program were retained. Ong wrote his analysis in FORTRAN compared with the older ALGOL programs of Duthie. This work proved a major contribution to the work at Strathclyde and yielded the **SADDLE** program. The new analysis was based on a new, more consistent shell theory than that previously used by Duthie, which was by Flügge. Both Arthur Leissa[13] and David Bushnell[14] present a practical critique of shell theory and from Leissa's work, Sanders' theory was implemented since it proved simple, consistent and equally accurate to that of Flügge.

The Sanders' theory uses the principle of virtual work. Since this is an energy theorem, it is energy consistent and as such produces no strain when rigid body motions are present. The theory is a two-dimensional one and avoids unnecessary approximations when using a three dimensional one. This allowed Ong to include the effects of initial imperfection into the strain-displacement relationships with ease.

Ong considered vessels which were perfectly circular or had initial imperfections, situated on flexible or rigid saddles and were welded or unwelded to the vessel shell. The contact to the vessel was modelled as a series of discrete areas or patches and also as a series of equivalent line loads each varying around the arc profile of the saddle. The method for calculating the stresses and displacements was similar to the Duthie analysis mentioned earlier. The interface reaction model of patch or line load representation was necessary since, for most cases although not all, the patch model

proved adequate. However, for the liquid fill case with a loose saddle, the line load model seemed to offer a better representation of the contact force at the horn. In the main, the difference in results between the two models was small although, with hindsight, a compromise between the two, that is, a patch load model with a line at the horn, proved to be a more reasonable representation.

The flexibility of the saddle was considered by Ong using two approaches. The first method employed an ***ANSYS***[15] finite element model, generated by the present author, and the second, a simpler approach, treated the flexible part of the saddle as a **'T'** section beam using Engineer's bending theory. In both of these methods, a unit load was applied and relative deflections at all other locations on the saddle contact surface were evaluated. The unit load was applied in both the radial and tangential directions. This procedure allowed the flexibility matrix for the saddle to be generated.

Ong generally found his theoretical work yielded good agreement with experimentally available results and with the findings of other researchers. His contribution improved and corrected the theoretical base, modernised the programming language and provided a flexible modular analysis tool with extended capabilities for other researchers to use.

F A MOTASHAR (1988)[16]

Motashar[16] overlapped with some of the work of Ong in the area of saddle supported pressure vessels. However, Motashar had several major contributions to make to the work at Strathclyde. The first was to review and examine the choice of shell theory mentioned earlier. Along with Ong, the Sanders' shell equations were employed in the further development of the saddle analysis programmes.

The question of uniform contact pressure was also addressed. Whilst Duthie had discretised the arc and Ong introduced variable interface pressure around the arc, the influence of varying the pressure across the saddle width had not yet been addressed.

Motashar thus divided the saddle width into a number of equal sized patches and ultimately developed a variable pressure grid to model non-uniform interface pressure across the width. The grid possessed the ability to weight the contact pressure area refinement to those areas where maximum change of pressure occurred. These areas also reflected the regions in the vessel where the maximum deformation gradients occurred. This method, which required separate runs for each grid mesh configuration, produced a refined grid whereby the pressure patches became progressively smaller towards the horn and towards the edges to the saddle plate. Higher stresses were found at the edges of the saddle as opposed to the centreline horn stresses evaluated by Duthie and Ong.

The present author believes that the design of the saddle itself governs the representation of the interface pressure loading onto the vessel. If the saddle is sufficiently stiff across the width, the Motashar representation is correct. However, if the saddle were well designed, then the uniform pressure model used by Duthie and Ong would be justified. In fact, the optimum design may well prove to concentrate the interface pressure map towards the centre of the saddle and dying out towards the edges of the saddle, thus reducing discontinuity stresses and relieving any unnecessary stress concentrations at the welds.

Motashar also brought to light the need for convergence testing when using the Fourier series method to represent the loadings and displacements. An exhaustive study concluded that a higher number of terms were required when a greater number of discrete areas was used. He also recognised that convergence should be checked for a particular vessel under analysis.

The saddle flexibility problem was also addressed using a three dimensional finite element approach since the Motashar shell analysis could cope with flexibility across the width. Again, the present author provided much on this aspect and helped develop, at this stage, the finite element model to generate the required saddle flexibility matrices. This work was extended to the study of vessels with support

diaphragms and also to the study of local loads through rigid rectangular attachments with variable interface pressure grids.

2.2.2 Survey of More Recent Work on Twin Saddle Supported Vessels

The main focus of the literature survey has been of work carried out at Strathclyde over a thirty-year period. Some comments have been made regarding the original work of L P Zick. However, this section concentrates on more recent work that is relevant to the work presented in this thesis. ***Stoneking and Sheth***[87] were first to implement a finite element analysis of the saddle support problem. ***Krivy and Filho***[17] also presented some finite element analysis results of the saddle support arrangement. ***Widera et al***[18-19] has recently provided some **qualitative** results using finite element analysis and ***Křupka***[20] produced a new design proposal for the limit carrying capacity of the shell in the region of the saddle support.

The most recent publications of Ong[21-23] provide a parameter study based on the Fourier series method developed while at Strathclyde. The method uses a basic stress equation, of the form originally developed by Křupka, but modified by a series of factors that characterise the behaviour of the individual parameters affecting the design. The work also includes the effect of the wear plate and incorporates factors to allow for seismic loading.

These papers provide useful comparisons for the methods developed by the present author.

J K Stoneking and K Sheth (1977)[87]

This work presents the first documented finite element analysis of the saddle support problem. The geometry of their test case was that of Wilson and Tooth[88]. Two support cases were studied. The rigid welded case assumed all nodes were fully constrained in all directions. For the loose case, infinitely stiff axial boundary elements were employed and these specified to take only compressive loads. In this manner, the interface pressures were determined using an iterative procedure. They also found

that the interface pressures were not constant across the width for the rigid saddle case. The resulting maximum stresses for the welded and loose cases were approximately the same. In addition, they found that the maximum stresses agreed well with the Zick result, this indicating lack of refinement in the FE model.

J Krivy and A S Filho (1986)[17]

These researchers present a computer-based method for the analysis of the twin saddle supported problem (CYLSAD). It is interesting to read their work since they have replicated the work of Tooth but at a rudimentary level. Their solution follows the pattern of analysis defined by Duthie in that the Navier method with trigonometric series are used to represent the displacements and a shell analysis, based on equations of ***Timoshenko***[24], is used to define the vessel behaviour.

Krivy and Filho identified the importance of the overall flexibility of the system, especially relating to the saddle geometry. They used a simple two dimensional finite element model to represent the stiffness and used nine contact points to relate this deformation to the shell. A brief description of the analysis procedure is provided. It is of a similar form to the Duthie method for ensuring compatibility at the interface.

Krivy and Filho present three main conclusions when comparing their results with the British Standard BS 5500:

- *BS 5500 gives results 10-20% lower than CYLSAD for moderately long vessels (no L/R values quoted)*
- *For short vessels, the BS 5500 values are too conservative*
- *The BS 5500 procedure should not be used for intermediate supports of cylindrical shells. For cross-sections which are very far from the end-plates, the error can be higher than 50%.*

No details are given regarding convergence of the Fourier series or on the number of contact areas or lines. It is the present author's opinion that these researchers have not

examined and investigated the work of Tooth and require to consider more of the relevant factors pertaining to this type of analysis.

G E O Widera et al (1987-88) [18-19]

The work of Widera[18-19] is the most recently available which contains results of a limited parameter study based on the finite element method. In these papers, the emphasis was to model the vessel and the saddle as a complete assembly and therefore try to incorporate some flexibility into the system. Widera used a coarse finite element model using twenty noded isoparametric shell elements, shown in Figure 2.3, which were contained within a program written by themselves (ASSHPV). All pre- and post-processing was carried out using MacDonnell Douglas software.

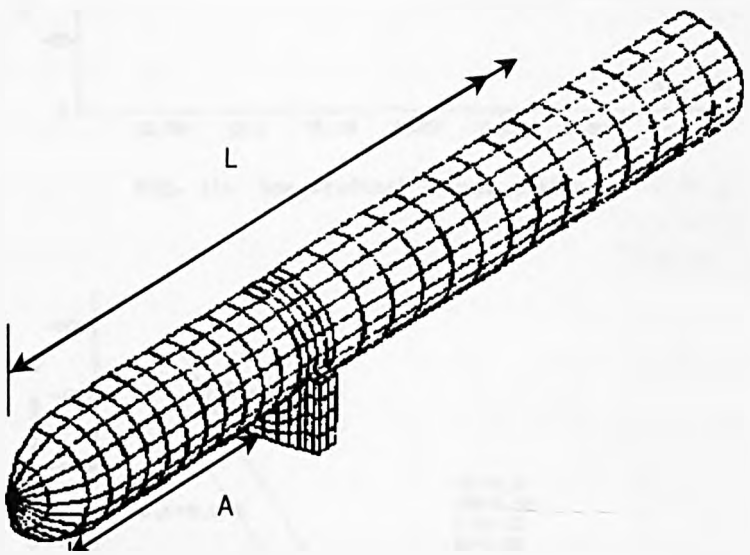

Figure 2.3 Finite element mesh used by Widera

In presenting his results, Widera makes use of dimensionless curves for the determination of the localised stresses. Two stress indices for the longitudinal and circumferential directions respectively were defined, c_ψ and c_θ, by the ratio of maximum stress intensity in the vessel to the nominal stress in the saddle support induced by the load Q. This gives:

$$c_\psi = 4c_1c_2\left(\sigma_\psi / Q\right) \text{ and } c_\theta = 4c_1c_2\left(\sigma_\theta / Q\right) \qquad \textbf{(2.1)}$$

where c_1 and c_2 represent the saddle contact area. Results were plotted for these stress indices against distance from the saddle horn in both the longitudinal and circumferential directions. In an attempt to provide non-dimensional design curves, his earlier results were re-plotted against the ratio of saddle centreline position to vessel length A/L.

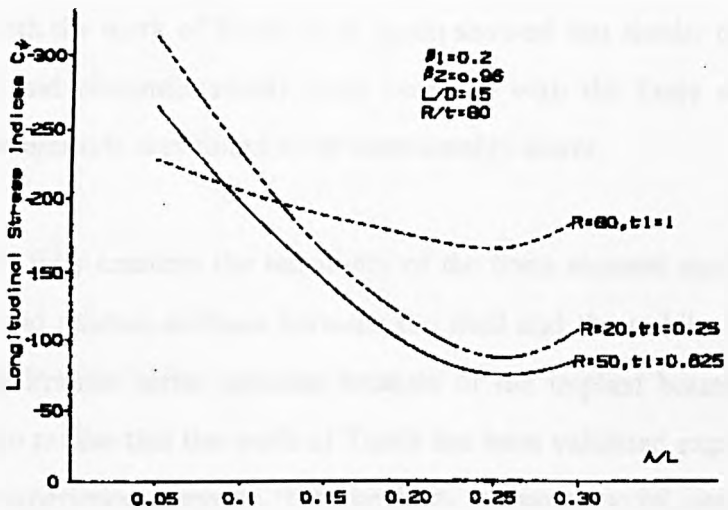

Fig. 14a Longitudinal stress indices

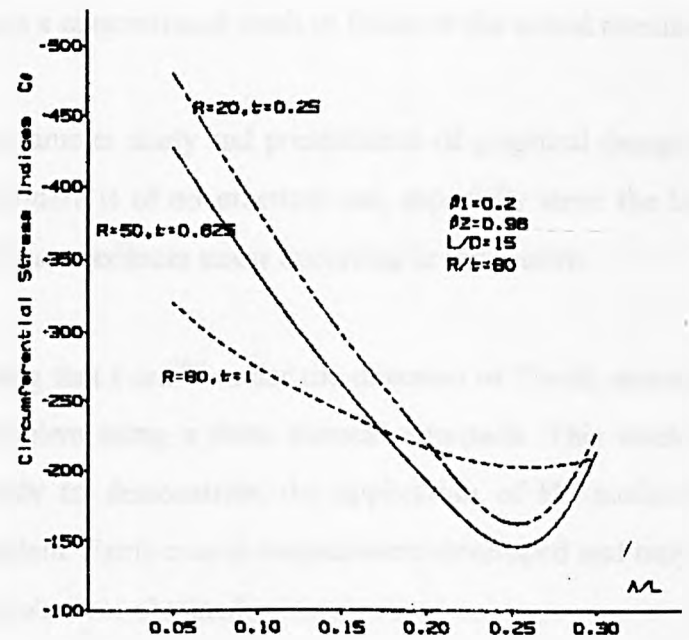

Fig. 14b Circumferential stress indices

Figure 2.4 Non dimensional stress indices plots for c_ψ and c_θ (after Widera)

Although the application of the finite element method to the saddle support problem should have resulted in an improved stress analysis of the maximum values occurring at the horn, Widera notes that the results obtained by his work can only be used in a '**qualitative**' manner. The values of maximum circumferential stress obtained were found to be some 30% lower. The radial displacement at the saddle centreline and midspan of the vessel was 28% and 63% lower at each position respectively. A comparison with the work of Tooth *et al*, again showed that similar distributions both longitudinally and circumferentially were obtained with the finite element analysis, however the magnitude was found to be considerably lower.

Widera did not fully examine the sensitivity of the finite element model in relation to mesh density and relative stiffness between the shell and the saddle. Widera is quick to criticise the Fourier series solution because of the implied boundary conditions, however fails to realise that the work of Tooth has been validated experimentally. The authors own experience suggests that the finite element model used by Widera is wholly inadequate for determining accurate stress results in the region of the horn. The distribution of stress at the horn varies rapidly over a very small angular distance and this requires a concentrated mesh to focus on the actual maximum stress.

Therefore, a parameter study and presentation of graphical design charts of the form presented by Widera is of no practical use, especially since the basic stress analysis fails to identify the maximum stress occurring in the system.

It is worth noting that Ford[64] under the direction of Tooth, attempted to analyse the twin saddle problem using a finite element approach. This work was very much a preliminary study to demonstrate the application of FE methods to the complex interaction problem. Fairly coarse meshes were developed and only qualitative results similar to Widera's were obtained.

V Křupka (1991)

An alternative method of solution to the problem of the saddle supported cylinder was first proposed by Křupka [20] in 1969. This dealt with the contact loaded shell by using the semi-bending Vlasov theory whereas Tooth *et al* used the general bending theory of shells. It is noted that the semi-bending theory ignores axial bending and was originally developed to model a rigid die pressing onto a cylinder rather than the cylindrical vessel supported on two saddles. Both methods, used independently of each other, reached similar conclusions. Radial and tangential interface forces were able to be calculated by the use of a computer. However, the advantage of the semi-bending theory is that the resulting relations can be expressed in a closed analytical form. A further review of the work of Křupka and of the accuracy of his method can be found in the literature review presented by Motashar.

In this most recent in a series of publications, Křupka has attempted to provide a **'design proposal'** for saddle supported vessels. The solution provides the stress at the horn in an infinitely long cylindrical shell which is then modified to take account of the saddle position at the flexibility of the end. The form of the solution is

$$\sigma_s = f_{as} f_{os} \frac{Q}{t^2} \sqrt{\frac{t}{r}} \qquad \textbf{(2.2)}$$

where Q is the total saddle reaction. Factors f_{os} and f_{as} are obtained from Figures 2.5a and b and thus allow the maximum stress to be evaluated. The coefficients, $\bar{k}$ and k in these figures, reflect the stiffening effect of the end and of the infinitely long cylinder respectively. These coefficients are obtained from the design curves shown below. In these, the saddle width, angle and distance from the end are all incorporated into two graphs. No effect of the wear plate or saddle flexibility is included. It is also worth noting that the shape and thickness of the end are not incorporated or characterised.

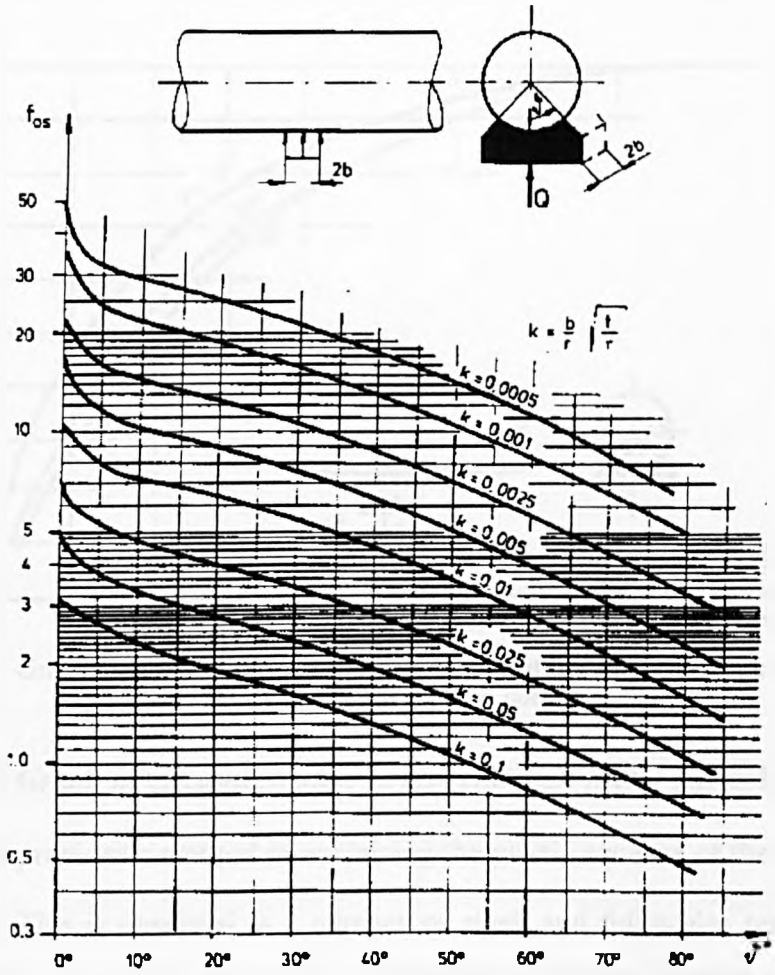

Fig. 2. Graph for the determination of the circumferential bending stress σ_{os} for an infinitely long shell.

Figure 2.5a Graph of circumferential stress reduction factor (Křupka 1991)

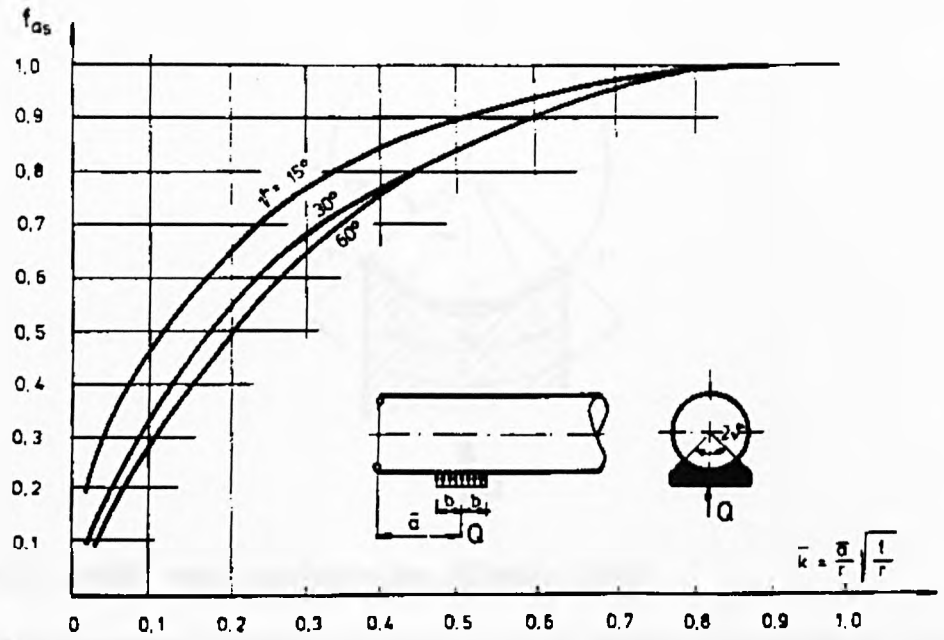

Fig. 3. Graph for the reduction of the circumferential bending stress with respect to the stiffening effect of the bottom.

Figure 2.5b Graph of circumferential stress reduction factor (Křupka 1991)

Křupka also provides a method of examining the plastic squeeze of the saddle into the vessel shell. This is observed in a number of small and full scales tests which have been carried out over a number of years. The plastic collapse condition can provide a limit for the maximum load carrying capacity for the vessel. However, in certain cases, a limited plastic state for a non-cyclic static load can produce a lower load carrying capacity than the shakedown effect. The form of this expression gives the limit plastic carrying capacity for a material yield of R_y as,

$$Q_{pl} = 2R_y s_o t\sqrt{\frac{t}{r}} \tag{2.3}$$

where R_y is the allowable yield stress, r and t have their usual meanings and s is the saddle periphery in contact with the vessel shell - shown in Figure 2.6. The value for s_o is given overleaf in Equation 2.4.

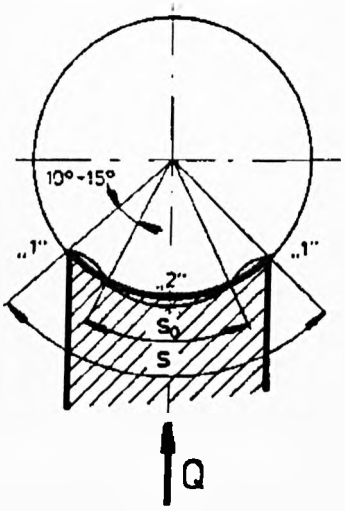

Figure 2.6 Saddle vessel contact region (Křupka 1991)

The solution assumes that there is a loss of contact between the vessel and saddle. In fact, Křupka recommends a reduction of 10° of the saddle angle in the calculation to minimise this effect, since any loss of contact will occur over this distance. This method may be adequate for the loose saddle condition but does not reflect the fully welded saddle, which maintains contact between the vessel and the support, see Figure 2.6. Thus, the new contact length becomes,

$$s_o = \frac{2\pi r}{360} 2(\theta - 10°) \tag{2.4}$$

In order to complete the design proposal, Křupka has addressed the problem of buckling in the region of the saddle support. In this treatment, he has presented an equation for the longitudinal membrane stress in the saddle region. This equation is similar in form to that for the circumferential stress shown above but has two new factors, f_{ax} and f_{ox}, which characterise the effects on the longitudinal stress of stiffening as defined previously. It is noted however, that the bucking is observed to occur at the nadir. Křupka addresses the assessment of this calculated longitudinal stress by comparing it with the result for the critical stress, for a vessel under a bending moment. However, he is careful to note that his treatment has oversimplified the problem but remains confident that his method is somewhat conservative.

A recent European standard[26] has provided allowable critical values of stress in pure compression and the case of a bending moment. The calculated value obtained by Křupka could be assessed against this. Further work on the buckling phenomenon (both circumferential and longitudinal) exhibited in the saddle region has been published by Kendrick and Tooth[27] and Tooth *et al*[81,82]. It is noted that the present work is limited to the elastic stress analysis of the saddle support region and the buckling problem has not been addressed.

L S Ong (1987-93)

Since 1986, Ong has published several papers relating to the saddle support problem. The majority of these papers are based on his thesis work, which has already been discussed earlier.

His first two papers[28-29] detail the Fourier series analysis using Sanders shell theory and the development of a computer program for cylindrical shell analysis. This is similar to that used in this thesis (although the writers program has been developed to cover additional cases and modified to run quicker and on a variety of machines). The salient points from the shell theory and Fourier series representation will be developed later since they were jointly developed at Strathclyde.

Ong's third paper on the subject[21] provides a parameter study which allows the calculation of the maximum stress at the horn for the unstiffened horizontal cylindrical shell. The parametric formula consists of various multiplying factors based on the Křupka equation shown earlier. Factors are introduced to account for the influences of saddle flexibility, saddle position, support spacing, support angle and width, together with the basic vessel dimensions. The parametric data is generated from the SADDLE program detailed previously. The parametric equation for the peak stress at the horn has the following form,

$$\sigma_{\phi o} = k_a k_c k_f k_\phi \frac{Q}{t}\sqrt{\frac{t}{r}} \qquad \textbf{(2.5)}$$

where the *'k'* factors represent the effects of location from one end, support spacing, the effect of the wear plate and different support design, and saddle support angle and Q is the total saddle reaction. These factors are obtained from tables of which contain the stress reduction for a given vessel configuration. Ong has also plotted the variation of each factor against a non-dimensional grouped parameter. These are included for convenience as Figures 2.7.

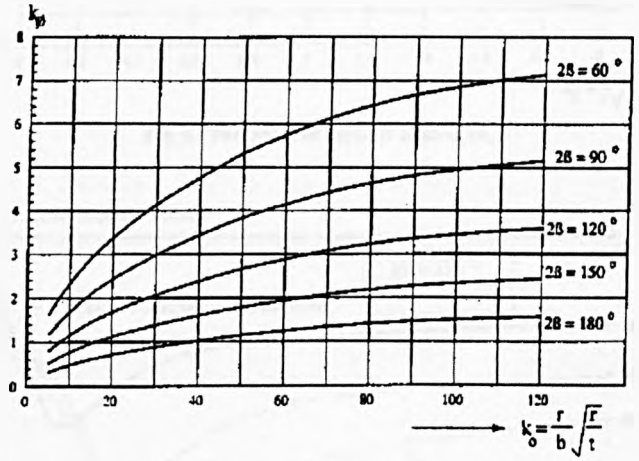

Fig. 4. The effect of saddle support angle.

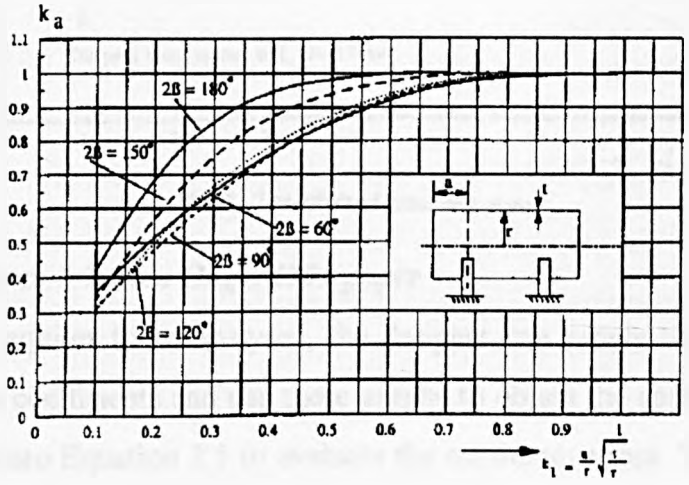

Fig. 5. The effect of support location from end.

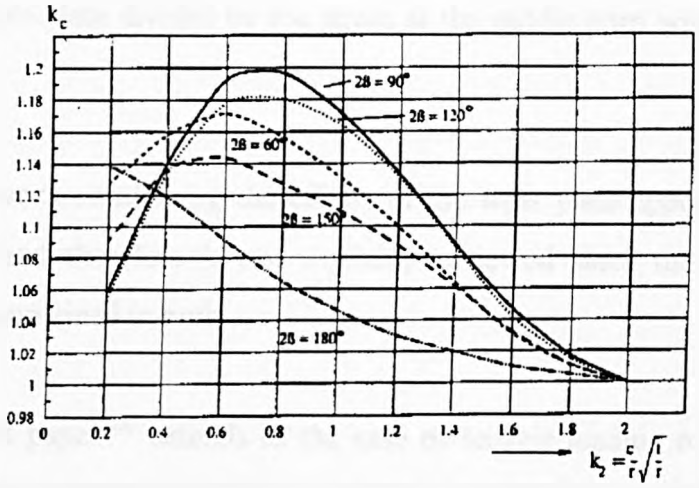

Fig. 6. The effect of support spacing (k_c).

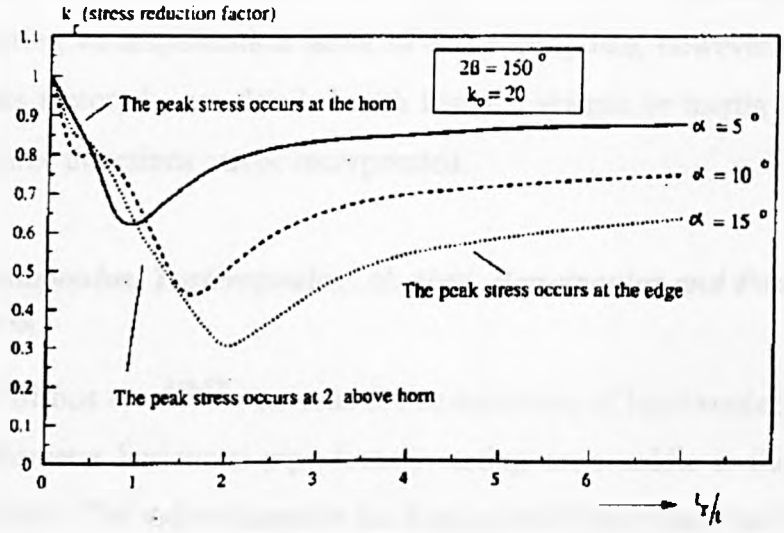

Fig. 7. The effect of extended plate.

Figure 2.7 Figures 4-7 from Ong's 1991 paper

When a vessel requires to be analysed, the designer can supply the geometric data into the abscissa coefficients and use these graphs to obtain the appropriate *k* factors and insert them into Equation 2.5 to evaluate the maximum stress. The effects of the wear plate and saddle flexibility are included in the analysis in an identical manner to that developed at Strathclyde during the time of White. The support is treated like a tapered cantilever 'I' beam and a flexibility matrix generated. This is a simpler technique to the finite element method which can also characterise the saddle flexibility. The present author provided several finite element saddle flexibilities for Ong during his time at Strathclyde for comparison with the tapered 'I' beam approach. The effects of the wear plate are defined as the peak stress with the

extended flexible plate divided by the stress at the saddle horn without the extended plate.

Much of this work considering the effects of the wear plate appear in Ong's fourth publication[22] and therefore is not explicitly reviewed since the same parametric information is contained in both.

His most recent paper[23] extends to the case of seismic loading on the twin saddle supported vessel. A stress amplification factor is defined to quantify the additional induced stress at the saddle support during ground motion. Ong has found that for most geometries, an amplification factor of 3 is appropriate, however, equations for an earthquake factor, k_e, are detailed such that the seismic or inertia coefficients in each of the three directions can be incorporated.

Bisbos, Thomopoulos, Tzaferopoulos, Al-Abed, Banoipoulos and Panagiotopoulos (1994-97) [49-53]

The work of Bisbos *et al*[49-53] concerns the computation of local contact loads acting on a small diameter horizontal pipe loosely resting on a saddle in the presence of Coulomb friction. The authors employ the Flügge shell theory and use Fourier series to generate flexibility coefficients. The non-linear boundary condition is treated by a two-stage algorithm which is repeatedly executed until convergence is reached. The first stage considers the tangential loads as given and determines regions of contact or non-contact. The second stage considers the normal loads as constant and sticking/slipping regions are computed. An example of the technique is provided for a progressively filled water pipe.

A S Tooth, W M Banks, C P Seah and B A Tolson(1994)

Tooth et al[89] progressed the earlier analysis work on saddles for isotropic materials, to incorporate a layered material system for glass reinforced plastic (GRP) systems. For liquid filled storage systems made from a GRP material, localised cracking can occurs in the region of highly localised bending stresses, which can occur in the

region adjacent to the saddle support. A thin shell approach was developed by Tolson[58], and a complementary test programme undertaken. Three full-sized vessels were strain gauged to provide measurements to validate the theoretical analysis. Using the shell analysis for layered systems, a parametric study was undertaken and a design approach presented, to enable the maximum strain to be determined for the symmetric laminated horizontal vessel.

S Naijie, Z Jitao and L Wenge (1996)

The authors[55] investigate the stress state in the saddle zone of twin saddle supported vessels in much the same manner as Tooth. In addition, some simple verification experiments have been undertaken on a suitable model. Thereafter, a double Fourier series expansion method is employed to analyse the problem. Contact pressure profiles are established in the usual manner and some comparisons made.

2.3 Literature Review - The Local Load Problem

This literature review presents a summary of the work carried out in the development of the main design methods found in most international pressure vessel standards for the design and analysis of local attachments. It is restricted to the case of the rigid attachment fully welded to a cylindrical shell. Other researchers have investigated the problems of rigid attachments on spheres and also flexible attachments such as nozzles in both cylindrical shell and spheres (e.g. Leckie and Penny[30]).

2.3.1 Summary of Current Methods for Local Load Analysis

There are two main design methods which have been generally adopted by industry for the calculation of stresses and deflections in circular cylindrical shells subject to local loads transmitted by rigid attachments. These methods are found in the British Standard BS5500[1] and the Welding Research Council Bulletin 107[31] respectively.

When considering the theoretical development of the background to each of these documents, it is clear that the methods are essentially the same for the treatment of

radial loads but differ slightly in the representation of moment loads. In addition, the format and presentation of each of the two methods is quite different but both methods contain graphs, tables and worksheets and are equally complex when performing hand calculations, due to the difficulty of accurate interpolation.

The analytical method is based on elastic, small displacement analysis. The loads and displacements are represented by Fourier series. By also considering the equilibrium of the shell, the displacements due to an externally applied load component are found by reducing the three partial differential equilibrium equations for the shell into a single eighth order differential equation in terms of the radial displacements. The Fourier series expression for the radial displacements and the external loadings are then substituted into the eighth order differential equation and this is then solved by a numerical routine. Ultimately, expansions for each of the three displacements can be found and the subsequent stress resultants obtained via the compatibility relationships.

It is worth noting that the load representation of the BS method is based on a single Fourier series expression of a line load followed by direct integration across the patch whereas the WRC method utilises double Fourier series representation. This is expanded in detail in the following sections. In both codes, the radial load is assumed to be uniformly distributed over the patch and the moment loading to be linearly distributed.

Since both methods are based on end-supported cylindrical shells and use Fourier series to represent the loading terms, there are certain restrictions to the use of the method. In general, the analysis assumes the loaded area is remote from the ends, typically the edge of the loaded region being no closer the half of the radius from the end of the cylinder. In addition, the assumption of uniformly distributed loading is maintained by restricting the maximum patch length to be one half of the vessel radius (ie. $C_x/r < 0.25$). Limitations to the circumferential length are based on experimental work of the Pressure Vessel Research Committee of the ASME and are presented in WRC Bulletin 107 as extra-modified curves. This data also appears as Figure G.1 of

BS 5500 Annex G giving those regions where the charts may be used. Typical values of circumferential patch size are limited to the circumferential length being less that half of the vessel radius for a radial load or axial moment and circumferential length being less that the vessel radius for a circumferential moment for example, $C_\phi / r \leq 0.25$ *and* $C_\phi / 2r \leq 0.25$. The BS method of handling the moment loads, in which equivalent uniformly loaded patches are employed, makes economic use of the design charts.

Each of the two main design codes is based on this fundamental philosophy although, in practise, the execution of the method is different.

2.3.2 WRC Bulletin 107

In the ASME Boiler and Pressure Vessel Code, no explicit rules are given for the analysis of local ***rigid*** attachments on shell, however, the designer is directed to the Welding Research Council Bulletin 107 by ***Wichman et al***[31]. The history of this document originates in the early 1950's with work sponsored by the Pressure Vessel Research Committee of the Welding Research Council who commissioned ***P P Bijlaard*** to undertake an analytical and experimental investigation into the stresses and deflections of pressure vessel nozzle connections subject to various external loadings.

Bijlaard reported his work in various publications [32-38], however the salient points are worth noting. In his analysis, the displacement and loading functions, e.g. Equation(2.6) below, were represented by double Fourier series expressions and the cylinder was assumed to be simply supported at each end. The cylindrical shell equations employed by Bijlaard were similar to those of Donnell[39]. The main output of his work was in the form of nomographs for design for each of the various load cases anticipated; deflections, bending moments and membrane forces in cylinders arising from the application of externally applied radial loads and bending moments.

$$P_r = \sum_{n=0,1,2..}^{\infty} P_{m,n} \cos\left(\frac{m\pi x}{L}\right) \cos n\phi$$

(2.6)

Note that the form of this equation for P_r assumes that x is measured from the centre of the vessel at the centreline of the load. The method of load transfer adopted by Bijlaard for an externally applied radial load was that of a uniform pressure profile distributed over the vessel surface. For the case of a moment loading, the load profile was assumed to be triangular in distribution, see Figure 2.8a-c. Each of these loads is permitted to act on a rectangular area. Circular and elliptical areas were treated by evaluating the equivalent rectangle and using the same analysis. That is to say, a circular area, of radius, r_o, is represented by an equivalent square of half-side length = $0.875r_o$ and an elliptical area by a rectangular area of sizes 0.42 times the major and minor axes of the intersection of the shell as shown in Figures 2.9a and b.

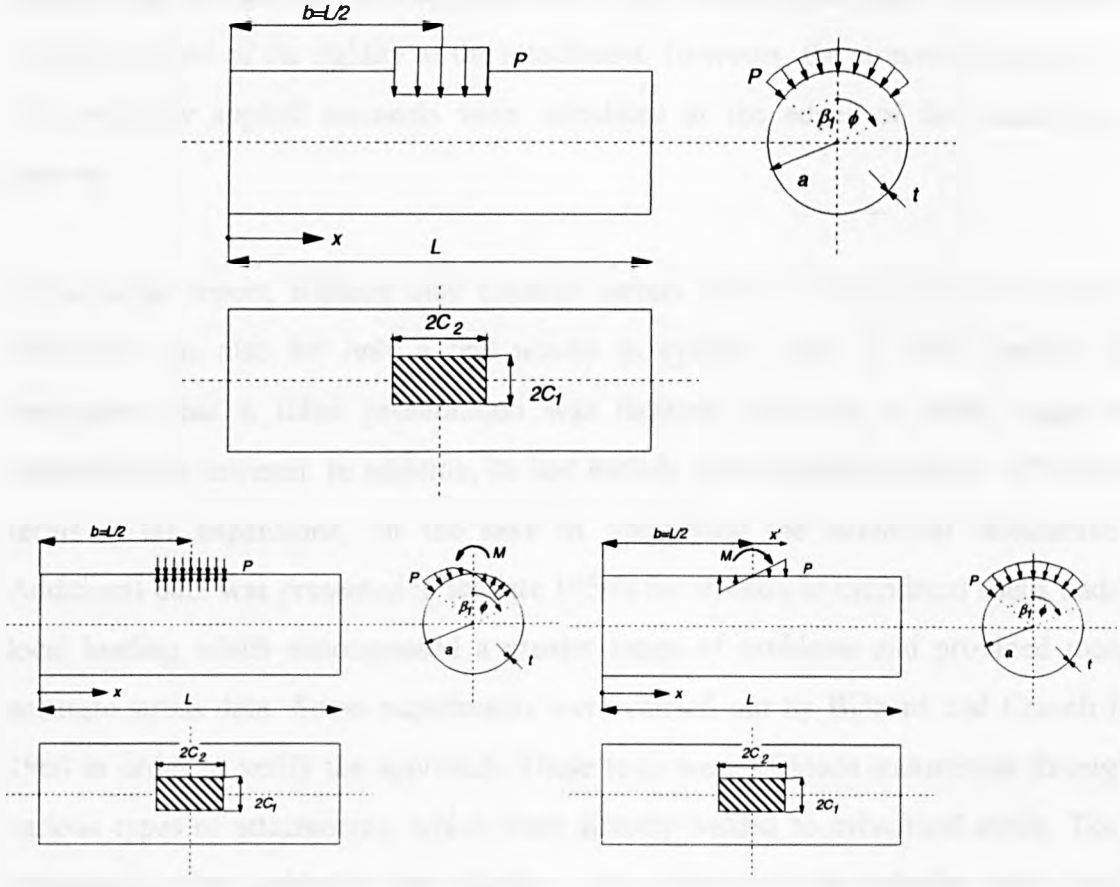

Figure 2.8a-c Radial and moment loads acting on a cylindrical shell

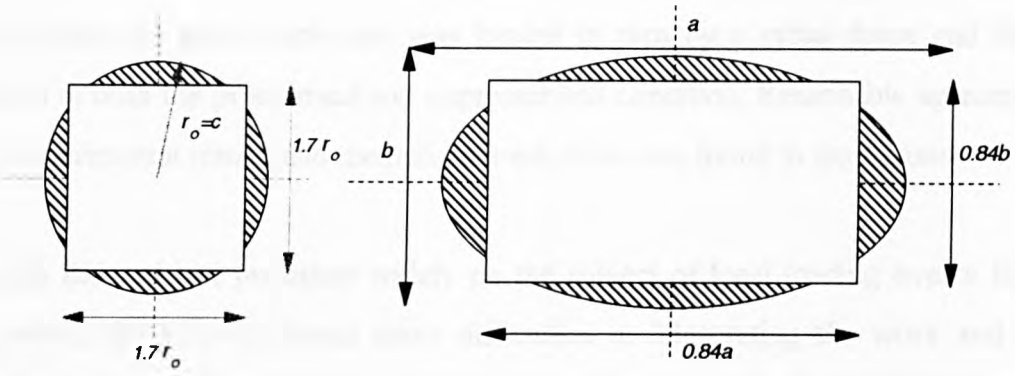

Figure 2.9a,b Equivalent rectangles for circular and elliptical patches

For the case of the externally applied radial load, the stresses presented in Bijlaard's reports and nomographs were located at the centre of the loaded area positioned at the geometric centre of the vessel. Although, in view of the welded construction of the detail, this location does not seem to be the natural position of the maximum stress. Bijlaard thus recommended that the values calculated at the centre of the loaded area, be used for the stresses located at the edge of the patch. This was done to take account of the rigidity of the attachment. However, the stresses presented for the externally applied moments were calculated at the edges of the loaded area anyway.

In his initial report, Bijlaard only covered certain cases of vessel radius to nozzle thickness, this also for only a few nozzle to cylinder radii. In later reports, he recognised that a fuller presentation was required and that a wider range of geometries be covered. In addition, he had initially used a limited number of Fourier terms in his expansions, for the sake of simplifying the numerical calculations. Additional data was presented in the late 1950's for stresses in cylindrical shells under local loading which encompassed a greater range of problems and provided more accurate stress data. Some experiments were carried out by Bijlaard and Cranch in 1960 in order to verify the approach. These tests were of loads transmitted through various types of attachments, which were directly welded to cylindrical shells. They comprised a pipe welded to the cylinder, a pipe welded to the cylinder with a hole introduced, a pipe with a reinforcing pad welded to the cylinder with a hole, a hollow rectangular section welded directly to the hole and lastly, a solid circular bar welded

to the cylindrical shell. Each case was loaded in turn by a radial force and both moments in both the pressurised and unpressurised condition. Reasonable agreement of the experimental results and theoretical predictions was found in most cases.

Although Bijlaard had published widely on the subject of local loading over a five-year period, the industry found many difficulties in interpreting the work and its limitations became evermore apparent. ***Wichman et al*** in 1965[31], were commissioned by the Welding Research Council to summarise all of Bijlaard's work and to extend the work to meet the requirements of industry. This work was presented, at that time, in a useful **'cook-book'** form and was published as the WRC Bulletin 107. The bulletin incorporated a description of the limitations of the original work and a comprehensive explanation of the changes made therein.

Although in wide use today, the main drawback with the bulletin, as a design tool, is that it contains a multitude of graphs. It contains graphical data for each stress resultant for each different load type, radial load, longitudinal moment and circumferential moment for a range of geometries. Graphs are also included for the evaluation of die-out effects. Using the information is complex and there is a real possibility of errors being made since, in many cases, the data may require interpolation between graphs for differing geometries.

2.3.3 BS 5500 Annex G

The British Standard 5500 has, contained within Annex G, rules for the evaluation of the stresses and deflections for local loads on cylindrical and spherical shells.

The origin of the method for loads transferred to cylindrical shells by rigid attachments is traced to a series of reports published by ***Kempner, Sheng and Pohle***[40] (1957) for the Knoll Atomic Power Laboratory and is based on the theoretical work of ***Hoff et al***[41] (1954). These reports produced graphs and tables of displacements, rotations and stress resultants for the case of a radial line load applied

at the zenith acting along part of the generator (i.e. in the axial direction) located at the mid-length of an end supported cylinder - as shown in Figure 2.10.

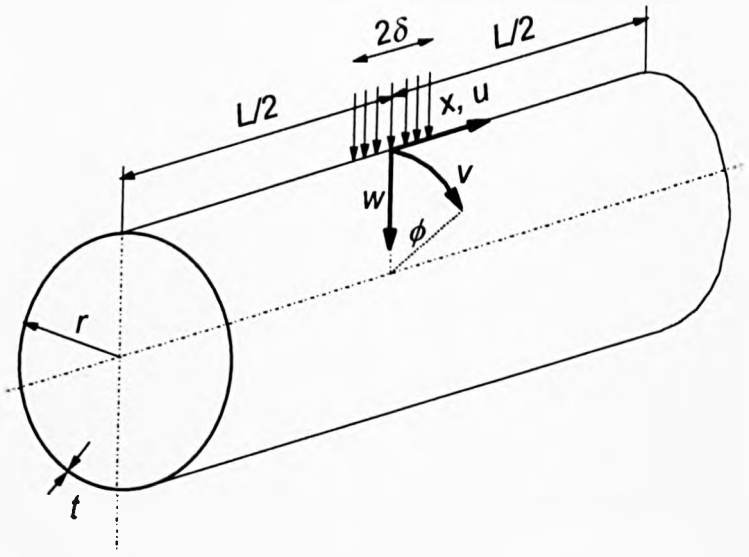

Figure 2.10 Line load acting on a generator

These line load results utilised a single Fourier series to represent the line load (Equation 2.7) and were later used to obtain the stresses and deflections for rectangular areas of loading by direct integration. This procedure was adopted by ICI, who developed their own version of the data in the form of a 'Mechanical Engineering Design Book', which was later included in BS 1515, 1965, Part 1, Appendix A. In 1976, with the writing of the master pressure vessel standard BS5500, which updated BS 1515 and incorporated data from various British Standards, the procedure was drafted into its present form as Appendix G.

$$P_r = \sum_{n=1,3...}^{\infty} P_m \cos\left(\frac{m\pi x}{L}\right) \tag{2.7}$$

The analysis of moment loadings generally assumes that the interface pressure distribution is triangular in form. However, in BS5500, the procedure adopted was to utilise the existing data for the radial load case, with its uniform rectangular profile, and to consider the moment as equivalent to two patches of uniformly distributed radial loading of length equal to one third of the loaded patch length. The forces on each patch are equal and opposite and act in directions consistent with the direction of the action of the moment.

It is worth noting that, as BS5500 was being written, the information from WRC Bulletin 107 was available for obtaining the longitudinal and circumferential moments cases using the triangular distribution. However, the code writers felt that the two equal and opposite radial patch approach minimised the number of graphs in the Standard, since only data for the uniform radial loading case need be presented. There remains, however, the question of the interaction effects between the two equal and opposite patches which complicates the procedure as presented in the Standard. Indeed, some designers have been known to carry out a moment loading analysis in accordance with Annex G and to ignore the effect of the second loaded area. In general, this approach provides a conservative result.

As a means of simplifying the procedure, worksheets are presented in the Standard in an attempt to aid the designer through the calculation. Even so, the procedure is complex and cumbersome and does not readily allow simple design changes to be easily made.

Some engineering software companies (e.g. Finglow, ESDU and Whessoe) have computerised the code. In their programs, the approach is to have digitised the graphical information, and thereafter produce routines that undertake the data interpolation. Where available, actual equations are used. Whilst this is of use in a Code design context, a preferred route would be to use the computer to carry out a more rigorous analysis, using the fundamental or basic equations rather than to have approximate data calculated. This approach would provide data that are more accurate for both stress analysis and fatigue assessments.

2.3.4 Other Approaches to the Local Loading of Cylindrical Vessels

In view of the fact that the methodology of BS 5500 is complex and cumbersome, several alternative approaches have been proposed which attempt to ease the effort in performing repetitive designs. There are three possible routes which may be followed

in developing these alternative approaches. The ***first*** is to provide a simplified method which may be used instead of the Standard.

To this end, work carried out at UMIST was carried out by ***Bedri et al***[42] provides a series of 'stress factors' for rectangular attachments. These factors were presented for three different load cases, i.e. radial force, circumferential and longitudinal moments. It is interesting to note that these charts incorporate the effect of the second loaded area in the moment cases thus eliminating one complete section of the calculation process, which is often ignored by designers. A similar approach is presented by ***Teixeira et al***[43] for local loadings on branch pipes. In both cases, the basic stress data is taken directly from BS 5500 Annex G and covers the range of vessel parameters stated in the Standard. However, no attempt was made to improve or 'correct' the values for the basic stress data. Despite the fact that this work has been available since 1983, it has never been incorporated into the Standard (***BS 5500***[1]).

The ***second*** alternative approach is to provide a suitable microcomputer program based on the basic shell equations. The double Fourier series solution used by Bijlaard has been programmed by ***Duthie and Tooth***[44] for various patch loading cases. More recently, ***Tooth and Nash***[45] have developed the double Fourier series solution using Sanders' shell equations and have programmed their solution on a personal computer. This method avoids the inaccuracy of graph reading and interpolation and allows a rapid analysis to be carried out for a wide range of loading cases which may not be covered by the Standard. This alternative approach is extended in the present work to cover those cases where the loading patch is not rectangular.

The ***third*** alternative method is to perform a **'design-by-analysis'** study of the problem using, say, finite element methods. This approach is discussed later in this work and is very useful for analysing individual problems but can be time consuming and onerous if there are a large number of cases which require to be considered. Problems with mesh refinement and stress categorisation arise with the use of finite

element analysis and there is often confusion and mis-interpretation when applying code rules and limitations to the output. This approach should not be used by the inexperience vessel engineer or indeed, finite element analyst. A depth of knowledge in both subjects is required.

2.4 Survey of More Recent Work on Local Loads

A review of more recent work, that is to say, work published since the present author began his investigations in 1985, has been mainly concentrated in analysing the interface contact pressure distribution under the local attachment. ***Hueilin and Santung***[46-47], ***Motashar and Tooth***[48] and ***Thomopoulos et al***[49-50] have analysed the case of the rigid attachment (or saddle) with a variable interface pressure distribution. ***Nadarajah, Tooth and Spence***[54,90,91], however, have used the finite element technique to investigate the influence of large displacement analysis for radial loading and the influence of the rigidity of the attachment, both acting separately and together.

Thomopoulos *et al*[49-50] have used the framework of the Flügge shell equations and have discretised the loaded areas into a regular number of patches. Fourier series are used to represent the loading via flexibility coefficients, which are obtained from the analysis. The boundary representation is non-linear and is formulated using a contact-Coulomb friction numerical algorithm, which is consecutively repeated until convergence is reached. The algorithm is carried out in two stages with the first considering tangential loads as given and those regions which are and are not in contact are determined. Thereafter, the normal loads are considered as constant and the sticking/slipping regions are computed.

Although principally concerned with the evaluation of the frictional contact loads for simple 'saddles' or attachments on pipe supports, Thomopoulos identifies that the method may be more general in application. For example, the more traditional pressure vessel saddle support may be analysed using the technique. In addition, he notes that multi supported systems incorporating frictional effects in the longitudinal direction may also be tackled. However, the technique is computer intensive with a

typical run for a simple pipe support taking over five hours for a single case, compared with 4-5 minutes using the present approach.

Hueilin and Suntung[46-47] presented an alternative method of evaluating the contact pressures for pad-reinforced structures. A mixed finite element method for the analysis of plate and shell problems has been developed which involves non-linear contact analysis. After defining the load vector for the problem, the flexibility matrix for the system is evaluated. Contact normals are identified on the two surfaces which may come into contact. A Coulomb friction model is used and mating pair of nodes are identified as being free, sticking (adhesion state) or slipping. Thereafter the continuity equations are modified and the contact forces and gaps (if any) are identified. A check is made for convergence and for the total load application and thereafter the nodal displacements and stresses are evaluated.

Two examples of the use of the mixed finite element formulation are presented. The first is a saddle support problem with the 'saddle' being represented as a stiff bracket plate with a flexible wrapper. Some 20 contact nodes were used to represent the contacting surfaces. The distribution of the contact forces on the saddle surface is shown below, in Figure 2.11. This represents a developed surface plot of the saddle/vessel contact area. It can be seen that maximum contact pressure peaks arise just below the saddle horn edge and these have a maximum value at the saddle centreline.

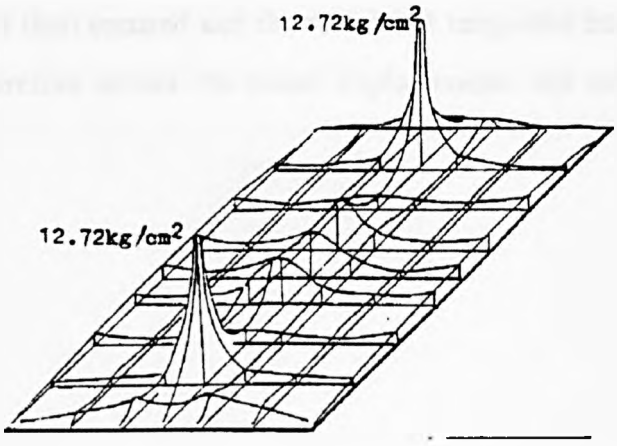

Figure 2.11 Contact Force Distribution on Saddle Surface (Hueilin and Suntung)

The second example highlighted is that of an axial moment acting on a large circular pad. In the British Standard, a triangular distribution is assumed for the load representation. The mixed FEM analysis of the distribution of contact forces on the pad shows that, in the main, the bulk of the interface pressure is concentrated at the weld regions located at the top and bottom of the loaded region. The major portion of the pad has little or no interface pressure value. The researchers carried out strain gauge tests in order to verify their method. Reasonable agreement was found for those regions where gauges could be sited. Comparison was also made with conventional finite element methods and some 30-40% improvement was found by the implementation of the mixed formulation.

Motashar and Tooth[48] examined the behaviour of the cylindrical vessel which is radially loaded through a rigid attachment which is of a rectangular plan form. The resulting radial and tangential interface forces between the vessel and the attachments are found assuming the attachment is fixed to the vessel at all points over the mating surface and is subject to a radial displacement. The double Fourier series solution, which is detailed in the present work, is extended to incorporate a number of equal size discrete areas as shown in Figure 2.12. The vessel flexibility is evaluated and compatibility equations enforced. Motashar's solution allows for a flexible attachment to be incorporated in the construction of the compatibility equations if the flexibility matrices can be found from, for example, a suitable finite element model. In their example, the flexibility matrices are set to zero and the attachment is assumed to be rigid. Equilibrium is then ensured and the radial and tangential interface pressures are evaluated. This therefore allows the vessel displacements and stress resultants to be found.

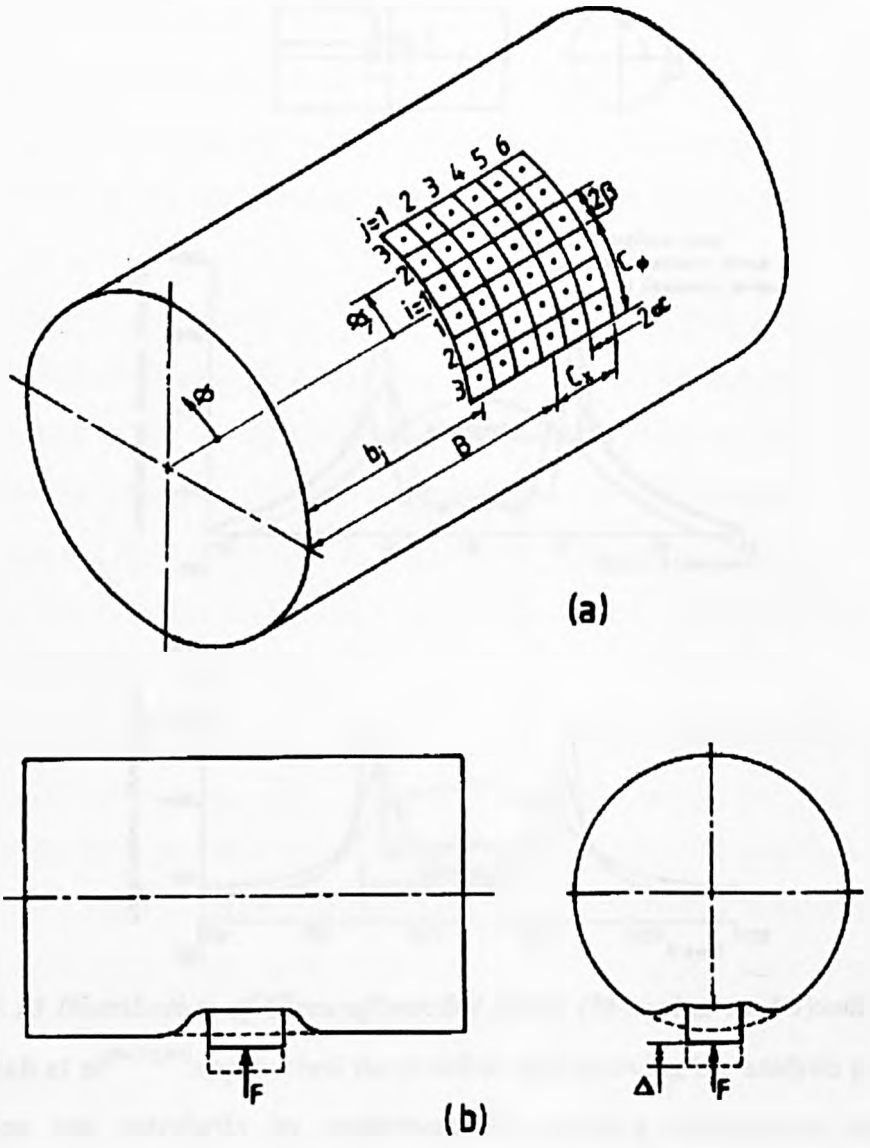

Figure 2.12 Rigid Attachment (a) Discrete Areas (b) Applied Force

Motashar concludes that the uniformly distributed interface pressure assumption is always unconservative and in the cases presented, the variable interface pressure analysis can be lead to peak stresses which are up to 37% higher. These peak stresses occur at the attachment edges in the local vicinity to the weld region - as shown in Figure 2.13.

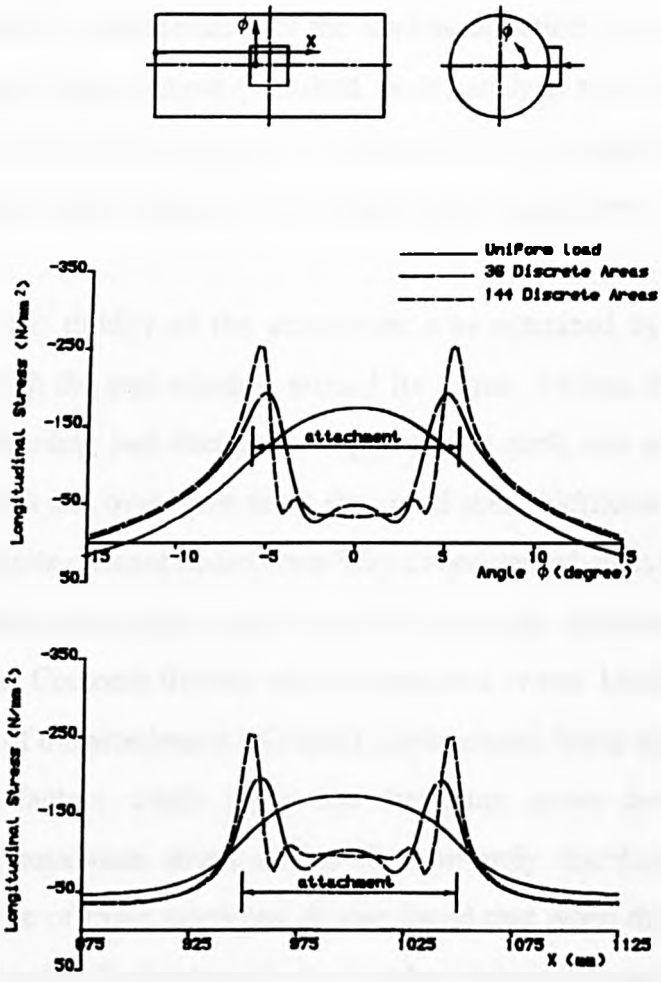

Figure 2.13 Distribution of Circumferential Stress (Motashar and Tooth 1988)

Nadarajah et al[54,90,91]approached the problem of improving the analysis presented in the codes and standards by examining the existing restrictions imposed by simplifications which were adopted at the time of writing. The Standard is based on the use of small displacement analysis for rotations and deflections to evaluate the code stress and displacement values. In addition, no account is taken of the complex interface pressure distribution, the codes assuming a simplified uniform distribution in the case of radially loaded attachments and linear (or equivalent) distributions for the externally applied moment cases.

Extensive finite element analyses were undertaken for a range of cases using large and small displacement analysis. The large displacement analysis resulted in higher peak stresses when the load was applied in towards the centre of the vessel and the opposite was the case when the loading direction was reversed. The small

displacement analysis is independent of the loading direction. A series of correction factors for the small displacement (standard, code) analysis were developed ranging from 0.92 for the load applied outwards to values of 1.45, 1.62 and 1.60 for the radial deflection, circumferential stress and longitudinal stress respectively.

The influence of the rigidity of the attachment was examined by generating finite element models with the pad attached around its edges. Various thicknesses of pad were examined including pad thicknesses equal to the shell, one and one half times thicker than the shell and over three times the vessel shell thicknesses. At the location of the welds, the finite element nodes were fully connected whereas in the location of the attachment area, the nodes were connected using gap elements. No mention is made as to whether Coulomb friction was incorporated or not. Uniform pressure was applied to the top of the attachment and small displacement, linear elastic analysis was employed. Stress factors which relate the maximum stress due to the loaded attachment to the maximum stress due to the uniformly distributed loading were plotted for the range of cases examined. It was found that when the pad is the same thickness as the vessel wall, the stress factor was less than unity over the whole range, therefore the pad stiffens the vessel and is sufficiently flexible to avoid increasing the edge stresses.

When both effects are analysed together, the large displacement analysis and the attachment rigidity did not significantly interact, i.e. they can be considered uncoupled. Therefore, in order to establish a simple way of combining the two effects, Nadarajah analysed a number of cases where the welded attachment was analysed using large displacement finite element analysis. These results were then compared with those obtained independently by combining the two modification factors together. This approach always gave a conservative result when comparing with the FE analysis, therefore simple multiplication of the two factors could be used as a design aid.

2.5 Aims of the Proposed Research

The present research deals with two specific problems, which are related. It is worth noting that the two previous sections **'Twin Saddle Problem'** and **'Local Patch Loading Problem'** can be solved using procedures that are based on the same fundamental equations. Each problem is tackled by employing **Sanders'** general theory of surfaces applied to a cylindrical shell. The choice of shell theory is based on the work of **A Leissa**, who presented a survey of thin shell theories under specific applications and showed that Sanders' equations were the most consistent and satisfactory. Thereafter, a double Fourier series approach allows the representation of the surface loading on the cylindrical shell and the development of a numerical solution that has been adapted for a variety of computer platforms.

The present work is concerned with examining the basis of current methods used in industry. In this, the background to the methods in the British pressure vessel standard BS 5500 and the ASME code are summarised and some attempt is made to verify their application. Solutions are developed and are then applied to a number of special cases for each problem.

Local load solutions are developed for rectangular shaped patches, which produce similar results to current code and standard approaches. New solutions are presented for patches that are circular and elliptical in form. In addition, stresses are now evaluated at the true maximum positions, as opposed to the approximate maximum location given in the literature. This provides reliable stress data for use in design and fatigue assessments. The solution thereafter is extended to cover steady state thermal stress problems including patch areas of heating or cooling and non-linear bell shaped thermal gradients.

The saddle support solution is developed and extended to incorporate flexible saddles with radial and tangential flexibility. From this, a full parameter study is undertaken and a new design methodology presented. This new approach incorporates all of the

main design parameters for a liquid filled vessel on twin saddles. The effects of the flexibility of the vessel head and saddle support are studied using finite element methods and suitable flexibility factors are supplied, where possible, for inclusion into the new design approach.

In addition, an overview is given of the use of finite element analysis in dealing with the design of complex pressure vessel details such as local loads and saddle supports.

3 THIN CIRCULAR CYLINDRICAL SHELL THEORY

This chapter presents the analysis of a thin circular cylindrical shell, simply supported at its end. The displacements and stresses are evaluated for the case where the cylinder is located horizontally and is subjected to various types of surface loading. Firstly, the differential equations which govern the behaviour of the cylindrical shell are derived. Thereafter, a double Fourier series expansion technique is employed to represent the surface loading, and a numerical solution for the equations describing the behaviour of the shell is established. The cases of a cylindrical vessel subjected to radial and tangential uniform patch loading are presented in detail, as they are used throughout this work.

3.1 Derivation of Thin Circular Cylindrical Shell Equations

The analysis developed within this thesis is based upon the improved thin shell theory proposed by Sanders'[12]. This has been developed almost entirely as a two-dimensional theory. This avoids certain complexities that arise when relating two and three-dimensional theories and makes for simpler implimentation whilst retaining consistency. Sanders' uses the principal of virtual work as the main tool for the derivation of his shell theory. This is presented in this section in some detail.

3.1.1 Geometry

The deformation of a **thin** shell can be completely defined by the displacement of its middle surface. The cylindrical co-ordinate system is used to define the middle surface and since the cylindrical shell has a constant radius of curvature along its circumference, then any point on the middle surface can be defined by two unique variables, x in the axial or longitudinal and θ in the circumferential directions. The middle surface displacements of the shell are defined as U, V and W in the x, θ and the surface normal directions respectively. Figure 3.1a shows the middle surface co-ordinates and positive directions of the shell displacements. Figures 3.1b and 3.1c show the stress resultants and couples which act on a section of the cylindrical shell parallel to its co-ordinates.

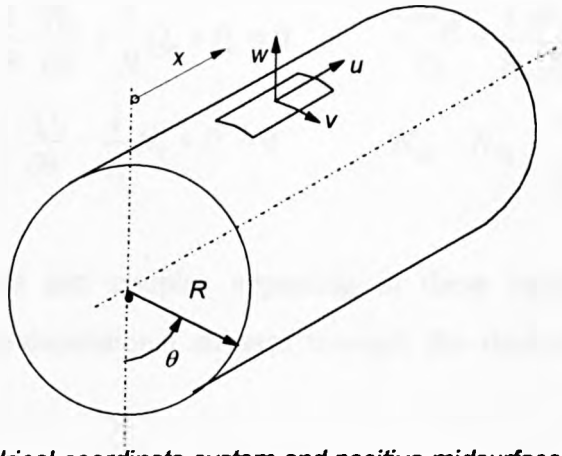

Fig 3.1a Cylindrical coordinate system and positive midsurface displacements

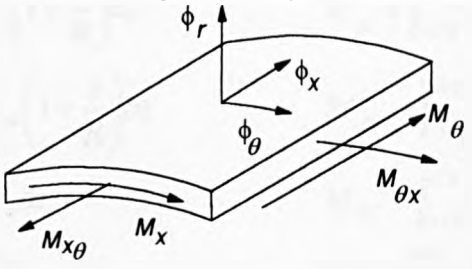

Fig 3.1b Couples and midsurface rotations

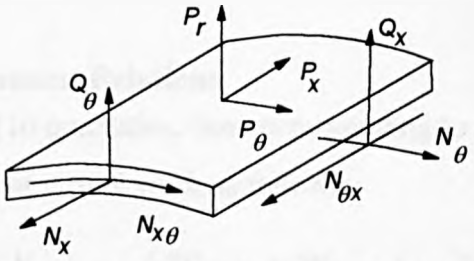

Fig 3.1c Stress resultants and loading components

Figure 3.1a-c Positive direction of displacements, stress resultants and loading

3.1.2 Equilibrium Equations

The equations of static equilibrium of the general shell element, which are quoted in Reference [12], are generally accepted and agreed upon[13]. The following equations are the equivalent equilibrium equations for a circular cylindrical shell:

$$\frac{\partial N_\chi}{\partial \chi}+\frac{1}{R}\frac{\partial N_{\theta\chi}}{\partial \theta}+P_\chi=0 \qquad \frac{\partial M_\chi}{\partial \chi}+\frac{1}{R}\frac{\partial M_{\theta\chi}}{\partial \theta}-Q_\chi=0$$

$$\frac{\partial N_{\chi\theta}}{\partial \chi}+\frac{1}{R}\frac{\partial N_\theta}{\partial \theta}+\frac{1}{R}Q_\theta+P_\theta=0 \qquad \frac{\partial M_{\chi\theta}}{\partial \chi}+\frac{1}{R}\frac{\partial M_\theta}{\partial \theta}-Q_\theta=0$$

$$\frac{\partial Q_\chi}{\partial \chi}+\frac{1}{R}\frac{\partial Q_\theta}{\partial \theta}-\frac{1}{R}N_\theta+P_r=0 \qquad N_{\chi\theta}-N_{\theta\chi}-\frac{1}{R}M_{\theta\chi}=0$$

(3.1)

The stress resultants and couples appearing in these equations are defined by integrations of three-dimensional stresses through the thickness of the cylinder as given below:

$$N_\chi=\int_{-t/2}^{t/2}\sigma_\chi\left(1+\frac{z}{R}\right)dz \qquad M_\chi=\int_{-t/2}^{t/2}\sigma_\chi\left(1+\frac{z}{R}\right)zdz$$

$$N_{\chi\theta}=\int_{-t/2}^{t/2}\tau_{\chi\theta}\left(1+\frac{z}{R}\right)dz \qquad M_{\chi\theta}=\int_{-t/2}^{t/2}\tau_{\chi\theta}\left(1+\frac{z}{R}\right)zdz$$

$$N_{\theta\chi}=\int_{-t/2}^{t/2}\tau_{\chi\theta}dz \qquad M_{\theta\chi}=\int_{-t/2}^{t/2}\tau_{\chi\theta}zdz$$

$$N_\theta=\int_{-t/2}^{t/2}\sigma_\theta dz \qquad M_\theta=\int_{-t/2}^{t/2}\sigma_\theta zdz$$

(3.2)

3.1.3 Strain-Displacement Relations

The strain expressions (10 quantities, one corresponding to each stress) are derived here using the principle of virtual work as follows:

$$\iint\left\{\left(\frac{\partial N_\chi}{\partial \chi}+\frac{1}{R}\frac{N_{\theta\chi}}{\partial \theta}\right)\delta U+\left(\frac{\partial N_{\chi\theta}}{\partial \chi}+\frac{1}{R}\frac{\partial N_{\theta\chi}}{\partial \theta}+\frac{1}{R}Q_\theta\right)\delta V\right.$$
$$+\left(\frac{\partial Q_{\chi\theta}}{\partial \chi}+\frac{1}{R}\frac{\partial Q_{\theta\chi}}{\partial \theta}-\frac{1}{R}N_\theta\right)\delta W+\left(\frac{\partial M_\chi}{\partial \chi}+\frac{1}{R}\frac{\partial M_{\theta\chi}}{\partial \theta}-Q_\chi\right)\delta\phi_\chi$$
$$\left.+\left(\frac{\partial M_{\chi\theta}}{\partial \chi}+\frac{1}{R}\frac{\partial M_\theta}{\partial \theta}-Q_\theta\right)\delta\phi_\theta+\left(N_{\chi\theta}-N_{\theta\chi}-\frac{1}{R}M_{\theta\chi}\right)\delta\phi_z\right\}d\theta dx=0$$

(3.3)

The integral must vanish by virtue of Equations (3.1). Expanding Equation (3.3) and integrating by parts yields:

$$\int_C \left[\begin{array}{l} \left(N_\chi \delta U + N_{\chi\theta}\delta V + Q_\chi \delta W + M_\chi \delta\phi_\chi + M_{\chi\theta}\delta\phi_\theta\right)d\theta + \\ \qquad\qquad \left(N_{\theta\chi}\delta U + N_\theta \delta V + Q_\theta \delta W + M_{\theta\chi}\delta\phi_\chi + M\theta\delta\phi_\theta\right)\dfrac{dx}{r} \end{array} \right]$$

$$-\int\int\{N_\chi\delta\left(\frac{\partial U}{\partial\chi}\right)+N_{\chi\theta}\delta\left(\frac{\partial V}{\partial\chi}-\phi_z\right)+N_{\theta\chi}\delta\left(\frac{1}{R}\frac{\partial U}{\partial\theta}+\phi_z\right)+N_\theta\delta\left(\frac{1}{R}\frac{\partial V}{\partial\theta}+\frac{W}{R}\right)$$

$$-M_\chi\delta\left(\frac{\partial\phi_\chi}{\partial\chi}\right)+M_{\chi\theta}\delta\left(\frac{\partial\phi_\theta}{\partial\chi}\right)+M_{\theta\chi}\delta\left(\frac{1}{R}\frac{\partial\phi_\chi}{\partial\theta}+\frac{1}{R}\phi_z\right)+M_\theta\delta\left(\frac{1}{R}\frac{\partial\phi_\theta}{\partial\theta}\right)$$

$$+Q_\chi\delta\left(\frac{\partial W}{\partial\chi}+\phi_\chi\right)+Q_\theta\delta\left(-\frac{V}{R}+\frac{1}{R}\frac{\partial W}{\partial\theta}+\phi_\theta\right)\}dxd\theta=0$$

(3.4)

The two double integrals extend over the region of the middle surface of the shell enclosed by the cylindrical curve C. According to the principle of virtual work these two integrals must equal each other. The first integral represents the virtual work of the forces acting on the cylinder whilst the second integral describes the virtual change in strain energy of the cylindrical shell. This leads to the following definitions of strain quantities:

$$\varepsilon_\chi=\frac{\partial U}{\partial\chi} \qquad K_\chi=\frac{\partial\phi_\chi}{\partial\chi}$$

$$\varepsilon_{\chi\theta}=\frac{\partial U}{\partial\chi}-\phi_z \qquad K_{\chi\theta}=\frac{\partial\phi_\theta}{\partial\chi_\chi}$$

$$\varepsilon_{\theta\chi}=\frac{1}{R}\frac{\partial U}{\partial\theta}+\phi_z \qquad K_{\theta\chi}=\frac{1}{R}\frac{\partial\phi_\chi}{\partial\theta}+\frac{1}{R}\phi_z$$

$$\varepsilon_\theta=\frac{1}{R}\frac{\partial V}{\partial\theta}+\frac{W}{R} \qquad K_\theta=\frac{1}{R}\frac{\partial\phi_\theta}{\partial\theta}$$

$$\gamma_\chi=\frac{\partial W}{\partial\theta}+\phi_\chi \qquad \gamma_\theta=\frac{1}{R}\frac{\partial W}{\partial\theta}-\frac{V}{R}+\phi_\theta$$

(3.5)

3.1.4 Simplification of Results

It is assumed that the work done by the maximum transverse shear stress acting through a distance equal to the maximum transverse shear strain times the thickness of the shell, is negligible in comparison with the total change in strain energy during deformation. From this assumption the two terms in the second integral of Equation

(3.4) which contain Q_x and Q_θ can be set to zero and the quantities ϕ_x and ϕ_θ can be expressed in terms of U, V and W:

$$\phi_\chi = -\frac{\partial W}{\partial \chi} \qquad \phi_\theta = \frac{V}{R} - \frac{1}{R}\frac{\partial W}{\partial \theta}$$

(3.6)

The rotation about the normal ϕ_Z is calculated by taking the surface curl of a displacement vector. The expression ϕ_Z becomes:

$$\phi_z = \frac{1}{2}\left(\frac{\partial V}{\partial \chi} - \frac{1}{R}\frac{\partial U}{\partial \theta}\right)$$

(3.7)

Substituting for ϕ_Z into equation 3.5, it follows that:

$$\varepsilon_{\chi\theta} = \varepsilon_{\theta\chi} = \frac{1}{2}\left[\frac{\partial V}{\partial x} + \frac{1}{R}\frac{\partial U}{\partial \theta}\right]$$

(3.8)

Combining the two expressions for twisting strain $K_{x\theta}$ and $K_{\theta x}$ and the expressions of the shear strain yields the following identity:

$$K_{\chi\theta} - K_{\theta\chi} = \frac{1}{2R}(\varepsilon_{x\theta} + \varepsilon_{\theta\chi}) = \frac{1}{R}\varepsilon_{\chi\theta}$$

(3.9)

Using expressions (3.8) and (3.9), the second integral of equation (3.4) (the change in strain energy integral) can be rewritten as:

$$\iint\{N_\chi \delta\varepsilon_\chi + (N_{\chi\theta} + N_{\theta\chi}) + \frac{1}{4R}(M_{\chi\theta} - M_{\theta\chi})\delta\varepsilon_{\chi\theta} + N_\theta \delta\varepsilon_\theta + M_\chi \delta K_\chi$$
$$+ \frac{1}{2}(M_{\chi\theta} + M_{\theta\chi})\delta(K_{\chi\theta} + K_{\theta\chi}) M_\theta \delta K\theta + Q_\chi \delta\gamma_\chi + Q_\theta \delta\gamma_\theta\} R dx d\theta$$

(3.10)

A new modified definition of the shear resultant, shear couple and twisting strain are introduced at this point. These are:

$$\overline{N}_{\chi\theta} = \frac{1}{2}(N_{\chi\theta} + N_{\theta\chi})$$

$$\overline{M}_{\chi\theta} = \frac{1}{2}(M_{\chi\theta} + M_{\theta\chi})$$

$$\overline{K}_{\chi\theta} = \frac{1}{2}(K_{\chi\theta} + K_{\theta\chi})$$

$$= -\frac{1}{R}\frac{\partial^2 W}{\partial\chi\partial\theta} + \frac{3}{4R}\frac{\partial V}{\partial\chi} - \frac{1}{4R^2}\frac{\partial U}{\partial\theta}$$

(3.11a,b,c)

A simplification is introduced here by neglecting the term (1/4*R*) ($M_{\chi\theta}$ - $M_{\theta\chi}$).

This is justified by the introduction of expression (3.11a), where (1/4*R*) ($M_{\chi\theta}$-$M_{\theta\chi}$) would be very small compared with 1/2 ($N_{\chi\theta}$+$N_{\theta\chi}$) or 1/2 ($M_{\chi\theta}$+$M_{\theta\chi}$). However, it is noted that ($N_{\chi\theta}$-$N_{\theta\chi}$) is not being neglected. Applying the above definitions and simplifications to Equation (3.10), it becomes:

$$\int\int\left\{N_\chi\delta\varepsilon_\chi + 2\overline{N}_{\chi\theta}\delta\varepsilon_{\chi\theta} + N_\theta\delta\varepsilon_\theta + M_\chi\delta K_\chi + 2\overline{M}_{\chi\theta}\delta\overline{K}_{\chi\theta} + M_\theta\delta K_\theta + Q_\chi\delta\gamma_\chi + Q_\theta\delta\gamma_\theta\right\}Rdxd\theta$$

(3.12)

3.1.5 Modified Equilibrium Equations

After introducing the new definitions and simplifications, the equilibrium equations require modification. This is carried out using the principle of virtual work. At this stage, the strain expressions are now expressible in terms of the displacements *U*, *V* & *W*. They are introduced into Equation 3.12 in the application of the principle of virtual work that leads to a new set of equilibrium equations. The expression for the virtual change in strain energy may now be written as:

$$\iint\{N_\chi\delta\left(\frac{\partial U}{\partial\chi}\right)+\overline{N}_{\chi\theta}\delta\left(\frac{\partial V}{\partial\chi}+\frac{1}{R}\frac{\partial U}{\partial\theta}\right)+N_\theta\delta\left(\frac{1}{R}\frac{\partial V}{\partial\theta}+\frac{W}{R}\right)+M_\chi\delta\left(\frac{\partial\phi_\chi}{\partial\chi}\right)$$
$$+\overline{M}_{\chi\theta}\delta\left(\frac{\partial\phi_\theta}{\partial\chi}+\frac{1}{R}\frac{\partial\phi_\chi}{\partial\theta}+\frac{1}{2R}\frac{\partial V}{\partial\chi}-\frac{1}{2R^2}\frac{\partial U}{\partial\theta}\right)+M_\theta\delta\left(\frac{1}{R}\frac{\partial\phi_\theta}{\partial\theta}\right)$$
$$+Q_\chi\delta\left(\frac{\partial W}{\partial\chi}+\phi_\chi\right)+Q_\theta\delta\left(\frac{\partial W}{\partial\theta}-\frac{V}{R}+\phi_\theta\right)\}Rdxd\theta=$$
$$\int_c[\left(N_\chi\delta U+\overline{N}_{\chi\theta}\delta V+M_\chi\delta\phi_\chi+\overline{M}_{\chi\theta}\left(\delta\phi_\theta+\frac{1}{2R}\delta V\right)+Q_\chi\delta W\right)Rd\theta$$
$$+\left(\overline{N}_{\chi\theta}\delta U+N_\theta\delta V+\overline{M}_{\chi\theta}\left(\delta\phi_\chi-\frac{1}{2R}\delta U\right)+M_\theta\delta\phi_\theta+RQ_\theta\delta W\right)dx]$$
$$-\iint\{\left(R\frac{\partial N_\chi}{\partial\chi}+\frac{\partial\overline{N}_{\chi\theta}}{\partial\theta}-\frac{1}{2R}\frac{\partial\overline{M}_{\chi\theta}}{\partial\theta}\right)\delta U+\left(R\frac{\partial\overline{N}_{\chi\theta}}{\partial\chi}+\frac{\partial N_\theta}{\partial\theta}+\frac{1}{2}\frac{\partial\overline{M}_{\chi\theta}}{\partial\chi}+Q_\theta\right)\delta V$$
$$+\left(-N_\theta+R\frac{\partial Q_\chi}{\partial\chi}+R\frac{\partial Q_\theta}{\partial\theta}\right)\delta W+\left(R\frac{\partial M_\chi}{\partial\chi}+\frac{\partial\overline{M}_{\chi\theta}}{\partial\theta}-RQ_\chi\right)\delta\phi_\chi$$
$$+\left(R\frac{\partial\overline{M}_{\chi\theta}}{\partial\chi}+\frac{\partial M_\theta}{\partial\theta}-RQ_\theta\right)\delta\phi_\theta\}dxd\theta$$

(3.13)

If the shell is to be in equilibrium, by the principle of virtual work, the left hand side of Equation (3.13) (the virtual change in strain energy) must equal the first integral in the right hand side (the virtual change in work done by forces on the shell). This implies the second integral on the right hand side (the area integral) must vanish. Since the virtual displacements are arbitrary and independent they cannot be set equal to zero, so all the five expressions (which are corresponding to the five virtual displacements) must vanish. Thus the following equilibrium conditions must hold:

$$\frac{\partial N_\chi}{\partial \chi}+\frac{1}{R}\frac{\overline{N}_{\chi\theta}}{\partial\theta}-\frac{1}{2R^2}\frac{\overline{M}_{\chi\theta}}{\partial\theta}=0$$

$$\frac{\partial \overline{N}_{\chi\theta}}{\partial \chi}+\frac{1}{R}\frac{\partial N_\theta}{\partial\theta}+\frac{1}{2R}\frac{\overline{M}_{\chi\theta}}{\partial\chi}+\frac{1}{R}Q_\theta=0$$

$$\frac{\partial Q_\chi}{\partial \chi}+\partial Q_\theta-\frac{N_\theta}{R}=0$$

$$\frac{\partial M_\chi}{\partial \chi}+\frac{1}{R}\frac{\partial \overline{M}_{\chi\theta}}{\partial\theta}-Q_\chi=0$$

$$\frac{\partial \overline{M}_{\chi\theta}}{\partial \chi}+\frac{1}{R}\frac{\partial M_\theta}{\partial\theta}-Q_\theta=0$$

(3.14)

These equations are the new modified equilibrium equations. The number of stress unknowns has been reduced from 10 to 8.

In previous derivations of shell theory, the number of unknown stress resultants and couples are reduced by making approximations in the expressions for the resultants in terms of integrals of stress through the thickness of the shell. In the present derivation, the reduction is made by combining some terms in a similar manner to those in the application principle of virtual work. This affects those terms associated with the work done during a small rotation about the normal to the shell. Using this approach, it is not necessary to eliminate any terms in the expressions for the stress resultants and couples in terms of integrals of stress through the thickness of the shell. Substituting for Q_χ and Q_θ in Equations (3.14) reduces the number of terms from five to three. Adding them to the external forces, they become:

$$\frac{\partial N_\chi}{\partial \chi}+\frac{1}{R}\frac{\overline{N}_{\chi\theta}}{\partial\theta}-\frac{1}{2R^2}\frac{\overline{M}_{\chi\theta}}{\partial\theta}+P_\chi=0$$

$$\frac{\partial \overline{N}_{\chi\theta}}{\partial \chi}+\frac{1}{R}\frac{\partial N_\theta}{\partial\theta}+\frac{3}{2R}\frac{\overline{M}_{\chi\theta}}{\partial\chi}+\frac{1}{R^2}\frac{\partial M_\theta}{\partial\theta}+P_\theta=0$$

$$\frac{\partial^2 M_\chi}{\partial \chi^2}+\frac{2}{R}\frac{\partial^2 M_{\chi\theta}}{\partial\chi\partial\theta}+\frac{1}{R^2}\frac{\partial^2 M_\theta}{\partial\theta^2}-\frac{1}{R}N_\theta+P_r=0$$

(3.15)

3.1.6 Stress-Strain Relations

The stress-strain relations depend on the mechanical properties of the material of the shell. In determining stresses analytically it is customary to assume that the material is elastic, isotropic, homogeneous and that it conforms to Hooke's Law, which states the strain is proportional to stress. These assumptions lead to the following stress-strain relations, with shell thickness, t:

$$Et\varepsilon_x = N_x - \nu N_\theta \qquad Et^3 K_x = 12(M_x - \nu M_\theta)$$
$$Et\varepsilon_\theta = N_\theta - \nu N_x \qquad Et^3 k_\theta = 12(M_\theta - \nu M_x)$$
$$Et\varepsilon_{x\theta} = (1+\nu)\overline{N}_{x\theta} \qquad Et^3 \overline{K}_{x\theta} = 12(1+\nu)\overline{M}_{x\theta}$$

(3.16a-f)

3.2 The Governing Equations

In order to obtain the governing equations for the circular cylindrical shell, the equilibrium equations, the compatibility equations and the constitutive relations can now be combined to develop the governing equations that determine the overall behaviour of the shell. Firstly, the stress-strain relations are written as follows:

$$N_x = D(\varepsilon_x + \nu\varepsilon_\theta) \qquad M_x = \frac{Dt^2}{12}(K_x + \nu K_\theta)$$
$$N_\theta = D(\varepsilon_\theta + \nu\varepsilon_x) \qquad M_\theta = \frac{Dt^2}{12}(K_\theta + \nu K_x)$$
$$\overline{N}_{x\theta} = D(1-\nu)\varepsilon_{x\theta} \qquad \overline{M}_{x\theta} = \frac{Dt^2}{12}(1-\nu)\overline{K}_{x\theta}$$

(3.17a-f)

Using the compatibility equations to substitute the strains or their equivalents in terms of the displacements, a set of stress resultants is obtained expressed in terms of the displacements and material properties:

$$N_\chi = D\left(\frac{\partial U}{\partial \chi} + \frac{\nu}{R}\frac{\partial V}{\partial \theta} + \frac{\nu W}{R}\right)$$

$$N_\theta = D\left(\frac{1}{R}\frac{\partial V}{\partial \theta} + \upsilon\frac{\partial U}{\partial \chi} + \frac{W}{R}\right)$$

$$\overline{N}_{\chi\theta} = D\frac{(1-\nu)}{2}\left(\frac{\partial V}{\partial \chi} + \frac{1}{R}\frac{\partial U}{\partial \theta}\right)$$

$$M_\chi = DkR^2\left(-\frac{\partial^2 W}{\partial \chi^2} - \frac{\nu}{R^2}\frac{\partial^2 W}{\partial \theta^2} + \frac{\nu}{R^2}\frac{\partial V}{\partial \theta}\right)$$

$$M_\theta = DkR^2\left(-\frac{1}{R^2}\frac{\partial^2 W}{\partial \theta^2} + \frac{1}{R^2}\frac{\partial V}{\partial \theta} - \nu\frac{\partial^2 W}{\partial \chi^2}\right)$$

$$\overline{M}_{\chi\theta} = DkR^2(1-\nu)\left(-\frac{1}{R}\frac{\partial^2 W}{\partial \chi \partial \theta} + \frac{3}{4R}\frac{\partial V}{\partial \chi} - \frac{1}{4R^2}\frac{\partial U}{\partial \theta}\right)$$

(3.18a-f)

Using the above set of relations to substitute for the stress resultants into the new equilibrium equations, a set of three partial differential equations known as the Differential Equations of the Bending Theory of Circular Cylindrical Shells results:

$$\left\{(Rd_\chi)^2 + \frac{(1-\nu)}{2}\left(1+\frac{k}{4}\right)d_\theta^2\right\}U + \left\{\left(\frac{(1+\nu)}{2} - \frac{3(1-\nu)k}{8}\right)(Rd_\chi)d_\theta\right\}V + \left\{\upsilon(Rd\chi) + \frac{(1-\nu)k}{2}(Rd_\chi)d_\theta^2\right\}W = -\frac{P_\chi R^2}{D}$$

$$\left\{\left(\frac{(1+\nu)}{2} - \frac{3(1-\nu)k}{8}\right)(Rd_\chi)d_\theta\right\}U + \left\{\frac{(1-\nu)}{2}\left(1+9\frac{k}{4}\right)(Rd_\chi)^2(1+k)d_\theta^2\right\}V + \left\{\frac{(\nu-3)k}{2}(Rd_\chi)^2 d_\theta + d_\theta - kd_\theta^3\right\}W = -\frac{P_\theta R^2}{D}$$

$$\left\{-\frac{(1-\nu)}{2}k(Rd_\chi)d_\theta^2 - \nu(Rd_\chi)\right\}U + \left\{\frac{(3-\nu)}{2}k(Rd_\chi)^2 d_\theta + kd_\theta^3 - d_\theta\right\}V + \left\{-k(Rd_\chi)^4 - 2k(Rd_\chi)^2 d_\theta^2 - kd_\theta^4 - 1\right\}W = -\frac{P_r R^2}{D}$$

(3.19a-c)

Or they can be written in the form:

$$a_1U + b_1V + C_1W = d_1$$

$$a_2U + b_2V + C_2W = d_2$$

$$a_3U + b_3V + C_3W = d_3$$

where:

$$a_1 = (Rd_\chi)^2 + \left(\frac{1-\nu}{2}\right)\left(1+\frac{k}{4}\right)d_\theta^2 \qquad c_1 = \nu(Rd_\chi) + \frac{(1-\nu)k}{2}(Rd_x)d_\theta^2$$

$$a_2 = \left(\frac{1+\nu}{2} - \frac{3(1-\nu)k}{8}\right)(Rd_\chi)d\theta \qquad c_2 = \frac{(\nu-3)k}{2}(Rd_\chi)^2 d_\theta - kd_\theta^3 + d_\theta$$

$$a_3 = \frac{(\nu-1)k}{2}(Rd_\chi)d_\theta^2 - \nu(Rd_\chi) \qquad c_3 = -k(Rd_\chi)^4 - 2k(Rd_\chi)^2 d_\theta^2 - kd_\theta^4 - 1$$

$$b_1 = \left(\frac{1+\nu}{2} - \frac{3(1-\nu)k}{8}\right)(Rd_\chi)d_\theta \qquad d_1 = \frac{-P_\chi R^2}{D}$$

$$b_2 = \left(\frac{1-\nu}{2}\right)\left(1+\frac{9k}{4}\right)(Rd_x)^2 + (1+k)d_\theta^2 \qquad d_2 = \frac{-P_\theta R^2}{D}$$

$$b_3 = \frac{(3-\nu)}{2}(Rd_\chi)^2 d_\theta + kd_\theta^3 - d_\theta \qquad d_3 = \frac{-P_r R^2}{D}$$

(3.20)

3.3 Solution of The Governing Equations

The equations, which govern the behaviour of the circular cylindrical shell, have been derived in the sections above. These equations involve partial derivatives of χ and θ, and thus are described as **partial differential** equations. The solution of such systems of equations is generally complex. It is sometimes very difficult to find the required solution for a set of partial differential equations. Normally, some mathematical compromise is made and a numerical soultion evaluated, provided sufficient accuracy can be established. In the present work, a **Fourier Series Expansion Technique** is used to find the solution for the governing equations of the circular cylindrical shell.

Certain assumptions are made here in order to make the Fourier expansion method applicable and the resulting solution easier to establish. The circular cylindrical shell is assumed to be horizontally located and simply supported at its ends. The latter assumption sometimes may not always be true. However, in such cases, correction factors can be added to make up for this. In addition, a restriction is placed such that only those cases where symmetry about the vertical plane exists are considered in this work, since such covers the main types of loading that occur; pressure, fluid and self weight.

3.3.1 The Fourier Series Representation of Surface Loading

Differential equations with simple forms, for example sines or cosines can be easily solved. However, there are many cases of complex functions, which describe the behaviour of a real physical system, which cannot be simply represented by simple sine or cosine waves. In such cases, their behaviour can be expressed by a series of sines and cosines, the summation of which is the equivalent to the actual behaviour at the component. Thus a series composed of sines and cosines is the termed the **Fourier Expansion** of the function. To represent the loading system on a cylindrical surface, a double Fourier series is required for each component in longitudinal, tangential and radial directions. The following expressions are used to represent the surface loading:

$$P_\chi = \sum_{m=0}^{\infty}\sum_{n=0}^{\infty} P_{\chi mn}\cos(n\theta)\cos\left(\frac{m\pi\chi}{L}\right)$$

$$P_\theta = \sum_{m=1}^{\infty}\sum_{n=1}^{\infty} P_{\theta mn}\sin(n\theta)\cos\left(\frac{m\pi\chi}{L}\right)$$

$$P_r = \sum_{m=1}^{\infty}\sum_{n=0}^{\infty} P_{rmn}\cos(n\theta)\sin\left(\frac{m\pi\chi}{L}\right)$$

(3.21a-c)

A particular solution of the differential equations, corresponding to each term of the surface loading, can now be found. The sum of these particular solutions thus represents the total solution of the differential equations. The displacement solution therefore has the form of the double Fourier series as follows:

$$U = \sum_{m=0}^{\infty}\sum_{n=0}^{\infty} P_{\chi mn}\cos(n\theta)\cos\left(\frac{m\pi\chi}{L}\right)$$

$$V = \sum_{m=1}^{\infty}\sum_{n=1}^{\infty} P_{\theta mn}\sin(n\theta)\cos\left(\frac{m\pi\chi}{L}\right)$$

$$W = \sum_{m=1}^{\infty}\sum_{n=0}^{\infty} P_{rmn}\cos(n\theta)\sin\left(\frac{m\pi\chi}{L}\right)$$

(3.22a-c)

Substituting, for a particular mode of the Fourier expansion, for P_x, P_θ, P_r, U, V and W from Equations (3.21) and (3.23) into Equations (3.20), yields a set of three algebraic equations:

$$A_1 U_{mn} + B_1 V_{mn} + C_1 W_{mn} = D_1 P_{\chi_{mn}}$$
$$A_2 U_{mn} + B_2 V_{mn} + C_2 W_{mn} = D_1 P_{\theta_{mn}}$$
$$A_3 U_{mn} + B_3 V_{mn} + C_3 W_{mn} = D_1 P_{r_{mn}}$$

(3.23a-c)

where:

$$A_1 = \lambda^2 + \frac{1-\nu}{2}\left(1+\frac{k}{4}\right)n^2 \qquad C_1 = \nu\lambda - \frac{(1-\nu)k}{2}\lambda n^2$$

$$A_2 = \left(\frac{1+\nu}{2} - \frac{3(1-\nu)k}{8}\right)\lambda n \qquad C_2 = \frac{(\nu-3)k}{2}\lambda^2 n - kn^3 + n$$

$$A_3 = \frac{(\nu-1)k}{2}\lambda n^2 - \nu\lambda \qquad C_3 = -k\lambda^4 - 2k\lambda^2 n^2 - kn^4 - 1$$

$$B_1 = \left(\frac{1+\nu}{2} - \frac{3(1-\nu)k}{8}\right)\lambda n \qquad D_1 = -\frac{R^2}{D}$$

$$B_2 = -\frac{1-\nu}{2}\left(\frac{1+9k}{4}\right)\lambda^2 + (1+K)n^2$$

$$B_3 = -\frac{(3-\nu)k}{2}\lambda^2 n + kn^3 - n$$

(3.24)

This may be written in matrix form as:

$$\begin{pmatrix} A_1 & B_1 & C_1 \\ A_2 & B_2 & C_2 \\ A_3 & B_3 & C_3 \end{pmatrix}\begin{pmatrix} U_{mn} \\ V_{mn} \\ W_{mn} \end{pmatrix} = D_1 \begin{pmatrix} P_{\chi mn} \\ P_{\theta mn} \\ P_{rmn} \end{pmatrix}$$

The solution of which is:

$$U_{mn} = D_1 \frac{\{(B_2C_3 - B_3C_2)P_{\chi mn} - (B_1C_3 - B_3C_1)P_{\theta mn} + (B_1C_2 - B_2C_1)P_{rmn}\}}{DEN}$$

$$V_{mn} = D_1 \frac{\{-(A_2C_3 - A_3C_2)P_{\chi mn} + (A_1C_3 - A_3C_1)P_{\theta mn} - (A_1C_2 - A_2C_1)P_{rmn}\}}{DEN}$$

$$W_{mn} = D_1 \frac{\{(A_2B_3 - A_3B_2)P_{\chi mn} - (A_1B_3 - A_3B_1)P_{\theta mn} + (A_1B_2 - A_2B_1)P_{rmn}\}}{DEN}$$

where:

$$DEN = A_1(B_2C_3 - B_3C_2) - A_2(B_1C_3 - B_3C_1) + A_3(B_1C_2 - B_2C_1)$$
$$= -k\left(\frac{1-\nu}{2}\right)\left\{(\lambda^2+n^2)^4 - 2n^2(\lambda^2+n^2)^2 - 4\lambda^2 n^2(\lambda^2+n^2-1) + n^4 + \left(\frac{1-\nu^2}{2}\right)\lambda^4\right\}$$

(3.25)

This represents the solution for a particular mode of Fourier expansion of the general loading system P_x, P_θ, and P_r; but it is simpler to consider each loading component at a time and superimpose them to obtain the total solution.

3.3.2 Longitudinal Loading Only

In this case, it is assumed that $P_\theta = P_r = 0$, thus $P_{\theta mn} = P_{rmn} = 0$ for all values of m & n. Equations (3.25) become:

$$U_{\chi mn} = D_1 \frac{(B_2C_3 + B_3C_2)P_{\chi mn}}{DEN}$$

$$V_{\chi mn} = D_1 \frac{(A_2C_3 - A_3C_2)P_{\chi mn}}{DEN}$$

$$W_{\chi mn} = D_1 \frac{(A_2B_3 - A_3B_2)P_{\chi mn}}{DEN}$$

(3.26a-c)

The total solution for the displacements of a circular cylindrical shell subjected to a general loading in the axial direction becomes:

$$U_{\chi mn} = \frac{R^2}{kD}\sum_{m=0}^{\infty}\sum_{n=0}^{\infty} ZLL \;\; P_{\chi mn}\cos(n\theta)\cos\left(\frac{m\pi\chi}{L}\right)$$

$$V_{\chi mn} = \frac{R^2}{kD}\sum_{m=1}^{\infty}\sum_{n=1}^{\infty} ZLT \;\; P_{\theta mn}\sin(n\theta)\cos\left(\frac{m\pi\chi}{L}\right)$$

$$W_{\chi mn} = \frac{R^2}{kD}\sum_{m=1}^{\infty}\sum_{n=0}^{\infty} ZLR \;\; P_{rmn}\cos(n\theta)\sin\left(\frac{m\pi\chi}{L}\right)$$

where:

$$ZLL = \frac{\left\{k\left(\frac{1-\nu}{2}\lambda^2\left(\lambda^2+n^2\right)^2 + \frac{1}{k}\right) + n^2\left(\left(\lambda^2+n^2\right)^2 - (3-\nu)\lambda^2 2n^2 + 1\right)\right\}}{DEN}$$

$$ZLT = kn\lambda\frac{\left\{\frac{1+\nu}{2}\left(\lambda^2+n^2\right) - \frac{1}{2}\left((3-\nu)\nu\lambda^2 - (1-3\nu)n^2 - \frac{1-\nu}{k}\right)\right\}}{DEN}$$

$$ZLR = \frac{\left\{-\lambda\left(kn^2(\lambda^2+n^2) - \frac{1-\nu}{2}(\nu\lambda^2 - n^2)\right)\right\}}{DEN}$$

$$DEN = \frac{1-\nu}{2}\left\{(\lambda+n^2)^4 - 2n^2\left(\lambda^2+n^2-4\lambda^2n^2(\lambda^2+n^2-1)+n^4+\frac{(1+\nu^2)}{k}\lambda^4\right)\right\}$$

(3.27)

Finding the solution for the displacements in the Fourier series form allows the determination of the stress resultants, which are expressed in terms of the displacements and their derivatives (Equations 3.18), in the same form:

$$N_\chi = \frac{R}{k}\sum_{n=0}^{\infty}\sum_{m=1}^{\infty}\{-\lambda ZLL + vmZLT + vZLR\}P_{\chi_{mn}}\cos(n\theta)\sin\left(\frac{m\pi\chi}{L}\right)$$

$$N_\theta = \frac{R}{k}\sum_{n=0}^{\infty}\sum_{m=0}^{\infty}\{nZLT + ZLR - v\lambda ZLL\}P_{\chi_{mn}}\cos(n\theta)\sin\left(\frac{m\pi\chi}{L}\right)$$

$$\overline{N}_{\chi\theta} = \frac{R(1-v)}{2k}\sum_{n=1}^{\infty}\sum_{m=0}^{\infty}\{\lambda ZLT - nZLL\}P_{\chi_{mn}}\sin(n\theta)\cos\left(\frac{m\pi\chi}{L}\right)$$

$$M_\chi = R^2\sum_{n=0}^{\infty}\sum_{m=1}^{\infty}\{(\lambda^2 + vm^2)ZLR + vmZLT\}P_{\chi_{mn}}\cos(n\theta)\sin\left(\frac{m\pi\chi}{L}\right)$$

$$M_\theta = R^2\sum_{n=0}^{\infty}\sum_{m=1}^{\infty}\{(n^2 + v\lambda^2)ZLR + nZLT\}P_{\chi_{mn}}\cos(n\theta)\sin\left(\frac{m\pi\chi}{L}\right)$$

$$\overline{M}_{\chi\theta} = R^2(1-v)\sum_{n=1}^{\infty}\sum_{m=1}^{\infty}\left\{n\lambda ZLR + \frac{3}{4}\lambda ZLT + \frac{1}{4}nZLL\right\}P_{\chi_{mn}}\sin(n\theta)\cos\left(\frac{m\pi\chi}{L}\right)$$

(3.28a-f)

3.3.3 Tangential Loading Only

In this case, it is assumed that P_x=P_r=0, thus P_{xmn}=P_{rmn}=0 for all values of m and n. Equations (3.25) now become:

$$U_\theta = D_1\frac{(B_3C_1 - B_1C_3)P_{\theta_{mn}}}{DEN}$$

$$V_\theta = D_1\frac{(A_3C_1 - A_1C_3)P_{\theta_{mn}}}{DEN}$$

$$W_\theta = D_1\frac{(A_3B_1 - A_1B_3)P_{\theta_{mn}}}{DEN}$$

(3.29a-c)

The total solution for the displacements of a circular cylindrical shell subjected to a general loading in the tangential direction become:

$$U_\theta = \frac{R^2}{kD}\sum_{n=0}^{\infty}\sum_{m=0}^{\infty}ZTLP_{\theta_{mn}}\cos(n\theta)\cos\left(\frac{m\pi\chi}{L}\right)$$

$$V_\theta = \frac{R^2}{kD}\sum_{n=1}^{\infty}\sum_{m=1}^{\infty}ZTTP_{\theta_{mn}}\sin(n\theta)\sin\left(\frac{m\pi\chi}{L}\right)$$

$$V_\theta = \frac{R^2}{kD}\sum_{n=0}^{\infty}\sum_{m=1}^{\infty}ZTRP_{\theta_{mn}}\cos(n\theta)\sin\left(\frac{m\pi\chi}{L}\right)$$

(3.30a-c)

where:

$$ZTL = kn\lambda \frac{\left\{\frac{1+\nu}{2}\left(\lambda^2+n^2\right)-\frac{1}{2}\left((3-\nu)\nu\lambda^2-(1-3\nu)n^2-\frac{1-\nu}{k}\right)\right\}}{DEN}$$

$$ZTT = \frac{\left\{k\left(\lambda^2+\frac{1-\nu}{2}n^2\right)\left(\lambda^2+n^2\right)^2+(1-\nu)\left(\lambda^2\left(1+\nu+k\nu n^2\right)+\frac{1}{2}n^2\right)\right\}}{DEN}$$

$$ZTR = -n\frac{\left\{k\left(\frac{3-\nu}{2}\lambda^4+(2-\nu)\lambda^2n^2+\frac{1-\nu}{2}n^4\right)+\frac{1-\nu}{2}\left((2+\nu)\lambda^2+n^2\right)\right\}}{DEN}$$

(3.31a-c)

Equations 3.18 for the stress resultants now become:

$$N_\chi = \frac{R}{k}\sum_{n=0}^{\infty}\sum_{m=1}^{\infty}\left\{-\lambda ZTL+\nu nZTT+\nu ZTR\right\}P_{\theta_{mn}}\cos(n\theta)\sin\left(\frac{m\pi\chi}{L}\right)$$

$$N_\theta = \frac{R}{k}\sum_{n=0}^{\infty}\sum_{m=0}^{\infty}\left\{nZTT+ZTR-\nu\lambda ZTL\right\}P_{\theta_{mn}}\cos(n\theta)\sin\left(\frac{m\pi\chi}{L}\right)$$

$$\overline{N}_\theta = \frac{R(1-\nu)}{2k}\sum_{n=0}^{\infty}\sum_{m=0}^{\infty}\left\{\lambda ZTT-nZTL\right\}P_{\theta_{mn}}\sin(n\theta)\cos\left(\frac{m\pi\chi}{L}\right)$$

$$M_\chi = R^2\sum_{n=0}^{\infty}\sum_{m=1}^{\infty}\left\{(\lambda^2+\nu n^2)ZTR+\nu nZTT\right\}P_{\theta_{mn}}\cos(n\theta)\sin\left(\frac{m\pi\chi}{L}\right)$$

$$M_\theta = R^2\sum_{n=0}^{\infty}\sum_{m=1}^{\infty}\left\{(n^2+\nu\lambda^2)ZTR+nZTT\right\}P_{\theta_{mn}}\cos(n\theta)\sin\left(\frac{m\pi\chi}{L}\right)$$

$$\overline{M}_{\chi\theta} = R^2(1-\nu)\sum_{n=1}^{\infty}\sum_{m=1}^{\infty}\left\{n\lambda ZTR+\frac{3}{4}\lambda ZTT+\frac{1}{4}nZTL\right\}P_{\chi_{mn}}\sin(n\theta)\cos\left(\frac{m\pi\chi}{L}\right)$$

(3.32a-f)

3.3.4 Radial Loading Only

In this case, $P_x = P_\theta = 0$. The total solution for the displacements and the stress resultants is obtained in a similar way as above:

$$U_r = D_1\frac{(B_1C_2-B_2C_1)P_{r_{mn}}}{DEN}$$

$$V_r = D_1\frac{(A_1C_2-A_2C_1)P_{r_{mn}}}{DEN}$$

$$W_r = D_1\frac{(A_1B_2-A_2B_1)P_{r_{mn}}}{DEN}$$

(3.33a-c)

where:

$$ZRL = \frac{\left\{-\lambda\left(kn^2(\lambda^2+n^2)-\frac{1-\nu}{2}\left(W\lambda^2-n^2\right)\right)\right\}}{DEN}$$

$$ZRT = -n\frac{\left\{k\left(\frac{3-\nu}{2}\lambda^4+(2-\nu)\lambda^2n^2+\frac{1-\nu}{2}n^4\right)+\frac{1-\nu}{2}(\lambda^2-n^2)\right\}}{DEN}$$

$$ZRR = \frac{\left\{\frac{1-\nu}{2}(\lambda^2+n^2)^2\right\}}{DEN}$$

(3.34a-c)

This yields,

$$U_r = \frac{R^2}{kD}\sum_{n=0}^{\infty}\sum_{m=0}^{\infty} ZLRP_{r_{mn}}\cos(n\theta)\cos\left(\frac{m\pi\chi}{L}\right)$$

$$V_r = \frac{R^2}{kD}\sum_{n=1}^{\infty}\sum_{m=1}^{\infty} ZRTP_{r_{mn}}\sin(n\theta)\sin\left(\frac{m\pi\chi}{L}\right)$$

$$W_r = \frac{R^2}{kD}\sum_{n=1}^{\infty}\sum_{m=1}^{\infty} ZRRP_{r_{mn}}\cos(n\theta)\sin\left(\frac{m\pi\chi}{L}\right)$$

$$N_\chi = \frac{R}{k}\sum_{m=1}^{\infty}(-\lambda ZLR+\nu mZRT+\nu ZRR)P_{r_{mn}}\cos(n\theta)\sin\left(\frac{m\pi\chi}{L}\right)$$

$$N_\theta = \frac{R}{k}\sum_{m=1}^{\infty}(nZRT+ZRR-\nu\lambda ZRL)P_{r_{mn}}\cos(n\theta)\sin\left(\frac{m\pi\chi}{L}\right)$$

$$\overline{N}_{\chi\theta} = \frac{R(1-\nu)}{2k}\sum_{m=0}^{\infty}\sum_{n=0}^{\infty}(\lambda ZRT-nZRL)P_{r_{mn}}\sin(n\theta)\cos\left(\frac{m\pi\chi}{L}\right)$$

$$M_\chi = R^2\sum_{n=0}^{\infty}\sum_{m=1}^{\infty}\left\{(\lambda^2+\nu m^2)ZRR+\nu mZRT)\right\}P_{r_{mn}}\cos(n\theta)\sin\left(\frac{m\pi\chi}{L}\right)$$

$$M_\theta = R^2\sum_{n=0}^{\infty}\sum_{m=1}^{\infty}\left\{(n^2+\lambda^2)ZRR+nZRT)\right\}P_{r_{mn}}\cos(n\theta)\sin\left(\frac{m\pi\chi}{L}\right)$$

$$M_{\chi\theta} = R^2(1-\nu)\sum_{n=0}^{\infty}\sum_{m=1}^{\infty}\left\{n\lambda ZRR+\frac{3}{4}\lambda ZRT+\frac{1}{4}nZRL\right\}P_{r_{mn}}\sin(n\theta)\cos\left(\frac{m\pi\chi}{L}\right)$$

(3.35a-i)

3.3.5 Boundary Conditions

The representation of surface loading using the double Fourier series expansion as described implies certain boundary conditions (cf. Duthie,White & Tooth, Ref [9]).

Since the origin of the co-ordinate system is taken at one end of the cylinder, as shown in Figure 3.1a, all the Fourier expansions and their derivatives containing the term sin ($m\pi x/L$), vanish at the end of the cylinder, i.e.

$$\frac{\partial U}{\partial x} = 0, \quad V = \frac{\partial^2 V}{\partial x^2} = 0 \quad \text{and} \quad W = \frac{\partial^2 W}{\partial x^2} = 0 \quad \text{at} \quad x = 0 \;\&\; x = L$$

This implies that the cylinder is supported in the tangential and radial directions, and the shell is free to rotate about a tangent to the edge. These are exactly the boundary conditions prescribed for a hinged support, and are applicable if the shell under consideration is part of an infinitely long tube stiffened by rigid diaphragms at regular intervals of length L. The present treatment is specifically concerned with the behaviour of a cylinder subjected to loading remote from the ends. Although these boundary conditions do not precisely describe the condition for all end closure configurations, they are sufficiently close for most problems encountered in practice. In the present work, the effect of the end closure is considered in Chapter 8.

If the vessel ends conform to the above boundary conditions, then the Fourier series expansions form the complete solution of the problem, and no complementary solution needs to be added to the particular solution, since both the governing differential equations and the boundary conditions of the problem are satisfied. However, in practice some deviations from these conditions are likely to occur, yet it is still possible to use the solution with confidence if the loading is applied some distance from the vessel ends.

3.4 Simply Supported Cylindrical Shell

The solution of the simply supported cylindrical shell has been presented in the previous section in Equations (3.26-35). The only unknowns in these equations are the surface loading terms P_{xmn}, $P_{\theta mn}$ and P_{rmn}. These terms can be found by multiplying both sides of Equations (3.21) by suitable orthogonal expressions. Integrating over the surface of the cylinder eliminates all but one of the terms used in each Fourier expansion. The following orthogonal identities are used in this process:

$$\int_o^L \sin(mx)\sin(m'x)dx = 0 \qquad if\ m \neq m'$$

$$= \frac{L}{2} \qquad if\ m = m'\ or\ m = m' = 0$$

$$\int_o^L \sin(mx)\cos(m'x)dx = 0 \qquad for\ all\ values\ of\ m\ and\ m'$$

$$\int_o^L \sin(mx)\cos(m'x)dx = 0 \qquad if\ m \neq m'$$

$$= \frac{L}{2} \qquad if\ m = m'$$

$$= L \qquad if\ m = m' = 0$$

(3.36)

For the case of **longitudinal loading**, multiplying both side of expressions (3.21) by cos ($n'x$) cos ($m'\pi x/L$)$dxd\theta$, and integrating over the surface of the cylinder, making use of orthogonality properties, the longitudinal loading coefficients are obtained.

$$P_{\chi_{mn}} = \frac{1}{\pi L}\int_o^L \int_o^\pi P_\chi dxd\theta \qquad (m = n = 0)$$

$$= \frac{2}{\pi L}\int_o^L \int_o^\pi P_\chi \cos\left(\frac{m\pi\chi}{L}\right)dxd\theta \qquad (m = 0, n = 1,2,3,....)$$

$$= \frac{2}{\pi L}\int_o^L \int_o^\pi P_\chi \cos(n\theta)dxd\theta \qquad (n = 0, m = 1,2,3,....)$$

$$= \frac{4}{\pi L}\int_o^L \int_o^\pi P_\chi \cos(n\theta)\cos\left(\frac{m\pi\chi}{L}\right)dxd\theta \qquad (m,n = 1,2,3,....)$$

(3.37)

For the case of **tangential loading,** multiplying both sides of Equations (3.21) by cos($n'\theta$) sin ($m'\pi x/L$)$dxd\theta$ and integrating over the surface of the cylinder, the tangential loading coefficients are obtained:

$$P_{\theta_{mn}} = \frac{4}{L\pi}\int_o^L \int_o^\pi P_\theta \sin\left(\frac{m\pi\chi}{L}\right)\sin(n\theta)dxd\theta$$

(3.38)

Similarly, the **radial loading** coefficients are obtained by multiplying both sides of Equation (3.21) by cos ($n'\theta$) sin ($m'\pi x/L$)$dxd\theta$ and integrating:

$$P_{r_{mn}} = \frac{2}{L\pi}\int_o^L \int_o^\pi P_r \sin\left(\frac{m\pi\chi}{L}\right) dx d\theta \qquad (n = 0, m = 1,2,3....)$$

$$= \frac{4}{L\pi}\int_o^L \int_o^\pi P_r \cos(n\theta)\sin\left(\frac{m\pi\chi}{L}\right) dx d\theta \qquad (m, n = 1,2,3.....)$$

(3.39)

By obtaining the surface loading coefficients, the displacements and stress resultants for defined surface loading case, could be obtained using Equations (3.26-35).

The case of a liquid filled shell imparts a hydrostatic load as shown in Figure 3.2

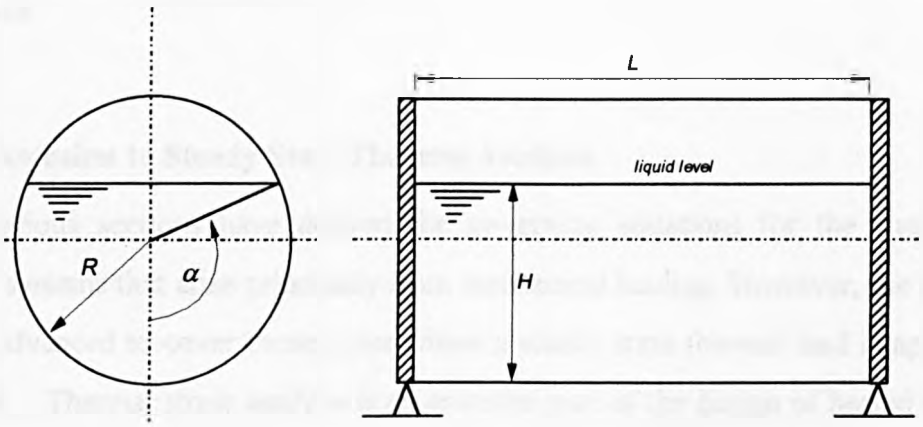

Figure 3.2 Simply supported cylindrical shell partially filled with liquid

The horizontal cylindrical shell is considered to be simply supported at both end and partially filled with a fluid of specific weight, ρ. The height of the fluid is shown by the angle, α, measured from the nadir which is taken as the base generator with ϕ=0. It is assumed that the fluid exects a radial pressure which is directly proportional to the depth at the point of consideration and that is remains constant along the shell length. The surface load on the cylindrical shell can thus be written as:

$$P_r = \rho R(\cos\theta - \cos\alpha) \qquad (-\alpha \le \theta \le \alpha)$$

(3.40)

The Fourier expansion coefficients for this case are obtained by substituting this expression into Equation 3.39 and integrating over the surface

$$P_{rmn} = \frac{4\rho R}{m\pi^2}(\sin\alpha - \alpha\cos\alpha) \qquad (n=0,\ m=1,3,5,\ldots)$$

$$= \frac{4\rho R}{m\pi^2}(2\alpha - \sin 2\alpha) \qquad (n=1,\ m=1,3,5,\ldots)$$

$$= \frac{8\rho R}{m\pi^2 n(n^2-1)}\{\sin(n\alpha)\cos\alpha - n\cos(n\alpha)\sin\alpha\} \qquad (n=2,4,6..,\ m=1,3,5,\ldots)$$

(3.41)

In a similar manner, the coefficients for the case of a cylinder subject to a uniform internal surcharge pressure, p, can be obtained as follows:

$$P_{rmn} = \frac{4p}{m\pi} \qquad (n=0,\ m=1,3,5\ldots)$$

(3.42)

3.5 Extension to Steady State Thermal Analysis

The previous sections have derived the governing equations for the shell under loading systems that arise principally from mechanical loading. However, the solution can be advanced to cover those cases where a steady state thermal load is applied to the shell. Thermal stress analysis is an essential part of the design of heated vessels, such as heat exchangers, hot oil storage containers and piping systems. These stresses arise from differential expansion or mechanical constraint of the system during overall temperature change. This can occur either by a thermal gradient through the vessel wall or by a variation of temperature over the vessel surface. The former is generally small in the case of thin walled vessels, however the latter can result in large magnitudes of stress when the thermal gradient is severe. Such conditions may arise from a design requirement of the process or alternatively from a fault condition when the liquid or gas flow is impeded and a local **'hot spot'** occurs.

In an earlier treatment of the **'hot spot'** problem by Wilson[62], the governing equations were effectively, apart from the temperature dependent terms, the Flügge shell equations. More recently, Bushnell[14] has shown that the Flügge equations have certain inconsistencies when resolving certain thermal stress problems. For this reason, the Sanders shell equations are employed throughout this thesis, since they avoid this problem.

3.5.1 Modified Governing Equations

The main modifications to the general shell equations arise from additional temperature terms which cause a rise in the overall stress. From Equations (3.17), the constitutive relations representing axial, circumferential and shear stress at a general point Z from the middle surface, with temperature term can be written,

$$N_\chi = D(\varepsilon_\chi + \nu\varepsilon_\theta) - Et\alpha\frac{T}{(1-\nu)} \qquad M_\chi = \frac{Dt^2}{12}(K_\chi + \nu K_\theta)$$

$$N_\theta = D(\varepsilon_\theta + \nu\varepsilon_\chi) - Et\alpha\frac{T}{1-\nu} \qquad M_\theta = \frac{Dt^2}{12}(K_\theta + \nu K_\chi)$$

(3.43)

These expressions are carried through the analysis in a similar manner to Equations (3.18-3.20); the only major change is the inclusion of the temperature terms in the direct stress resultant expressions.

$$N_\chi = D\left(\frac{\partial U}{\partial\chi} + \frac{\nu}{R}\frac{\partial V}{\partial\theta} + \frac{\nu W}{R}\right) - Et\alpha\frac{T}{(1-\nu)}$$

$$N_\theta = D\left(\frac{1}{R}\frac{\partial V}{\partial\theta} + \frac{\partial U}{\partial\chi} + \frac{W}{R}\right) - Et\alpha\frac{T}{(1-\nu)}$$

$$M_\chi = DkR^2\left(-\frac{\partial^2 W}{\partial\chi^2} - \frac{\nu}{R^2}\frac{\partial^2 W}{\partial\theta^2} + \frac{\nu}{R^2}\frac{\partial^2 W}{\partial\theta}\right)$$

$$M_\theta = DkR^2\left(-\frac{1}{R^2}\frac{\partial^2 W}{\partial\theta^2} + \frac{1}{R^2}\frac{\partial V}{\partial\theta} - \nu\frac{\partial^2 W}{\partial\chi^2}\right)$$

(3.44)

This leads to the general equilibrium relations expressed in matrix form as shown in Equation (3.20).

3.5.2 Fourier Expansion Solution

A particular solution of these equations may be obtained by expressing the displacements and loading in the form of Equations (3.22). The temperature loading is also included,

$$U = \sum_{m=0}^{\infty}\sum_{n=0}^{\infty} U_{mn}\cos(n\theta)\cos\left(\frac{m\pi\chi}{L}\right)$$

$$V = \sum_{m=1}^{\infty}\sum_{n=1}^{\infty} V_{mn}\sin(n\theta)\sin\left(\frac{m\pi\chi}{L}\right)$$

$$W = \sum_{m=1}^{\infty}\sum_{n=0}^{\infty} W_{mn}\cos(n\theta)\sin\left(\frac{m\pi\chi}{L}\right)$$

$$T = \sum_{m=1}^{\infty}\sum_{n=0}^{\infty} T_{mn}\cos(n\theta)\sin\left(\frac{m\pi\chi}{L}\right)$$

(3.45a-d)

The choice of this expansion for the temperature indicates that the loading is symmetric with respect to the generator passing though ϕ =0. They also imply that the end constraints have zero temperature at x=0 and L, although the approach can handle cases when the entire vessel is subject to thermal load. A detailed description of the boundary conditions required by the above equations is given by Duthie and Tooth[44].

When the series expansions are substituted into the matrix equation above, a similar matrix Equation (3.24) is obtained, the only difference being the load coefficients,

$$d_1 = a^2(1+\nu)\frac{\alpha m\pi}{L}T_{(n,m)}$$

$$d_2 = -a(1+\nu)\alpha n T_{(n,m)}$$

$$d_3 = -a(1+\nu)\alpha T_{(n,m)}$$

(3.46a-c)

This allows the matrix equation to be solved as Equations (3.25). The displacements are found initially and then the required stress resultants can be obtained.

3.5.3 Fourier Series Representations of Applied Loading

The only unknowns are therefore the loading terms $T_{(n,m)}$. These terms are found by expressing the loading system in double Fourier series form as detailed in Section 3.4. the form of the equation is similar to that for the radial load and therefore by a similar procedure, the loading term can be written for all values of ***m*** and ***n*** as,

$$T_{mn} = \frac{2}{L\pi}\int_o^L \int_o^\pi T \sin\left(\frac{m\pi\chi}{L}\right) dx d\theta \qquad (n = 0, m = 1,2,3.....)$$

$$= \frac{4}{L\pi}\int_o^L \int_o^\pi T \cos(n\theta)\sin\left(\frac{m\pi\chi}{L}\right) dx d\theta \qquad (m, n = 1,2,3.....)$$

(3.47)

These expressions can be utilised once an equation or relationship has been chosen to fully describe the thermal loading term, T. Substitution into the above and applying an integration allows the stress resultant equations to be solved to give the mid-surface displacements and stress resultants. This approach is of particular value in dealing with thermal loadings distributed over discrete areas and can deal with uniformly and non-uniformly distributed loading as shown by Panayotti[83,84]

3.6 Notes on the Fourier Series

The Fourier series expansion technique has many advantages making it attractive to be used for the solution of differential equations. One of its merits is that any function can be expressed in sine and cosine terms, which make it easy to be differentiated and manipulated.

The main drawback lies in the fact that it is an infinite series and in order to establish the **exact value** of the represented function, an **infinite** or large number of terms requires to be summated. However, recent advances in computer facilities have made this problem of less importance, since the large number of Fourier series terms can be considered in a relatively short computing time. In practice, most engineering applications allow for an approximate solution to be acceptable. One further point is that the Fourier series expansion approach is more easily ported to a computing platform than alternative solutions, which may involve the use of complex numerical routines.

3.6.1 Fourier Series Limit and Rate of Convergence

As stated previously an approximate value of a function, represented by a single Fourier series is obtained by summing up a number of terms of the series. The more

terms considered, the closer the value obtained is to exact solution. For simple functions, the so called **Fourier Integrals** can be used as a limit of a series to give the value of that function at all points. Fourier integrals are obtained using **sine or cosine integrals,** which are tabulated in numerous handbooks. This is normally true when the function is simple, but in most engineering applications this may not be the case. It is thus necessary to rely on the **rate of convergence** of the series. One of the properties of the Fourier series is that the contribution of high order terms to the solution is less than that of lower order terms. The rate of convergence of a series is the rate at which its coefficients approach zero. The convergence of the series depends on several factors, such as the continuity of the function, the number of terms selected in the series, the rate of change of the function (rapidly changing functions are slower to converge), and the period of the function (short period functions converge faster than functions with long periods).

The displacement and stress functions of a cylindrical vessel, which have been derived earlier in this chapter, are complicated functions. They comprise double Fourier expansions and contain many parameters, which ultimately makes it difficult to judge the number of terms required in achieving a sufficiently accurate result. Users of such solutions should always ensure convergence by performing successive runs and comparing the rates of convergence for the required target quantity (stress, displacement result etc.) With modern computers, double Fourier series solutions with between 200 - 1000 terms in each series can be computed in a reasonable time.

4 ANALYSIS OF LOCAL LOADS ON CYLINDRICAL SHELLS

4.1 Introduction

During the life of the pressure vessel it is often subjected to a wide variety of loading conditions, all of which must be considered during design. In many instances the internal pressure is not the dominant form of loading and special attention has to be given to other load cases which combined together could cause premature failure of the vessel.

The local loading of supports and lifting brackets, which are welded to the vessel, is such a case and although the resulting stresses are generally not excessive, checks must be made to establish their value. When a radial force or a bending moment is applied to the attachment, the interface forces between the attachment and the vessel are, as in the twin saddle problem, rather complicated. Their distribution depends upon the relative rigidities of the vessel and the attachment. For example, if the attachment is very rigid compared with the vessel, one would expect the interface forces to be concentrated round the outer edges of the attachment. A further complication for the welded attachment is that it is only fixed to the vessel round its outer edges.

As mentioned earlier in Chapter 2.3, neither the British Standard 5500 nor the Welding Research Council Bulletin 107 attempt to handle these and other intractable modelling problems, but when the contact area is relatively small, they assume a simplified form for the interface force distribution between the vessel and attachment. For example, when a radial load is applied, the assumption is that the interface loading is uniformly distributed. A further simplification is that the attachments are rectangular or square with boundaries that coincide with the parallel circle profile, associated with the coordinate and the axial generator x, as shown in Figure 4.1.

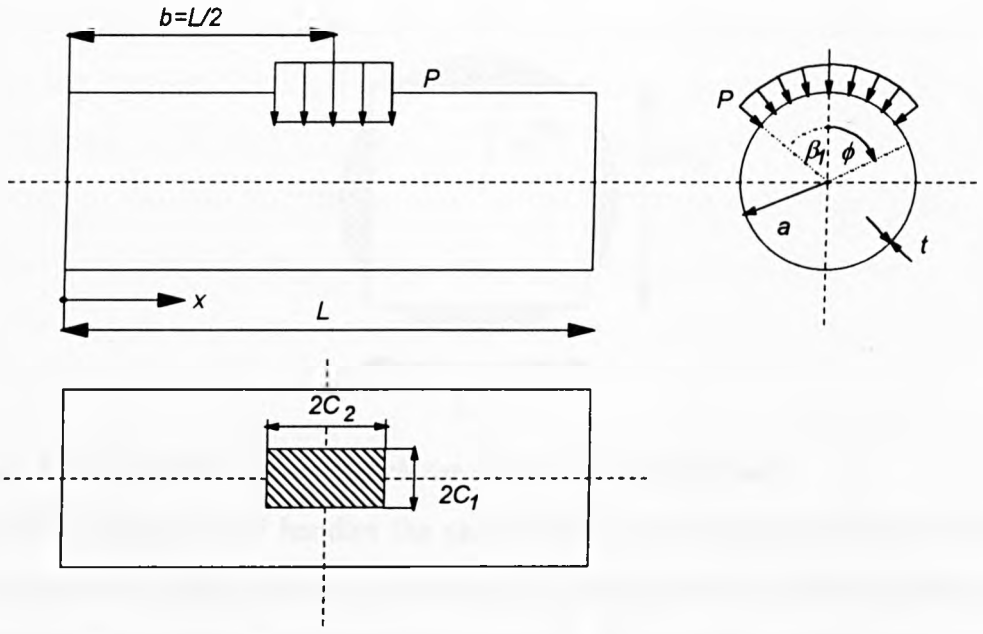

Figure 4.1 Radial loading on a rectangular patch

This enables the applied load to be expressed as a double Fourier series form by

$$P_r = \sum_{m=1}^{\infty} \sum_{n=0}^{\infty} P_{r_{mn}} \cos(n\theta) \sin\left(\frac{m\pi x}{L}\right)$$

Forms of this type, (Equations 3.21 and 3.22), can be used in the shell equations to derive the vessel displacements and stress resultants.

In the absence of a more precise analytical method, the local loading of nozzles in cylindrical vessels can be analysed by assuming the nozzle behaves like a cylindrical attachment. This can be handled, as in the early versions of WRC Bulletin 107 by assuming that the circular patch is equivalent to a square patch of side lengths equal to 1.75 r_o. This provides a square patch with a notional area marginally smaller (2.5%) than that of the circular attachment. A similar approach is given in BS 5500 where a slightly smaller area is assumed by using a value of 1.70 r_o for the equivalent square patch as shown in Figure 4.2. More recently, a supplement to WRC Bulletin 107, WRC Bulletin 297, has been provided, which enables more adequate modelling of the nozzle and vessel to be achieved. In this, the nozzle wall thickness can be included in the derivation of the local load stresses.

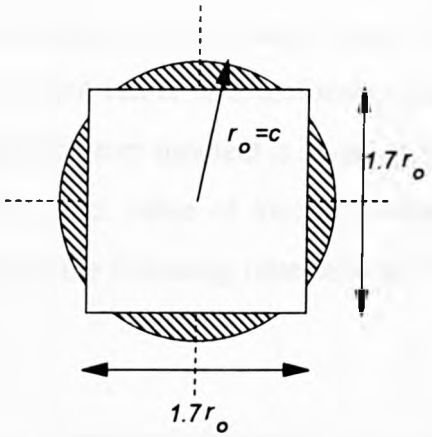

Figure 4.2 Equivalent square patch for circular loaded regions

While WRC Bulletin 297 handles the case of the nozzle subject to local loads, the requirement still exists to obtain a more rigorous analysis for the circular patch, which avoids the **'equivalent square patch'** approach. The solution given in this chapter address these problems and provide an analysis which can handle both mechanical and thermal loading. It can be programmed for a micro computer in a manner described earlier by the present author[45]. As in the earlier studies the assumption that the interface loading is uniform, for the radial load case, is retained.

The solution for the rectangular patch subject to radial, tangential and longitudinal shear loads has been previously described. However, the case of moment loading, in both the tangential and longitudinal directions requires to be addressed. Therefore, in order to encompass the full variation of loading conditions, the solutions for both moment loads and a thermal load case are derived.

The extension to the circular and elliptical patch is also developed. Again, the patch is subjected to radial direct load, to both the tangential and longitudinal moment loads and also to the thermal patch load case.

4.2 Loading Intensity Representation

In pressure vessel and piping system analysis, the vessel engineer is given the applied loading as forces and moments resulting from a piping system analysis. The shell must be capable of withstanding these loads in order to maintain the integrity of the vessel.

However, in the present analysis described herein, each loaded area is subject not to forces and moments directly but rather to a uniform or triangularly varying pressure, this depending on whether a force or moment is being applied.

In order to represent the correct value of loading pressure intensity acting on the relevant patch size and shape, the following relationships were obtained.

Radial Load *P*

For a radial force of value P acting on a patch area, the uniform loading intensity p is given by:

$$p = \frac{P}{area}$$

where, for a rectangular patch of dimensions $2c_1$ and $2c_2$, the area is Area$=4c_1c_2$ and, for an elliptical patch with major and minor axes of dimensions $2a_o$ and $2b_o$, the area is Area $=\pi a_o b_o$

A circular patch is a special case of the elliptical patch with radius $c=a_o=b_o$. Hence, for a radial load on a circular patch the area is given by, Area $=\pi c^2$.

External Moment *M* on a Rectangular Patch

The loading intensity for an external moment M acting on a rectangular patch can be found by considering an element of the rectangular patch subject to a load intensity p_y at a distance y from the x-x axis as shown below (Figure 4.3). The radial load dP acting on the elemental strip at this distance is given by:

$$dP = p_y(2c_2 dy)$$

From the geometry of the figure, p_y could be expressed in terms of maximum loading p as:

$$p_y = p\frac{y}{c_1}$$

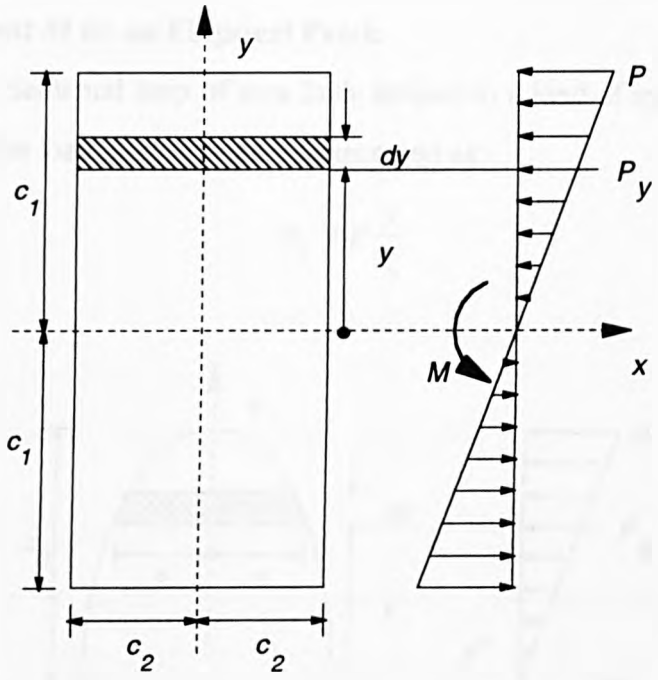

Figure 4.3 External moment on a rectangular patch

The moment *dM* acting on the elemental area about the x-x axis is:

$$dM = dP \times y$$

$$= p\frac{y}{c_1}(2c_2 dy)y$$

And therefore, for the whole rectangular area,

$$M = \frac{2pc_2}{c_1}\int_{-c_1}^{c_1} y^2 dy$$

$$= \frac{4}{3}pc_1^2 c_2$$

or

$$p = \frac{3M}{c_1 \times \text{Area}}$$

where,

$$\text{Area} = 4c_1 c_2$$

External Moment *M* on an Elliptical Patch

Considering the elemental strip of area $2xdy$ subject to a load of intensity p_y as shown in Figure (4.4), the load intensity can be expressed as:

$$p_y = p\frac{y}{a_o}$$

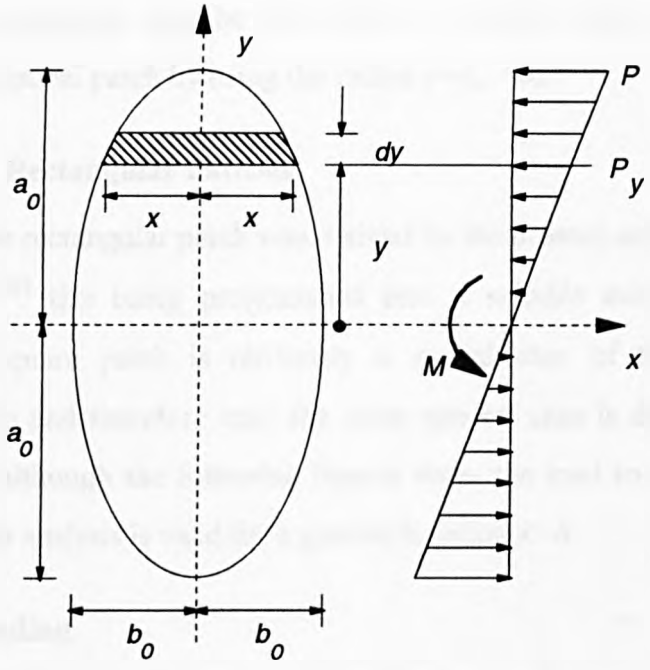

Figure 4.4 External moment on an elliptical patch

By a similar procedure as shown previously for the rectangular case, the total moment for the whole elliptical area is given by:

$$M = \frac{2p}{a_o}\int_{-a_o}^{a_o} xy^2 dy$$

The general elliptical equation, $(x/b_o)^2 + (y/a_o)^2 = 1$ can be rewritten in terms of x as:

$$x = b_o\sqrt{1-\left(\frac{y}{a_o}\right)^2}$$

The total moment then becomes,

$$M = \frac{2pb_o}{a_o}\int_{-a_o}^{a_o} y^2\sqrt{1-\left(\frac{y}{a_o}\right)^2}\,dy$$

By substituting $y = a_o \sin\theta$ and $dy = a_o \cos\theta$ and integrating yields,

$$p = \frac{4M}{a_o \times \text{Area}} \quad \text{for a circumferential moment and}$$

$$= \frac{4M}{b_o \times \text{Area}} \quad \text{for a longitudinal moment}$$

where

$$\text{Area} = \pi a_o b_o$$

Similar explicit expressions may be derived for a circular patch using the above relations for the elliptical patch by using the radius $c=a_o=b_o$.

4.3 Square and Rectangular Patches

The solution for the rectangular patch was derived by the present author as part of his Master's thesis [56,45] this being programmed into a suitable microcomputer. The solution for the square patch is obviously a special case of the more general rectangular solution and therefore only the more general case is detailed here. It is worth noting that although the following figures show the load to be located at the vessel midpoint, the analysis is valid for a general location $x=b$.

4.3.1 Radial Loading

On considering a uniformly distributed radial loading of value, ***P***, acting on a rectangular patch located symmetrically about the generator $\phi = 0$, and at a distance ***b*** from one end of the vessel, then the radial load can be described as,

$$P_r = \begin{cases} p \text{ in the region } -\beta_1 \le \phi \le \beta_1 \text{ and } (b-c_2) \le x \le (b+c_2) \\ 0 \qquad\qquad\qquad\qquad\qquad\qquad \text{otherwise} \end{cases} \tag{4.1}$$

where $\beta_1=c_1/a$. Using Equations 3.39 and noting the new integration limits $(b\text{-}c_2)$ to $(b+c_2)$ and 0 to β_1, the loading expressions can be stated as follows:

$$P_{r_{mn}} = \frac{2}{L\pi}\int_{b-c_2}^{b+c_2}\int_0^{\beta_1} P_r \sin\left(\frac{m\pi x}{L}\right) dx d\theta$$

$$= \frac{4p\beta_1}{m\pi^2}\sin\frac{m\pi b}{L}\sin\frac{m\pi c_2}{L} \quad (n=0,\ m=1,2,3,.....)$$

$$= \frac{4}{L\pi}\int_{b-c_2}^{b+c_2}\int_0^{\beta_1} P_r \cos(n\theta)\sin\left(\frac{m\pi x}{L}\right)dxd\theta$$

$$= \frac{8p}{mn\pi^2}\sin\frac{m\pi b}{L}\sin\frac{m\pi c_2}{L}\sin(n\beta_1) \qquad (m,n=1,2,3,.....)$$

(4.2*a*,*b*)

When $c_1=c_2$ then the rectangular patch solution becomes that of the square patch.

4.3.2 Moment Loading

Two cases are envisaged, namely longitudinal and circumferential moment loading. The loads are assumed to be idealised as radial loading of a triangular pressure distribution.

For the **'longitudinal moment'** on a rectangular patch, consider a moment, ***M***, uniformly distributed along a short length in the circumferential direction acting on the rectangular patch.

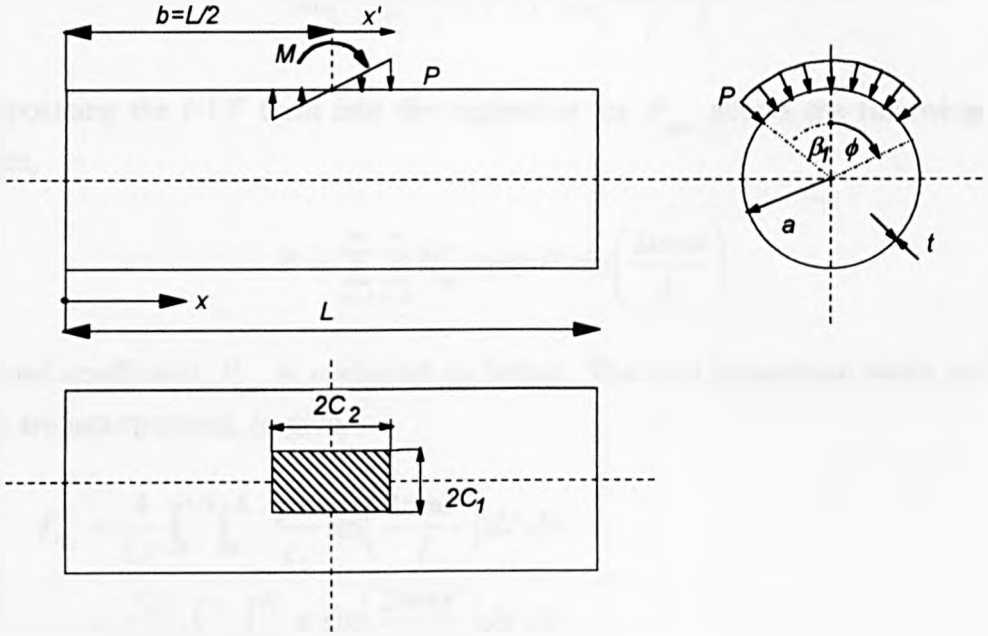

Figure 4.5 Longitudinal moment on a rectangular Patch

The external moment is applied by radial loads proportional to the distance from $x=b=L/2$, represented by:

$$P_r = \begin{cases} \dfrac{px'}{c_2} & \text{in the region } -\beta_1 \le \phi \le \beta_1 \text{ and } -c_2 \le x' \le c_2 \\ 0 & \text{otherwise} \end{cases}$$

(4.3)

where $x'=x-L/2$; $\beta_1=c_1/a$ and p is the maximum load intensity of the radial loads. The radial load may be represented as an odd function of x' with period $L=2b$. Hence,

$$P_r = \sum_{m=1}^{\infty}\sum_{n=0}^{\infty} P_{r_{mn}} \cos(n\theta)\sin\left(\frac{2m\pi x'}{L}\right)$$

Expanding the last term of the above equation, substituting $x'=x-L/2$ gives,

$$\sin\left(\frac{2m\pi x'}{L}\right) = (-1)^m \sin\left(\frac{2m\pi x}{L}\right)$$

Incorporating the $(-1)^m$ term into the expansion for $P_{r_{mn}}$ allows the following to be written,

$$P_r = \sum_{m=1}^{\infty}\sum_{n=0}^{\infty} P_{r_{mn}} \cos(n\theta)\sin\left(\frac{2m\pi x}{L}\right)$$

The load coefficient $P_{r_{mn}}$ is evaluated as before. The new integration limits and load terms are incorporated, to give,

$$\begin{aligned} P_{r_{mn}} &= \frac{4}{L\pi}\int_0^{L/2}\int_0^{\beta_1} \frac{px'}{c_2}\sin\left(\frac{2m\pi x'}{L}\right)dx'\,d\theta \\ &= \frac{4p}{L\pi c_2}\int_0^{c_2}\int_0^{\beta_1} x'\sin\left(\frac{2m\pi x'}{L}\right)dx'\,d\theta \\ &= \frac{pL\beta_1}{m^2\pi^3 nc_2}(-1)^m\left(\sin\left(\frac{2m\pi c_2}{L}\right) - \frac{2m\pi c_2}{L}\cos\left(\frac{2m\pi c_2}{L}\right)\right) \quad (n=0, m=1,2,3,.....) \\ &= \frac{8}{L\pi}\int_{c_2}^{c}\int_0^{\beta_1} \frac{px'}{c_2}\cos(n\theta)\sin\left(\frac{2m\pi x'}{L}\right)dx'\,d\theta \\ &= \frac{2pL}{m^2\pi^3 nc_2}(-1)^m\left(\sin\left(\frac{2m\pi c_2}{L}\right) - \frac{2m\pi c_2}{L}\cos\left(\frac{2m\pi c_2}{L}\right)\right)\sin(n\beta_1)\ (m,n=1,2,3,.....) \end{aligned}$$

(4.4*a,b*)

For the **'circumferential moment'** on a rectangular patch, consider a moment, M, uniformly distributed along a short length in the longitudinal direction acting on the rectangular patch. The external moment is applied by radial loads of maximum intensity p which do not vary with x represented by:

$$P_r = \begin{cases} \dfrac{p\phi}{\beta_1} & \text{in the region } -\beta_1 \le \phi \le \beta_1 \text{ and } (b-c_2) \le x \le (b+c_2) \\ 0 & \text{otherwise} \end{cases}$$

where $\beta_1 = c_1/a$.

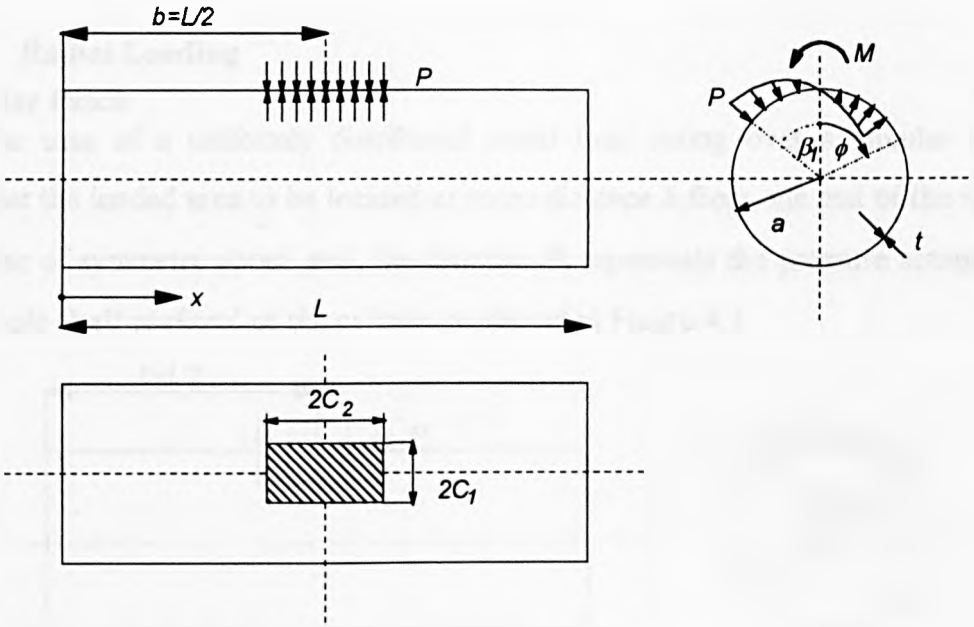

Figure 4.6 Circumferential moment on a rectangular patch

The loading can be expressed by the following Fourier expansion,

$$P_r = \sum_{m=1}^{\infty}\sum_{n=0}^{\infty} P_{r_{mn}} \sin(n\phi)\sin\left(\frac{m\pi x}{L}\right)$$

This expression is similar to equation 3.39 and by introducing the loading and limits, we find,

$$P_{r_{mn}} = \frac{4}{L\pi}\int_{b-c_2}^{b+c_2}\int_{0}^{\beta_1} \frac{p\phi}{\beta_1}\sin(n\phi)\sin\left(\frac{m\pi x}{L}\right)dx\,d\phi$$

$$= \frac{8p}{mn^2\pi^2\beta_1} \sin\frac{m\pi b}{L}(\sin(n\beta_1) - \beta_1\cos(n\beta_1))\sin\left(\frac{m\pi c_2}{L}\right) \quad (m,n = 1,2,3.....) \tag{4.6}$$

4.4 Circular and Elliptical Patches

Circular and elliptical patches represent the contact area of a number of local loading connections. For example, when vessel legs are attached to the cylindrical shell, they are often located at some angle to the surface normal, thus defining an elliptical contact area. In addition, the true circular and elliptical patch solution can be used in place of the approximate equivalent square or rectangle approach suggested by the codes and standards.

In the present work, the solutions for circular and elliptical patches subject to radial loads and longitudinal and circumferential moments are outlined.

4.4.1 Radial Loading

Circular Patch

For the case of a uniformly distributed radial load acting over a circular patch, consider the loaded area to be located at some distance *b* from one end of the vessel. Because of symmetry about ϕ=0, the function P_r represents the pressure acting over the whole '**half surface**' of the cylinder as shown in Figure 4.7

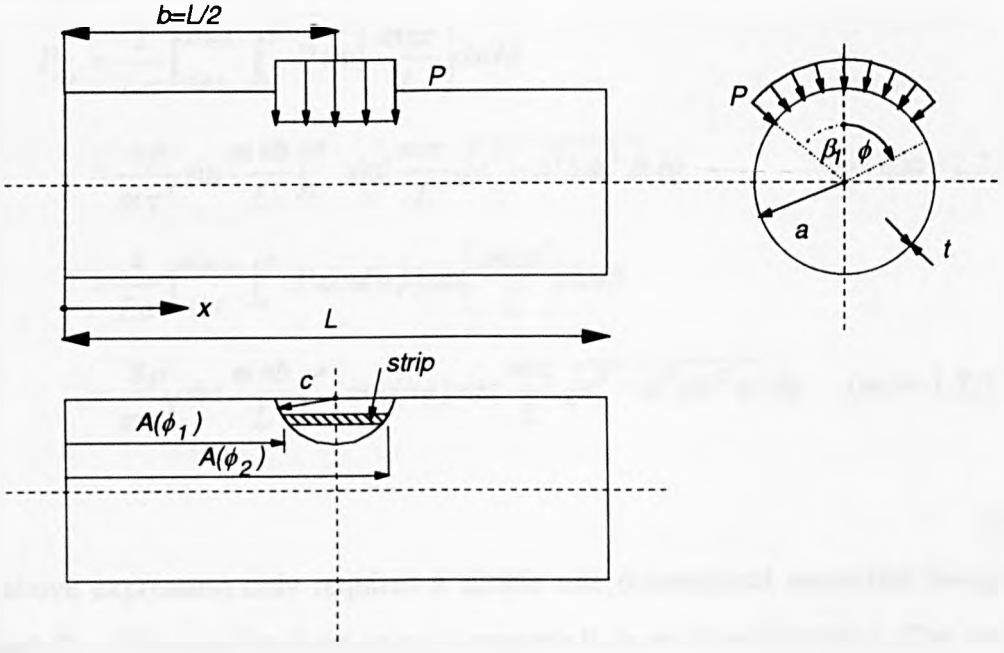

Figure 4.7 Radial load acting on circular patch

Outside the boundary, the loading is zero ie. $P_r = 0$; inside the boundary, however the load intensity $P_r = P$.

The boundary is the variation of x with ϕ acting around the loaded area perimeter as is defined by:

$$P_r = \begin{cases} p \text{ in the region } -\beta \le \phi \le \beta \text{ and } (b-c) \le x \le (b+c) \\ 0 \qquad\qquad\qquad\qquad\qquad\qquad \text{otherwise} \end{cases}$$

(4.7)

and

$$A(\phi_1) = b - \sqrt{c^2 - a^2 \sin^2 \phi}$$

$$A(\phi_2) = b + \sqrt{c^2 - a^2 \sin^2 \phi}$$

(4.8*a,b*)

where: $0 \le \phi \le \beta$

The loaded area is divided into a number of axial strips, the length of which are obtained from $A(\phi_1)$ and $A(\phi_2)$ as shown in Figure 4.7. Therefore, substituting these limits into Equation (4.7), yields,

$$P_{r_{mn}} = \frac{2}{L\pi} \int_{A(\phi_1)}^{A(\phi_2)} \int_0^{\beta} P \sin\left(\frac{m\pi x}{L}\right) dx d\phi$$

$$= \frac{4p}{m\pi^2} \sin\frac{m\pi b}{L} \int_0^{\beta} \sin\left(\frac{m\pi}{L}\sqrt{c^2 - a^2 \sin^2 \phi}\, d\phi\right) \qquad (n=0, m=1,2,3,.....)$$

$$= \frac{4}{L\pi} \int_{A(\phi_1)}^{A(\phi_2)} \int_0^{\beta} P \cos(n\phi) \sin\left(\frac{m\pi x}{L}\right) dx d\phi$$

$$= \frac{8p}{m\pi^2} \sin\frac{m\pi b}{L} \int_0^{\beta} \cos(n\phi) \sin\left(\frac{m\pi}{L}\sqrt{c^2 - a^2 \sin^2 \phi}\; d\phi\right) \qquad (m,n=1,2,3,.....)$$

(4.9*a,b*)

The above expression only requires a simple one dimensional numerical integration for each $P_{n,m}$. This may be done using Simpson's Rule or Filon's Method. The example detailed later is based on the former method which, for the illustrated case, was both

easier to use and as accurate as Filon's Method. In order to reduce the integration time, especially with regard to mounting the routine onto microcomputers, the half angle β can be assumed small so that $sin\phi=\phi$.

Elliptical Patch

The analysis of the **elliptical patch** is used for the cases of oblique nozzles and elliptical patches. The method derived above for the circular patch is extended to derive the loading terms for a radial load acting on an elliptical patch by redefining Equations (4.8a,b) and integrating.

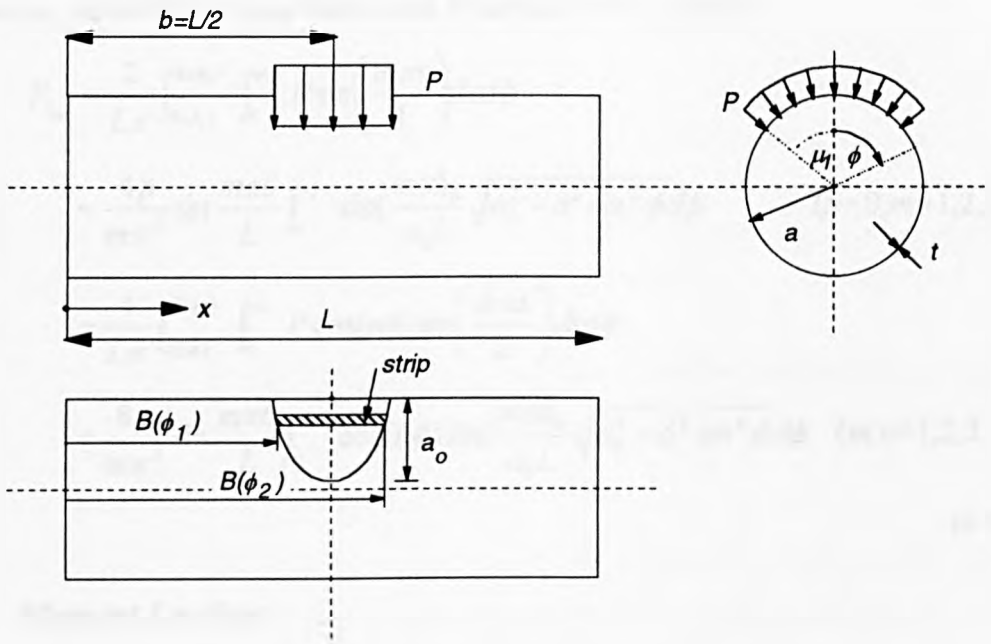

Figure 4.8 Radial Load acting on an Elliptical Patch

By considering a uniformly distributed radial load of intensity p, acting on an elliptical patch located symmetrically about the generator ϕ=0, and at a distance b from one end of the vessel, then,

$$P_r = \begin{cases} p \text{ in the region } -\mu_1 \le \phi \le \mu_1 \text{ and } (b-b_0) \le x \le (b+b_0) \\ 0 \qquad\qquad\qquad\qquad\qquad\qquad \text{otherwise} \end{cases} \tag{4.10}$$

where $\mu_1 = a_0/a$.

The boundary is the variation of x with ϕ acting around the loaded area perimeter as is defined by:

$$B(\phi_1) = b - \frac{b_0}{a_0}\sqrt{a_0^2 - a^2\sin^2\phi}$$

$$B(\phi_2) = b + \frac{b_0}{a_0}\sqrt{a_0^2 - a^2\sin^2\phi} \qquad \textbf{(4.11}a,b\textbf{)}$$

where: $0 \le \phi \le \mu_1$

As in the case of the circular patch, the loaded area is divided into a number of axial strips, the length of which are obtained from $B(\phi_1)$ and $B(\phi_2)$ as shown in Figure 4.8. Therefore, substituting these limits into Equation (4.11), yields,

$$P_{r_{mn}} = \frac{2}{L\pi}\int_{B(\phi_1)}^{B(\phi_2)}\int_0^{\mu_1} P\sin\left(\frac{m\pi x}{L}\right)dx\,d\phi$$

$$= \frac{4p}{m\pi^2}\sin\frac{m\pi b}{L}\int_0^{\mu_1}\sin\left(\frac{m\pi b_0}{a_0 L}\sqrt{a_0^2 - a^2\sin^2\phi}\,d\phi\right) \qquad (n=0, m=1,2,3,.....)$$

$$= \frac{4}{L\pi}\int_{B(\phi_1)}^{B(\phi_2)}\int_0^{\mu_1} P\cos(n\phi)\sin\left(\frac{m\pi x}{L}\right)dx\,d\phi$$

$$= \frac{8p}{m\pi^2}\sin\frac{m\pi b}{L}\int_0^{\mu_1}\cos(n\phi)\sin\left(\frac{m\pi b_0}{a_0 L}\sqrt{a_0^2 - a^2\sin^2\phi}\,d\phi\right) \quad (m,n=1,2,3,.....)$$

(4.12*a,b*)

4.4.2 Moment Loading

As stated previously for the rectangular patch, there are two loading cases that require analysis, namely longitudinal and circumferential moment loading.

The moment loading cases have been derived for a rectangular patch earlier and the moment loading is assumed to be equivalent to a radial loading with a triangular pressure distribution. This assumption assumes that the attachment has the same degree of flexibility, as the vessel.

Circumferential Moment - Circular Area

For the case of '**circumferential moment**' loading ***M***, uniformly distributed along a short distance in the longitudinal direction, acting over a **circular area**, the loading

can be represented by a triangularly distributed radial load of maximum intensity p. For this case the loading can be expressed using the following expression.

$$P_r = \begin{cases} \dfrac{p\phi}{\beta} & \text{in the region } -\beta_1 \le \phi \le \beta_1 \text{ and } (b-c_2) \le x \le (b+c_2) \\ 0 & \text{otherwise} \end{cases} \tag{4.13}$$

where $\beta_1 = c/a$.

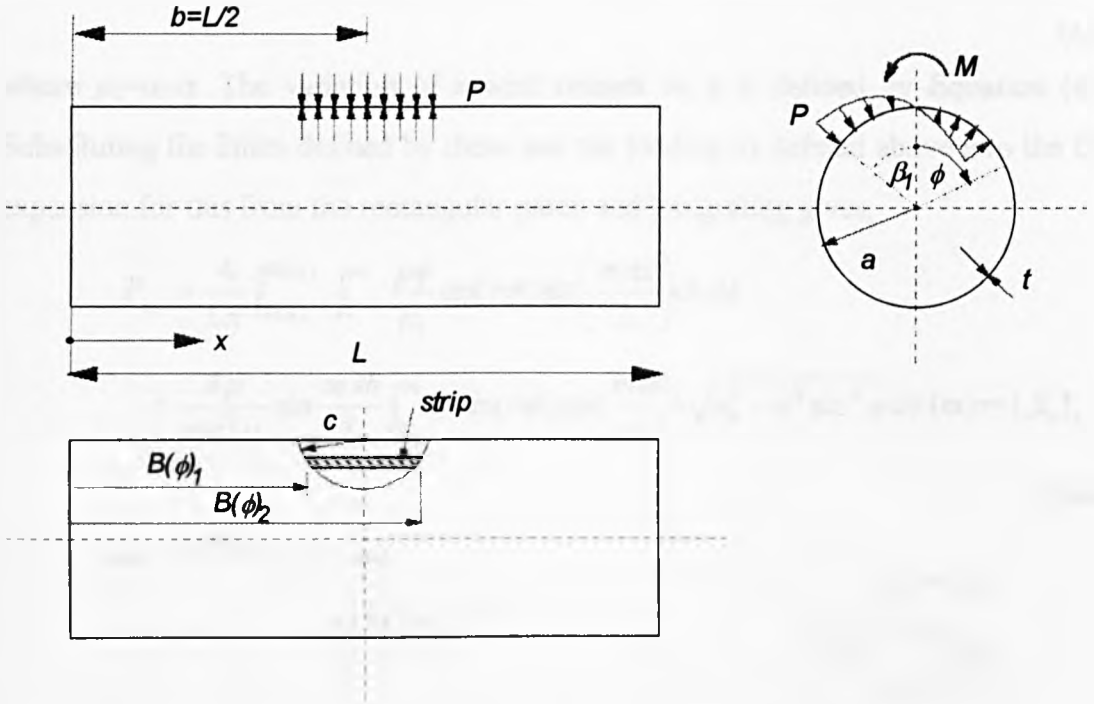

Figure 4.9 Circumferential moment load acting on a circular patch

The variation of x with respect to ϕ is defined by Equation (4.7). Substituting the limits defined by these and the loading as defined above into Equation (4.9) (the first expansion for this from the rectangular patch) and integrating gives,

$$P_{r_{mn}} = \frac{4}{L\pi}\int_{B(\phi_1)}^{B(\phi_2)} \int_0^{\beta} \frac{p\phi}{\beta_1}\sin(n\phi)\sin\left(\frac{m\pi x}{L}\right)dx\,d\phi$$

$$= \frac{8p}{m\pi^2\beta_1}\sin\frac{m\pi b}{L}\int_0^{\beta} \phi\sin(n\phi)\sin\left(\frac{m\pi}{L}\sqrt{c^2 - a^2\sin^2\phi}\right)d\phi \quad (m,n=1,2,3,.....) \tag{4.14a,b}$$

Circumferential Moment - Elliptical Area

For the **elliptical patch**, subjected to the same **circumferential moment** loading, using the same assumptions as for the circular patch, the loading term can be expressed as:

$$P_r = \begin{cases} \dfrac{p\phi}{\mu_1} & \text{in the region } -\mu_1 \le \phi \le \mu_1 \text{ and } (b-b_0) \le x \le (b+b_0) \\ 0 & \text{otherwise} \end{cases}$$

(4.15)

where $\mu_1=a_0/a$. The variation of x with respect to ϕ is defined by Equation (4.9) Substituting the limits defined by these and the loading as defined above into the first expansion for this from the rectangular patch and integrating gives,

$$P_{r_{mn}} = \frac{4}{L\pi}\int_{B(\phi_1)}^{B(\phi_2)}\int_0^{\mu_1} \frac{p\phi}{\mu_1}\sin(n\phi)\sin\left(\frac{m\pi x}{L}\right)dxd\phi$$

$$= \frac{8p}{m\pi^2\mu_1}\sin\frac{m\pi b}{L}\int_0^{\mu_1} \phi\sin(n\phi)\sin\left(\frac{m\pi b_0}{a_0 L}\sqrt{a_0^2 - a^2\sin^2\phi}\right)d\phi \quad (m,n=1,2,3,.....)$$

(4.16*a*,*b*)

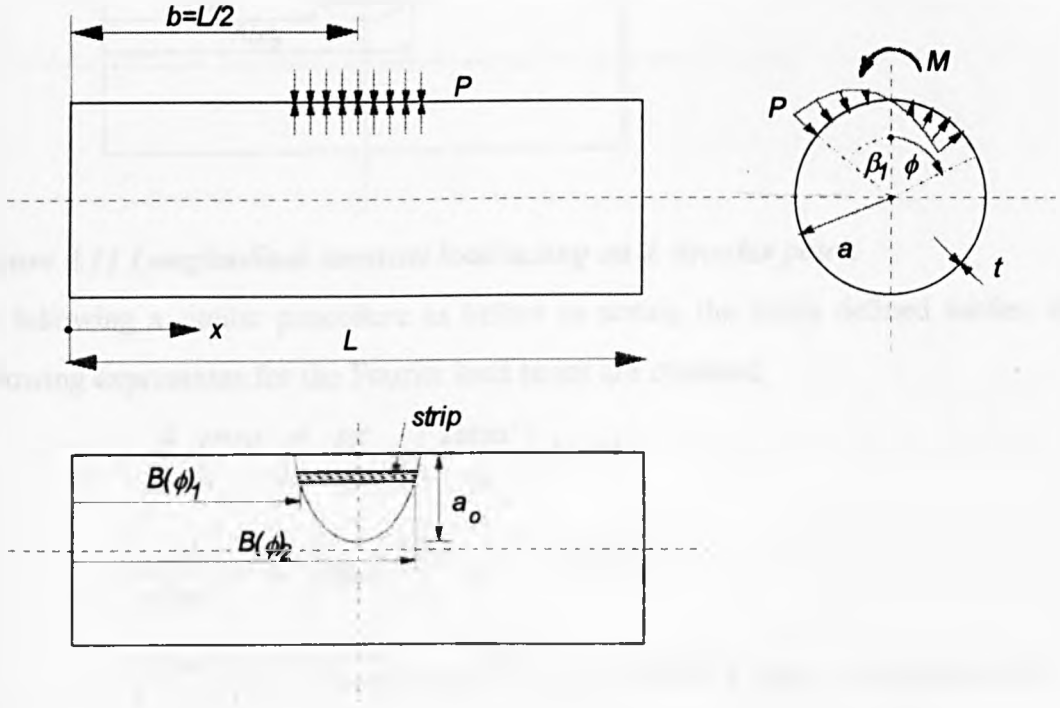

Figure 4.10 Circumferential moment load acting on an elliptical patch

Longitudinal Moment - Circular Area

For the case of **'longitudinal moment'** loading M, uniformly distributed along a short distance in the longitudinal direction, acting over a **circular area**, the loading can be represented by a triangularly distributed radial load of maximum intensity p. For this case the loading can be expressed using the following expression.

$$P_r = \begin{cases} \dfrac{px'}{c} \text{ in the region } -\beta \le \phi \le \beta \text{ and } -c \le x' \le c \\ 0 \qquad\qquad\qquad\qquad \text{otherwise} \end{cases} \tag{4.17}$$

where $x'=x=L/2$; $\beta_1=c/a$ and p is the maximum load intensity.

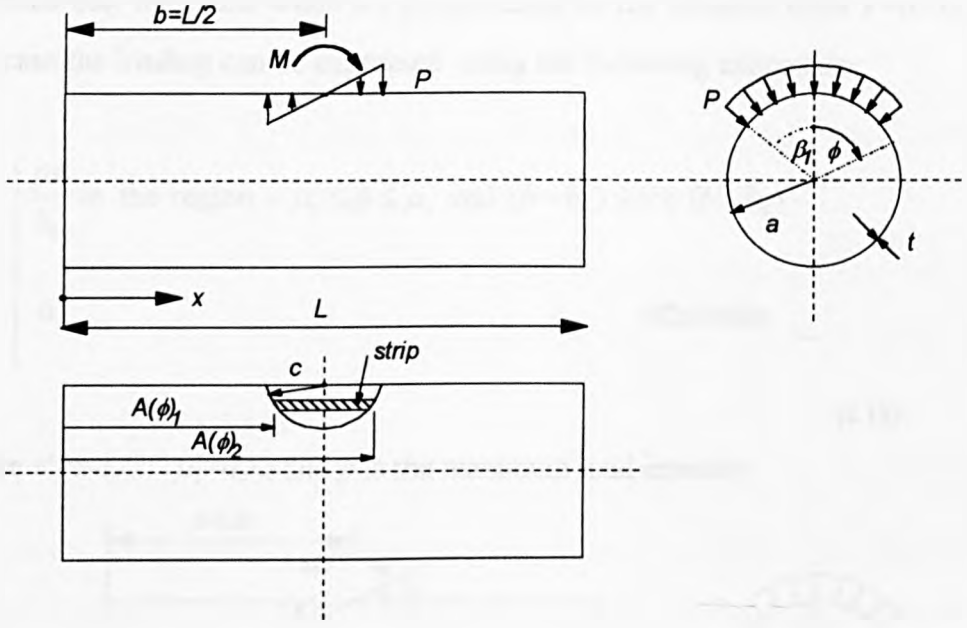

Figure 4.11 Longitudinal moment load acting on a circular patch

By following a similar procedure as before as noting the limits defined earlier, the following expressions for the Fourier load terms are obtained,

$$P_{r_{mn}} = \frac{4}{L\pi}\int_0^{A(\phi_2)} \int_0^{\beta} \frac{px'}{c}\sin\left(\frac{2m\pi x'}{L}\right)dx'\,d\theta$$

$$= \frac{pL}{m^2\pi^3 c}(-1)^m \int_0^{\beta}\left(\sin\left(\frac{2m\pi}{L}\sqrt{c^2 - a^2\sin^2\phi}\right)\right.$$

$$\left. -\left(\frac{2m\pi}{L}\sqrt{c^2 - a^2\sin^2\phi}\cos\left(\frac{2m\pi}{L}\sqrt{c^2 - a^2\sin^2\phi}\right)\right)\right)d\phi \quad (n=0, m=1,2,3,.....)$$

$$= \frac{8}{L\pi}\int_0^{A(\phi_2)} \int_0^{\beta} \frac{px'}{c}\cos(n\phi)\sin\left(\frac{2m\pi x'}{L}\right)dx'\,d\theta$$

$$= \frac{2pL}{m^2\pi^3 c}(-1)^m \int_0^{\beta} \cos(n\phi)\left(\sin\left(\frac{2m\pi}{L}\sqrt{c^2 - a^2\sin^2\phi}\right)\right.$$

$$\left.-\left(\frac{2m\pi}{L}\sqrt{c^2 - a^2\sin^2\phi}\cos\left(\frac{2m\pi}{L}\sqrt{c^2 - a^2\sin^2\phi}\right)\right)\right)d\phi \quad (m,n=1,2,3,.....)$$

(4.18*a*,*b*)

Longitudinal Moment - Elliptical Area

For the case of **longitudinal moment** loading *M*, uniformly distributed along a short distance in the longitudinal direction, acting over an **elliptical area**, the loading can be represented by a triangularly distributed radial load of maximum intensity *p*. It is assumed that the radial loads are proportional to the distance from $x=b=L/2$. For this case the loading can be expressed using the following expression.

$$P_r = \begin{cases} \dfrac{px'}{b_0} \text{ in the region } -\mu_1 \le \phi \le \mu_1 \text{ and } (b-b_0) \le x' \le (b+b_0) \\ 0 \qquad\qquad\qquad\qquad\qquad\qquad \text{otherwise} \end{cases}$$

(4.19)

where $x'=x-L/2$; $\mu_1=a_0/a$ and *p* is the maximum load intensity.

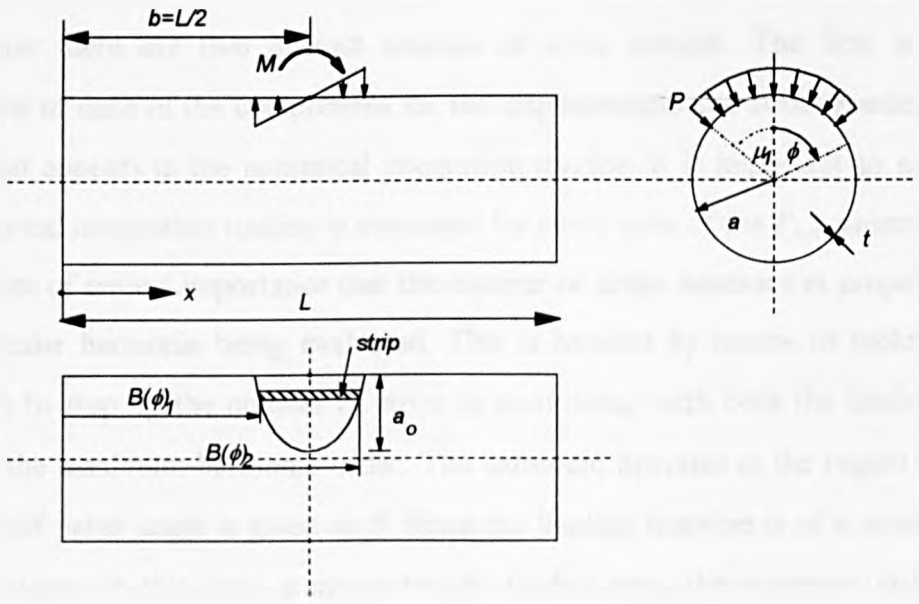

Figure 4.12 Longitudinal moment load acting on an elliptical patch

By following a similar procedure as before as noting the limits defined earlier, the following expressions for the Fourier load terms are obtained,

$$P_{r_{mn}} = \frac{4}{L\pi}\int_0^{B(\phi_2)} \int_0^{\mu_1} \frac{px'}{b_0}\sin\left(\frac{2m\pi x'}{L}\right)dx'd\phi$$

$$= \frac{pL}{m^2\pi^3 b_0}(-1)^m \int_0^{\mu_1}(\sin\left(\frac{2m\pi b_0}{a_0 L}\sqrt{a_0^2 - a^2\sin^2\phi}\right)$$

$$-\left(\frac{2m\pi b_0}{a_0 L}\sqrt{a_0^2 - a^2\sin^2\phi}\cos\left(\frac{2m\pi b_0}{a_0 L}\sqrt{a_0^2 - a^2\sin^2\phi}\right)\right)d\phi \quad (n=0,m=1,2,3,.....)$$

$$= \frac{8}{L\pi}\int_0^{B(\phi_2)} \int_0^{\mu_1} \frac{px'}{b_0}\cos(n\phi)\sin\left(\frac{2m\pi x'}{L}\right)dx'd\phi$$

$$= \frac{2pL}{m^2\pi^3 b_0}(-1)^m \int_0^{\mu_1} \cos(n\phi)(\sin\left(\frac{2m\pi b_0}{L}\sqrt{a_0^2 - a^2\sin^2\phi}\right)$$

$$-\left(\frac{2m\pi b_0}{a_0 L}\sqrt{a_0^2 - a^2\sin^2\phi}\cos\left(\frac{2m\pi b_0}{a_0 L}\sqrt{a_0^2 - a^2\sin^2\phi}\right)\right)d\phi$$

$$(m,n=1,2,3,.....)$$

(4.20*a*,*b*)

4.5 Accuracy of Solution

The inherent problem with any numerical solution is that of accuracy, and in this type of solution there are two distinct sources of error present. The first is in the summation of each of the components for the displacements and stress resultants and the second appears in the numerical integration routine. It is important to note that the numerical integration routine is evaluated for every term of the $P_{n,m}$ summation. It is therefore of critical importance that the number of strips increases in proportion to the particular harmonic being evaluated. This is handled by means of including an algorithm to step up the number of strips in accordance with both the loaded patch size and the maximum harmonic order. The harmonic operates in the region $0<\phi<\pi$, and the half patch angle is given as β. Since the loading function is of a cosine form and represents, in this case, a symmetrically loaded area, the minimum number of strips for a given harmonic can be obtained from the ratio of half patch angle to half

wave length. This is then modified in a suitable form for incorporation into the Simpson's Rule numerical integration routine.

$$N_{min} = INT\left(\frac{2n\beta}{\pi} + 1\right)(\times 4) + 1 \tag{4.21}$$

The above equation shows the minimum number of strips, N_{min}, to be 5 for the first harmonic with a small patch size. As the patch size or harmonic order rises, the number of strips increases proportionally (ie. n=2,3,4,.. N_{min}=9,13,17,..) thereby maintaining sufficient accuracy.

A detailed description of the significance of varying the number of terms for the Fourier Series summations is given by Duthie and Tooth[9].

4.6 Some Illustrative Examples

Example 1 - Radial Load on a Circular Area

The first example is of a direct radial load applied to a 300mm dia. circular pad attached at the mid-point of a 2m diameter, 10mm thick, 10m long cylindrical steel vessel (E=200,000 N/mm^2, ν= 0.3). A value of 10,000N is applied to the pad and the displacements and stress resultants calculated.

The results shown in Figures 4.13a,b describe the variation of the component stress resultants around the profile x=L/2. The graphs shown in Figures 4.13c,d show the variation along the length of a generator located from the centre of the patch. The results presented also include the **'equivalent'** square patch values as obtained from a Fourier series representation of the BS5500 patch (c=0.85r_0) and the ASME VIII patch (c=0.875r_0).

A finite element solution is also included, modelling the above geometry using 80 ANSYS SHELL61 axisymmetric harmonic conical shell elements. The direct radial loading is again expressed as a Fourier expansion with 100 summations allowing non-axisymmetric loads to be represented.

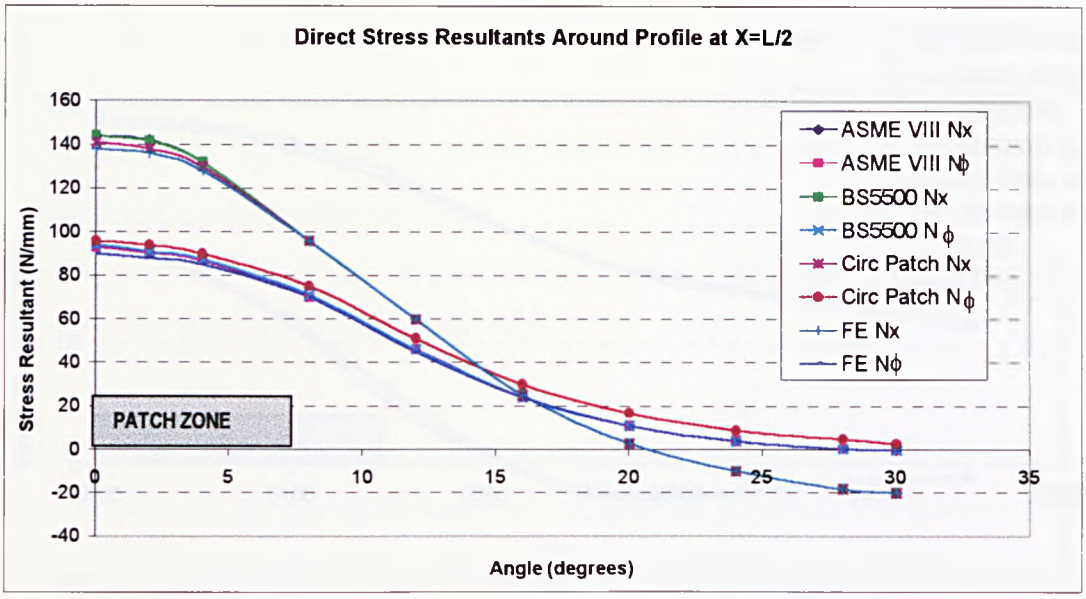

Figure 4.13a Direct stress resultants for radial load on circular patch example around profile at x=L/2

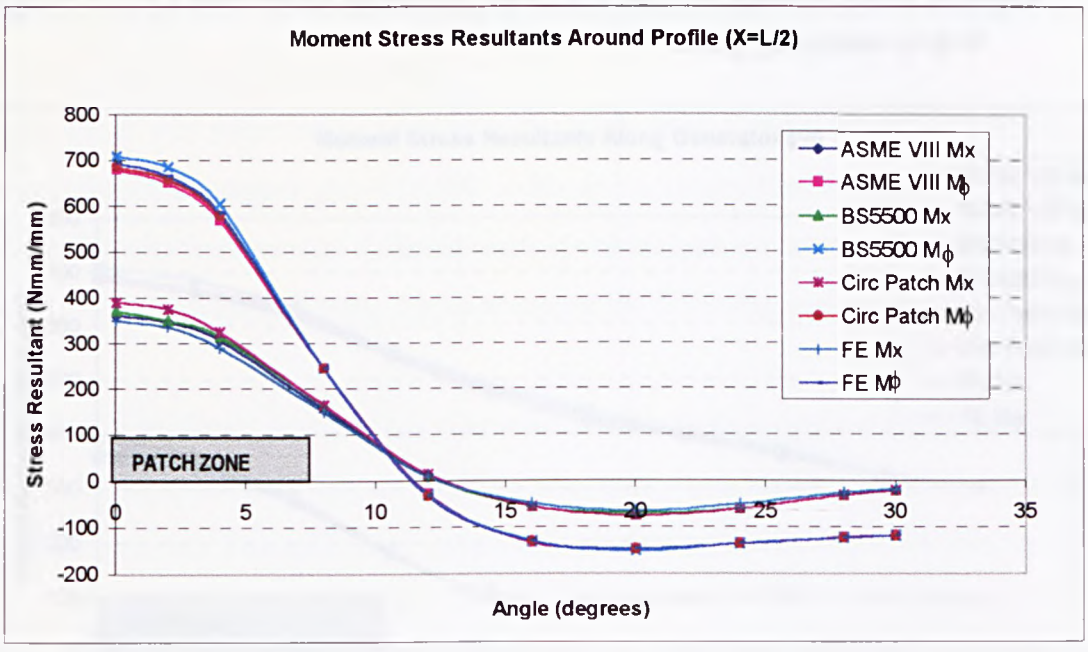

Figure 4.13b Moment stress resultants for radial load on circular patch example around profile at x=L/2

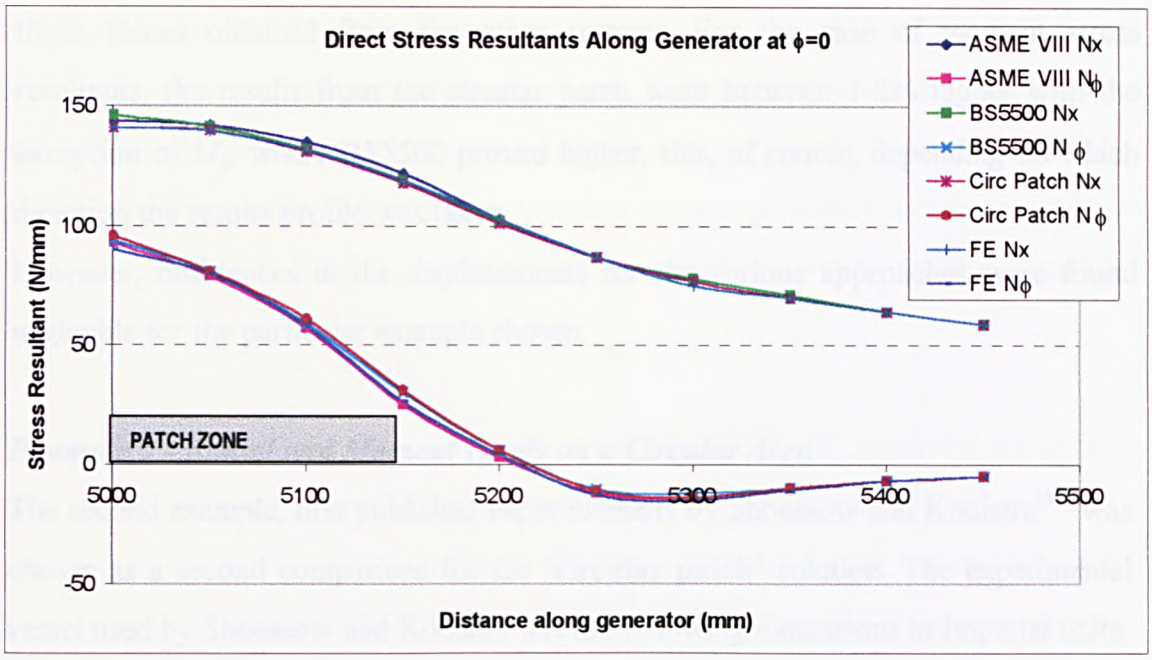

Figure 4.13c Direct stress resultants for radial load on circular patch example along generator at $\phi=0$

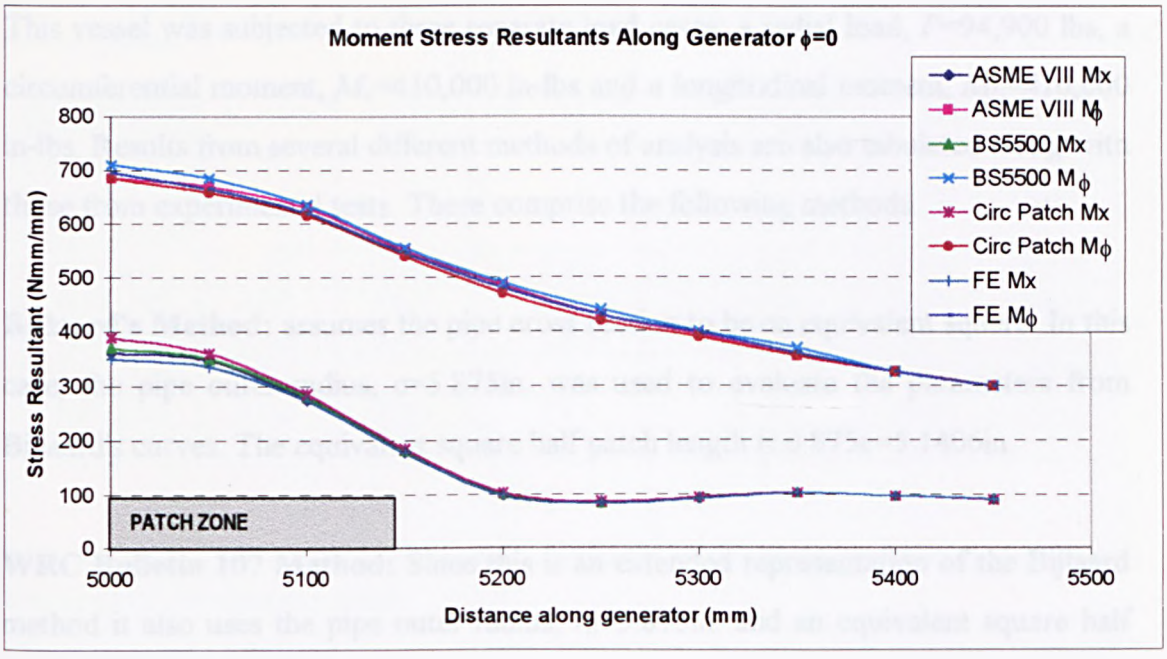

Figure 4.13d Moment stress resultants for radial load on circular patch example along generator at $\phi=0$

From these graphs (Figures 4.13a-d), it can be seen that for the direct stress resultants, N_x and N_ϕ the circular patch solution yields results some 1-4% higher than

those values obtained from the other sources. For the case of moment stress resultants, the results from the circular patch were between 1-2% higher with the exception of M_ϕ where BS5500 proved higher, this, of course, depending on which direction the results profile was taken.

However, differences in the displacements for the various approaches were found negligible for the particular example chosen.

Example 2 - Radial and Moment Loads on a Circular Area

The second example, first published experimentally by Shoessow and Kooistra[65] was chosen as a second comparison for the '**circular patch**' solution. The experimental vessel used by Shoessow and Koositra has the following dimensions in Imperial units: Mean radius R=28 in., length L=71 in., wall thickness t=1.3 in., outer diameter of attachment pipe d_0=11.75 in., length of pipe L_0=90 in. with material property values E=3x10^7 lb/in^2 and Poisson's ratio, ν = 0.3.

This vessel was subjected to three separate load cases: a radial load, P=94,900 lbs, a circumferential moment, M_c=410,000 in-lbs and a longitudinal moment, M_L=410,000 in-lbs. Results from several different methods of analysis are also tabulated along with those from experimental tests. These comprise the following methods.

Bijlaard's Method: assumes the pipe cross section to be an equivalent square. In this case, the pipe outer radius, c=5.875in. was used to evaluate the parameters from Bijlaard's curves. The equivalent square half patch length is 0.875c=5.1406in.

WRC Bulletin 107 Method: Since this is an extended representation of the Bijlaard method it also uses the pipe outer radius, r_0=5.875in. and an equivalent square half patch length is 0.875r_0=5.1406in.

BS 5500 Appendix G: In this case, the mean radius of the pipe, r_m=5.4375in. is used to find an equivalent square with sides of half length equal to 0.85r_m=4.622in.

Finite Element Method: Runs were performed using the ANSYS finite element program using a quarter symmetric model using 8-noded shell elements. The load is applied as a pressure acting over a circular area based on the pipe mean radius, c=5.4375in. The results for the moment loading are not presented here but could be obtained using the ANSYS harmonic element with non-axisymmetric loading capability.

Fourier Series Solutions: In each of the cases, '**FORTRAN**' programs using the solutions described herein, were used with 100 terms in each series with 10 integration steps within each summation. These results are based on the mean radius of patch, c=5.4375in. '**RECTAN**' shows the results for a square BS patch using the Fourier solution, whilst '**CIRCLE**' refers to the present circular/elliptical patch solution.

Table 4.1 Comparison of alternative methods of analysis for radial loading (P) for circular patch

	$M_\phi / M_c c$	$M_x / M_c c$	$-N_\phi / (M_c / Rc)$	$-N_x / (M_c / Rc)$	σ_ϕ (psi)	σ_x (psi)
Shoessow & Kooistra (experiments)	-	-	-	-	-31000	-24000
Bijlaard	0.079	0.051	2.356	2.688	-32610	-24200
WRC 107	0.093	0.061	2.654	3.432	-38321	-29635
BS 5500	0.094	0.062	2.959	2.815	-39285	-28195
FE Analysis	-	-	-	-	-36677	-35088
RECTAN	0.090	0.065	2.991	2.948	-38250	-29525
CIRCLE	0.088	0.064	3.353	2.924	-38474	-29329

Table 4.2. Comparison of alternative methods of analysis for circumferential loading (M_c) for circular patch

	$M_\phi / M_c c$	$M_x / M_c c$	$-N_\phi / (M_c / Rc)$	$-N_x / (M_c / Rc)$	σ_ϕ (psi)	σ_x (psi)
Shoessow & Kooistra (experiments)	-	-	-	-	-25000^{+} -27000^{++}	-16000^{+} -23500^{++}
Bijlaard	0.081	0.042	0.832	1.482	-23280	-14220
WRC 107	0.094	0.040	0.866	1.092	-26995	-13021
BS 5500	0.112	0.056	0.929	1.038	-31970	-17266
RECTAN	0.109	0.060	0.765	1.393	-30675	-18933
CIRCLE	0.102	0.067	0.998	1.560	-29294	-21065

Table 4.3. Comparison of alternative methods of analysis for longitudinal moment loading (M_l) for circular patch.[•]

	$M_\phi / M_c c$	$M_x / M_c c$	$-N_\phi / (M_c / Rc)$	$-N_x / (M_c / Rc)$	σ_ϕ (psi)	σ_x (psi)
Shoessow & Kooistra (experiments)	-	-	-	-	-13500[+] -13000[++]	-16500[+] -16000[++]
Bijlaard	0.039	0.048	2.592	1.482	-13910	-14620
WRC 107	0.040	0.066	2.592	1.092	-16141	-19282
BS 5500	0.061	0.065	1.787	1.038	-20194	-19569
RECTAN	0.049	0.074	2.753	1.393	-18781	-21578
CIRCLE	0.056	0.068	2.871	1.560	-20977	-20147

- Maximum value of outer surface stress.
- [+,++] Denote the stress calculated at the top and inverted positions respectively from test data.

For the radial load case, it can be seen from Table 4.1 that the codes methods and the results from the new solution (CIRCLE) are in good agreement but the analytical solutions are higher than the experimentally measured results. This is probably due to the unclear exact position of the gauges on an edge, compared with the maximum location, which is at the centre of the patch, for the analytical methods. The moment load cases show better agreement, since the analytical methods evaluate the maximum at the edge of the loaded area. Again, the new solution provides results slightly higher than the experimental values. Thus, the new method can be stated to be conservative in design.

Example 3 - Radial and Moment Loads on an Elliptical Area

The general solution for the elliptical patch enables the problem of an attached pipe or nozzle, which has its axis inclined to the main vessel centrelines and generators, to be analysed. Since no available data exists for direct comparison for the elliptical patch case, a typical vessel has been analysed and graphs have been provided Figures 4.14-4.16. These show the variation of the maximum stress values for a range of ratios of the major and minor axes of the ellipse.

For this case, the vessel parameters are as follows: mean vessel radius R=1000mm; thickness of vessel t=10mm; length of vessel L=8000mm; elastic modulus E=200,000N/mm^2; Poisson's ratio ν=0.3.

The patch size ratio a_0/b_0 (i.e. circumferential/axial half lengths) has been varied from 0.643 to 1.556. When $a_0/b_0 > 1$ the computed values of stress correspond to a 150 mm outer diameter pipe inclined in the circumferential direction. The maximum ratio of $a_0/b_0 = 1.556$ corresponds to an oblique angle of approximately 50° from the normal. This value is equal to the maximum recommended oblique angle for a nozzle in BS 5500. When $a_0/b_0 < 1$ the values correspond to the same diameter pipe, but this time inclined in the axial direction. The minimum ratio of $a_0/b_0 = 0.644$ again is equal to a maximum oblique angle of 50°.

The stresses have been derived for the three load systems; radial load, circumferential moment and longitudinal moment for the range of a_0/b_0 values quoted. The same magnitude of load was applied to each elliptical patch in turn. In each case the load was applied at the vessel centre $b=L/2$. The values of these were as follows:

Total radial load, P **= 10,000 N**
Circumferential moment, M_c **= 1,000,000 Nmm**
Axial moment, M_L **= 1,000,000 Nmm**

The maximum values of stress have been computed for these three load cases using the following approaches:

(a) The analysis presented in this chapter for the elliptical patch, representing the load as indicated, by a double Fourier series technique;

(b) Assuming the ellipse is equivalent to a rectangle of side 0.84× the major and minor axes of the ellipse (this ratio is proposed by BS 5500 for this case). It is identified as **'Equiv. Rect.'** Using the equivalent rectangle, the radial loading is assumed to be distributed uniformly over the patch and the moment loading is assumed to produce a triangular distribution of radial loads. The double Fourier series is again used;

(c) Using the same equivalent rectangle and the BS 5500 Charts. In this the radial loading is assumed to be uniformly distributed and the moment loading to be equivalent to two equal & opposite radial load patches. This is shown as **'BS 5500'**

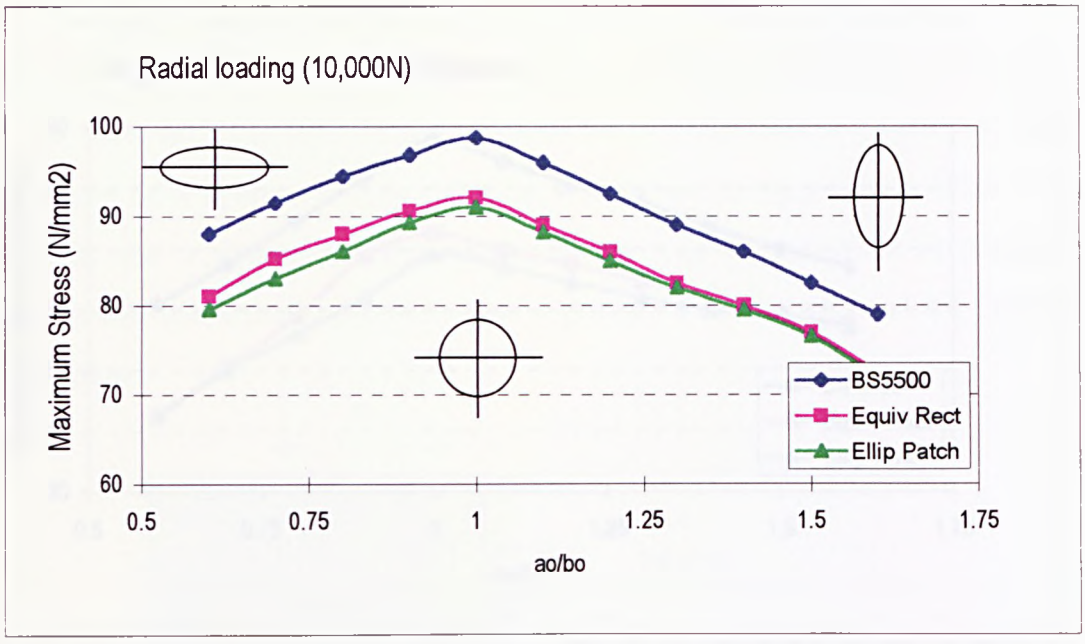

Figure 4.14 Maximum stress variation for elliptical patch subject to radial load

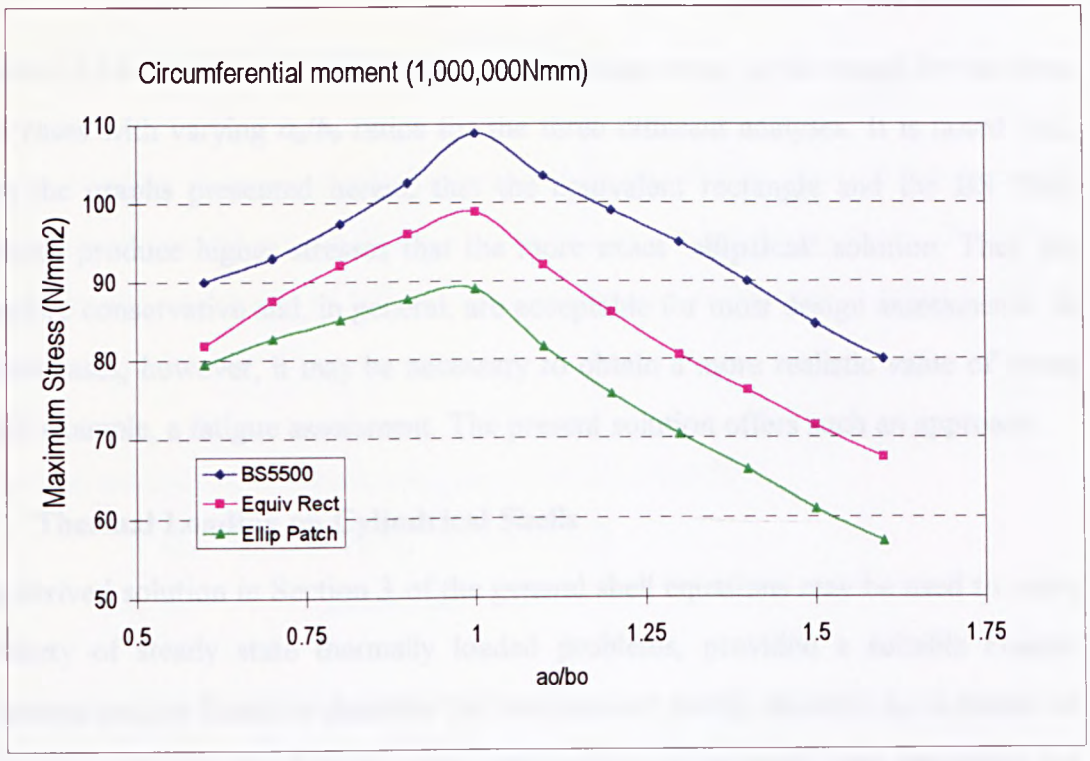

Figure 4.15 Maximum stress variation for elliptical patch subject to circumferential moment

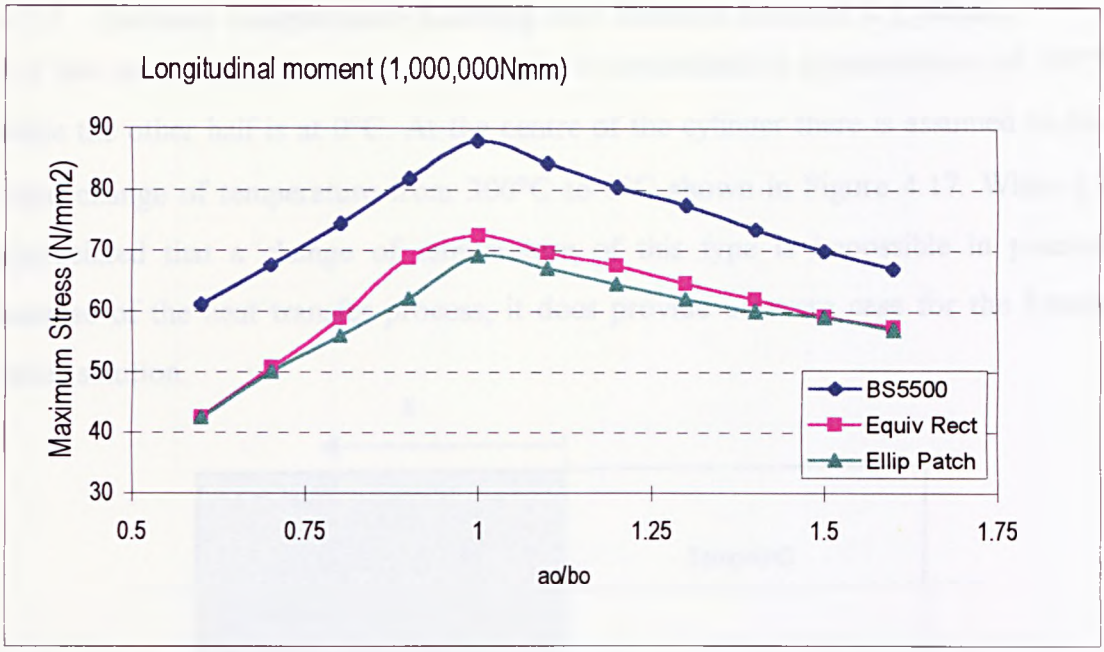

Figure 4.16 Maximum stress variation for elliptical patch subject to longitudinal moment

Figures (4.14-16) show the variation of the maximum stress in the vessel for the three load cases with varying a_0/b_0 ratios for the three different analyses. It is noted that, from the graphs presented herein, that the equivalent rectangle and the BS 5500 methods produce higher stresses that the more exact **'elliptical'** solution. They are therefore conservative and, in general, are acceptable for most design assessments. In certain cases, however, it may be necessary to obtain a more realistic value of stress in, for example, a fatigue assessment. The present solution offers such an approach.

4.7 Thermal Loading on Cylindrical Shells

The derived solution in Section 3 of the general shell equations may be used to solve a variety of steady state thermally loaded problems, provided a suitable Fourier expansion can be found to describe the temperature profile desired. As a means of illustration of how the Fourier series approach may be used, two examples are described in detail. The first is a rather hypothetical case where one half of the vessel is maintained at temperature T_1, with the other half at temperature T_2. The second case is the more realistic one of a **'hot-spot'** acting at a certain cylinder location.

4.7.1 Uniform Temperature Loading over Discrete Areas of A Cylinder

For this case, the left hand of the cylinder is maintained at a temperature of 300°C while the other half is at 0°C. At the centre of the cylinder there is assumed to be a rapid change of temperature from 300°C to 0°C shown in Figure 4.17. While it is appreciated that a change of temperature of this type is impossible in practice, because of the heat transfer process, it does provide a severe case for the Fourier series solution.

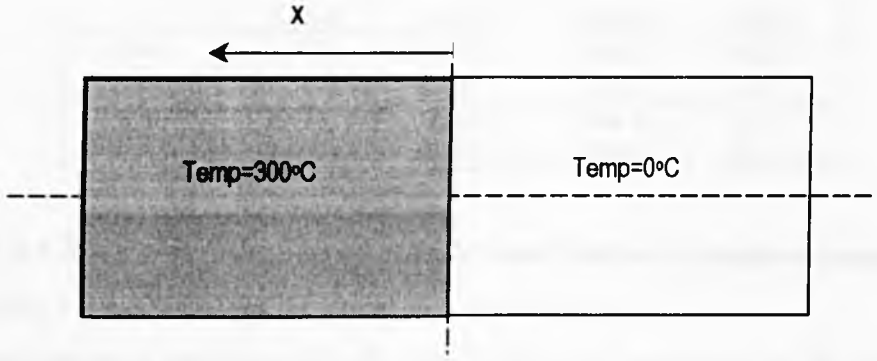

Figure 4.17 Partially heated cylinder

Furthermore, it is possible to obtain another solution to this hypothetical case using the edge bending equations from classical shell theory. In this, the two halves of the cylinder are allowed to expand freely. The displacements and slopes at $x=L/2$ are then matched by the application of self-equilibrating forces - in this case, a radial line load around the cylinder at $x=L/2$.

The temperature term, T, representing this profile is given by:

$$T = t_0, \quad (0 \le \phi \le 2\pi), \quad (0 \le x \le L/2)$$
$$= 0, \quad \text{otherwise} \tag{4.22}$$

To compare the two approaches, a steel cylinder of length 4000mm and 1500mm diameter with 10mm wall thickness is considered. The temperature in the region $0 < x < 2000$ is at 300°C whilst the remainder of the cylinder is at 0°C.

The following table shows the comparison of the two solutions, the figures in parenthesis being obtained from the Fourier solution using 500 terms in each series.

x^* (mm)	w (mm)	M_x (Nmm/mm)	M_ϕ (Nmm/mm)	N_ϕ (N/mm)
0	1.350 (1.350)	0.000 (-0.039)	0.000 (-0.012)	3456 (4.40)
2	1.390 (1.390)	301.3 (294.1)	90.40 (82.22)	3353 (1564)
6	1.470 (1.470)	850.9 (851.1)	255.3 (255.3)	3149 (3524)
10	1.549 (1.549)	1333 (1337)	400.0 (401.1)	2947 (3392)
20	1.741 (1.741)	2273 (2273)	682.0 (681.8)	2456 (2423)
60	2.352 (2.352)	3337 (3337)	1001 (1001)	892.2 (896.1)
100	2.674 (2.674)	2362 (2362)	708.5 (708.5)	67.71 (66.29)

Table 4.4. Classical infinite heated cylinder and Fourier expansion comparison

* In this case, x is measured from the centreline at the heat junction

The comparison is excellent for all values with the exception of N_ϕ close to the hot/cold junction. The reason for this is that at this junction, the temperature as predicted by the Fourier series solution is part way between 300°C and 0°C. The N_ϕ values reflects this and shows a reduction very close to the junction in readiness to the compressive value in the cold section. The classical result goes from -3456N/mm to +3456N/mm in zero length. However because of the nature of the Fourier series solution, it does take some finite length for the approximation to map the step change. For real temperature distributions, it is felt that the Fourier analysis would cope quite adequately.

4.7.2 The 'Hot-Spot'

The case of the localised '**hot-spot**' provides a more realistic test of the Fourier series method. The hot spot may take the form of some predetermined shape which will represent the actual steady-state condition. In this particular problem, the temperature function will take the form of a '**bell-shaped**' temperature profile acting over a rectangular (or square) section at the cylinder profile x-b and at the zenith $\phi=\pi$ of the vessel as shown in Figure 4.18. This function, first proposed by Wilson[62], has a variation in both the axial and circumferential directions. It is restricted to the

rectangular patch for this case, that is $(\pi-\beta) \leq \phi \leq (\pi+\beta)$, $(b\text{-}c) \leq x \leq (b+c)$ and can be represented in this region by the following function,

$$T = \frac{t_0}{4}\left(1-\cos\frac{\pi}{c}(x-(b-c))\right)\left(1-\cos\frac{\pi}{\beta}(\phi-(\pi-\beta))\right)$$

$$= 0 \text{ otherwise}$$

(4.23)

Such a distribution may arise, for example, from a flow restriction within a vessel, or from loss of insulation. It is expressed in Fourier series form and then incorporated into the solution.

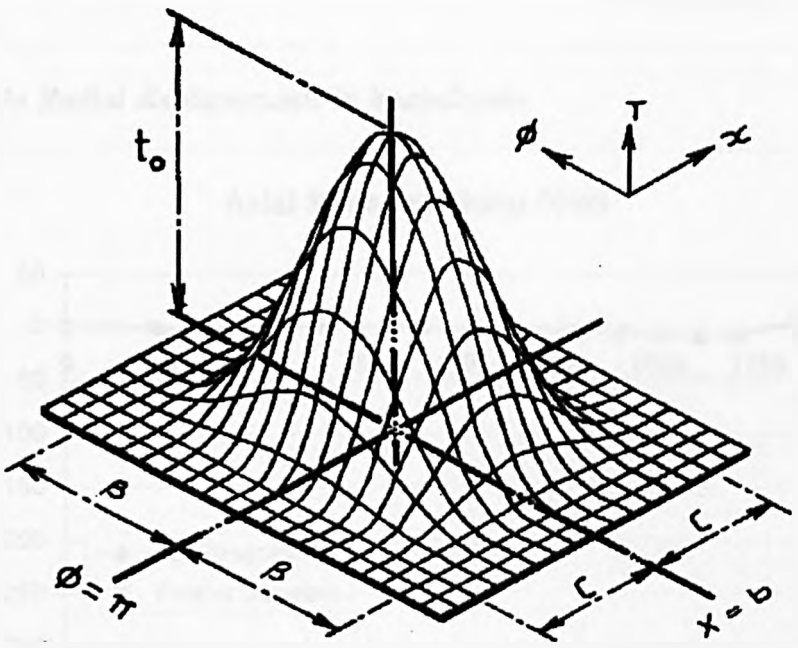

Figure 4.18 Bell shaped temperature distribution over hot-spot

As an illustrative example, the bell-shaped hot spot was applied to the steel cylinder with dimensions as per Section 4.7.1. The hot spot was applied over a square patch 300×300 mm centred about the vessel profile ($x=L/2$) and the zenith ($\phi=\pi$) with a maximum temperature, t_0=150°C. The radial displacements w, and the stress resultants and stresses were obtained for this thermal loading.

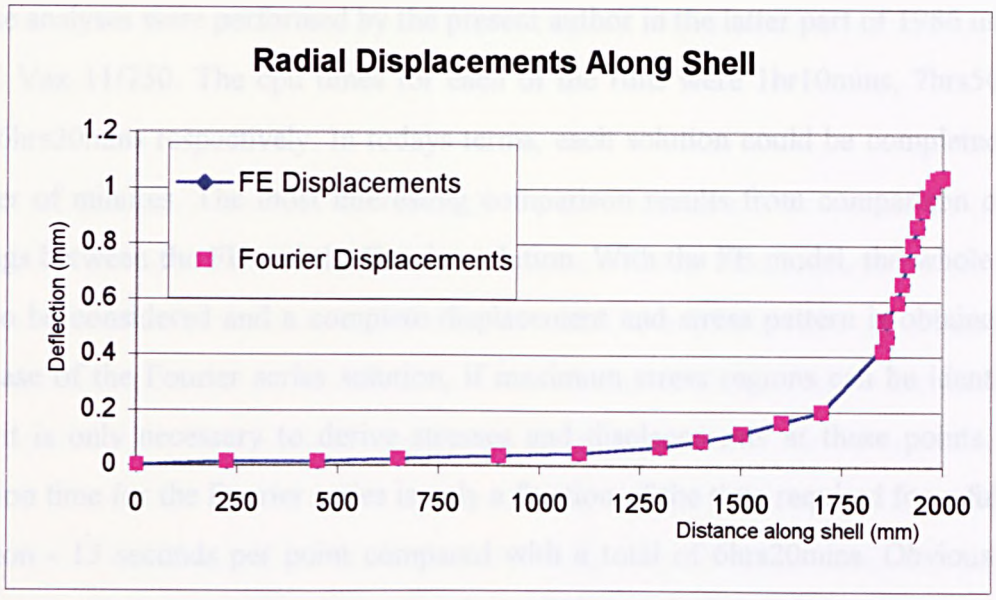

Figure 4.19a Radial displacements in heated zone

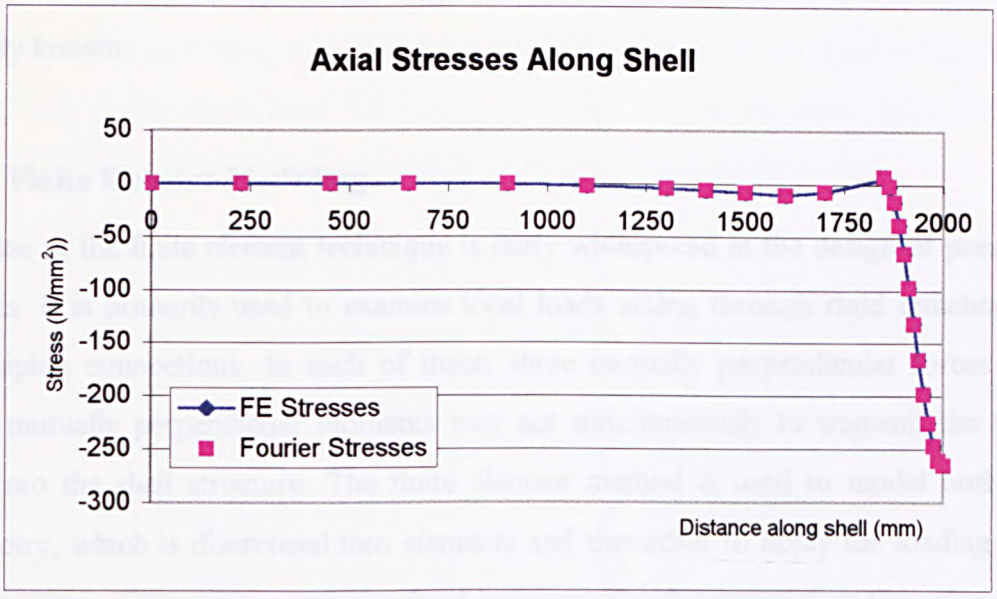

Figure 4.19b Axial stresses in heated zone

These results were compared with those obtained from the ANSYS finite element program. One quarter of the shell was modelled using quadrilateral shell elements with both membrane and bending capabilities. Three different models were used and detailed below.

Model	Element Type	Elements in Heated Zone	Total Elements	Total Nodes	Maximum Displacement	Max. Axial Stress N/mm^2
1	4-noded	9x9	586	567	1.04502 mm	-261.958
2	8-noded	9x9	586	1801	1.04536 mm	-262.816
3	8-noded	24x24	855	969	1.04841 mm	-264.092

These analyses were performed by the present author in the latter part of 1986 using a DEC Vax 11/750. The cpu times for each of the runs were 1hr10mins, 7hrs50mins and 6hrs20mins respectively. In todays terms, each solution could be completed in a matter of minutes. The most interesting comparison results from comparison of the timings between the FE and the Fourier solution. With the FE model, the whole shell has to be considered and a complete displacement and stress pattern is obtained. In the case of the Fourier series solution, if maximum stress regions can be identified, then it is only necessary to derive stresses and displacements at these points. The solution time for the Fourier series is only a fraction of the time required for a full FE solution - 13 seconds per point compared with a total of 6hrs20mins. Obviously as the power of the computer increases these differentials will reduce, however, the Fourier series will always be the more efficient if the location of the maximum is already known.

4.8 Finite Element Modelling

The use of the finite element techinique is fairly widespread in the design of pressure vessels. It is primarily used to examine local loads acting through rigid attachments and piping connections. In each of these, three mutually perpendicular forces and three mutually perpendicuar moments may act simultaneously to transmit the local load into the shell structure. The finite element method is used to model both the geometry, which is discretised into elements and thereafter to apply the loading into the structure. The problem is then solved in terms of stiffness and then the solution is evaluated to give displacements, strains and, lastly, stresses.

The finite element techinique is of use since it allows the exact geometry to be modelled. This feature of the process makes use of sophisticated modelling commands which are now available in most modern systems. These include features such as arcing, dragging, calculation of exact intersections of lines and planes and volumes, component sweeping, extrusion and so on. By suitable application of these

utilities within the system, it is possible to produce a realistic model for most pressure vessel problems.

After the geometry has been established, the main shapes are discretized to provide the finite element mesh. Experience is required when deciding on the level of refinement to use in a particular situation. Often, it is helpful to have an indication of the expected stress system, so that a sufficient number of elements are concentrated in the required area of interest. If specific stress concentations are to be examined, the number of elements may be high (say greater than 10,000), however, a large number of pressure vessel problems can be reduced to a simpler model using the physical properties of the system, e.g. symmetry, axisymmetry and so on.

With regard to modelling local loading problems, such as the patch-type loading on cylindrical shells, these may be simulated using several different finite element techniques, each making use of a specific physical property of the system.

4.8.1 Modelling using 2D Axisymmetric Shells

This class of problem models the vessel as a series of connected line segments and assumes the geometry is a solid of revolution. This type of analysis is most commonly used to examine shell/head discontinuity problems under internal pressure. The main restrictions are that no account can be taken of the geometry of openings or attachments that are non-axisymmetric. In addition, the thickness of each shell is constant, therefore, it is difficult to look at localised stresses, arising from say, weld build up. In addition, the thickness of the shell must be small in relation to its radius (say $R/t > 10$), to satisfy the assumptions inherent in shell analysis.

A facility exists in most modern codes to allow the input of non-axisymetric loads which can be fitted with a Fourier-type series. In this, a sine or cosine series is used to model the loading and using the harmonic postprocessor, the resulting stresses can be found at specific locations by sweeping around the shell at chosen discrete angles (say every 5°). Whilst this type of analysis has certain restrictions, it can be of use in

initially examining a problem before expending considerable effort in a much more complex analysis.

4.8.2 Modelling using 3D Shells

The use of 3D isoparametric shell elements allows the analyst to model the problem in three dimensions. This type of analysis is the most common for pressure vessel problems. The main restrictions are similar to those of the axisymmetric shell elements and include the *R/t* ratio, limited to greater than 10, element shape limitations on aspect ratio and skew angle, limitations on connected element wall thickness, since only a centreline approach is used. A linear stress distribution is implied through the thickness of the shell. Since only the midsurface of the shell need be modelled, results are output on a surface basis. Results are available for the top, middle or bottom surface and this must be defined prior to outputting numerical values or contour plots. However, care must be taken in establishing which surface is top or bottom especially when stress intensity values are requested.

Even with the above restrictions, the major advantage of this type of analysis is that a truly three dimensional loading may be applied directly to the model. In addition, graphical contour plots are available on each of the three surfaces which can be directly viewed to give a 'full-field' description of the stress distribution.

4.8.3 Modelling using 3D Bricks

The three dimensional brick model is used only when the three dimensional shell model proves inadequate. These situations arise when changes in wall thickness occur and through thickness effects are being investigated. Examples of these analyses are, nozzle/shell intersections with and without pads, areas of weld build-up, thick plate to thin shell attachments, and so on. Using 3D brick elements demands that the geometry be described in terms of volumes, therefore the modelling time associated with this type of analysis is considerably greater. However, this method is the only available techinque for obtaining non-linear through thicknesses effects since it discretises the vessel thickness explicitly.

In addition, a major point of concern is the process whereby stress obtained from a 3D brick model are **'linearised'** in order to obtain membrane and bending stresses which can be assessed against the requirements of pressure vessel codes such as BS5500 and ASME VIII Division 2. Prior to the advent of FEA, it was usually possible, with simple mechanics or shell discontinuity analysis, to separate primary and secondary stress, in the light of the fundamental failure mechanisms which the code addresses, since the equilibrium calculations were done manually. This is not obvious with finite element results, and in particular with the results of using continuum elements.

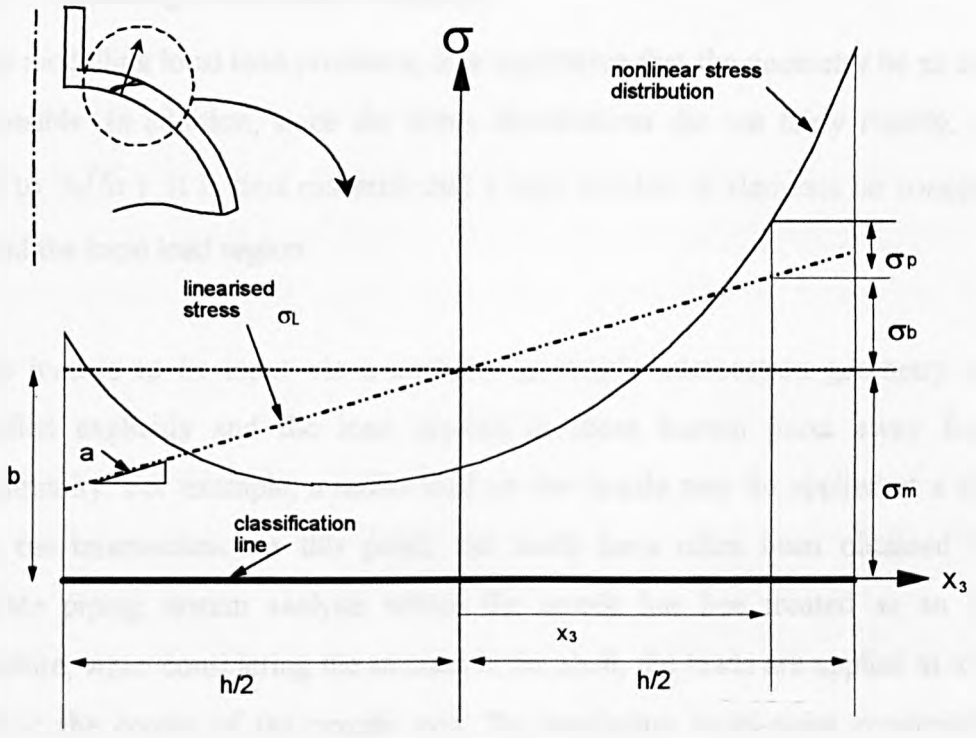

Figure 4.20 Stress linearisation through a 3D vessel wall

The linearisation procedure is based on beam bending stress and attempts to define an *equivalent linear stress distribution* on a classification line (CL); thus if z measures distance along the CL then the equivalent linearised stress is,

$$\sigma_L = az + b$$

where the coefficients a and b are determined from the calculated finite element stresses. This can be accomplished from the conditions that the total bending moment for the actual and linearised bending stresses must be the same, and that the total direct force from the linearised stress should be zero. The membrane stress is

calculated as the average stress through the wall and the bending stress is found by evaluating the linearised stress at the inner and outer surfaces and subtracting the membrane. The peak stress is obtained from,

$$\sigma_p = \sigma - \sigma_m \pm \sigma_b$$

However, there is much debate regarding which stresses (or stress intensities) should be linearised and which classification line (or plane) should be used, and indeed, what should be done with the resulting linearised stresses. Therefore, these additional difficulties compound the analysis of local load problems using 3D brick elements.

4.8.4 Modelling Local Load Problems

When modelling local load problems, is is imperative that the geometry be as accurate as possible. In addition, since the stress distributions die out fairly rapidly, (within $2\sqrt{rt}$ to $3\sqrt{Rt}$). It is thus essential that a high number of elements be concentrated around the local load region.

If the load is to be input via a nozzle, the nozzle intersection geometry may be modelled explicitly and the load applied at some known point away from the discontinuity. For example, a radial load on the nozzle may be applied at a distance from the intersection. At this point, the loads have often been obtained from a separate piping system analysis where the nozzle has bee treated as an anchor. Therefore, when considering the stresses in the shell, the loads are applied at a known point at the centre of the nozzle axis. By employing multi-point constraints (i.e. treating the applied load point as rigid), the nozzle is thus forced to transfer the load into the shell. In this manner, the correct nozzle flexibility is introduced.

If the load is input via an attachment and pad, the correct method of analysis is to model both the attachment and pad and use contact elements to introduce the appropriate interface pressures which transfer the load to the shell. This method is quite onerous and involves a high degree of competence in using the finite element system. More often, these problems are simplified by assuming the attachments and pad are considerably more rigid than the vessel shell. The attachment and pad are

neglected and the load is directly applied to the shell via pressure loads or via master-slave multi-point constraints. Even so, the distribution of the interface pressure remains unknown.

For the purposes of this work, the three dimensional shell elements have been used throughout since a linear through thickness stress distribution is assumed. Even using this simplifying assumption, run times for the models can still be high, this being attributed to the number of elements required in order to achieve the correct mesh refinement.

4.9 Comments

The Fourier series approach has been used with the Sanders shell theory to provide a method which can be used to analyse stresses and displacements occurring in the regions local to square, rectangular, circular and elliptical patch attachments on cylindrical vessels. Loading may be either direct radial force or moment or thermal loading.

The solution has been used to compare the well-tried BS 5500 and ASME VIII approaches of using an equivalent **'square'** patch to evaluate the required values. In general, the circular patch solution yielded results, which were 1-4% higher than the corresponding equivalent square patch for force resultants and 1-2% higher for moment resultants. However, differences in the displacements for the various approaches were found negligible for the particular example chosen. Further validation of the analysis was provided by the finite element results.

The solution can handle the cases where moments are applied through a circular patch in both the x and ϕ directions and ultimately in the 45° plane. The solution is also able to analyse the case of loading applied to an annular pad for loading transmitted from, say, a support fabricated from pipe welded directly to the shell. This presents a direct method for the analysis of intersecting structures such as pressure vessel shells, nozzles and supports, oil rig nodes and so on. The solution, as shown earlier, by

means of modification of the boundary conditions for the case of the elliptical patch, by redefining the $B(\phi)$ equations, yields a solution for the problem of oblique attachments. Here the BS values are always conservative.

The case of the steady-state thermal patch has also been addressed. Although only a few simple cases are presented herein, the same capability exists for extension to other problems as for the radial load case, since the form of representation is the same. The solution by Duthie and Tooth gives many more examples of the different loading functions, which may be applied. One interesting case is that of the stress relieving of a nozzle, whereby the heat is input via a thermal pad often annular in form. The circular patch solution can be combined with the thermal extensions to the general shell equations and Fourier series solution to solve this problem using superposition.

This work was published by the author in References [45], [59], [66] and [67].

5 ANALYSIS OF CYLINDRICAL SHELLS ON SADDLE SUPPORTS

5.1 Introduction

The analysis of a horizontal cylindrical vessel supported on twin saddle supports could be assumed to be similar to the local loading problem since the contact area is normally a rectangular patch. However, since the encompassed arc angle, often denoted the **'saddle wraparound angle'** is relatively large (in the range 60°to 180°) contact between the vessel and the support cannot be assumed to produce a uniform value of interface pressure. When a vessel is subjected to local loading over a small region of its surface it is often assumed that the loading is uniformly distributed over the small region of the bracket or lifting lug. This implies that the loading system takes up the displaced shape of the vessel surface in the loaded region. This is one of the main assumptions made in the previous chapter and is also relevant in the context of *BS5500 Annex G.*

However, this is clearly not the case when a vessel is loaded through a rigid attachment such as a saddle support and over a large wraparound angle, since contact between the vessel and the attachment may be lost in some regions due to the relative flexibility of the vessel and possible lack of fit of the saddle. It has been well established, both by analytical and experimental means, that highly concentrated reaction forces occur at the horns of saddle supports. This occurs for saddles which are both welded and loose fitting, however, for the latter is has been noted that contact may be lost over a small arc immediately below the saddle horn. Therefore, it is fundamental that the correct distribution of the interface pressures be identified and accurately determined.

A general summary of the available solutions developed at Strathclyde is shown. The development of the method and extension of a Fortran program for the analysis of this problem is presented in detail although much of the presentation can be found in the work of Ong[11], Motashar[16], Warrender[57] and Tolson[58]. It is worth summarising the contributions made by each of these researchers towards a solution. The problem

was first tackled by Forbes[84] during 1964 to 1967, who provided the original approach. He developed an ALGOL program based on the shell equations of Flügge. Thereafter, his work was modified by Duthie and changed slightly by White. Ong updated the work for Sanders' equations and developed the code for the analysis of an unstiffened cylindrical shell either simply supported at it ends or supported on twin saddles. The program had the capability of taking into consideration the 'out-of-roundness' of the shell, this being caused by poor workmanship or as a result of a local dent. The out-of-roundness was modelled using a Fourier series fit to a number of radial measurements at discrete points around the circumference on up to five profiles along the shell. The program could also handle self-weight and hydrostatic loading conditions in conjunction with some of the local load cases mentioned earlier. In addition, the case of side loads can also be accommodated. The solution assumed discrete areas of contact around the saddle in the circumferential direction but assumed uniform contact across the width. The program was developed using DEC Fortran 77 for a VAX computer running VMS.

Warrender utilised Ong's program to study the case of the GRP vessel with chopped strand mat construction. For that case, the material is assumed homogeneous and isotropic, therefore allowing a single equivalent Young's modulus and Poisson's ratio to be input. His work included comparisons of experimental and theoretical strain values for the rigid support. Since the relative flexibilities of the GRP and steel saddles were quite different, a rubber insert was used by Warrender to 'cushion' the vessel and therefore reduce the maximum stress levels at the horn. This simplified analysis was incorporated into the program to allow the rubber interface solution to be assessed. The present author developed the coding for Warrender to allow the inclusion of friction to be introduced to the contact area between the vessel and the saddle. This restricted the movement of the saddle in the circumferential direction in proportion to the reaction forces present at the point of contact. As in the program developed by Ong, Warrender assumed uniform contact across the saddle width.

Motashar developed a similar solution to Ong's program but for the perfectly circular cylindrical vessel supported on twin saddles. However, his main interest was in the distribution of the interface pressure around the circumference and across the width. The saddle area was sub-divided into various **'meshes'** or grids and the relative merits examined. He concluded that there were some high interface peaks found at the edges of the saddles but a general uniformity across the width for most cases. To a certain extent, the accuracy of the solution depended on the number of discrete areas and the number of Fourier series terms used to model the step changes. Motashar devoted a large proportion of his time to examining solution convergence and the sensitivity to the numbers of terms in the axial and circumferential directions. Some finite element work was carried out to examine the effects of the saddle flexibility. This work was an extension of both White and Ong.

Tolson[58] provided a further version of the computer programs to run on the SUN workstation running UNIX. Her analysis included the case of the saddle support not welded to the vessel and incorporated the use of friction effects. She also included the discretisation of the saddle across the width as used by Motashar. Using the finite element method, the flexibility of the steel saddle with rubber interface was modelled, this being somewhat more realistic than the simplified analysis carried out by Warrender. But most significantly, her contribution was to extend the analysis to cover the case of the orthotropic GRP vessel containing a number of composite layers. Much of her work was verified by her own experiments carried out on full-size vessels.

In this section, the general solution is summarised and presented for the saddle support problem. This consists of two main steps, the first being the determination of the interface pressures between the saddle and vessel. In the second step, the interface pressures or reactions are applied as known external forces to the case of a cylinder which is simply supported at its ends. The resulting stresses and displacements may therefore be determined at any point on the vessel. Since there is no closed form solution to the determination of the saddle/vessel interface pressures

an appropriate solution must be obtained by assuming that the distribution of the pressure can be simulated by a finite number of unknown discrete forces.

The following assumptions are made.

1. Deformations are small.
2. The vessel and support are linear elastic.
3. The contacting surfaces are smooth with matching curvatures and thus have continuous first derivatives.
4. Each contact node is capable of exerting normal and tangential reaction forces.
5. For the present case, the interface pressure distribution is assumed constant across the saddle width. However, Motashar and Tolson assumed a discretized variation across the width.
6. There is no relative slip between contact nodes.

5.2 Interface Pressure Distribution

The interface pressure distribution and its modelling presents a key area of investigation in the saddle support problem. If it is not modelled correctly, the resulting stresses will not be realistic. If the distribution is incorrect, the maximum stresses may occur at locations other than the horn, typically beneath the saddle in some cases. This implies that, in real cases, a fatigue crack could initiate and propogate undetected, originating from the weld on the internal underside of the saddle. If the contact interface pressure distribution is correct but has the wrong magnitude, then the determination of the fatigue life may be in error by a significantly large amount since the allowable fatigue life is plotted against stress range on a log-log scale.

In order to determine the interface pressures between the saddle and the vessel, the saddle contact area is divided into a number of discrete areas, each of which is subject to unknown uniformly distributed pressures in both the radial and tangential directions. For ease of calculation, the early work carried out by Tooth *et al* assumed that these pressures were of constant magnitude across the saddle width. This assumption is such that the saddle has a degree of flexibility in the radial direction across the width and is comparitively stiff in the axial direction, therefore avoiding

pressure high spots across the width. The discrete areas used in this type of analysis therefore consist of a range of uniform pressure patches disposed round the saddle arc and of axial length equal to the saddle width.

A more complete analysis has been provided by Motashar. In this treatment, the saddle width was subdivided into a number of discrete areas as shown in Figure 5.1. Three cases were analysed with 3, 5 and 7 discrete areas across the width. The three dimensional nature of the saddle was then considered in the generation of the flexibility matrix of the support.

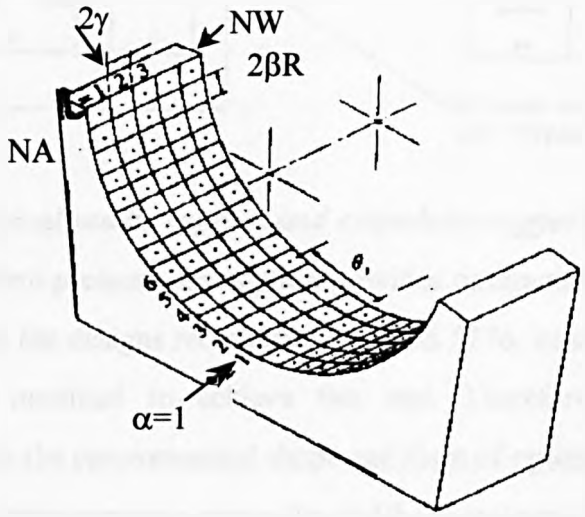

Figure 5.1 Saddle interface showing discretisation across width (after Motashar)

It was found that when a saddle with substantial radial stiffening was employed the interface pressure had peak values at the edges of the support. At the other extreme, when the saddle top plate was not adequately stiffened, peak values of the interface pressure occurred at the saddle centre profile with zero values at the edges. Neither of these saddles provides optimum support to the vessel. It could well be that many of the saddle designs suggested in the dimensional standard BS 5276[63] (and shown in Figure 5.2) i.e. having a central web with top and bottom plates in the form of a stiffened 'I' beam, fall within this latter category. That is to say, in general they do not provide support at the edges of the saddle. These saddles can be improved by stiffening the projecting web at the saddle horn with an end plate.

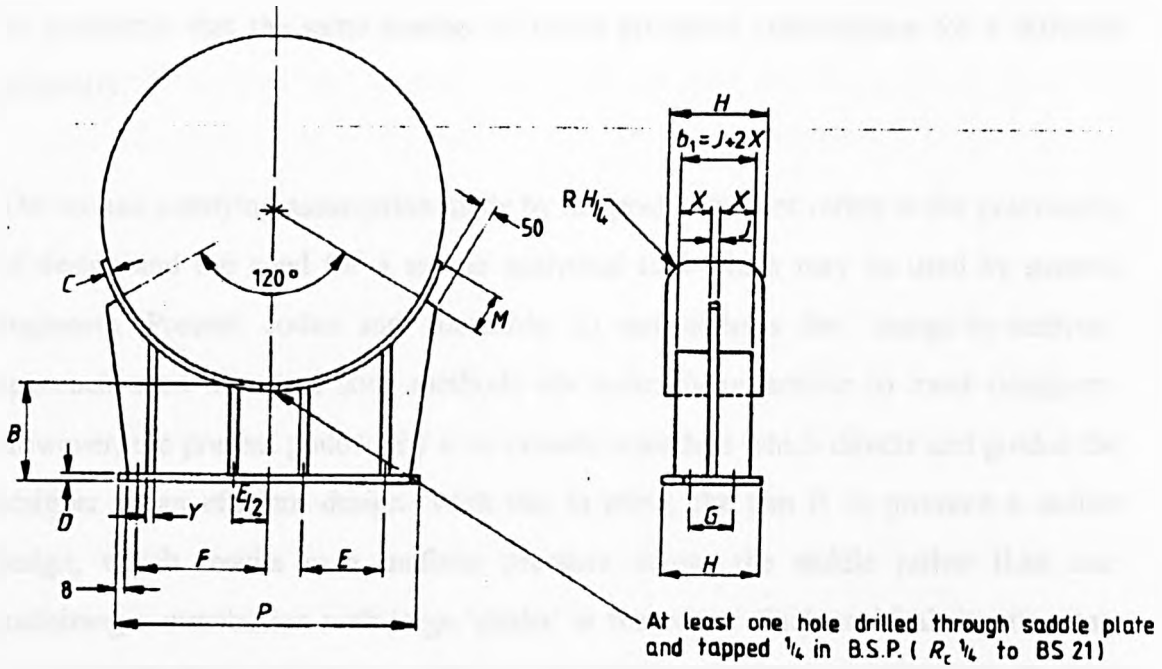

Figure 5.2 Typical saddle support and extended wrapper plate (after BS 5276)

Since the uniform pressure assumption provides optimum support for the vessel, it is considered that the designs recommended in BS 5276, as shown in Figure 5.2, should ultimately be modified to achieve this end. Therefore, in anticipation of this improvement to the recommended shape and form of optimum saddle, the assumption of uniform interface pressure across the width is employed in the present work.

The present author realises the importance of correctly discretizing the saddle interface pressure profile both in the circumferential and axial directions. However, for the purposes of the present work, the assumption of uniform pressure across the width is made. This is justified in two ways. Firstly, the uniform interface pressure distribution analysis is somewhat simpler and for the purposes on the parameter study, takes considerably less run-time than the '**variable pressure across the width**' solution. The sensitivity of the more complex solution is noted by both Motashar and especially Tolson who comments, ***'Convergency should be checked for any vessel to be considered to establish the correct number of terms used to obtain an accurate solution.'*** Motashar found that there could be a wide variation in answer depending on the number of terms and the number of discretized patches used, i.e. if say, 200 terms in each series were used for a particular geometry and configuration, there was

no guarantee that the same number of terms produced convergence for a different geometry.

The second justifying assumption made by the present author refers to the practicality of design and the need for a simple analytical tool which may be used by general engineers. Present codes and standards do not address the 'design-by-analysis' approach used here and such methods are normally unfamiliar to most designers. However, the present philosophy is to present a method which directs and guides the designer to an efficient design. With this in mind, the aim is to produce a saddle design, which results in a uniform pressure across the saddle rather than one containing a distribution with large 'peaks' at the edges. Such an ideal situation can be achieved by introducing a new design of saddle that introduces an element of radial flexibility across the width and avoids the hard edge of the rigid saddle. Some comments are made regarding the design, which incorporates a treatment of the saddle flexibility across the width in Chapter 9 of this work.

The analysis used here, therefore, assumes a variable pressure distribution around the saddle arc angle and a uniform pressure profile across the saddle width. This is similar to that used by Ong. A typical distribution of the interface pressure around the arc angle is shown typically below in Figure 5.3.

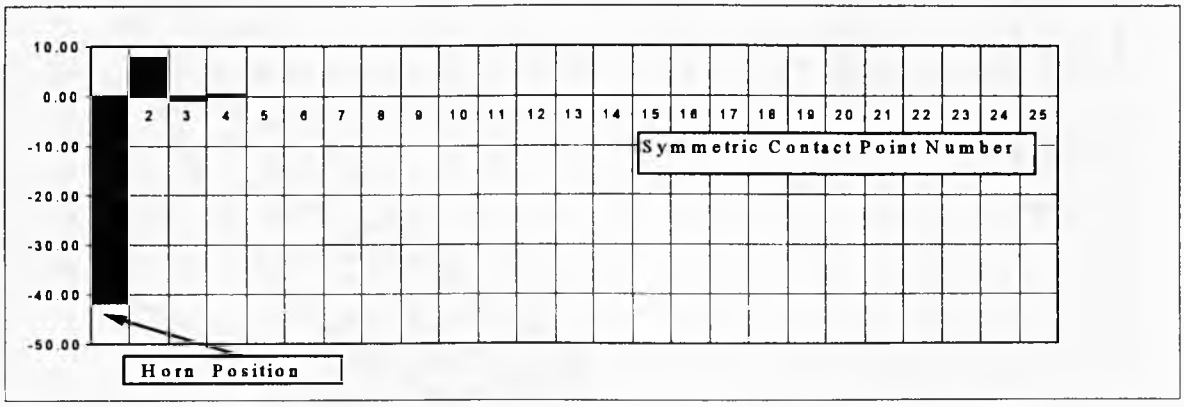

Figure 5.3 Interface pressure profile for 50 contact areas on a rigid saddle

The figure above shows that values of radial interface pressure at the saddle centre profile for the discrete contact areas round the saddle arc. In this, it can be observed

that there are large concentrations of pressure acting towards the horn of the saddle. These concentrations also change sign which indicates that the vessel is deforming dramatically in that region. In fact, the pressure profile distribution is one indicator used to determine the required level of flexibility needed to reduce the maximum stresses that occur at the horn.

The number of contact areas can be varied. If the number of discrete areas increases, these can be, in some cases, a more accurate representation of the interface pressure profile. However, using 50-60 interface pressure contact points has been shown acceptable for most cases. If significantly more discrete areas are introduced into the analysis, the number of Fourier terms in the circumferential direction must be increased to cope with the smaller patch size. Figure 5.4 shows the layout of these discrete areas.

The following diagram shows the saddle and the distribution of the discrete areas around the saddle width.

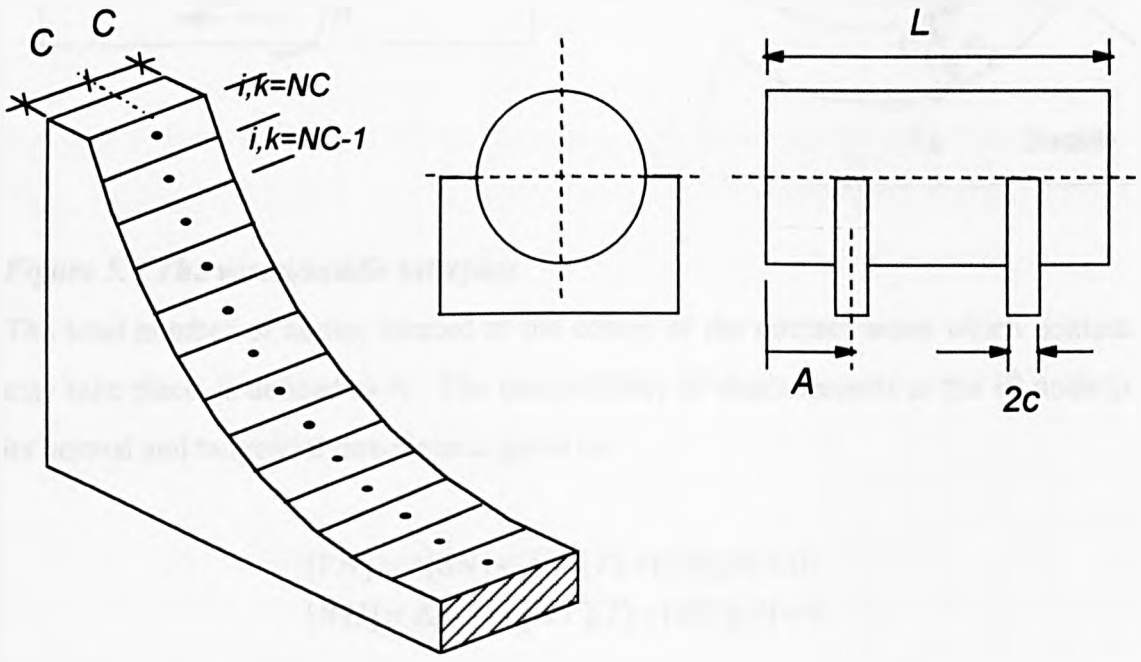

Figure 5.4 Saddle and distribution of the discrete areas around the saddle width

5.3 Compatibility of Displacements for Two Bodies in Contact

The present solution caters for the case where the saddle is located symmetrically around the vessel circumference, although the Ong solution can handle the unsymmetric case. Since in this work the symmetric case is considered, only half of the saddle angle need be considered and subsequently discretised. The compatibility of the radial and tangential displacements caused by the interface pressure forces at the centres of the discrete areas is enforced.

The basic contact problem is shown in Figure 5.5 below:

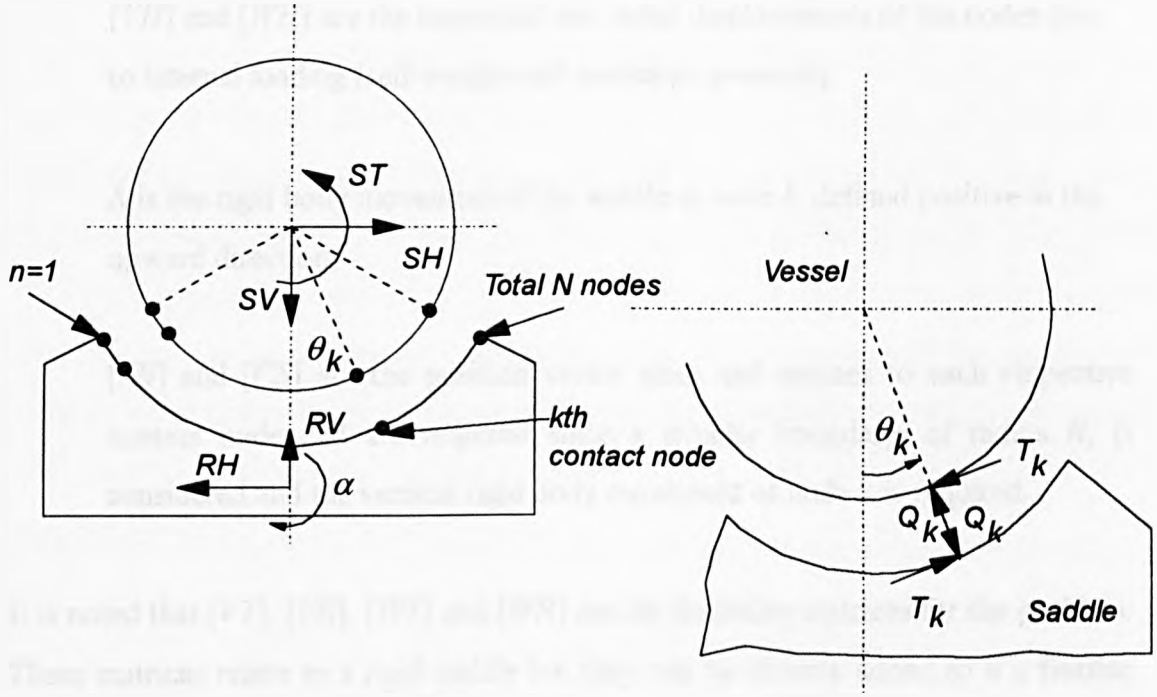

Figure 5.5 The vessel/saddle interface

The total number of nodes, located at the centre of the contact areas which contact may take place, is defined as N. The compatibility of displacements at the k^{th} node in its normal and tangential directions is given by:

$$[VH] = \Delta[SN] + [VT][T] + [VR][P] = 0$$
$$[WH] = \Delta[CS] + [WT][T] + [WR][P] = 0 \qquad \textbf{(5. 1)}$$

where:

$[T]$ and $[P]$ are the tangential and radial interface pressures,

$[VT]$ and $[VR]$ are the tangential displacements of the nodes due to tangential and radial interface pressures,

$[WT]$ and $[WR]$ are the radial displacements of the nodes due to tangential and radial interface pressures,

$[VH]$ and $[WH]$ are the tangential and radial displacements of the nodes due to internal loading (self-weight and surcharge pressure),

Δ is the rigid body movement of the saddle at node k, defined positive in the upward direction,

$[SN]$ and $[CS]$ are the position vector sines and cosines to each respective contact node and are required since a circular boundary, of radius R, is considered and the vertical rigid body movement of node k is required.

It is noted that $[VT]$, $[VR]$, $[WT]$ and $[WR]$ are the flexibility matrices for the problem. These matrices relate to a rigid saddle but they can be directly added to if a flexible system requires to be considered. This is done by directly inputting and adding to these matrices if a specific set of flexibility matrices is generated by external means, e.g. by experimental measurement or by the use of the finite element method. When a flexible system is considered, the equations therefore change to:

$$\begin{aligned}[VH]-\Delta[SN]+[VT][T]+[VTS][T]+[VR][P]+[VRS][P]=0\\ [WH]-\Delta[CS]+[WT][T]+[WTS][T]+[WR][P]+[WRS][P]=0\end{aligned} \quad \textbf{(5.2)}$$

where

[*VTS*], [*VRS*], [*WTS*], and [*WRS*] are the introduced flexibility matrices for the flexible support system.

Examples of a flexible system can include a fabricated flexible saddle or the use of a rubber interface on a rigid saddle. Any support system for which a small displacement flexibility matrix can be generated can be incorporated in the above analysis. This is discussed more fully in Chapter 9, where some examples of a flexible saddle are presented.

5.4 Equilibrium Equations

Having examined the compatibility of the system, the solution is completed by considering the overall equilibrium of the system. After the interface pressure solution is completed, the presence of the unknown rigid body displacement, Δ, means there are three unknowns and only two equations as defined by Equations (5.1) or (5.2). The third equation is introduced by enforcing the overall equilibrium of the system. By considering the equilibrium, the total weight , which consists of the vessel self-weight, weight of contents, and the end weight (if considered), must equal the sum of the vertical components of the interface forces previously determined. The equilibrium equation can be expressed as:

$$-[CS]^T[P]+[SN]^T[T]=S \tag{5.3}$$

where S is the total weight divided by $(16\beta RC)$, R being the vessel radius, C is the half saddle width and β the half saddle angle.

5.5 Interface Pressure and Stress Analysis Solutions

Since the unknowns are all now obtainable, it is possible to obtain various solutions. The first, as previously described, is the analysis for rigid supports. In this, all of the elements of Equation (5.1) are used. The second case is that of the frictionless saddle which is obtained by simply making $[T]=0$. For the frictional saddle, $[T]=\mu[P]$ where μ is the coefficient of friction between the saddle interface and the vessel.

Although no further reference is made to these solutions, they were first coded by the present author for Warrender in 1985.

These simple models can be back-substituted into Equations (5.1-5.3) and new expressions for the interface pressure [P] and the rigid body displacement, Δ, can be found. Having completed the solution for the interface pressure values, the resulting stresses must be evaluated. Using the interface pressures, a solution for the displacements, U, V and W of the vessel and the resulting stresses and strains can be found. For the case considered here, the stress resultants and displacements can be obtained using Equations (3.35a-i).

The loading terms can allow superposition of cases. Typical cases include internal surcharge pressure, hydrostatic fluid loading, vessel self-weight and external radial and tangential interface pressure loadings. Since the saddle has been subdivided into a number of discrete areas, then summation has to take place for all the centres of the discrete areas and their respective interface pressure values. This means that there is a summation within the loading coefficient term and an extra loop within the program.

Full details of the intermediate steps can be found in References [11], [16] and [58] and in the main comment steps within the program listings found in the Appendices.

5.6 Choice & Comparison of Loading System-Line, Patch& Line+Patch Models

From the work of Ong, it was found that two models were possible to relate the distribution of the interface pressure to the discretised area over which it acted. The first model was the '**Patch Load Model**'. In this, the interface pressure was assumed to act over the whole patch as previously described. However, in some cases, this did not give a good comparison with the experimental vessels. It proved useful in the rigid saddle case but somewhat poorer in the case of the loose saddle.

A better model for the loose saddle was the '**Line Load Model**'. In this, the total force did not act over the whole area but was summed to provide an equivalent line

force acting as a uniform line load at the centre of the area, i.e. at the contact node position. This provided much better agreement for those cases where the patch load model was found inadequate.

Ong covered these two cases separately. Here, in order to provide a good 'all-round' model for use as a design tool, which would provide realistic results for all cases, the **'Line+Patch Model'** has been developed by the author. This essentially comprises the patch load model but has the last patch on either horn expressed as a line load acting at the centre of the outer area as shown in Figure 5.5. This solution tends to model the rigid edge effect which occurs at the horn of the saddle and as a result presents the more severe and hence conservative result for designers.

The **line+patch model** has been used throughout this work for the generation of parametric data for use in the design method.

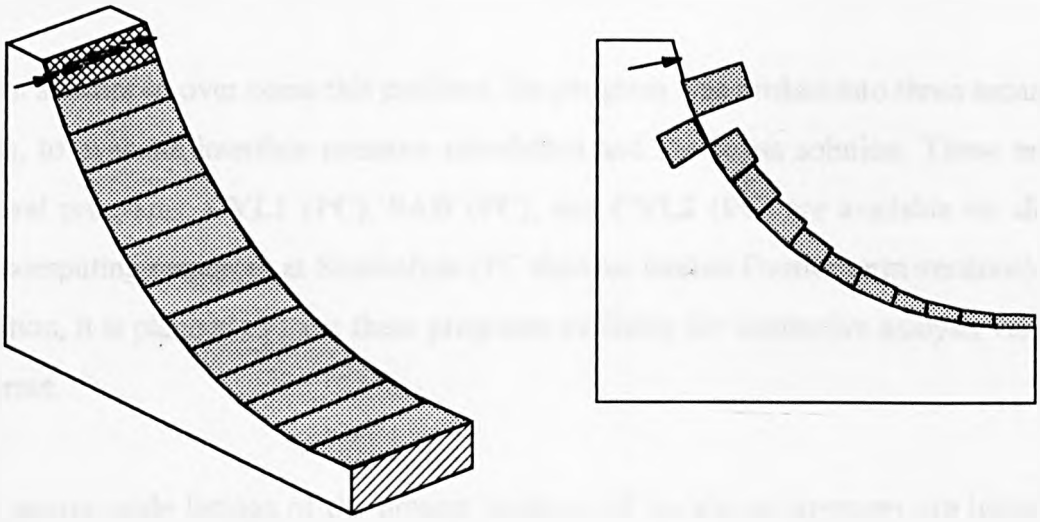

Figure 5.5 Line + patch model schematic showing typical interface distribution

5.7 Computer Programs

The original computer programs based on Sanders' theory were developed by Ong. Since then most of the researchers at Strathclyde have modified or adapted these programs to suit various machines or to incorporate specific routines or capabilities which were not originally available.

Ong's programs have been substantially changed by the present author for some of the subsequent workers. Most of these changes have required recoding for different operating systems, MS-DOS and UNIX variants, and for different versions of Fortran. Some moves have been made towards a rewrite in the C language, for porting to a Windows version, has taken place although this is not complete as yet.

The computer programs now run on Sun and Silicon Graphics workstations and also on the PC. The PC version of the program requires carefully manipulation due to the 640K memory limit and since no overlays have been used, only a restricted number of terms can be incorporated ie. around 300 terms in each direction. This limit is due to the size of the arrays, which require to be open at any given time in the solution. With a modern PC, solution times with 300×300 for a single point can be evaluated in tens of seconds with a typical analysis, searching for the maximum value over a grid of discrete points being solved in less than five minutes.

As an attempt to over come this problem, the program was broken into three separate parts, to evaluate interface pressure calculation and the stress solution. These more general programs, **CYL1 (PC)**, **SAD (PC)**, and **CYL2 (PC)** are available on all of the computing resources at Strathclyde (PC denotes limited Fourier term versions). In addition, it is planned to have these programs available for interactive analysis via the Internet.

The source code listings of the present versions of the above programs are included as Appendices 1, 2 and 3 respectively.

6 A PARAMETER STUDY AND DESIGN METHODOLOGY FOR THE TWIN SADDLE PROBLEM

6.1 Introduction

It is generally accepted that the existing design procedure for the design of twin saddle supported vessels does not provide a rigorous method of determining the maximum stresses at the most critical regions. This means that the stresses obtained from the procedure cannot be used with adequate certainty for use in determining the fatigue life assessment of the component.

Although current international design codes have made available a **'design'** method for twin saddle supported vessels, based on the work of Zick[2] in 1951, the approach is semi-empirical and was validated experimentally for a limited number of relatively small diameter (approx. 6ft. dia.) vessels. Despite this, it has been in use for many years and has been used successfully to design larger diameter vessels even though Tooth has shown, in certain cases, that the actual maximum stresses at the horn indicate the Zick method is unconservative, with an error as high as 50%.

The success of the Zick method in design is due to its relative simplicity and that it can be performed by hand. It is also partly due to the reduced allowable stresses quoted in the design codes, which seem to counterbalance the apparent error in the method. For example, in the case of the maximum stress intensity at the horn, which is a secondary bending stress, the British Standard BS 5500 permits an allowable stress intensity of ***1.25f***, where ***'f'*** is the design strength for the material, based on approximately two thirds of the yield strength of the material. If a more rigorous assessment is employed, the British Standard permits, through rules in the ***'design-by-analysis'*** section, Annex A, secondary bending stress intensities to rise to ***3f***.

However, although the Zick method can be, and has been, effectively used for design, it remains necessary to provide a more accurate design tool for use in safety and integrity assessments especially where **fatigue failure** may be prevalent. In such assessments, accurate maximum stresses are required in order to predict the

appropriate fatigue life of the vessel. Accurate stresses may be obtained using the SADDLE programs described previously, however, that procedure is complex and requires to be computer based. Moreover, it can take some considerable time to perform a full design study, especially where multiple runs are envisaged, i.e. when altering the different parameters and trying to optimise the saddle/vessel configuration. Therefore, as a design tool, it is preferable to have a suitable hand calculation method, or at least one that can be easily computerised on a PC either by direct programming or through the use of a simple spreadsheet.

The aim of this chapter is therefore to present the philosophy and scope for a new design methodology and parameter study with the objective of producing a simplified analysis based on the output from the SADDLE program.

6.2 Scope of the Study

With the aim of providing a new design methodology, a reasonable starting point is the generation of accurate stress data from the SADDLE program. The rigid saddle case is considered since this produces the maximum stresses. This data must then be examined for variations and trends that will, after defining the main governing parameters, highlight any geometric relationships and their interdependence. Thereafter, these parameters must be isolated and their individual influences examined and quantified. This procedure has the advantage of allowing the effect of any individual parameter to be understood since it may be varied when performing a design study. Therefore, it is essential that specific tasks be identified, in determining the scope of the study, which target the desired effects and influences.
The specific tasks identified have been categorised as follows: -

1. To carry out a comprehensive parameter study for the maximum horn stress and its location using the present SADDLE analysis for the twin saddle supported vessel.
2. To examine other areas of the vessel in accordance with those areas identified by the British Standard BS 5500.

3. To study the influence of the vessel ends upon the maximum stresses that occur at the support regions. This to be undertaken using finite element techniques to represent the variation in flexibility of different end types and differing locations of the support for the end.
4. To present the results from the above in a suitable form to assist the design methodology.

6.3 Maximum Stress Locations

From a study of the stress system of the twin saddle supported vessel, the maximum stresses generally occur in the horn region of the saddle support. These stresses often reach their maximums in the vessel during the hydraulic test and in some instances, under operating conditions. The maximum stress is known to be the circumferential stress component located at the outside surface of the horn region of the vessel. The horn is defined as the uppermost point of the saddle when viewed along the vessel axis as shown in Figure 6.1

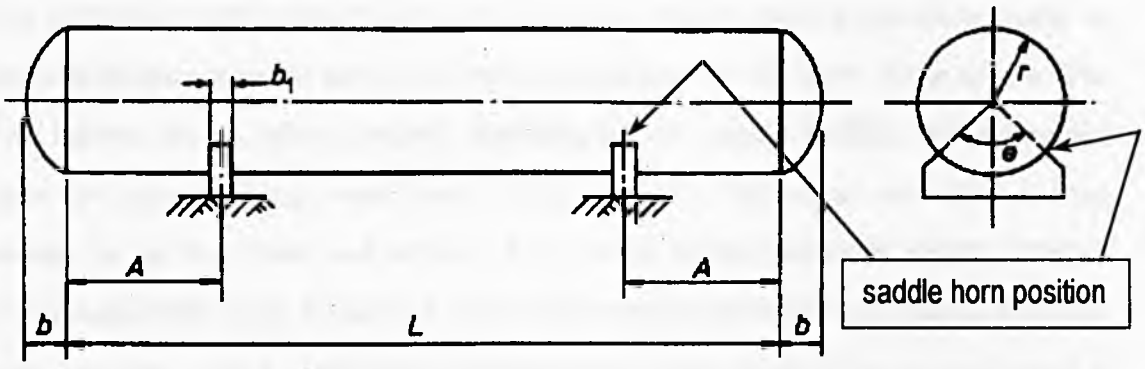

Figure 6.1 Location of the assumed maximum stress position ~ the saddle horn

From a study of the literature, previous investigators assumed that the maximum stress occurs exactly at the horn of the saddle, that is to say, if the saddle wraparound angle θ were 120^0, then the maximum stresses are found to be located in the circumferential direction on the outside surface of the vessel adjacent to the weld or at the edge of the saddle if not fully welded.

At the start of this parameter study, the present researcher wrongly followed this approach and carried out extensive studies based on this assumption. The result of

this was that when carrying out tests for the location of the maximum stress, in most instances, the position maximum stress did not necessarily fall at the exact horn location.

In order to provide the correct maximum values for use in the parameter study, irrespective of location, results were output every 1/10th of a degree in order to examine the exact location of the maximum stress. The survey region analysed was defined by the position of the saddle horn angle and a results zone, upto five degrees either side of the horn edge was examined. It was found that, depending on the flexibility of the system and the size and width of the contact areas, the maximum stress location varied from the horn position by up to one or two degrees. In fact, most results showed the maximum stress location to lie just under the saddle edge. This location of maximum stress has not been examined experimentally since it is difficult to position a suitable strain gauge in this region.

The parameter study carried out, and reported in this chapter, is therefore based on actual maximum stresses and not on stresses measured at the horn of the saddle. The two figures shown below present distributions of outside surface circumferential stress for a typical 'long vessel' case. A 'long vessel' is defined as one which is long enough to be free from end effects. As a result of the increased length, stresses become artificially high. Figure 6.2 details the variation in the circumferential direction and shows that, for a saddle horn position of 60°, the maximum measured stress is located just to the left of the 60° position, as mentioned earlier. Figure 6.3 shows the variation of circumferential stress along the length of the vessel plotted at the location of the horn of the saddle. From this study and a detailed investigation of the location of the maximum, it was observed that the maximum stress was located at the horn ± 1 to 2°.

Since the circumferential stress is the most significant and therefore most important for the majority of cases, only this stress will be described in further detail.

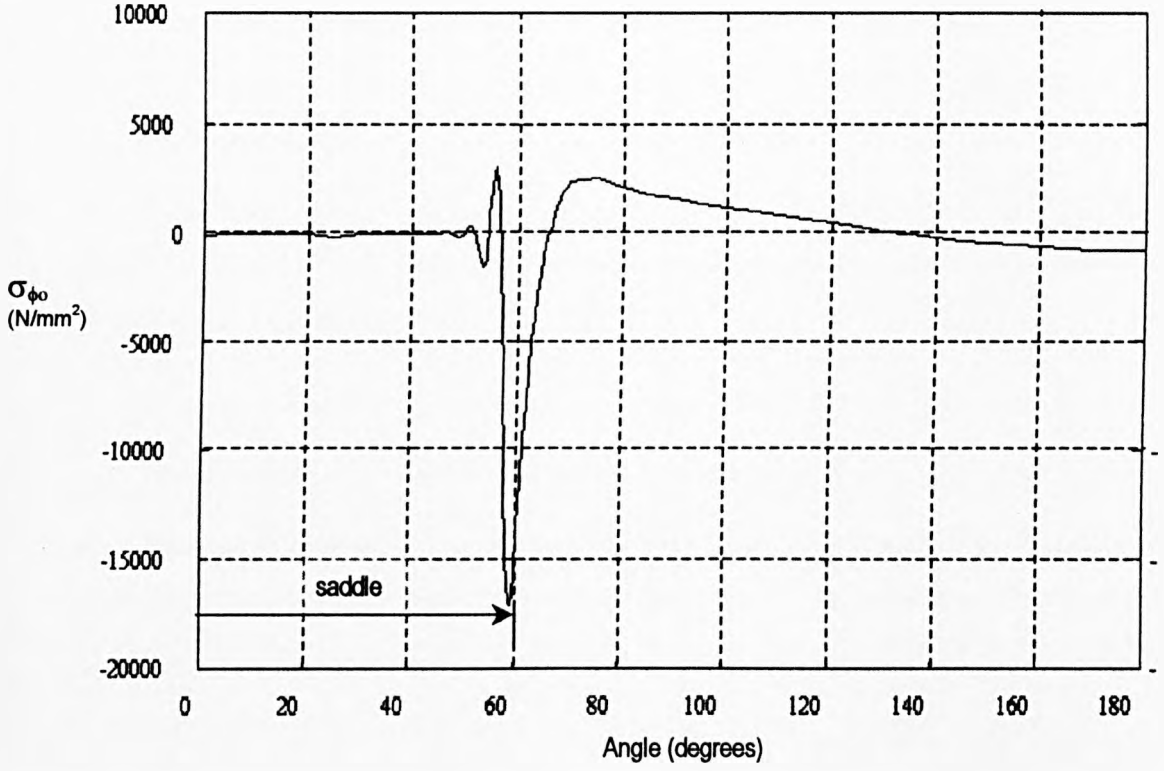

Figure 6.2 Circumferential stress distribution in the circumferential direction

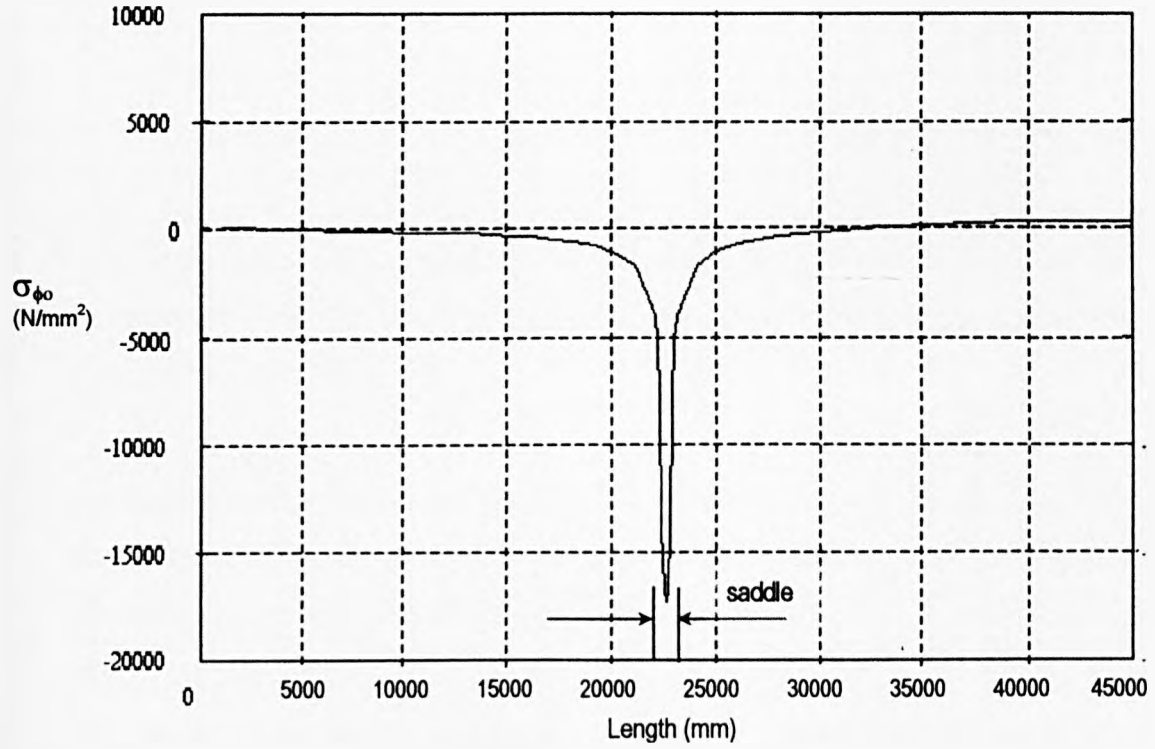

Figure 6.3 Circumferential stress distribution in the longitudinal direction

6.4 Distribution of Interface Pressure Across the Saddle Width

For the present analysis, it is assumed that the saddle design is such that a uniform interface pressure is present between the saddle wrapper and the vessel shell. In some cases of saddle design, a poor distribution of interface pressure results and peak values arise at the hard edges of the saddle across the width. Where a rigid saddle support has been used then a complete analysis using the approach suggested by Motashar is recommended.

6.5 Influence of the Number of Terms & Discrete Areas

According to the theory used for the calculation of the stresses and displacements, three numeric parameters have a significant importance on the results. These comprise the double Fourier series term numbers, **'m'** and **'n'**, which are associated with the sine and cosine series respectively and also the number of discrete areas, **'N'**, into which the contact surface between the saddle and the vessel is divided. The effect of each of these parameters must be examined prior to commencing the parameter study. Firstly, the double Fourier series expansion for the loading system representation is written as follows:

$$P_{m,n} = \sum_{m=0}^{\infty}\sum_{n=0}^{\infty} P \sin\frac{m\pi x}{L}\cos n\phi \; d\phi\, dx \qquad \textbf{(6. 1)}$$

From this expression, it is clear that the 'm' coefficient influences the loading in the longitudinal direction and 'n' is associated with the loading profile in the circumferential direction.

Obviously, the number of terms which are chosen for both the 'm' and 'n' values will have a great influence on the value of the maximum stress results obtained. This can be clearly seen, for example, if a cylindrical shell subject to a single rectangular radially loaded patch is chosen, as per the solutions described in Chapter 4. If the problem is modelled using a double Fourier series approach, it is evident that the greater the number of terms used, the more accurate the loading representation, and

therefore the stresses obtained. In single patch-type problems, even when say 100 terms are used, there can be a significant lack of agreement between the ideal loading distribution and the Fourier representation. This is shown in Figure 6.4. It is also dependent on the ratio of the patch size to the main dimension to which the Fourier function is fitted, i.e. vessel length in the longitudinal direction and vessel circumference in the circumferential direction.

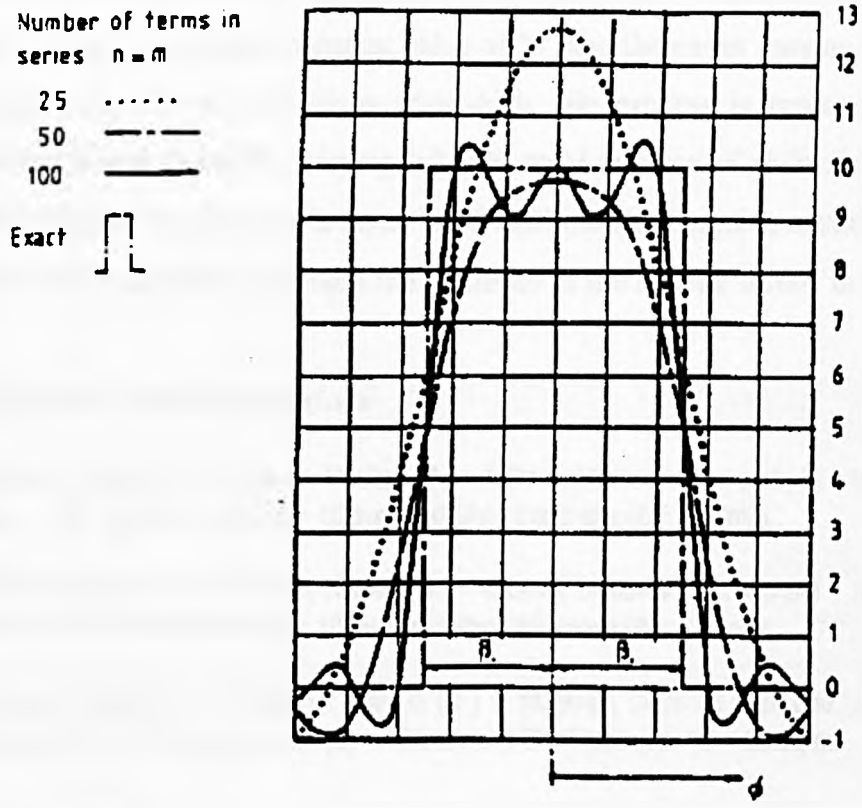

Figure 6.4 Fourier series representation of rectangular loaded patch (after Duthie)

Figure 6.4 shows the graph of the Fourier series expression shown as Equation 6.1 when viewed in the circumferential direction. A magnitude of load of 10 units is desired and each trace represents the function for an input number of terms, 25, 50, and 100. As the number of terms increases, it can be seen that the graph of the function becomes nearer the exact 'step-function' solution.

Although previous researchers had used 100 terms in each series, the optimum number of terms for both 'm' and 'n' must be determined. This is set against the criterion of achieving the desired accuracy, whilst maintaining a reasonable computing solution time for the calculation.

For the purposes of comparison, three typical 'real' vessel geometries are selected for comparison, these corresponding to cases tested experimentally by Tooth, with documented stresses obtained from strain gauge readings. A comparison of experimental and analytical results is found later in Table 6.8. The effects of varying 'm' and 'n' are investigated using the dimensions of Case 1. The convergence of the Fourier series and the significance of each of the Fourier terms is examined by choosing a fairly large constant value of 'n' and thereafter varying 'm' over a suitable range, say, 50 to 600 terms afterwhich, the process is repeated by keeping 'm' constant and thereafter varying 'n'. The total number of divisions used to represent the load used in this case is equal to 60 uniform sized patches around the saddle angle. The following tables highlight the influence of the Fourier terms 'm' and 'n'.

Test Case Vessel Dimensions

Case 1: Length (***L***) = 7315mm, Radius (***R***) = 458mm, Distance from end (***A***) = 1410mm, Saddle angle (θ) = 150°, Saddle width (***b***) = 102mm and Shell thickness (***t***) = 3.33mm.

Case 2: Length (***L***) = 7315mm, Radius (***R***) = 458mm, Distance from end (***A***) = 1410mm, Saddle angle (θ) = 150°, Saddle width (***b***) = 102mm and Shell thickness (***t***) = 4.67mm.

Case 3: Length (***L***) = 54858mm, Radius (***R***) = 1829mm, Distance from end (***A***) = 6858mm, Saddle angle (θ) = 162°, Saddle width (***b***) = 762mm and Shell thickness (***t***) = 26.6mm.

m terms	50	100	200	300	400	600
Max. Stress (N/mm^2)	-258.45	-261.9	-258.2	-257.03	-257.42	-257.41
Location (degrees)	74.3	74.3	74.3	74.3	74.3	74.3

Table 6.1 Influence of parameter 'm' for constant n=200 and 2N=60 (for Case 1)

n terms	50	100	150	200	300	400
Max. Stress (N/mm^2)	-247.5	-258.64	-258.26	-257.41	-258.24	-257.77
Location (degrees)	74.1	74.3	74.3	74.3	74.3	74.3

Table 6.2 Influence of parameter 'n' for constant m=600 and 2N=60 (for Case 1)

It can be seen from Tables 6.1 and 6.2 that an increase in 'n' above, say 50 to 100 terms, does not lead to a significant variation in the stress values obtained. Similarly, a

value above, say 200 terms in 'm', produces little or no effect in the stress results obtained. However, although m = n = 200 would provide a very accurate solution for Case 1, it is noted that this is a relatively short vessel and has a moderately loaded patch size. That is, *L/R* is small and *b/L* is high, therefore the number of terms required to achieve convergence is low. A similar behaviour was noted for Case 2.

However, it is recognised that for longer vessels where the patch size to vessel length ratio is much smaller, a much higher number of terms in the longitudinal direction ('m' terms) will be required to adequately represent the loading distribution. When considering Case 3, this effect was quite pronounced. In this case, a significantly longer vessel length was used, and the governing sine series parameter, 'm', was increased to 600 to provide an adequate load representation.

m terms	50	100	200	300	400	600
Max. Stress (N/mm^2)	-416.72	-421.29	-413.22	-409.43	-410.91	-410.78
Location (degrees)	80.5	80.6	80.5	80.6	80.6	80.6

Table 6.3 Influence of parameter 'm' for constant n=200 and 2N=60 (for Case 3)

n terms	50	100	150	200	300	400
Max. Stress (N/mm^2)	-	-410.17	-409.85	-410.78	-411.63	-411.58
Location (degrees)	-	80.5	80.5	80.6	80.6	80.6

Table 6.4 Influence of parameter 'n' for constant m=600 and 2N=60 (for Case 3)

With this in mind, the full parameter study, which is based on artificially long vessels was carried out using 600 'm' terms in the longitudinal direction and 200 'n' terms for the circumferential direction. This was justified by extending the full range of the investigation of the influence of the 'm' and 'n' parameters over the range ($100 \leq m \leq 800$; $100 \leq n \leq 500$). After carrying out this investigation, it was decided to fix 'm' at 600 terms and 'n' at 200 terms for the parameter study for an optimum solution, i.e. providing sufficient accuracy in a reasonable computing time. The time per scan of 20 points on a Silicon Graphics 4D-35G workstation is approximately 7.5 minutes.

The significance of the number of contact patches required for a reasonable solution must also be examined. A logical method of determining the total number of discrete contact areas, $2N$, may be to represent both the maximum stress and the stress at the horn as a function of $\frac{\beta}{2N}$, where β is the total saddle wraparound angle and $2N$ is the total number of discrete areas on the saddle, and then to take the extrapolated converging value between the two obtained curves. This method is based on the assumption that the maximum stress should normally be located at the horn of the saddle. The required value of $2N$ would result in convergence of the two curves. Some tests of these methods were made for the three actual vessel geometries described earlier and the variation of maximum stress and horn stress against $\frac{\beta}{2N}$ for the $2N$ range 30 to 110 is plotted below.

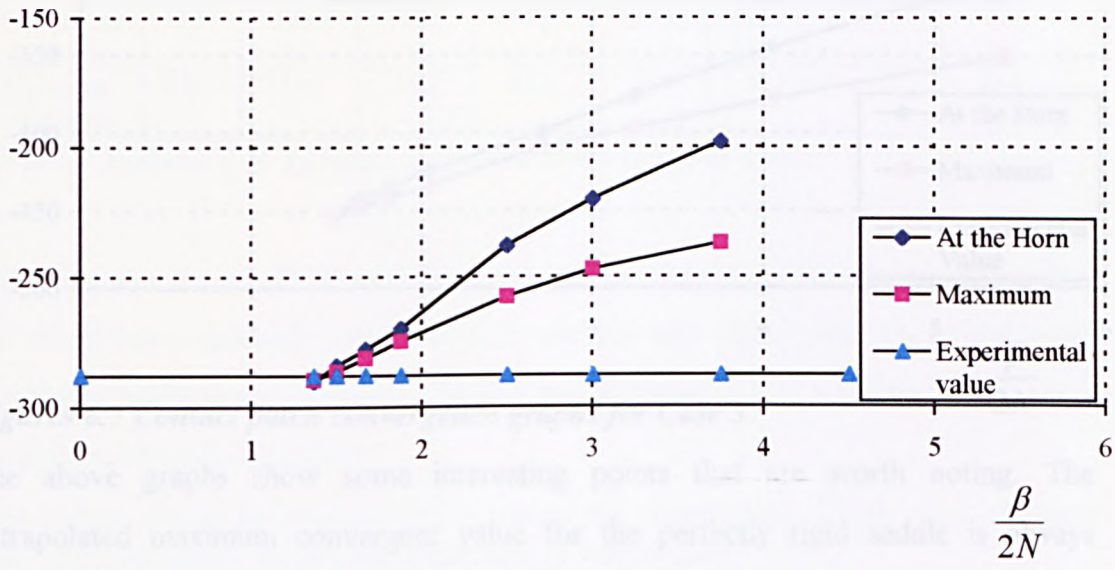

Figure 6.5 Contact patch convergence graphs for Case 1

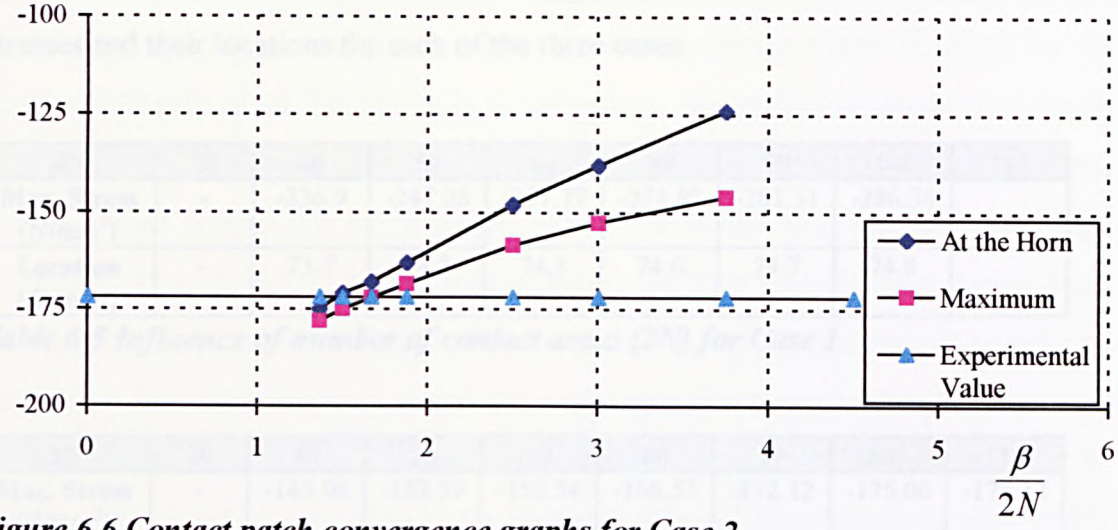

Figure 6.6 Contact patch convergence graphs for Case 2

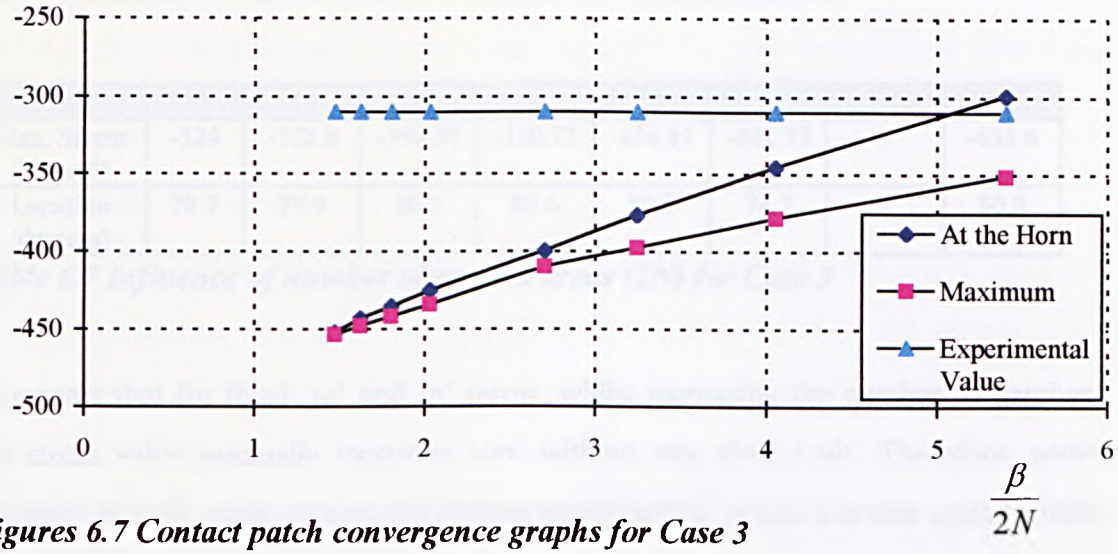

Figures 6.7 Contact patch convergence graphs for Case 3

The above graphs show some interesting points that are worth noting. The extrapolated maximum convergent value for the perfectly rigid saddle is always greater than the measured experimental value found for the vessel supported on real saddles. In addition, these cases presented here represent the most stiff saddle configurations and real saddles would allow a reduction in the limiting value. A reasonable maximum number of contact areas could be perceived to be around 50-60, by ensuring $\frac{\beta}{2N} = 1.5$ or so. In Case 3, the experimental value is much lower than the converging curves. The saddle used in for this case was of a semi-rigid nature and had

a degree of radial flexibility. The following tables show the calculated maximum stresses and their locations for each of the three cases.

2N	20	40	50	60	80	90	100	110
Max. Stress (N/mm^2)	-	-236.9	-247.28	-257.77	-274.93	-281.31	-286.36	
Location (degrees)	-	73.7	74.3	74.3	74.6	74.7	74.8	

Table 6.5 Influence of number of contact areas (2N) for Case 1

2N	20	40	50	60	80	90	100	110
Max. Stress (N/mm^2)	-	-145.96	-152.59	-158.54	-168.53	-172.12	-175.08	-178.12
Location (degrees)	-	73.6	74.2	74.3	74.6	74.7	74.8	74.8

Table 6.6 Influence of number of contact areas (2N) for Case 2

2N	20	40	50	60	80	90	100	110
Max. Stress (N/mm^2)	-324	-378.8	-398.59	-410.75	-434.11	-441.73	-	-453.6
Location (degrees)	78.7	79.9	80.3	80.6	80.7	74.7	-	80.8

Table 6.7 Influence of number of contact areas (2N) for Case 3

It appears that for fixed 'm' and 'n' terms, whilst increasing the number of patches, the stress value gradually increases too, without any clear limit. Therefore, some measure must be made against the known experimental values and this used to limit the number of contact patches.

(The values shown in brackets are included for comparison. These were obtained using the new design method detailed later in this chapter)

Units (N/mm^2)	**Experimental Stresses**		**SADDLE Program for Rigid Saddle, (2N=50)**		**BS 5500**
	Flexible	Rigid	Computer	**Design Method**	
Case 1	-120	-290.5	-247.35	*(-237.27)*	-120.7
Case 2	-70.4	-174.7	-152.59	*(-148.06)*	-63.1
Case 3	-186.2	-310.2*	-398.59	*(-393.80)*	-194.7

Table 6.8 Comparison of maximum stresses obtained by the various methods.

* denotes the use of the semi-rigid saddle

For the first two cases shown, the stress found either by the SADDLE program or by the design methods appears to lie between the experimental values obtained for the rigid and flexible cases. For the third vessel, that is, the longest of the three, it would appear that only 20 patches seem necessary. It is noted that, in this case, the saddle was not rigid around the entire saddle angle. The saddle was formed from a rigid saddle (150°) with two 6° flexible extensions on the wear plate forming a total angle of 162°. It should be stated that for the actual vessels, the saddles are not completely flexible or rigid and therefore, it appears reasonable that the solution obtained using 50 discrete areas per saddle would be of sufficient accuracy for most applications. In addition, this leads to a solution in a reasonable time, whereas solutions with higher numbers for m, n, and 2N can be over twenty minutes per point.

In conclusion, for the parameter study, the numbers of Fourier series terms were fixed at m=600 and n=200 with the number of discrete areas per saddle at 2N=50.

6.6 Parametric Studies

A full parameter study for the hydraulic case is presented since this loading condition generally produces the highest value of stress in the horn region of the vessel. There are a number of geometric parameters that require to be investigated in order to identify the effect each has on the maximum stress and indeed, on each of the other parameters. The effect of each variable is required in order to provide a versatile design procedure.

For general design of twin saddle supported pressure vessels, the use of the Fourier series technique provides a solution in a shorter time than using, say the finite element technique. However, the time taken can still be considerable using the Fourier series approach, especially if many design iterations are required. The decision was therefore taken to provide results for the maximum stress (i.e. the circumferential stress at the horn) as provided by the SADDLE program in a closed form - i.e. by a single equation, if this were at all possible. The requirements of such an equation would be to incorporate all the results of the parametric survey and allow the engineer to optimise the design by varying any individual parameter. It is noted that the design

method proposed by Křupka used an equation, which can be directly extracted from his analysis. This equation is shown in Chapter 2 as Equation (2.2). However, since the present treatment is based on a more complex numerical approach, there is no **'natural'** single equation or expression, which can characterise or represent the behaviour and interaction of the various parameters.

It is also noted at this point, that a similar method to the present work has recently been published by Ong[21]. In this, he attempts to **'force'** a single equation by defining a basic stress in the form of the Křupka equation and thereafter to provide a series of modification factors which correct the basic stress value and ultimately give similar answers to the output from the Fourier series program since Křupka made use of a 'semi-bending' shell theory. The present author does not believe this to be a realistic approach since forcing these results into the form proposed by Křupka may introduce unnecessary errors by the curve fitting procedures employed. The approach suggested herein, developed in 1990 and published in 1991[60] is to obtain a basic stress, which 'naturally' results from the plotted variation of maximum stress. This basic stress is thereafter progressively modified by a number of geometric and physical factors. The suggested form of the equation is written as:

$$\sigma_{max} = \sigma_b . F_w . F_b . F_\theta . F_A . F_D . F_L . F_e . F_f \tag{6.2}$$

where the coefficients of the equation are defined as follows:-

σ_b = peak stress at the horn for theoretical vessel (Basic Stress)

F_w = weight of contents factor

F_b = saddle width factor

F_θ = saddle wraparound angle factor

F_A = rigid end factor

F_D = saddle interaction factor

F_L = length change factor

F_e = end flexibility factor

F_f = saddle flexibility factor

These coefficients are discussed in detail.

It is worth noting that an allowance for the change in material properties is not explicitly mentioned in the equation shown above. It has been assumed, in the present analysis, that the vessel is fabricated from steel with a Young's modulus of 200,000 N/mm^2 and a Poisson's ratio of 0.3. However, some computer runs were carried out in order to investigate the effects of the material properties and it was found that the peak stress was independent of the Young's modulus value, E, and therefore this material constant is not included in parametric representation. It should be noted, however, that the vessel displacements and strain values **are** dependant on the modulus which would therefore need to be included in those cases where strain is the limiting criterion, as for GRP vessels. The influence of differing Poisson's ratios was found to be small and is therefore also neglected. This implies that the equation can be used for materials other than steel.

6.6.1 Basic Stress Values, σ_b

From some preliminary studies, it was apparent that the ends of the vessel have an important influence on the results obtained from the SADDLE program. In general, the vessel ends provide some support of the shell near the major plane of stiffening. This will in turn, affect the stresses obtained at the horn of the saddle. That is to say, as the support moves towards the vessel end, the effect of extra support for the cylindrical shell provided by the dished head will reduce the maximum horn stresses.

This effect was noted by Zick, and was incorporated in his analysis by using a reduction factor in the calculated stress. It was based on the ratio of the distance from the end of the vessel to the saddle centreline position to the vessel radius, A/R. Zick proposed that if the saddles were positioned such that A/R is less than a half of the cylindrical shell radius, then the stresses at the horn would reduce by a quarter. If the saddle were positioned up to A/R equal to a full radius, then linear interpolation would be allowed form the full value at A/R=1 to a quarter of the full value of maximum stress at A/R=0.5. Although this method appears to incorporate some stiffening factor

for the end effects, there is no theoretical justification for such an approach noted in the literature, and provided in the Standard, BS5500.

In addition, the problem is compounded by the fact that the Fourier series method, by definition, generates zero stresses and displacements at the ends, since the axial deformation is characterised by a sine series. Therefore, a graph of the sine function must have a zero value when the required location x, is equal to zero or L. This phenomenon can be physically represented as an infinitely stiff dished head.

Therefore, a first step in the identification of a basic stress was to eliminate the effect of the overstiff dished end. It was found that if the saddles were located at an appropriate distance of $9R$ from the ends the influence of the ends was negligible. In fact, the end effects were almost negligible after a distance approaching $6R$, but and additional $3R$ was introduced to ensure the stress effects had fully decayed, as shown in Figure 6.8

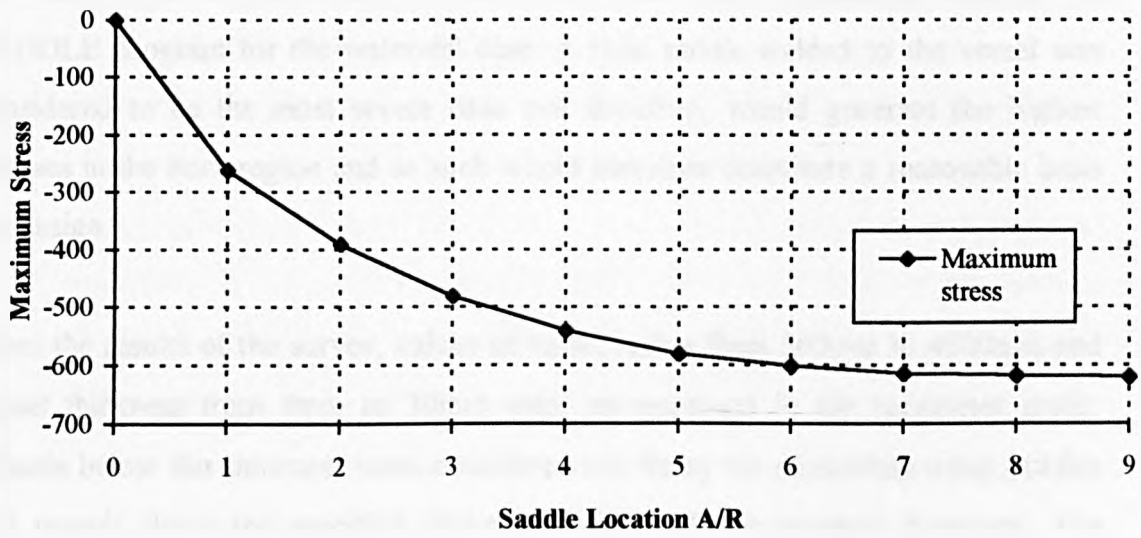

Figure 6.8 Graph of stress variation along extended vessel (L=36R)

Similar effects were also found in those cases where the two saddles were brought close together. Again, Zick incorporated this effect in his analysis by assuming that if the vessel geometry were such that $L/R>8$, no interaction would be present. However, if the vessel geometry were such that $L/R<8$ then the bending component of the stress would be multiplied by $8R/L$. In addition, industry standard convention is for the saddles to be positioned at approximately the quarter points of the cylinder, i.e.

A/L=0.25. In fact, finite element work done by the present author and also by Widera[18,19] shows that the optimum position is approximately A/L=0.22, this taking account of the extra weight introduced by the vessel dished head.

Therefore, the 9R end-effect length was doubled and found adequate to avoid saddle interaction. Thus to allow the saddle centreline parameters to be considered in isolation, a theoretical vessel of length equal to 36R was formulated. The saddles are therefore located at a distance of 9R from the ends. The maximum value of the stress at the saddle horn in this vessel is referred to as the Basic Stress, σ_b.

In order to define the scope of the parameter study, a survey was carried out and information was obtained from vessel designers and manufacturers in both the UK and USA. This identified a typical range of horizontal vessel sizes currently in use and supported on twin saddles. Using this information as a bound for radius and thickness, the basic stress for the series of theoretical vessels was obtained by running the SADDLE program for the water-fill case. A rigid saddle welded to the vessel was considered to be the most severe case and therefore, would generate the highest stresses in the horn region and as such would therefore constitute a reasonable basis for design.

From the results of the survey, values of vessel radius from 500mm to 4000mm and vessel thickness from 4mm to 30mm were encompassed in the parameter study. Vessels below this thickness were considered too flimsy for supporting using saddles and vessels above the specified thickness limit would be pressure dominant. The saddle angle and width were chosen to be 120 degrees and 0.2R wide respectively. These values were chosen since they represented the normal lowest value of the parameter, however some companies use smaller saddle angles of 60° and 90° for temporary saddles in shop construction and testing and also for transportation purposes. The 120-degree value is consistent with the smallest angle quoted in BS 5500. A width of $\sqrt{30D}$ (where D is in mm) is also used as a means of determining the

saddle width but the present definition of $0.2D$ (and multiples of this dimension) seems a more straightforward calculation.

In an extensive curve fitting exercise, using the SADDLE program with m=600 and n=200 for the Fourier terms, and inputting the long vessel dimensions as above, and by scanning for the maximum stresses, irrespective of their location in the immediate vicinity of the horn, equations were obtained for the basic stress for this load condition. These values are tabulated in Table 6.8. It is noted that the magnitudes of these stresses are, of course, fictitious and are intended to be modified by the various factors shown in Equation 6.2. In addition, the shell analysis is based on 'small displacement theory', which would in practise limit the movement of the shell wall to a magnitude in the order of the wall thickness.

The table is divided into three parts.

- The lower left hand corner of the table (denoted **'NOT REAL VESSELS'** is that part of the table where the thickness is considered to be too weak for the vessel only to be supported by saddles. The shell would be too flimsy and no horizontal vessel could be built with such dimensions.
- The opposite right hand corner of the table is that region where the internal pressure is dominant, i.e. the thickness would be defined by the internal pressure loading and not the saddle support condition.
- The main part of the table is the most interesting since it represents the major range of vessel geometries most commonly built by industry. This portion, therefore, is the main focus of the study.

	4	6	8	10	12	14	16	18	20	22	24	26	28	30
500	-1067.2	-532.3	-326.3	-223.7	-164.3	-126.4	-100.8	-82.5	-68.9	-58.6	-50.5	-44.0	-38.8	-34.4
750	-3225	-1601.3	-976.5	-667.2	-489.4	-377.0	-300.8	-264.4	-206.1	-175.2	-151.1	-131.9	-116.3	-103.4
1000	-7047.8	-3514.5	-2135.9	-1454.3	-1064.6	-818.7	-652.6	-534.6	-447.3	-380.7	-328.5	-286.8	-253.0	-224.9
1250		-6485.5	-3934.1	-2671.1	-1950.1	-1497.2	-1192.1	-975.5	-815.7	-694.1	-599.1	-523.2	-460.8	-410.6
1500		-11599	-6529.3	-4405.6	-3207.4	-2456.6	-1953.3	-1596.9	-1334.3	-1134.6	-978.8	-854.8	-754.0	-670.9
1750			-9310	-6847.5	-4906.1	-3745.1	-2907.4	-2425.7	-2025.1	-1720.9	-1483.8	-1295.0	-1141.9	-1016.1
2000			-13736	-9336.5	-7831.8	-5431.6	-4285.4	-3489.7	-2910.0	-2455.5	-2129.2	-1857.5	-1637.3	-1456.1
2250				-12723	-9385.3	-7256.6	-6010.0	-4830.5	-4014.2	-3403.5	-2930.6	-2555.0	-2251.2	-2001.4
2500				-17297	-12705	-9738.0	-7679.9	-7042.0	-5386.7	-4543.6	-3904.3	-3401.2	-2995.1	-2661.6
2750					-16460	-12661	-10054	-8182.3	-6695.4	-5980.6	-5079.7	-4411.5	-3878.3	-3446.8
3000		NOT REAL			-20802	-16042	-12769	-10419	-8674.5	-7307.1	-7025.5	-5628.5	-4926.4	-4368.5
3250		VESSELS				-19912	-15878	-12976	-10817	-9169.0	-7865.7	-6735.1	-6215.7	-5449.9
3500						-24294	-19405	-15879	-13252	-11240	-9667.9	-8406.8	-7350.0	*6593.8
3750							-23368	-19146	-17518	-13576	-11682	-10171	-8941.6	-7313.7
4000							-27782	-22792	-19056	-16188	-13937	-12138	-10678	-9473.9

Table 6.9 Basic stress values for the range of vessels encompassed by the parameter study

The first equation, generated by geometric regression across the radius/thickness surface, was geared to the SI system and is shown as follows:-

$$\sigma_b = 0.00052 R^{2.702} t^{-1.669} \qquad \textbf{(6. 3)}$$

where R and t are the vessel mean radius and wall thickness of the vessel respectively in millimetres. This equation gave σ_b values of ±1.5% of that predicted by running the full SADDLE program for a 36R long vessel, within the range of values in the main portion of the table, that is the unshaded portion. However, if the full table were considered, the error rises to -6 to +1.5% of the computed result. The additional error is generated by attempting to curve-fit to the **'NOT REAL VESSELS'** part of the table, and therefore the equation was deemed reasonable for the majority of cases.

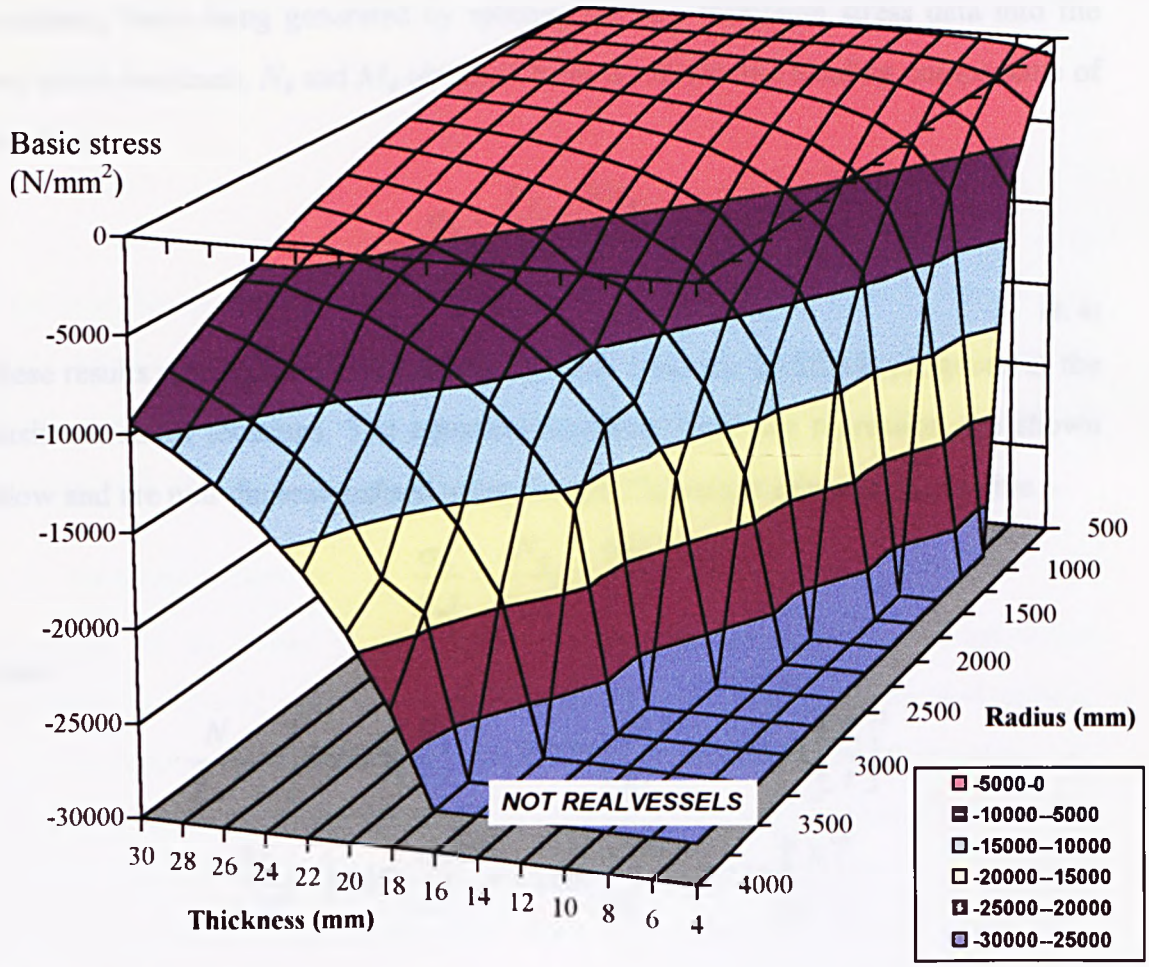

Figure 6.9 Surface plot of Basic Stress variation across geometry range

It is noted that Figure 6.9 surface plot highlights the variation in the basic stress value for a $36R$ long vessel with the 120°, $0.2R$ saddle positioned at the quarter point and this over the range $500<R<4000$ and $4<t<30$. By entering the required radius and thickness into the base basic, the maximum stress is obtained by tracking the surface contours and establishing the intersection value. The surface plot is intended for visualisation only. In order to be consistent with the SI approach, the units of this basic stress are N/mm^2, however this introduces a constant (0.00052) accommodates the units of stress such that when R and t are entered in mm, the resulting stress is given in N/mm^2.

A second approach was therefore considered which would result in non-dimensional equations, these being generated by splitting the raw maximum stress data into the two stress resultants, N_ϕ and M_ϕ obtained from the direct and bending components of the stress.

$$\sigma_b = \frac{N_\phi}{t} \pm \frac{6M_\phi}{t^2}$$

(6. 4)

These results represent the components of stress from the SADDLE programs at the maximum stress locations. The equations resulting from the regression are shown below and are non-dimensionalised using the specific weight of water, γ_w, to give :-

$$\frac{\sigma_b}{\gamma_w t} = \frac{N_\phi}{\gamma_w t^2} \pm \frac{6M_\phi}{\gamma_w t^3}$$

where:

$$\frac{N_\phi}{\gamma_w t^2} = \left[560.65\left(\frac{R}{t}\right)^{0.1} + 307.85\left(\frac{t}{R}\right)^{0.2} - 858.31\right]\left[\frac{R}{t}\right]^2$$

$$\frac{M_\phi}{\gamma_w t^3} = \left[9.18\left(\frac{R}{t}\right)^{0.1} + 61.68\left(\frac{t}{R}\right)^{0.2} - 27.18\right]\left[\frac{R}{t}\right]^3$$

(6. 5 a-c)

Within the range $35 < R/t < 300$, these equations give maximum errors of 3% for N_ϕ and 2% for M_ϕ. In each case these are over-estimates, thus providing a conservative basic stress. However, the previous expression is preferred since these equations were developed using stress data based on 200×200 terms for each Fourier series.

6.6.2 Weight of Contents Factor F_w

All runs performed using the SADDLE program assume the vessel self-weight to be zero and the vessel loading to be full of water. This is of use especially when comparing against strain gauge results. However, it may arise that a vessel contains contents which have a different specific gravity from that of water. This change of specific gravity, together with a weight correction for the capacity of the actual vessel of length, L, can be incorporated using the weight of contents coefficient, F_w, which is given by:

$$F_w = \left(\frac{L}{36R}\right)\rho \tag{6.6}$$

where ρ is the specific gravity of the liquid. It has been found that the vessel self-weight can be included by using an equivalent specific gravity, where the **'new'** specific gravity is modified in the ratio of the differences in weight with and without the vessel self-weight.

6.6.3 Geometric Factors

The design of the vessel is known to be dependant on a number of geometric parameters as defined earlier, namely, the saddle width, saddle angle, end effects, saddle interaction and the effect of vessel length to radius. Considerable time was spent in attempting to isolate the effects of each individual parameter and to thereafter generate closed-form equations which would describe the behaviour of these interactions. However, in investigating these interactions, the errors which were resulting when the parameters were **combined** proved excessive and it was clear that

the **'closed-form'** approach would not yield simple expressions which would provide useable, accurate results. As an alternative, it was found that, by using fourth order polynomial equations to represent the behaviour of each parameter, accurate results were forthcoming within acceptable error limits.

Therefore, the effect of each geometric parameter is considered for a range R/t ratios i.e. 25, 50, 75, 100, 125, 150, 175, 200, 250, 300 (i.e. which is typical of the range of industrial vessels surveyed earlier). For each ratio, a regression curve fitting exercise was undertaken using Microsoft Excel V5.0. Linear interpolation for intermediate R/t ratios between two already calculated R/t results can be easily obtained.

6.6.3.1 Saddle Width Factor, F_b

The values for the basic stress were generated based on the practical limits of saddle width. BS5500 prescribes the minimum saddle width, b, to be $\sqrt{30D}$ where D is the vessel diameter in millimetres. As an alternative, it is possible to use a value of b based on a fraction of the radius, for example, $b = 0.2R$, which provides a more conservative result and maintains consistent use of the variable R. Hence values of the basic stress were obtained for the same R and t ranges previously described using saddle width values from $0.1R$ to $0.5R$ in intervals of $0.1R$. If the saddle width changes alone, the maximum stress equation becomes:

$$\sigma_{max} = \sigma_b . F_b$$

which, when rearranged, gives the equation:

$$F_b = \frac{\sigma_{max}}{\sigma_b}$$

(6. 7 a,b)

where σ_b is calculated for an R/t ratio for which F_b is calculated.

F_b is graphed as a function of the saddle width to give the following curves, shown in Figure 6.10

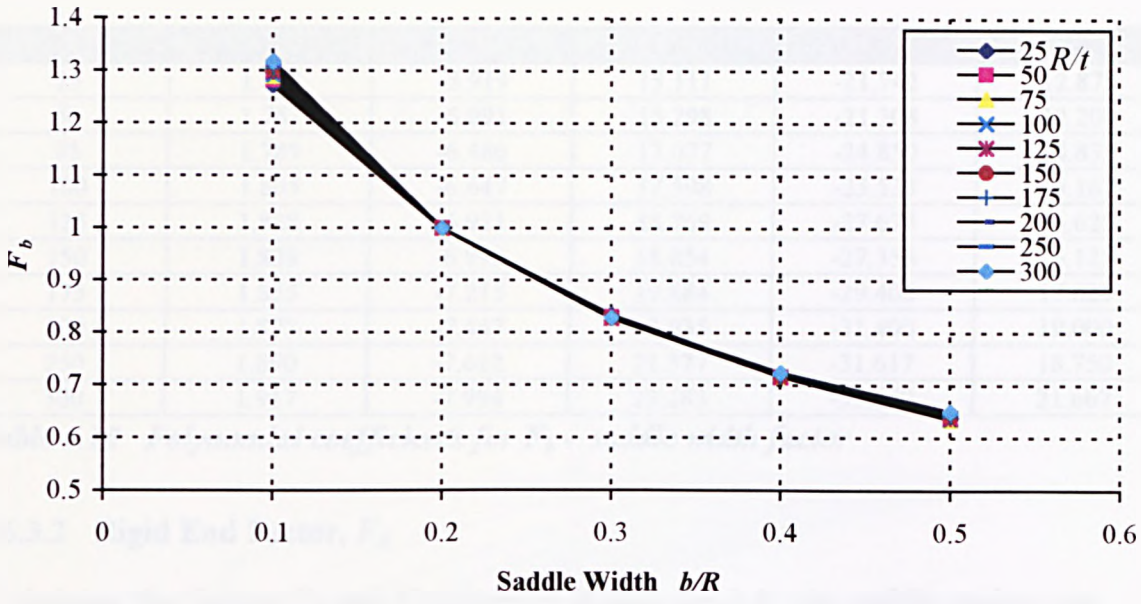

Figure 6.10 Graph of saddle width factor, F_b

From this figure, which shows that the effect of R/t is almost negligible, it is apparent that the maximum stress decreases as the saddle width increases. This is a reasonable result because as the support width increases, the force arising from the reaction between the saddle and the vessel is distributed over a slightly larger surface area. In addition to this, it can be observed that the curves lie quite close to one another for the various R/t ratios plotted. This indicates the limited influence of both the thickness and the radius when the width parameter, b, is fixed.

As shown in the Table 6.10, the saddle width factor F_b can be evaluated from a fourth order polynomial to obtain the best correlation, where:

$$F_b = a_0 + a_1 x + a_2 x^2 + a_3 x^3 + a_4 x^4 \qquad \textbf{(6. 8)}$$

with $x = b/R$ in polynomial expression.

R/t	a_0	a_1	a_2	a_3	a_4
25	1.733	-5.919	15.111	-21.742	12.875
50	1.757	-6.091	15.298	-21.308	12.208
75	1.789	-6.486	17.077	-24.850	14.833
100	1.805	-6.647	17.598	-25.533	15.167
125	1.828	-6.921	18.769	-27.675	16.625
150	1.838	-6.996	18.854	-27.358	16.125
175	1.855	-7.215	19.884	-29.408	17.625
200	1.873	-7.447	20.935	-31.400	19.000
250	1.890	-7.612	21.377	-31.617	18.750
300	1.917	-7.994	23.283	-35.550	21.667

Table 6.10 Polynomial coefficients for F_b - saddle width factor

6.6.3.2 Rigid End Factor, F_A

In deriving the factors F_b and F_θ (given in section 6.6.3.4), the saddle region was isolated by considering a vessel $36R$ long. To allow the method to encompass the full range of vessel configurations, the effects of the rigid end and of the other saddle have to be considered. In the Fourier series solution, it is assumed that the end does not deform in the plane of its profile. The way in which this assumption influences the peak stress at the horn was investigated by performing a number of SADDLE runs where the saddle centerline distance from the end, A, was varied but the overall vessel length remained constant. Plotting values of the rigid end factor, F_A, at the horn against R/t for a range of A/R values from the quarter points, $A=9R$ to $A=0.2R$ yields Figure 6.10. This figure allows the appropriate end effect factor, F_A, to be selected for use when the support is located at a particular A value. If the saddle position changes alone, the maximum stress equation becomes:

$$\sigma_{max} = \sigma_b . F_A$$

which, when rearranged, gives the equation:

$$F_A = \frac{\sigma_{max}}{\sigma_b}$$

(6. 9 a,b)

where σ_b is calculated for an R/t ratio for which F_A is calculated.

In addition, the following equation is obtained:

$$F_A = a_0 + a_1 x + a_2 x^2 + a_3 x^3 + a_4 x^4 \qquad \textbf{(6. 10)}$$

where $x=A/R$ in polynomial expression.

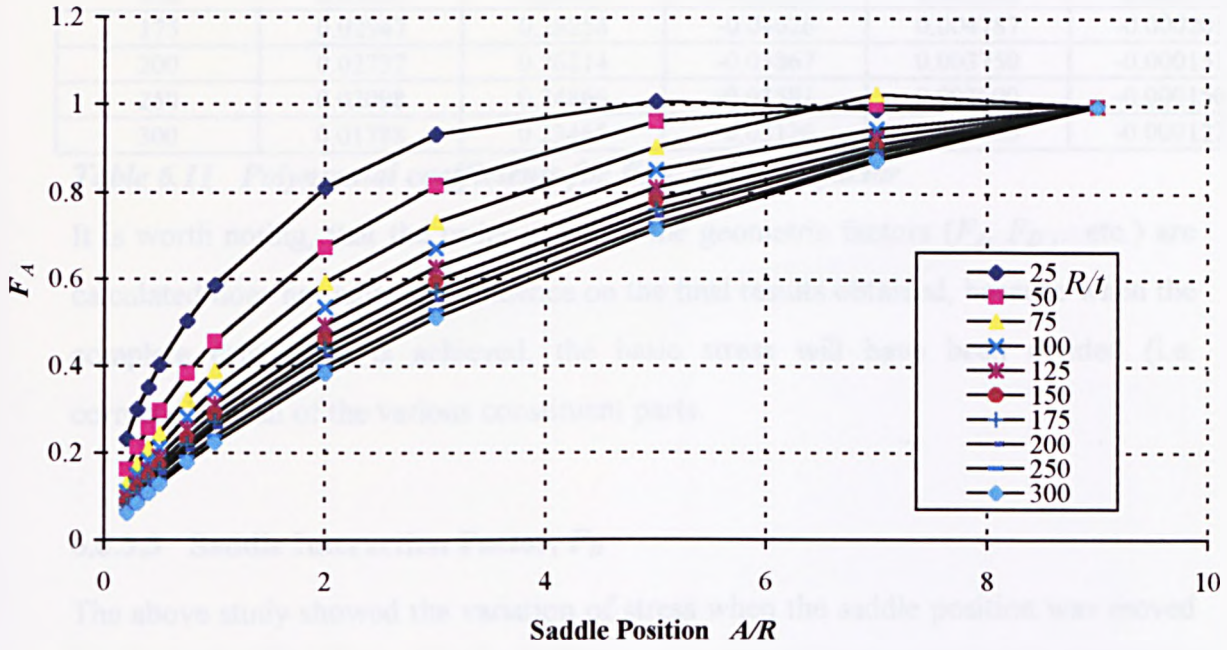

Figure 6.11 Graph of rigid end factor, F_A

The curves above show that as the saddles are moved closer to the ends, the smaller is the resulting maximum stress value obtained. This is due to a reduction in the bending moments induced by the ends.

From the curves above, it appears that the influence of A is bigger when the R/t ratio is increased. For $R/t=25$, the influence of A is negligible within the range $3.5R<A<9R$, but for the other ratios the influence of A is important over the whole interval.

The variation of F_A allows linear interpolation to be made for different R/t ratios. In Table 6.11, it can be seen that the polynomial coefficients are for the fourth order expression for F_A,

R/t	a_0	a_1	a_2	a_3	a_4
25	0.14621	0.55498	-0.13428	0.014198	-0.000551
50	0.08909	0.44585	-0.09151	0.009231	-0.000369
75	0.06572	0.38390	-0.71364	0.006990	-0.000270
100	0.05054	0.34826	-0.06336	0.006414	-0.000264
125	0.04093	0.32083	-0.05656	0.005812	-0.000242
150	0.03417	0.29953	-0.05098	0.005278	-0.000221
175	0.02947	0.28258	-0.04626	0.004787	-0.000201
200	0.02737	0.26214	-0.03867	0.003750	-0.000151
250	0.02098	0.24866	-0.03581	0.003600	-0.000150
300	0.01788	0.23465	-0.03126	0.003066	-0.000127

Table 6.11 Polynomial coefficients for F_A - rigid end factor

It is worth noting, that the order in which the geometric factors (F_A, F_D ,...etc.) are calculated does not have any influence on the final results obtained, because when the complete calculation is achieved, the basic stress will have been divided (i.e. corrected) by all of the various constituent parts.

6.6.3.3 Saddle Interaction Factor, F_D

The above study showed the variation of stress when the saddle position was moved nearer to the rigid end. A similar procedure was adopted to investigate the interaction effects between the saddles which are located a distance D apart. As the two saddles are positioned closer together, the influence of the second on the first becomes significant. The F_D factor, which represents this behaviour, is plotted in Figure 6.12 against R/t for various values of D/R where $D=(L-2A)$. D/R was varied from 18, the mid-dimension of the *36R* vessel, to a lower value of 2. If the saddle interaction position changes alone, the maximum stress equation becomes:

$$\sigma_{max} = \sigma_b . F_D$$

which, when rearranged, gives the equation:

$$F_D = \frac{\sigma_{max}}{\sigma_b}$$

(6. 11a,b)

where σ_b is calculated for an R/t ratio for which F_D is calculated.

In addition, the following equation is obtained:

$$F_D = a_0 + a_1 x + a_2 x^2 + a_3 x^3 + a_4 x^4$$

(6. 12)

where $x=D/R$ in polynomial expression.

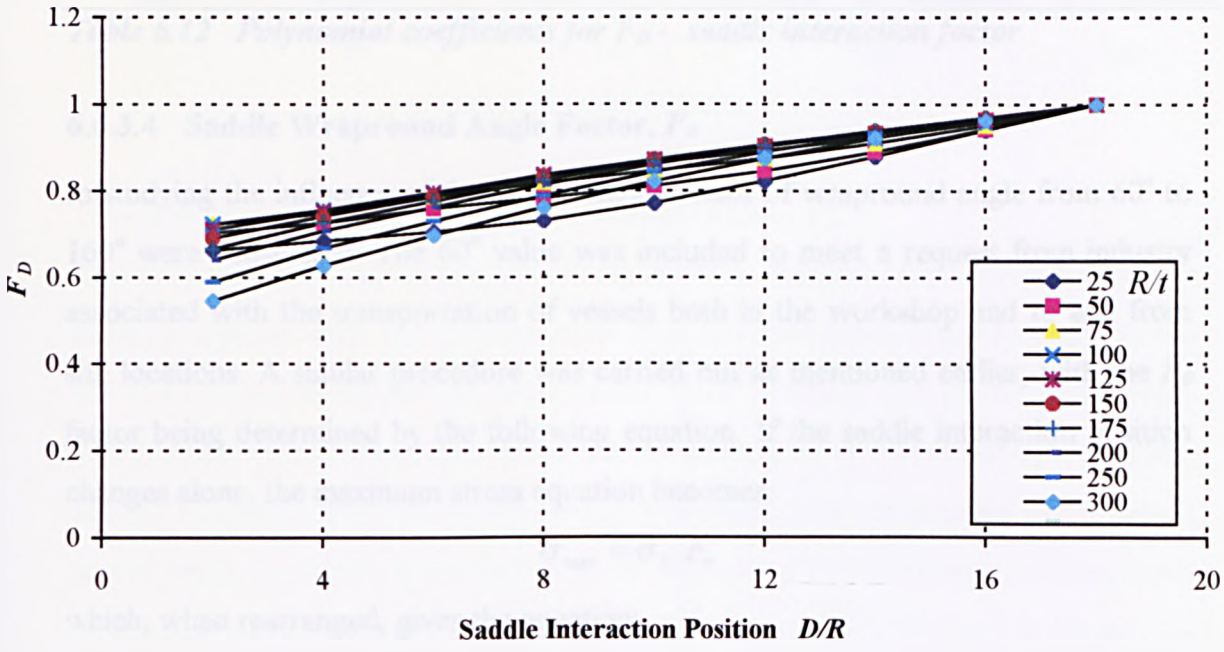

Figure 6.12 Graph of saddle interaction factor, F_D

It is noticeable that as the saddles move closer together, the resulting maximum stress at the horn increases. Obviously, there will come a point where the saddles are so close that they act as one. This has not been considered in this study. The variation is explained by the fact that for a certain D value, as the end sections become longer, they introduce a larger bending moment which, in turn, leads to a larger maximum stress value in the horn region. This effect is similar, in principle, to the influence of the A dimension.

The F_D factor which represents this behaviour is given as a fourth order polynomial equation with coefficients as shown as the Table 6.12,

R/t	a_0	a_1	a_2	a_3	a_4
25	0.63783	0.016572	-0.002274	0.000266	-7.16E-6
50	0.66755	0.019146	-0.001266	0.000092	-1.33E-6
75	0.69860	0.008906	0.001551	-0.000140	4.36E-6
100	0.68000	0.007285	0.002474	-0.000214	5.87E-6
125	0.67898	0.012773	0.001992	-0.000183	4.89E-6
150	0.64491	0.021468	0.000935	-0.000112	3.04E-6
175	0.60577	0.030931	-0.000267	-0.000033	1.08E-6
200	0.56838	0.038209	-0.001084	0.000020	-0.21E-6
250	0.50338	0.046902	-0.001904	0.000076	-1.64E-6
300	0.45423	0.049776	-0.001978	0.000086	-2.02E-6

Table 6.12 Polynomial coefficients for F_D - saddle interaction factor

6.6.3.4 Saddle Wraparound Angle Factor, F_θ

In studying the influence of the saddle angle, values of wraparound angle from 60° to 160° were considered. The 60° value was included to meet a request from industry associated with the transportation of vessels both in the workshop and to and from site locations. A similar procedure was carried out as mentioned earlier, with the F_θ factor being determined by the following equation. If the saddle interaction position changes alone, the maximum stress equation becomes:

$$\sigma_{max} = \sigma_b . F_\theta$$

which, when rearranged, gives the equation:

$$F_\theta = \frac{\sigma_{max}}{\sigma_\theta}$$

(6. 13a,b)

where σ_b is calculated for an R/t ratio for which F_θ is calculated.

In addition, the following equation is obtained:

$$F_\theta = a_0 + a_1 x + a_2 x^2 + a_3 x^3 + a_4 x^4$$

(6. 14)

where $x = \theta$ in radians in the polynomial expression.

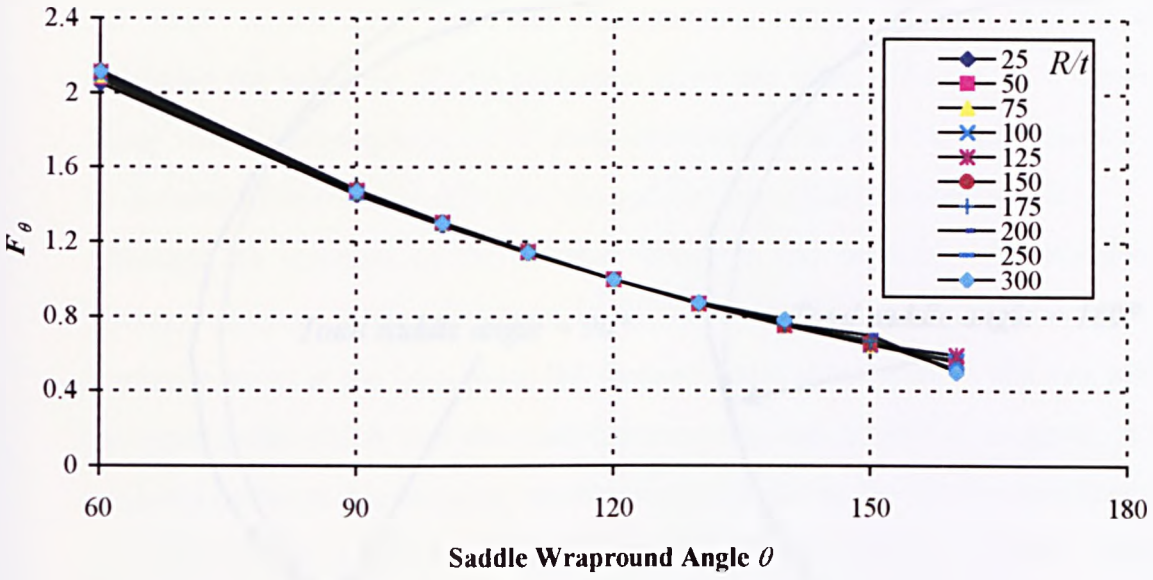

Figure 6.13 Graph of saddle wraparound angle factor, F_θ

The above curves indicate that the influence of the R/t ratio, for a fixed wraparound angle, is approximately the same for all of the cases considered. Some divergence was observed at higher wraparound angle values. This is mainly due to the larger angle which must encompassed by each of the 50 contact areas. Therefore, if a greater number of contact areas were employed in such cases, then convergence of the curves would result. From the above curves, it can be noticed that the stress decreases with an increase of the wraparound angle. This effect arises since the angle is bigger, the forces must be distributed over a larger area (i.e. the support wraps around a larger area of shell) which in turn, gives lower stresses in the vessel. In addition, the increase in wraparound angle provides stiffening of the shell in the radial direction at the saddle centreline profile, which helps to minimise the circumferential bending effects. This effect can be clearly seen when considering the resulting deformation from a finite element analysis. The finite element plots shown in Figures 6.14a,b highlight the difference in the deformation between two vessels with saddle wraparound angles of 90° and 160° respectively.

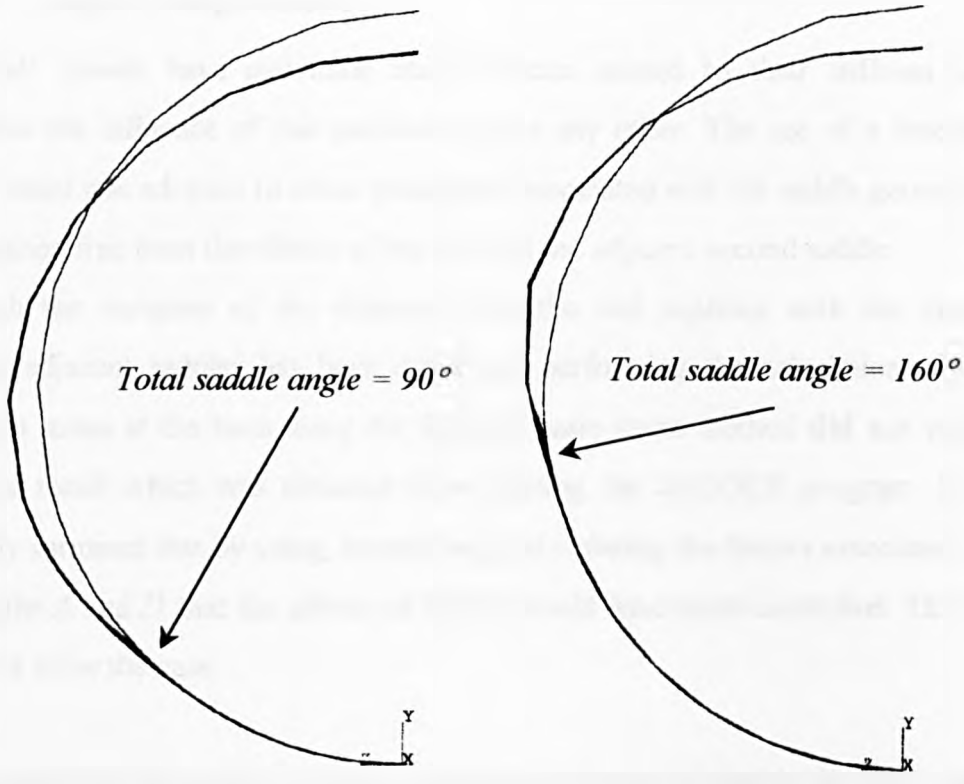

Figure 6.14a,b Finite element plots of deformed vessel profile at saddle centreline location - saddle wrapround angle of 90° and 160°

The coefficients of a fourth order polynomial which represents the factor F_θ are given in Table 6.13,

R/t	a_0	a_1	a_2	a_3	a_4
25	3.83590	-0.03791	0.000158	0	0
50	3.90584	-0.03876	0.000159	-0.0000004	0
75	4.04122	-0.04313	0.000216	-0.0000007	0
100	4.68385	-0.06828	0.000571	-0.0000290	0
125	4.72200	-0.07110	0.000642	-0.0000035	0
150	4.40982	-0.05769	0.000440	-0.0000022	0
175	2.09028	0.040349	-0.001045	0.0000074	0
200	2.94341	0.005759	-0.000545	0.0000043	0
250	2.37512	0.029811	-0.000912	0.0000067	0
300	1.74637	0.056508	-0.001322	0.0000094	0

Table 6.13 Polynomial coefficients for F_θ - saddle wrapround angle factor (note: $x = \theta$ in radians)

6.6.3.5 Length Change Factor, F_L

All **'real'** vessels have individual characteristics related to their stiffness which determine the influence of one parameter upon any other. The use of a theoretical **'long'** vessel was adopted to allow parameters associated with the saddle geometry to be examined free from the effects of the end and the adjacent second saddle.

Although the variation of the distance from the end together with the distance between adjacent saddles has been examined, performing the calculations for the maximum stress at the horn using the factored basic stress method **did not** provide the same result which was obtained from running the SADDLE program. It was originally surmised that by using, introducing and isolating the factors associated with the lengths A and D that the effects of length would have been controlled. This was found not to be the case.

It was found that in order to correct a theoretical vessel of length, say $36R$, where $A=9R$ and $D=18R$, to, for example, a vessel of length $18R$, with $A=4R$ and $D=10R$, the modifications using the polynomial factors F_A and F_D were inadequate. An additional factor to allow for the length change, F_L, was required. This was obtained by comparing many cases of shortened **'theoretical'** vessels with the SADDLE result for the actual case. It is noted that for this factor, the phrase **theoretical** refers to a result for a shortened vessel using the factor method based on a $36R$ long vessel which has been modified by the factors F_A and F_D for the appropriate length.

The values of the new length change factor, F_L, obtained were plotted against L/R for all R/t values. These curves are based on the following approach. For many shortened "theoretical" vessels, F_L is defined as follows.

If the vessel length changes from $L=36R$, the length change factor becomes:

$$F_L = \frac{\sigma_{max}}{\sigma_b . F_A . F_D} \qquad \textbf{(6. 15)}$$

where F_A and F_D are the calculated factors for the particular vessel.

In order to determine the appropriate length change parameter, for a given vessel length, L, it a feasible that a variety of saddle locations may be employed and not solely the quarter point locations. The F_L factor was calculated, for various saddle locations, at appropriate distances of A equal to $L/4$, $L/6$, $L/8$, and $L/10$ from the ends. The following fourth order polynomial equation is obtained:

$$F_L = a_0 + a_1 x + a_2 x^2 + a_3 x^3 + a_4 x^4 \qquad \textbf{(6. 16)}$$

where $x=L/R$ in the polynomial expression.

The final value of F_L is then ***the mean of the four cases*** calculated above. Using this procedure, the factors F_L found for each L/R and R/t are fitted into curves. The mean value is chosen in order to minimise the error associated with each different configuration. This means that the solution is equally accurate across the full range of the available saddle positions. However, some of the extreme saddle positions are unrealistic and these positions have been removed from the scope of the curve fit. Vessels whose length is greater than $20R$ must not have saddles positioned closer than $A=L/6$ to the end; that is the range $L/6 \leq A \leq L/4$ is acceptable for vessels with $L>20R$. This restriction prevents very long vessels having saddles situated too close to the ends of the vessel and introducing high bending stresses at the vessel mid-section. The form of the graph shown in Figure 6.15 shows that, as a smoothing curve, the effect of R/t is quite small. This is to be expected since the F_L parameter operates not only as a geometric function but corrects any errors introduced previously by the compound factors. If a larger error band were permitted, the effect of the length change factor could be replaced by a single curve. This curve indicates that the additional effects of both of these parameters, F_A and F_D, have been taken into account by the F_L factor.

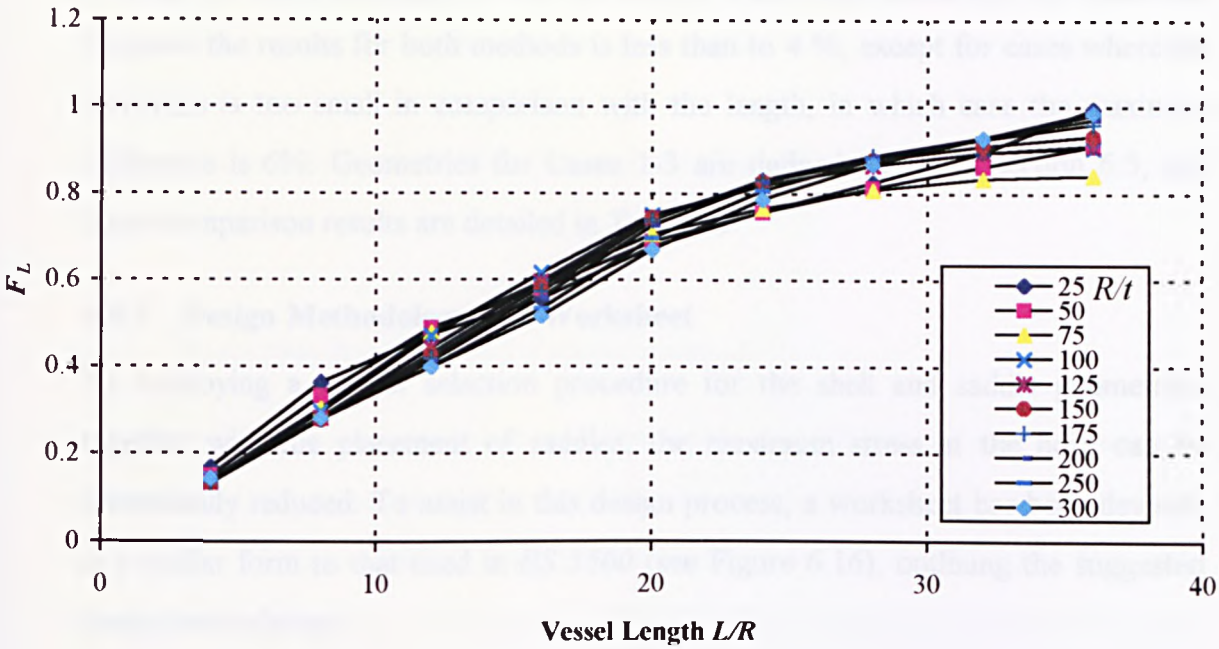

Figure 6.15 Graph of length change factor, F_L

The values of F_L can be represented by a fourth order polynomial equation as shown on Table 6.14,

R/t	a_0	a_1	a_2	a_3	a_4
25	-0.053702	0.065643	-0.002351	0.0000517	-4E-7
50	-0.084688	0.065522	-0.001856	0.0000283	-2E-7
75	-0.032241	0.041286	0.000617	-0.0000575	8E-7
100	0.027463	0.018664	0.002856	-0.0001317	16E-7
125	0.066444	0.003717	0.004032	-0.0001659	19E-7
150	0.089579	-0.003488	0.004514	-0.0001767	20E-7
175	0.100234	-0.005717	0.004505	-0.0001709	19E-7
200	0.095531	-0.001799	0.003912	-0.0001455	16E-7
250	0.084560	0.005450	0.002825	-0.0000997	10E-7
300	0.059512	0.017537	0.001403	-0.0000457	4E-7

Table 6.14 Length change factor F_L (note: x = L/R in the polynomial expression)

6.6.4 Verification of the Design Method

Results obtained by this hand calculation method were compared with those calculated by the SADDLE program for different geometries within a range of R/t between 25 to 250.

Among the cases envisaged to test the design, it has been found that the difference between the results for both methods is less than to 4 %, except for cases where the thickness is too small in comparison with the length, in which case the maximum difference is 6%. Geometries for Cases 1-3 are defined earlier in section 6.5, and some comparison results are detailed in Table 6.8

6.6.5 Design Methodology and Worksheet

By employing a careful selection procedure for the shell and saddle geometries, together with the placement of saddles, the maximum stress at the horn can be dramatically reduced. To assist in this design process, a worksheet has been devised, in a similar form to that used in *BS 5500* (see Figure 6.16), outlining the suggested design methodology.

In the worksheet, the designer may input the basic shell dimensions. Saddle dimensions are also introduced at this stage, these being obtained from a suitable dimensional standard for the particular vessel radius used. Ratios of the key variables are then evaluated. These ratios are used in calculating the appropriate factor associated with a particular variable and served to check the applicability of the method for the proposed geometry. The basic stress factors are found in turn for all the variables described earlier. The basic stress, σ_b, as given in Equation (6.3) is presented here. The alternative form given in Equations (6.5) may also be used, although preferably not for very long vessels. The basic stress is then combined with each factor to give the maximum stress in the vessel at the horn of the saddle.

This value is then assessed against the stress limit imposed for this type of loading. It is the opinion of the author that for the purposes of assessing the total stress in the shell at the horn of the saddle, this may be categorised as **primary plus secondary bending**. When this value is limited to 3 times the design stress (f or S_m) for the chosen material. However, this approach may be unconservative since the nature of

the stress may not be wholly secondary (see Chapter 7). If the maximum stress exceeds the imposed limit, the designer is presented with a number of options. Any variable can be altered, e.g. saddle wraproud angle increased, this resulting in a different factor being selected for that variable. The new value of maximum stress is then obtained.

6.6.6 Illustrative Example and Fatigue Analysis

In order to illustrate the procedure and then apply to a fatigue analysis, the example of a vessel (***Case 3***) has been chosen. It may be assumed that the vessel has been in service for 20 years and a fatigue assessment is to be carried out. This will demonstrate some of the problems that may arise using BS5500 calculated stresses. The vessel has an inside diameter of 3658mm (12ft.), tangent length of 54864mm (180ft.), thickness of 26.6mm (1.05in.), with 762mm (30in.) wide, 162^{O} wraproud saddles located at 6858mm (22.5ft.) from each end. The vessel is made from steel and is subject to a daily cycle of filling and emptying liquid butane, which has a specific gravity of 0.63, and has had 10 hydrotests during routine inspections. On this basis, a fatigue assessment to BS 5500 requires to be carried out.

Calculation of Maximum Stress in Support Region

The example vessel was originally designed using the present method in BS 5500, which is based on the Zick approach. The maximum circumferential stress at the horn (f_6) calculated for this condition is found to be **-178.1N/mm^2**. The design stress for the vessel, f or S_m, is taken as **193N/mm^2** (corresponding to a specified yield stress of 42,000psi). On this basis, the maximum stress at the horn must not exceed $1.25f$ which gives a value of **-241.3N/mm^2**. The vessel therefore satisfies the requirements of BS 5500.

Using the improved Fourier series/shell analysis (SADDLE), the maximum stress at the vessel horn is **-398.6N/mm^2**. When the worksheet method is used for the same vessel, the following terms are found:

Basic stress	=	**1470.0 N/mm^2**
Weight contents factor F_w	=	**0.833**
Saddle width factor F_b	=	**0.705**
Saddle wrapround factor θ	=	**0.548**
Rigid end factor F_A	=	**0.846**
Saddle interaction factor F_D	=	**1.000**
Length change factor F_L	=	**0.984**

Substituting the appropriate values for the factors into Equation (6.3), the maximum stress at the horn is equal to **-393.8N/mm^2**. The accuracy of the proposed method is clearly noted in the above value that is within 1.2% of the actual program value.

Since the worksheet method is a **'design-by-analysis'** approach, the design stress intensity limit is ***3f* or *3S$_m$***. For the above example, this value is **579N/mm^2**. Again, the calculated stresses fall within the ***3f*** limit and the vessel design is satisfactory, for the shakedown requirement of the maximum load cycle range, which is the hydrotest.

Fatigue Assessment

In order to assess the fatigue life of the vessel, under the action of repeated filling and emptying, the method set out in BS 5500 Annex C (previously Enquiry Case 5500/79) is used. The first step in the assessment is to identify the various events experienced by the critical region, in this case, the support region, which will give rise to fluctuating stresses. Attention is confined in this example, to the hydrotest and the butane fillings.

Using the worksheet result, the stress range for the hydrotest (S_{r1}) is 393.8N/mm^2 and for the butane, with specific gravity of 0.63, (S_{r2}) is 393.8×0.63 = 248.1N/mm^2.

Over the twenty-year period, the total number of cycles is as follows:

For the hydrotest, $n_1 = 10$

For the butane fillings, $n_2 = 365 \times 20 = 7300$

According to Annex C, the fillet welds at the horn of the saddle may be classified as a '*G*' type weld. The *S-N* curves of the form $S_r^m N = A$ for this assessment are provided in Figure C.3 and Equation C.5 of the Enquiry Case. The appropriate *S-N* equations are:

$$S_r^3 N = A = 2.50 \times 10^{11} \quad \text{and} \quad m = 3 \quad \text{for } N < 10^7 \text{ cycles}$$

$$S_r^5 N = A = 2.05 \times 10^{14} \quad \text{and} \quad m = 5 \quad \text{for } N > 10^7 \text{ cycles}$$

where S_r is the stress range and N is the number of cycles from the fatigue curve. The constants for the *S-N* curve, m and A, are found from Table C.1 of the Annex.

Taking into the account, the effect of the material and the thickness of the vessel in the support region, the following equation gives the fatigue life as a function of the stress range, S_{ri}:

$$N = A\left(S_n \frac{2.09 \times 10^5}{E}\right)^{-m}\left(\frac{22}{e}\right)^{m/4}$$

where E is the actual Young's modulus, e is the wall thickness (if e < 22mm then the value of 22mm should be used, otherwise the actual value should be used) and m is the index associated with S_r of the fatigue equation shown above.

In the present case, E=207,000 N/mm^2 and e=26.6mm. Using these values in the above fatigue equations, the number of cycles N are:

For the hydrotest:

$$2.50 \times 10^{11}\left(393.8 \times \frac{2.09}{2.07}\right)^{-3}\left(\frac{22}{26.6}\right)^{3/4} = 3449 \text{ cycles}$$

For the butane fillings:

$$2.50\times10^{11}\left(248.1\times\frac{2.09}{2.07}\right)^{-3}\left(\frac{22}{26.6}\right)^{3/4}=13794 \text{ cycles}$$

Applying the Miner's cumulative damage rule then leads to:

$$\sum\frac{n_i}{N_i}=\frac{10}{3449}+\frac{7300}{13794}=0.532 \quad \leq 1$$

The condition of the damage rule has therefore been met and the vessel/support arrangement can be judged safe from a fatigue point of view.

6.7 Comments

An existing rather complex analysis for twin saddle supported vessels has been parameterised and presented in a simple worksheet form. The maximum stresses occurring in the region of the horn of the saddle are categorised as **secondary bending** and as such uses **3*f*** (or $3S_m$) as the design criterion when all loads are considered.

It is also considered that, in those design cases where fatigue loading is specified, the Zick analysis may be inappropriate and the proposed approach should be adopted. It may also be used, to carry out a residual life assessment on existing plant, which have been subject to fatigue loading.

It is hoped that, with the incorporation of the factors for saddle and end closure flexibility, this method may prove the basis for a new hand calculation method suitable for incorporation into vessel Standards and Codes.

The first form of this work was published in Reference [60]. The design method contained therein is programmed into a MathCAD spreadsheet in Appendix 9 of the thesis.

Suggested working

Cylindrical shell supported on twin saddles
Simplified hand calculation for maximum stress

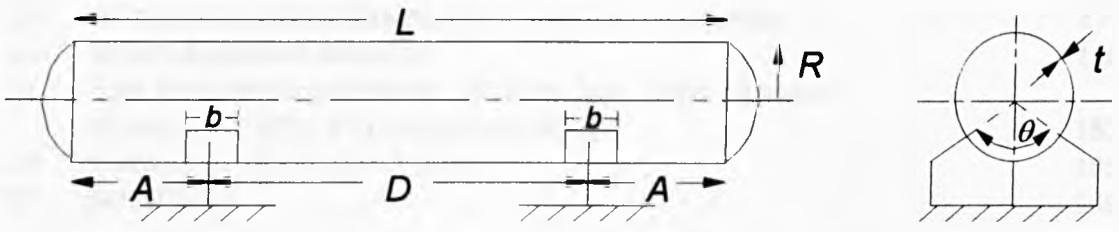

Vessel Parameters			**Ratios**	
Mean radius	R	=	R/t =	A/R =
Thickness	t	=	L/R =	D/R =
Shell length	L	=	**Note: The following limits apply :-**	
Saddle angle	θ	=	$0.1\,R \le b \le 0.5\,R$	
Saddle width	b	=	$A \le L/4$ (for $L > 20R$ & $L/6 < A < L/4$)	
Saddle distance from tan line	A	=	$25 \le R/t \le 625$	

Maximum stress equation factors:			
Weight factor		$F_W = \left(\frac{L}{36R}\right)\rho$	=
Saddle width factor	*Table 1*	F_b	=
Saddle wraparound angle factor	*Table 2*	F_θ	=
Rigid end factor	*Table 3*	F_A	=
Saddle interaction factor	*Table 4*	F_D	=
Length change factor	*Table 5*	F_L	=

Equation for σ_b

$$\sigma_b = 0.00052R^{2.702}t^{-1.669} \quad =$$

Maximum stress at horn

$$\sigma_{max} = \sigma_b . F_W . F_b . F_\theta . F_A . F_D . F_L \quad =$$

Figure 6.16 Design method working form

7 FINITE ELEMENT ANALYSIS OF TWIN SADDLE SUPPORTED VESSELS

7.1 Introduction

The advent of the finite element technique in stress analysis has allowed many industry sectors to analyse complex structures that cannot be directly addressed using classical mechanics approaches. The use of the technique is now widespread, this being due to the ease of use of modern finite element codes together with the rapidly increasing computing power-price ratio. Finite element analysis is presently perceived as the standard **'design tool'**, capable of addressing the majority of stress analysis problems where no obvious classical solution is readily available.

In the pressure vessel industry, finite element analysis is normally used in those cases where ***'design-by-rule'*** procedures are violated. A typical case is when a nozzle diameter to shell diameter exceeds the prescribed limits, and compensation pads are required, the additional material can only be applied to those cases where the *d/D* ratio is less than 0.33. Therefore, it is the industry accepted practice to analyse nozzles with pads with larger *d/D* ratios by finite element methods and thereafter assess the resulting stresses and deflections against some alternative rules, such as those stated in Annex A of BS 5500. These limitations address the possible failure modes of the vessel and attempt to ensure the structural integrity of the vessel is maintained.

The saddle support problem is also one of those problematic areas where ***a 'design-by-analysis'*** approach can be adopted to provide accurate values for the stresses in key areas as required for fatigue assessment. In cases where there is, for example, a complex loading arrangement such as local loads or nozzles located near saddles or the case of multi-saddle support systems, a solution using a finite element program is normally considered. Although the application of finite element analysis to this class of problem is considered attractive, applying the technology can be fraught with difficulty. Not only that, ensuring the results are satisfactory and the subsequent interpretation demands specialised knowledge and experience. Such problems arise

especially when the stress gradients vary rapidly over such a small zone. It is these and other difficulties that make the modelling and analysis of the stress systems arising at the horn of the saddle support so complex.

To this end, it is suggested that the design methodology, developed in the earlier chapters, presents a more **'useful'** design tool which is preferred over standard finite element analysis. This chapter, therefore, describes the difficulties associated with constructing a suitable finite element model of a twin saddle supported pressure vessel and interrogating the stress system obtained. In addition, a parametric model is developed which allows the end effects of the pressure vessel head to be examined, the results of which are described in a subsequent chapter.

In addition, comments are made regarding the suitability of the finite element technique with respect to twin saddle supported problems. Although other investigators have addressed the problem using finite element analysis, the results produced have been qualitative rather than quantitative. However, the present work attempts to provide guidelines for the modelling and analysis of such problems using finite element systems and to comment on the suitability of the technique in accommodating the support condition. All analysis carried out during this work was carried out using the ANSYS Finite Element Systems from Swanson Analysis Systems Inc. (now ANSYS Inc.)

7.2 Description of the Model

In constructing a suitable finite element model of a problem, it is imperative that the analyst has a complete understanding of the expected stress distribution, especially in the case of the twin saddle supported vessel. From the literature described earlier, the stress distribution in the area surrounding the saddle horn shows that the maximum stresses rise and fall very rapidly over a few degrees in the local vicinity of the saddle horn. In addition, the effects of the saddle flexibility are known to have a considerable effect on the location and magnitude of the maximum value.

In this study, the aim is to develop a satisfactory FE model which is capable of assessing the influence that a rigid saddle has on the maximum stresses in the vessel,

with particular reference to the magnitude and location of such stresses. In addition to this, the option for introducing various head closure configurations will be incorporated into the model in Chapter 8. In addition, much effort has been concentrated into choosing the most appropriate element type and mesh design. However, since the selected boundary condition can generate a mathematical 'sharp corner', comparisons with experimental results are made in order to limit asymptotic stress results to a physically realistic value. Figure 7.1 shows the element mesh used.

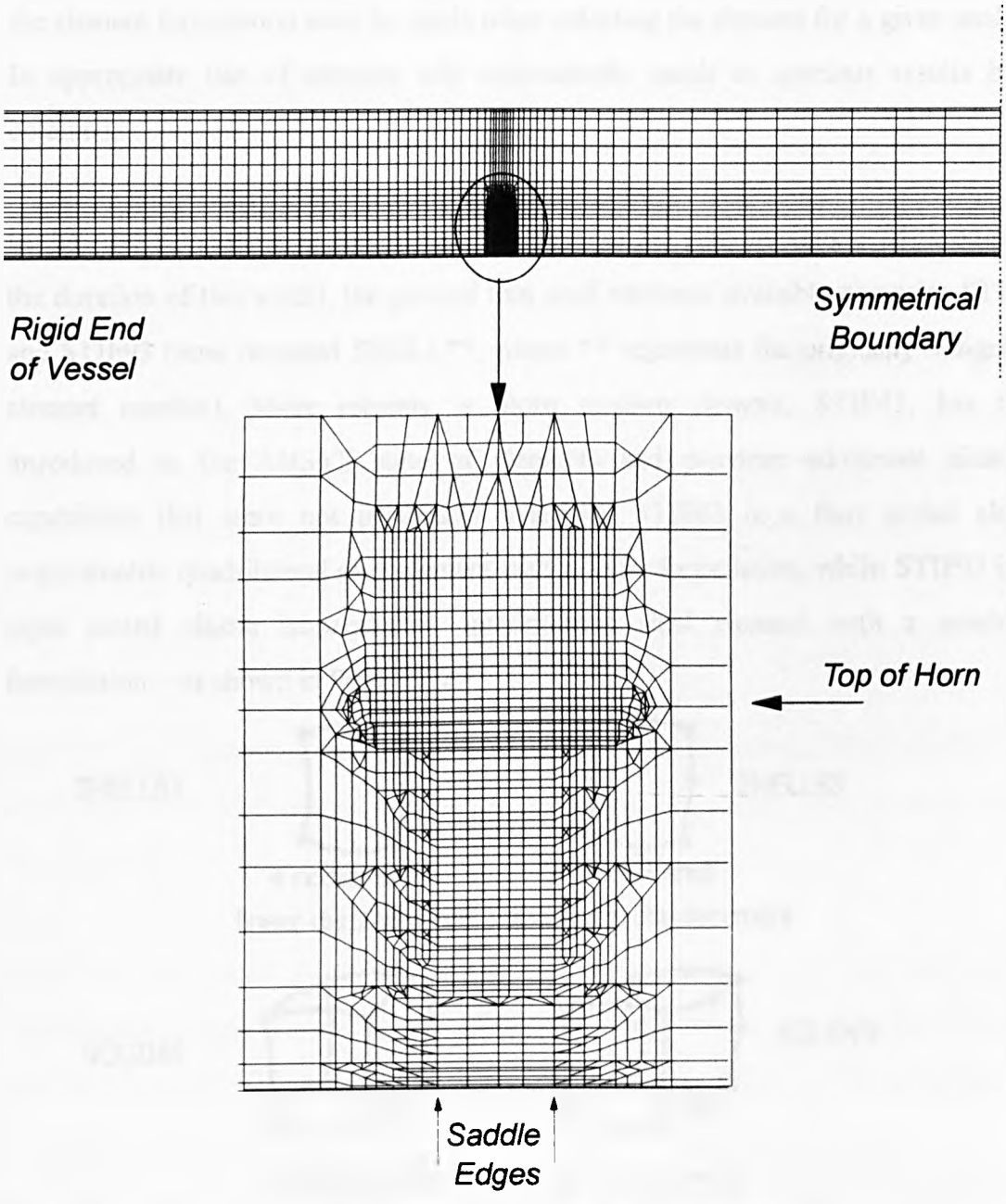

Figure 7.1 View of twin saddle supported vessel with symmetry constraints and zoomed view of the local fine mesh at the saddle horn

7.3 Element Types

The choice of element in any finite element model should be such that the element adequately describes the behaviour of the structure and makes use of any physical attributes that the structure may possess. In this particular case, the vessel has the property of being thin with respect to its radius and therefore, thin shell elements can be selected to model the overall behaviour of the vessel, although, as shown below, brick elements may be used. Careful consideration of the mathematical approach of the element formulation must be made when selecting the element for a given analysis. In appropriate use of element will undoubtedly result in spurious results being obtained.

In the ANSYS system, at Revisions 4.3A through 5.3 (the versions used throughout the duration of this work), the general thin shell elements available comprise STIF63 and STIF93 (now renamed SHELL**, where ** represents the originally designated element number). More recently, a more modern element, STIF43, has been introduced to the ANSYS suite of elements and provides additional plasticity capabilities that were not previously available. STIF63 is a four noded elastic isoparametric quadrilateral shell element with a linear formulation, whilst STIF93 is an eight noded elastic isoparametric quadrilateral shell element with a quadratic formulation ~ as shown in Figure 7.2.

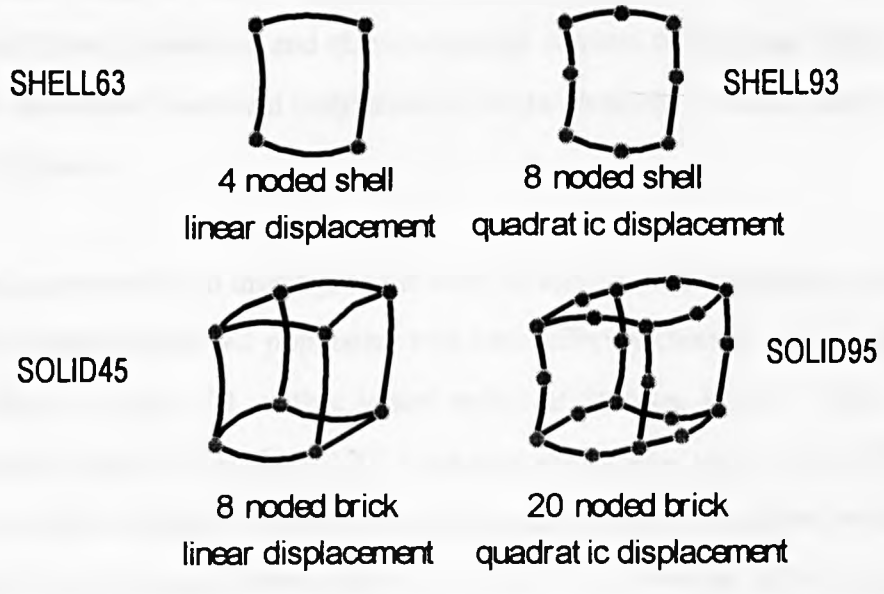

Figure 7.2 Standard element types used for pressure vessel analysis

It is worth recalling that the 4 noded shell and the 8 noded brick have a ***linear displacement*** formulation and the 8 noded shell and the 20 noded brick have a ***quadratic displacement*** formulation. The order of the interpolation function affects the variation of the function across the element. This becomes even more important when considering stress results since these are essentially the derivative of displacement results, thus linear displacements' become constant stress and quadratic displacement becoming a linear stress variation.

It is worth recalling that these elements require a numerical integration routine to enable calculation of the displacements. The most common integration routine used in finite element codes is the ***Gaussian Quadrature*** rule and therefore the resultant values for the function are always interior to the element nodal points. These locations are known as ***Gauss points***. The higher the order of quadrature, the closer the result at the Gauss point is to the actual value at the node.

The most important difference between the two element types is such that modelling using the STIF63 element produces an assemblage of flat shells which discretise the curved surface, whilst meshing using STIF93 curved shell elements produces a better approximation to the true geometry. However, the penalty for implementing the eight noded curved shell element is that it generates considerably more degrees of freedom and hence requires more computing power and disk space. All shell elements used possess three translations and three rotational degrees of freedom. Fuller descriptions of the theoretical basis and restrictions of these elements can be found in the ANSYS User Manuals.

A test case was run to investigate the level of accuracy, performance and run time for a given mesh density but populated with two different element types. Using the mesh described in Figure 7.1, with a vessel radius of 500mm, length = 36R, thickness of 10mm and saddles of angle of 120° located at the quarter points. The STIF93 element was therefore selected because of accuracy, albeit greater run times resulted, and this element type was used throughout this work. The following table compares various degrees of mesh refinement using STIF63 and STIF93 elements.

Model No.	Element Type	No. of Elements	Maximum Stress	Relative Run Time
1	STIF63	3320	-396.5 N/mm^2	1.0
2	STIF93	3320	-465.2 N/mm^2	2.6

Table 7.2 Element performance values (comparative times for an SG Iris computer)

As the maximum stresses are known to be located in the region of the horn of the saddle, a concentration of elements was introduced into this area - Figure 7.1. Since, the stress distribution varies both longitudinally and circumferentially in this region, a regular grid of rectangular STIF93 elements were generated in order to ensure that the shape functions would behave as accurately as possible. Convergence was checked by increasing the number of elements in the regular grid from two four noded shell elements either side of the saddle centreline to a final model comprising four eight noded shell elements located symmetrically about the horn centreline. The level of discretisation was necessary since the stress gradients are asymptotic at either end of the saddle horn.

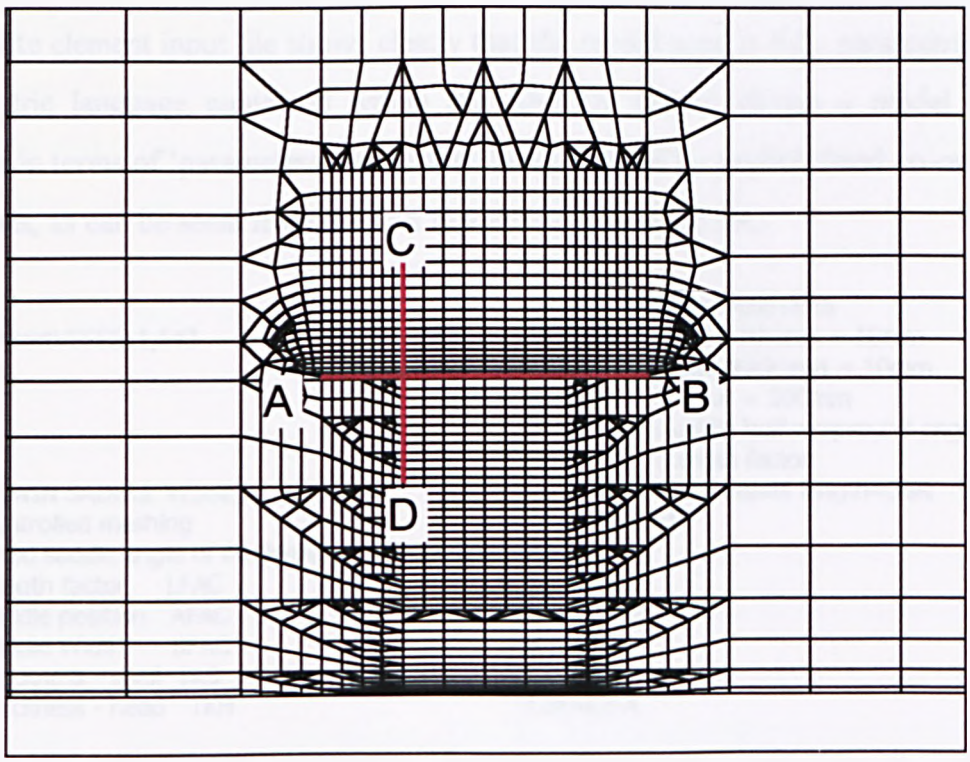

Figure 7.3 Zoomed plot showing mesh refinement and position of results lines

Figure 7.3 shows the finite element mesh in the region of the saddle contact area. The top left corner of the saddle is located at the intersection of the **A-B** and **C-D** lines. It can be seen that there is a regular mesh of eight elements across the width of the saddle and that the region directly above and below the saddle horn centre contains a very regular group of rectangular undistorted elements. In addition, the saddle contact area itself is meshed with regular shaped elements in order to maintain their performance.

Previous work by Widera, employed finite element analysis but it is the present authors consideration that the model was not sufficiently refined to ensure accurate results. This is principally due to the rapidly changing bending stress field in the vicinity of the saddle horn edges. The total quarter model size comprised some 3320 elements representing the vessel. In the saddle support region, it was assumed that the radial, tangential and axial displacements were zero, that is to say, the support was totally rigid. The choice of boundary condition is discussed later.

The finite element model file, which was created, is listed in Appendix of this thesis. The finite element input file shows clearly that the model used is fully parametric. The parametric language contained within the ANSYS system allows a model to be created in terms of 'parameters' rather than being defined by explicit fixed co-ordinate locations, as can be seem from the first few lines of the input file,

```
/PREP7
/GET,40,testVESSEL1,F43
AFAC=9
:L90
/PREP7
/nopr
/TITLE,TWIN SADDLE VESSEL
C*** Controlled meshing
C*** Fixed saddle angle of 60 degrees
C*** Length factor     LFAC
C*** Saddle position   AFAC
C*** Saddle Width      BFAC
C*** Thickness - shell  TKS
C*** Thickness - head   TKH
C*** DEFINE PARAMETERS
TKS=10    !Shell thickness = 10mm
TKH=10    !Head thickness = 10mm
R=500     !Radius = 500mm
ANG=60    !Saddle half wraproud angle=60
LFAC=36   !Length factor
L=LFAC*R !Total vessel length=36R
C*** AFAC=9
A=AFAC*R
BFAC=0.2
B=BFAC*R
B2=B/2
L2=L/2
L2A=L2-A
```

For the purposes of this model, the following syntax is used:

TKS	-	Shell thickness variable
TKH	-	Head thickness variable
R	-	Shell radius variable
ANG	-	Saddle half angle variable
LFAC	-	Length factor multiplier (L=LFAC*R)
AFAC	-	Saddle position, *A*, multiplier (A=AFAC*R)
BFAC	-	Saddle width, *B*, multiplier (B=BFAC*R)
REF1, REF2 & AREF	-	Various mesh refinement parameters

All geometry definition can be achieved by assigning numbers to the above parameters and running the model input file. The geometry is automatically created and meshed, ensuring that the regular grid is maintained and that as the saddle is moved (by altering the value of **AFAC**), all element sizes and shapes, are within the ANSYS allowable limits for shape, taper and skew.

Multiple runs are carried out using the ANSYS macro language. Samples of this are shown in Appendix 7 and these listings can be modified to allow any or all of the parameters to be the main variable when undertaking a parameter study.

7.4 Boundary Conditions and Loading

The boundary conditions associated with the saddle support problem make use of the two planes of symmetry which the vessel possesses. These planes lie along the axis of the vessel and at the profile located midway along the vessel length. Therefore, only one quarter of the vessel need be modelled and suitable symmetry boundary conditions are applied to ensure no out-of-plane displacements or rotations can exist. In order to investigate the stress distribution in this area, it was decided, on the basis of needing to derive results suitable for comparison with the Fourier series method, that a rigid saddle constraint should be adopted. This constraint, in reality, can be perceived to be a concrete or heavily reinforced saddle configuration with extensive support in the radial direction. Another justification for such an approach is that, in real situations, saddle construction can be quite variable, even though there exists a British Standard which gives guidelines and recommendations on saddle dimensioning. Therefore, it is quite possible that fabricators will produce, by accident or ignorance, an overly stiff saddle, which may therefore be considered as rigid. Therefore, in order to represent the 'worst-case' scenario, a rigid boundary is adopted

which will generated the largest maximum stress values, for comparison with the more ideal case assumed in the parametric study.

The mesh is also capable of solving various other problems including the incorporation of a flexible saddle, various configurations of 'rigid' saddle and the inclusion of the interface pressure profile generated by the SADDLE program as an initial condition.

There are a number of possible boundary conditions, which may be applied at the vessel saddle juncture. Firstly, the entire contact area may be fully fixed in all six degrees of freedom. This can be thought of as 'gluing' the saddle contact region to a rigid surface. The second option would be to only fully fix the saddle edges whereby contact is only enforced at the welds. Other options would allow the rotational degrees of freedom to be active and therefore introduce a measure of flexibility into the shell. However, it became clear that fully fixing the entire area produced results, which were much higher than those of the Fourier series analysis, whereas only fixing the edges produced distorted stress patterns. Therefore, in order to produce realistic stress results appropriate to the welded edge with a rigid foundation, it was found that the most effective boundary condition arose when the nodes at the edges of the saddle and/or at the saddle profile located by horn centreline were chosen to be constrained. For the present work, only the saddle and horn edges were constrained. The fully parametric ANSYS input file allows any of the above boundary conditions to be employed.

```
C*** Constraints acting on areas
csys,11
nrot,all
csys,0
symbc,0,1,L2
symbc,0,3
C*** Displacement constraints - Please select
C*** Select areas only
C*** Left Hand Part
arsel,,1,47
C*** Right Hand Part
arasel,,121,167
C*** Get nodes from areas
narea,1
d,all,all,0
nall
arall
C*** Add in load option
apsf,all,,,0,2,R*2,9.81E-6
wsort,x
afwrit
C***finish
```

```
C*** Constraints acting on lines
csys,11
nrot,all
csys,0
symbc,0,1,L2
symbc,0,3
C***Displacement constraints-Please select
C*** Select edges only
C*** Left Hand Edge
lsrsel,,2,54,4
lsasel,,13,29,16
lsasel,,53,63,10
lsasel,,70,147,7
C*** Add in Top Edge
lsasel,,148,151,3
lsasel,,370,372,2
C*** Add in Right Hand Edge
lsasel,,240,250,10
lsasel,,257,290,3
lsasel,,295,299,4
lsasel,,304,369,5
C*** Optional Centreline
lsasel,,4,56,4
lsasel,,25,45,20
lsasel,,61,152,7
C*** Get nodes from lines
nline,1
d,all,all,0
nall
lsall
C*** Add in load option
apsf,all,,,0,2,R*2,9.81E-6
C***finish
```

It is noted **from the above listings** that all nodes are rotated into the correct cylindrical co-ordinate system allowing the appropriate boundary conditions to act in the proper manner. Nodal rotation also implies that the results will be output such that radial, circumferential and longitudinal values will be available after the analysis is complete.

The head closure region of the model was designed to have various options, to allow the flexibility of the head to be examined. The results of these studies are presented in Chapter 8. However, in the present series and in order to make comparisons with the theoretical analysis of the SADDLE program, the vessel head was defined as fully rigid, i.e. the cross section of the vessel remains circular at the end of the vessel.

7.5 Automatic Mesh Refinement and Convergence

During the investigations of the effects of the flexibility of the dished head, it was noticed that warnings associated with element distortion were flagged when the saddle moved nearer the end. This was caused by the mesh refinement definition (REF1, REF2 and AREF) which assumed a 'fixed' level of mesh refinement in the saddle region which was based on the dimensions associated with the initial starting point of the parameter study i.e. $A=9R$, for a $36R$ long vessel. However, modifications to the file were introduced which allowed the meshing routines to improve the element density in the transition regions as and when required as the saddle region moved towards the end of the vessel, i.e. when $A/R<0.5$ then the

element mesh density inside the fixed zone alters in proportion to prevent element distortion. This check is incorporated at the end of the ANSYS input file as shown:

```
*IF,AFAC,LE,2.0,:L95
AFAC=AFAC-2.0
*GO,:L90
:L95
*IF,AFAC,LE,0.6,:L96
AFAC=AFAC-0.5
*GO,:L90
:L96
*IF,AFAC,LE,0.3,:L97
AFAC=AFAC-0.3
*GO,:L90
:L97
/EOF
```

7.6 Finite Element Results

The resulting stress gradients are shown in Figure 7.5 for the stress intensity values plotted along the axial and circumferential directions as described by Figure 7.3. These figures show that the stress gradient changes dramatically in the region of the horn apex. The magnitude and location of these twin peaks varies depending on the location of the saddle on the vessel and the results presented herein reflect only the magnitude irrespective of location. It is noted that over-constraining the model generates asymptotic values from a finite element analysis, since in this treatment, the saddle is represented as a rigid structure. These 'peaks' cannot have been detected experimentally due no doubt, to the difficulty in obtaining strain gauge results adjacent to the saddle horn weld and to the fact that real saddles, however rigid they may appear, are slightly flexible in the saddle horn region. The distribution of stress intensity shown in Figures 7.4a and b, point toward asymptotic values at the location representing the saddle edge. The magnitude of the stress will tend to infinity as the mesh is repeatedly refined and as the stress gradient continues to rise. The experimental value is superimposed onto the finite element output and corresponds to the average stress across the saddle width, as shown in Figure 7.4a. These results correspond to the vessel dimensions detailed in section 7.3, page 174, with a reduced specific gravity of 0.1.

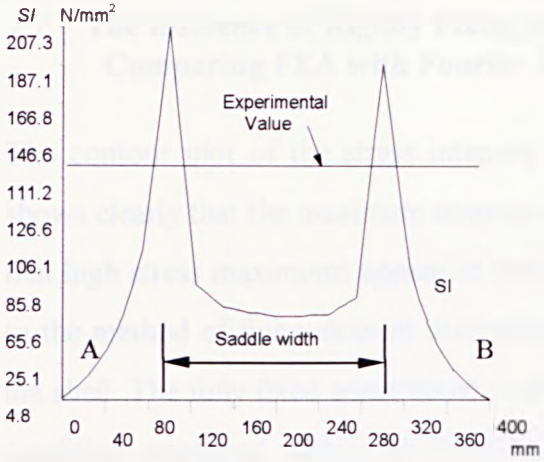

Stress Intensity Variation in Horn Region across Axial Distance A-B (Figure 7.3)

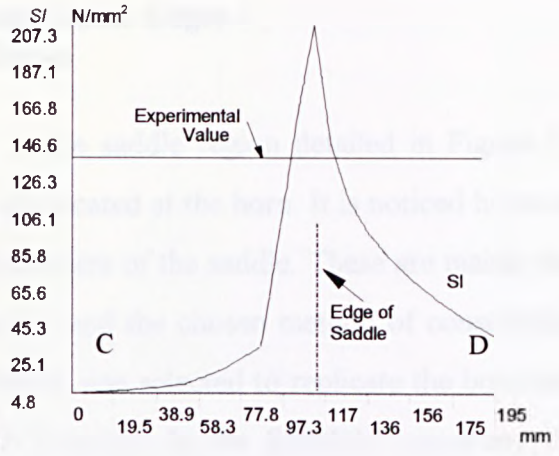

Stress Intensity Variation in Horn Region around Profile C-D (Figure 7.3)

Figure 7.4a,b Stress intensity gradients in axial and circumferential directions

Figure 7.5 shows a typical colour contour plot of the stress intensity values found at the saddle horns. The positions of the boundary conditions applied to represent the rigid saddles are shown as blue triangular constraints. The highly localised nature of the resulting stresses at the horn is clearly shown. The outer surface is plotted and the maximum compressive value (MN) is shown as blue. Red contours represent areas of tensile stress.

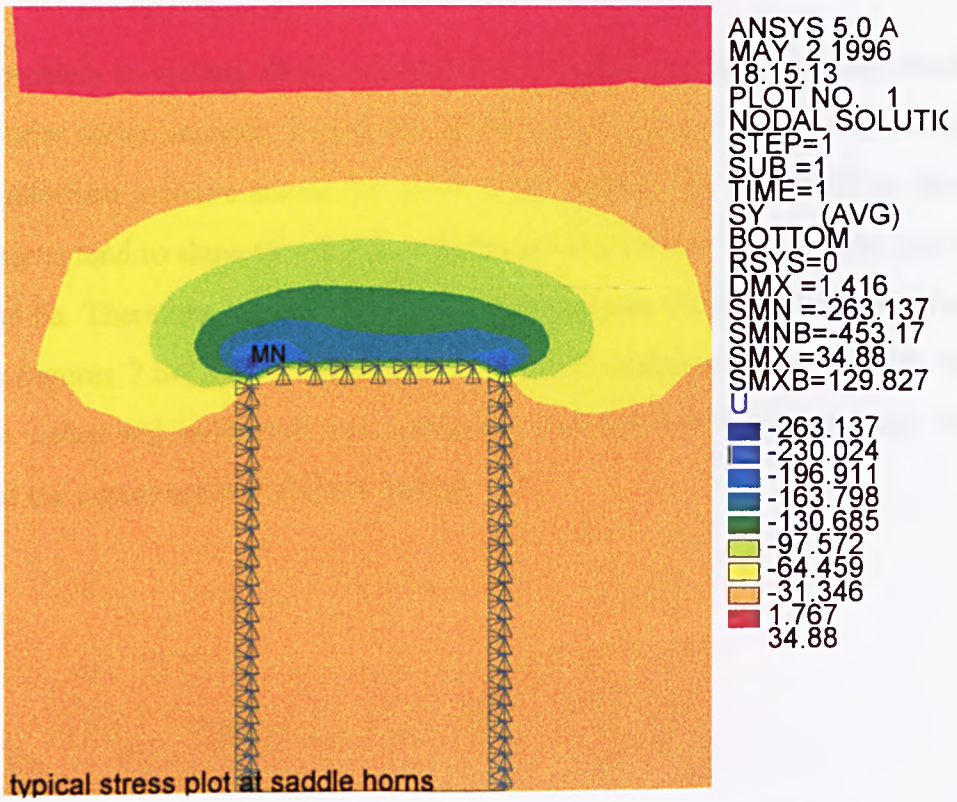

Figure 7.5 Contour plot of outside circumferential stress at saddle horn

7.7 The Influence of Rigidly Fixing the Saddle Edges - Comparing FEA with Fourier Series

The contour plot of the stress intensity in the saddle region detailed in Figure 7.5 shows clearly that the maximum stresses are located at the horn. It is noticed however that high stress maximums appear at both corners of the saddle. These are mainly due to the method of finite element discretisation and the chosen method of constraining the shell. The fully fixed constrained condition was selected to replicate the boundary condition employed within the SADDLE program. In the SADDLE program, the saddle centre profile is constrained and the saddle width supported by the appropriate uniform interface pressure. The finite element equivalent of a single constrained profile at the saddle centreline is too severe and therefore the saddle edges were fixed, that is, only the nodes at the edges of the saddle were constrained. The practical implication of this is that at the juncture between the loading lines (i.e. each corner of the saddle), the applied force is distributed over a point (i.e. a very small 'area') which consequently generates high stresses. These stresses do not arise in real situations.

The main problem in making direct comparisons between the finite element results and the Fourier series analysis, is that the SADDLE program assumes a uniformly distributed interface pressure across the width of the saddle. The results of the finite element analysis tend to show that this is probably not the case, at least for the case of the rigid saddle. Therefore, a graph of the average stresses on each patch has been drawn (see Figures 7.6-7.8), for Cases 1-3 as detailed earlier. For each graph, the mean stress value was evaluated and compared with the SADDLE program, the BS5500 and the experimentally derived values.

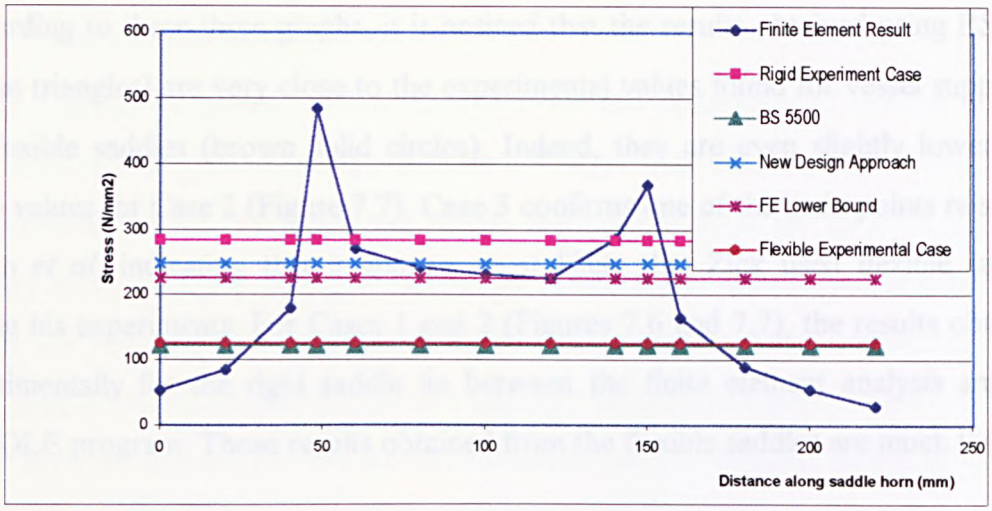

Figure 7.6 Stress distribution across saddle horn (Case 1)

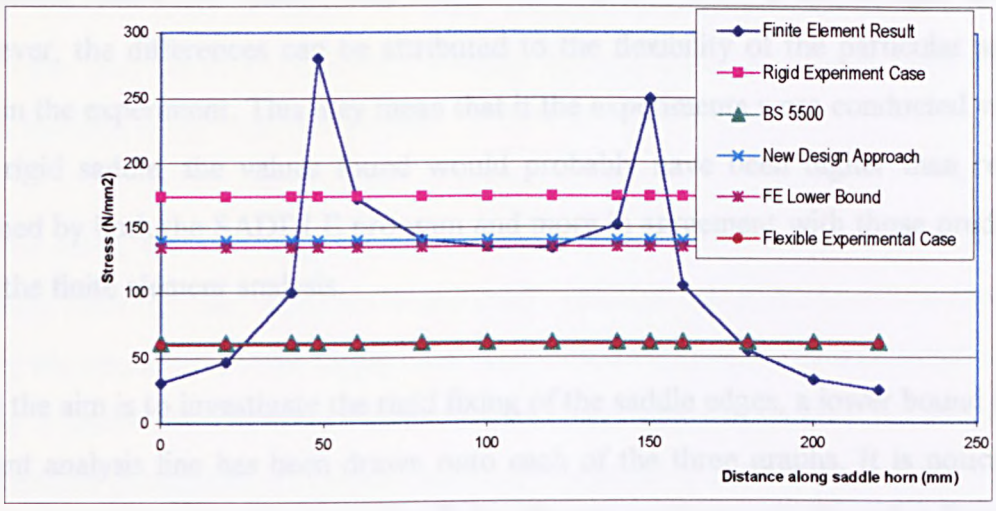

Figure 7.7 Stress distribution across saddle horn (Case 2)

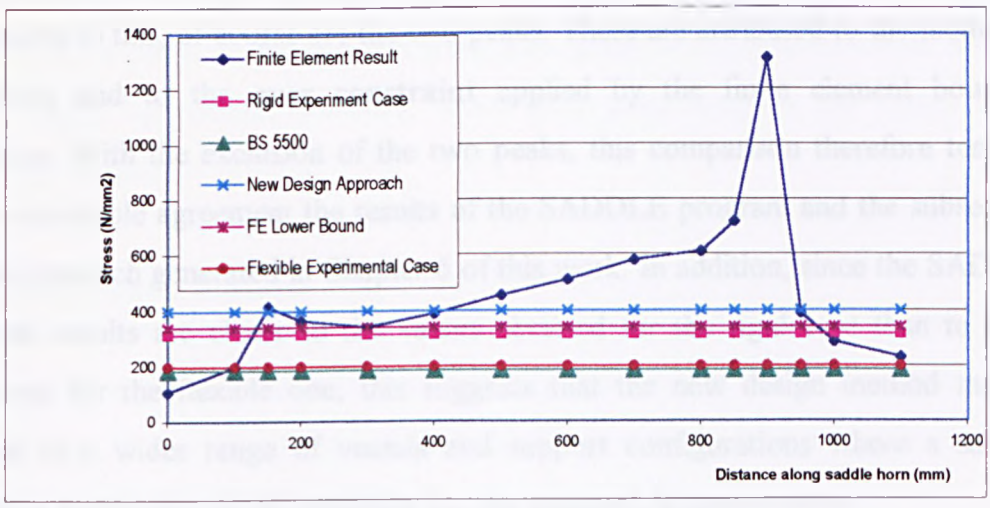

Figure 7.8 Stress distribution across saddle horn (Case 3)

According to these three graphs, it is noticed that the results obtained using BS5500 (green triangles) are very close to the experimental values found for vessel supported on flexible saddles (brown solid circles). Indeed, they are even slightly lower than these values for Case 2 (Figure 7.7). Case 3 confirms one of the main points raised by Tooth *et al*, indicating that it appears most likely that Zick used flexible saddles during his experiments. For Cases 1 and 2 (Figures 7.6 and 7.7), the results obtained experimentally for the rigid saddle lie between the finite element analysis and the SADDLE program. Those results obtained from the flexible saddles are much lower.

As for Case 3 (Figure 7.8), both the finite element analysis and the SADDLE program calculated values are higher than those found experimentally for a rigid saddle. However, the differences can be attributed to the flexibility of the particular saddle used in the experiment. This may mean that if the experiments were conducted with a fully rigid saddle, the values found would probably have been higher than results obtained by both the SADDLE program and more in agreement with those predicted from the finite element analysis.

Since the aim is to investigate the rigid fixing of the saddle edges, a lower bound finite element analysis line has been drawn onto each of the three graphs. It is noticeable that the lower bound value from the finite element analysis and the value from the SADDLE program are found to be very close to one another. However, the exceptions to this, of course are the two peaks. These are attributed to the method of modelling and to the **over constraint** applied by the finite element boundary condition. With the exclusion of the two peaks, this comparison therefore tends to show reasonable agreement the results of the SADDLE program and the subsequent design approach generated in Chapter 6 of this work. In addition, since the SADDLE program results are closer to the values obtained for the rigid case than to those measured for the flexible one, this suggests that the new design method may be applied to a wider range of vessels and support configurations where a suitable flexibility factor may not be available, i.e. the approach is conservative.

7.8 Nature of Maximum Stress

Using a design-by-analysis (DBA) approach for the assessment of stresses that are calculated by using finite element analysis is fraught with difficulty. Since the 1960's, the predominant tool for DBA was elastic thin shell analysis and as such, the rules employ many of these concepts, especially in the stress categorisation procedures which are required to assess the integrity of the vessel. Many researchers have attempted to develop robust procedures for use with finite element analysis which will either separate stresses into the recognised membrane and bending shell type stresses or to generate procedures for limit load evaluation.

Finite element analyses based on shell elements readily provide membrane and membrane plus bending component stresses. Results from this analysis type can be easily assessed using code procedures.

In some cases, where through thickness variations may not be linear, solid, brick type elements must be used. Analyses where solid continuum elements based on elasticity theory are employed do not supply shell type stresses automatically and therefore this makes it more difficult to fit into the traditional assessment method. Therefore, linearisation procedures to extract constant (membrane) and linear (bending) stress distributions have been suggested but have some limited applicability are not valid for all pressure vessel components. To date codes and standards authorities have not settled on one preferred method and work is on going to this end. However, there are some simple approaches available, which may point towards the nature of the resulting stresses.

Reduced Modulus Methods

The reduced modulus method was originally developed as a stress categorisation tool for piping systems but was later extended to cover a wider range of pressure vessel applications. These methods attempt to classify stresses by comparing the simulated inelastic response of a material with ideal primary and secondary stress. Many researchers have contributed towards this work. Most notably, Dhalla[69,70] who, while

assessing clamped pipes, found that stresses tend to redistribute due to the presence of the geometric non-linearity and thus could be considered as secondary, with secondary stress limits applied. In this, stress categorisation was not actually undertaken, rather the effect of local inelasticity was examined by iterative elastic analyses in which highly loaded regions were systematically weakened by reduction of the local modulus of elasticity in order to simulate the effect of local inelasticity. This approach was less time consuming than that of a full non-linear analysis. In addition, the need for complex non-linear material models was also removed. Dhalla extended his work to cover more general pressure vessel components.

Roche[71], Marriot[72], Seshadri [73],[74]and Mackenzie & Boyle[75-79] have all contributed extensively to the development of reduced modulus methods. A full list of references can be found in a literature review undertaken by Chan[80]. These include the development of stress classification procedures, lower bound limit load theorems, GLOSS analysis (generalised local stress strain analysis) and elastic compensation methods. The basis of each of the methods is similar to Dhalla's approach although variations in procedures and implementation have proved complex and time consuming. Many individual pressure vessel components have been assessed and presented in the literature. By considering many geometrical variations, many of the methods noted herein have been shown to have strengths and weaknesses. Even today, ASME, and other code writing bodies, have not wholly implemented reduced modulus methods.

Normalised Stress Strain Plot

Using a procedure developed by Dhalla, the nature of the stresses arising at the saddle horn is examined. In this, the procedure is based on apportioning elastically calculated stresses at highly loaded regions into primary & secondary components and applying appropriate stress limits to these stresses. Dhalla's method is summarised as follows:
Perform an elastic analysis and identify the most highly stressed regions of the structure noting the effective stress and strain, σ_A and ε_A.

Estimate the inelastic strain, ε_P corresponding to the elastic calculated stress. This is generally taken to be a rough estimate such as 1% membrane strain as defined in the ASME code.

Calculate the minimum secant modulus & assign to the most highly stresses zones

$$E_M^S = \frac{\sigma_A}{\varepsilon_P}$$

Perform at least three elastic analyses assuming reduced elastic moduli varying between the original modulus, E, and the minimum estimated modulus, E_M, for the most highly stresses regions. This establishes a trend in relaxation due to the simulated inelasticity.

Plot the effective stresses and strains for the original and reduced modulus analyses to define several points, R for each reduced analyses. Lines, defined as mixed response lines, are drawn between the elastically calculated point A, and the reduced points, R on the normalised plot, shown as Figure 7.9

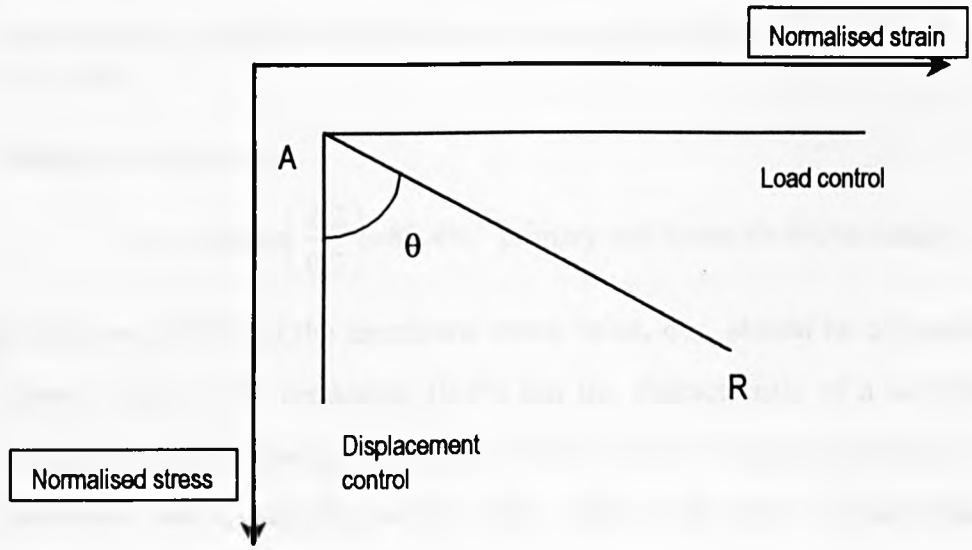

Figure 7.9 Normalised stress-strain plot (after Dhalla)

Dhalla defines the mixed response in terms of the rotation, θ. The rotation with respect to the 100% displacement controlled line determines the percentage of elastic stress, which should be classified as primary or secondary. If θ=0°, then the stress component is taken as 100% displacement controlled, hence 100% secondary stress. If θ=90°, then the stress is taken as 100% load controlled, hence 100% primary stress. For a mixed response, the amount of primary stress is calculated as ***PSF***=θ/90.

Applying this to the saddle problem for Case 3 geometry, results in the following diagram being constructed (Figure 7.10)

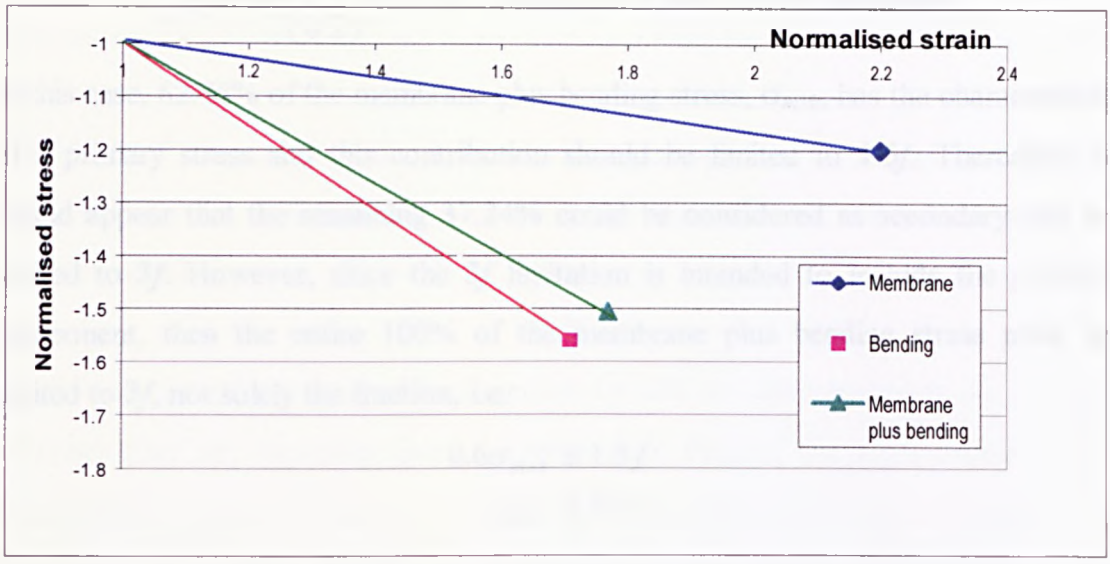

Figure 7.10 Normalised stress-strain plot for saddle supported cylinder (Case3)

Examining the gradients of each line allows an estimation of the nature of the stresses to be made.

Membrane stress, σ_m

$$\sigma_m = \arctan\left(\frac{2.2}{0.2}\right) = 89.4\% \quad \text{primary and hence } 10.6\% \text{ secondary}$$

In this case, 89.4% of the membrane stress value, σ_m, should be compared with the primary limit, f. The remaining 10.6% has the characteristic of a secondary stress. Neither BS 5500 Annex A nor ASME VIII Division 2 makes mention of secondary membrane stress category which often exhibits the same characteristics as the secondary stress category. Since the membrane stress has a predominately primary characteristic, for the case shown, the following limits should be observed,

$$0.894\sigma_m \leq f$$
$$\sigma_m \leq f$$

Membrane plus bending stress, σ_{m+b}

$$\sigma_m = \arctan\left(\frac{2.2}{0.2}\right) = 89.4\% \quad \text{primary and hence } 10.6\% \text{ secondary}$$

In this case, 62.76% of the membrane plus bending stress, σ_{m+b}, has the characteristic of a primary stress and this contribution should be limited to **1.5*f***. Thereafter, it would appear that the remaining 37.24% could be considered as secondary and be limited to **3*f***. However, since the **3*f*** limitation is intended to include the primary component, then the entire 100% of the membrane plus bending stress must be limited to **3*f***, not solely the fraction, i.e.

$$0.6\sigma_{m+b} \leq 1.5f$$
$$\sigma_{m+b} \leq 3f$$

7.9 Run Times

One of the important factors, which must be considered when choosing a design method, is the time for calculation. During this study, timings were measured in order to compare the relative performances of the finite element analysis and of the SADDLE program using two different reasonably powerful computers. The SADDLE program was run using 600 and 200 terms in each of the respective Fourier series (m and n numbers).

In Table 7.2, 'per case' for the saddle PROGRAM is a series of results for a single vessel with a line of results at 10 subdivided intervals. For the FEA result, this pertains to the quarter model described previously.

Computer Type	SADDLE program	Finite Element Analysis
486 PC		N/A
SUN Sparc 1+	45 min / case	60 min / case
APOLLO	12 min / case	35 min / case

Table 7.2. Solution run times

According to this table, running the SADDLE program appears somewhat faster than the equivalent finite element run. And it may be stated that as the results obtained with the SADDLE program are comparable with those found with the finite element analysis, the first method appears to be more appealing than the second. Indeed, since the proposed design method of Chapter 6 yields results which are almost identical to the SADDLE program, and the new method may be mounted on a simple PC or hand held calculator, it is believed this is the most beneficial method of providing an accurate solution.

At the time of writing, powerful computers are still not wide spread in the industry although they are becoming more commonplace. Indeed, the main problem with employing finite element analysis in most UK design offices is the lack of experienced finite element analysts. However, if the proposed design method were used, then typically, thetime taken to mount on a spreadsheet is less than 1 hour and thereafter solutions are available in seconds. Hence, if an analysis route is being considered based on both time of calculation and the degree of accuracy expected, then the design method presented herein appears to be the best choice over FEA methods.

8 THE INFLUENCE OF THE FLEXIBILITY OF THE VESSEL END ON THE TWIN SADDLE PROBLEM

8.1 Introduction

In previous chapters, a design methodology and worksheet have been developed for twin saddle supported cylindrical vessels in which one of the major assumptions is that the cylinder has totally rigid ends. In practice, dished ends are usually formed into a ***hemispherical***, ***torispherical***, ***ellipsoidal*** or ***flat*** profile, each possessing some degree of flexibility. This is a longstanding problem, and to date there is no robust approach present for designers to assess the effect of the end closure on the stresses at the saddle horn. Results of extensive finite element studies are presented in this chapter which demonstrate the influence of the dished end flexibility on the maximum stress in the vessel at the location of the horn of the saddle. This allows the generation of a '***new flexibility factor***' for incorporation into the simple design method already proposed. The factor is given in Equation 6.2 as F_e.

The analysis of pressure vessels supported on twin saddles is generally performed using a method first presented by Zick. This method employed a modified beam and ring analysis which, in turn, yielded a mathematical model for the vessel and saddle arrangement. The modifications were such that the predicted values of the method agreed with the experimental values available at that time. As indicated earlier, recent work by Tooth *et al* has indicated that Zick's treatment for the vessel, full of fluid, predicts stresses which are in reasonable agreement with experimental values only when a flexible saddle is used. When a more rigid saddle is employed, the method underestimates the maximum stresses which occur in the vessel. These stresses, located at the horn of the saddle on the outside surface of the vessel, may in some cases have a magnitude of twice the value predicted by Zick's method.

Advances have been made in understanding the stress systems associated with support regions of these vessels since Zick's treatment was first proposed. An alternative analysis method proposed by Tooth *et al*, has shown that the twin saddle

support problem may be adequately modelled using shell analysis and a double Fourier series approach. In this, the specified loadings of vessel self-weight, liquid contents and pressure loadings are represented by double Fourier series. The interaction forces and the radial and tangential interface pressures, between the vessel shell and the saddle support are the major unknowns of the problem. These forces are determined using classical small displacement shell equations for the vessel and by enforcing compatibility and equilibrium at the shell/saddle interface. The displacement functions are also represented by double Fourier series of the form,

$$u = \sum_{m=0}^{\infty}\sum_{n=0}^{\infty} u_{m,n} \cos(\frac{m\pi x}{L})\cos(n\phi)$$

$$v = \sum_{m=1}^{\infty}\sum_{n=1}^{\infty} v_{m,n} \sin(\frac{m\pi x}{L})\sin(n\phi)$$

$$w = \sum_{m=1}^{\infty}\sum_{n=0}^{\infty} w_{m,n} \sin(\frac{m\pi x}{L})\cos(n\phi)$$

(8.1)

The choice of this type of expansion for both the load and displacement indicate that the loading system is symmetric with respect to the generator passing through the nadir of the vessel at $\phi = 0$. They also imply that certain boundary conditions must exist at the ends of the vessel. Since the origin of the co-ordinate system is taken to be at one end of the cylinder, all the Fourier expansion terms or their derivatives, containing the term $\sin(m\pi x/L)$, vanish at the ends of the cylinder. This implies that,

- The ends cannot deform in the plane of their profile
- No rigid body displacement of the ends can occur
- The ends cannot carry applied axial loading
- Generators are free to rotate in a plane normal to the profile

If the vessel ends conform to the above boundary conditions then the Fourier expansions provide a complete solution to the governing differential equations of the problem, as detailed by Duthie and Tooth[3]. In practice, however, there will be some

deviation from this theoretical boundary condition since most practical pressure vessels utilise hemispherical, torispherical or semi-ellipsoidal dished ends. In some cases, however, a vessel may have an end closure which maintains the circularity and is very rigid compared with the vessel flexibility. In such cases, for example a high pressure vessel closed at the ends by a thick bolted blank flange, the vessel shape will remain completely circular under loading and the boundary conditions noted above are satisfied. In this situation, plotting a graph of displacements and stresses along the vessel axis would show that the values tend to zero at the ends of the vessel. Realistically, there will be some value of stress and displacement allowed at the end of the cylinder, due to the actual flexibility of the dished end. To adequately represent the vessel behaviour these effects must ideally be incorporated into the analysis.

8.2 Treatment in the British Standard - BS 5500

The importance of the end flexibility becomes increasingly important when the saddle support is located near the end of the vessel. Zick recognised that there would be a 'stiffening effect' present when the saddle was situated near to the vessel end. In his analysis, it was assumed that the shell could be represented as an arch loaded with a shear stress. Thereafter, the distribution of circumferential bending stress resultant can be found and in all cases, the maximum value was found to be at the horn of the saddle. The value of this moment can be expressed in the following form, using BS 5500 notation,

$$M_{max} = K_6 W_1 R \tag{8.2}$$

where W_1 is the load carried by one saddle and R is the vessel radius. The value K_6, is given in the table below (Table 8.1) for saddle positions $A/R \geq 1.0$. If the saddle is located near the vessel end, then substantial stiffening is anticipated and these values are reduced by a factor of 4 in the region $A/R < 0.5$. Intermediate values are found by linear interpolation.

A/R	Saddle Angle θ (degrees)			
	120	135	150	165
≤ 0.50	0.0132	0.0103	0.0079	0.0059
≥ 1.00	0.0528	0.0413	0.0316	0.0238

Table 8.1 Values of K_6 for use in BS5500 equation

For vessels of length greater or equal to $8R$, the bending moment generated at each horn is assumed to be supported over an effective vessel length of $4R$. The saddle also supports a direct load which is supported over the portion of shell stiffened by contact of the saddle, i.e. over a distance of (b_1+10t). Therefore, the total maximum circumferential stress, f_6, at the horn is,

$$f_6 = -\frac{W_1}{4t(b_1+10t)} - \frac{3}{2}K_6\frac{W_1}{t^2} \qquad \text{for } L/R \geq 8$$

For shorter vessels, the bending moment is assumed to be carried by $L/2$.

This results in the following equation,

$$f_6 = -\frac{W_1}{4t(b_1+10t)} - \frac{12}{Lt^2}K_6 W_1 r \qquad \text{for } L/R < 8$$

(8.3a,b)

In these equations, the symbols are defined as follows:

L = vessel parallel length

t = vessel wall thickness

b_1= saddle width

8.3 Present Treatment

From work detailed in Chapter 6 and in Reference [60] by the present author, the maximum stress at the horn can be expressed by the use of a 'basic stress' quantity which represents the stress for an imaginary vessel of length L=36R chosen such that the saddle horn stresses evaluated at this location are free from the influence of the vessel ends. Thereafter, a detailed study was carried out to enable the various controlling parameters to be isolated and quantified. An equation of the following form was employed using ***'factors'*** to represent the influences of the various

parameters and to allow the basic stress to be modified and related to the configuration of the real vessel under analysis.

The maximum stress at the horn can be expressed as,

$$\sigma_{\max} = \sigma_b . F_w . F_b . F_\theta . F_A . F_D . F_L$$

where,

F_w = factor associated with the vessel weight

F_b = factor associated with the saddle width

F_θ = factor associated with the saddle angle

F_A = factor associated with the saddle position

F_D = factor associated with the saddle interaction

F_L = factor associated with the vessel length

(8.4)

The stress evaluated by this equation is the maximum circumferential stress on the outside surface of the vessel. Its position is not always located at precisely the same geometric location, this depends on the configuration under consideration. In some cases, the maximum stress location can be situated above or, more often just underneath the saddle horn position. Indeed, the maximum stress location also moves axially across the saddle horns between the two saddle edges. This depends on the position of the saddle in relation to the vessel end points. If the saddle is located at the vessel quarter points, the maximum stress location is slightly offset from the saddle centre profile in the direction of the vessel end. As the saddle position is located nearer the end of the vessel, the maximum stress location moves across the saddle horn edge towards the inside edge of the saddle plate i.e. closer to the mid-span position.

However, using the rigorous shell analysis, the predicted maximum stress rapidly reduces as the saddle position is located the vessel end, since the Fourier series solution demands zero displacement at the ends of the cylinder.

8.4 Modelling the Flexibility of the Vessel Dished End

The flexibility of the vessel end has been analysed using finite element techniques. Four configurations of an end have been studied and their flexibilities characterised. These comprise, hemi-spherical, semi-ellipsoidal (2:1), flat and rigid heads. The local finite element mesh for each head is shown below in Figure 8.1.

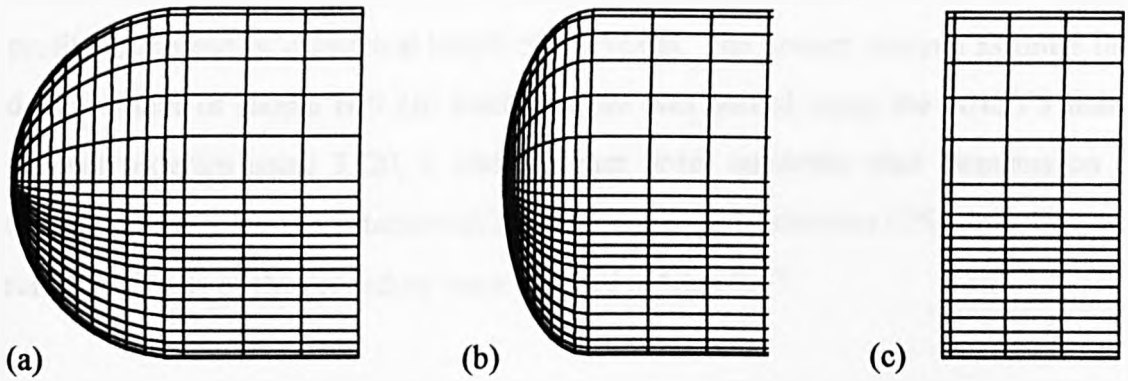

Figure 8.1a-c. Finite element meshes for the various head types

In addition to the vessel end being modelled accurately, due consideration must be given to the local mesh in the region of the saddle horn. Previous work by Widera[18,19], employed finite element analysis but the present author considers that the model was not sufficiently refined to ensure accurate results. This is principally due to the rapidly changing bending stress field in the vicinity of the saddle horn edges. Although Widera modelled the end explicitly, there is no indication that he investigated the influence of the end closure stiffness. The mesh used in the locality of the saddle is shown as Figure 7.1. In the saddle support region, it was assumed that the radial, tangential and axial displacements were zero at the saddle edges, that is, the support was totally rigid at these locations.

8.5 Parameter Study

Using the local mesh geometries described in Chapter 7, with the vessel length equal to $36R$, a parameter study was carried out for the four head configurations. The range of thickness variations encompassed the following ranges,

$$50 \leq \frac{R}{t} \geq 300 \quad ; \quad 0.5 \leq \frac{t_{head}}{t_{shell}} \geq 2.0$$

(8.6)

where t_{head} and t_{shell} are the end and shell thicknesses respectively. The saddle position was varied from $A=9R$ which is approximately the quarter point for the theoretical vessel free from end effects to a distance of $A=0.3R$ which brings the saddle location to a position very near the vessel end weld. The symbol A is equal to the saddle centre profile to the end of cylindrical length of the vessel. The present analysis assumes the default width of saddle is $0.2R$. Each analysis was solved using the ANSYS finite element program using 3320, 8 noded higher order quadratic shell elements on a Silicon Graphics Iris workstation taking approximately 15 minutes CPU time for each run. The details of the procedure were outlined in Chapter 7.

8.6 Finite Element Results

From the results of the parameter study, a graph of **'end flexibility factor'**, F_e was obtained for a range of different saddle positions when the R/t ratio was varied from 50 to 300, for the three head types referred to in Figure 8.1. Typical output values for the maximum stresses are shown in Tables 8.2 and 8.3. for the cases where R/t=100.

Head Type	A=9R	A=7R	A=5R	A=3R	A=1R	A=0.5R
Rigid	-199.4	-182.1	-184.5	-179.6	-164.9	-155.6
Flat	-202.6	-188.4	-192.6	-188.3	-167.7	-155.1
Ellipsoidal	-203.6	-188.3	-193.8	-191.7	-176.1	-166.4
Hemispherical	-205.1	-188.4	-195.3	-193.1	-181.3	-171.1

Table 8.2 Maximum stress values for various saddle positions and head types (R/t=100) in N/mm²

t_b / t_s	A=9R	A=7R	A=5R	A=3R	A=1R	A=0.5R
0.5	-203.6	-188.4	-193.9	-191.9	-176.6	-166.4
0.75	-203.6	-188.2	-193.9	-191.8	-176.4	-166.4
1.0	-203.6	-188.3	-193.8	-191.7	-176.1	-166.4
1.5	-203.6	-188.2	-193.8	-191.6	-176.1	-166.4
2.0	-203.6	-188.2	-193.6	-191.4	-176.0	-166.4

Table 8.3 Maximum stress values for various saddle positions and thickness ratios for a semi-ellipsoidal head (R/t=100) in N/mm²

It is noted that the values appear to be independent of the head type used and also of the head to shell thickness ratio **within reasonable limits**. In view of this, Figure 8.4 can be plotted - it is applicable for all head types and head to shell thickness ratios.

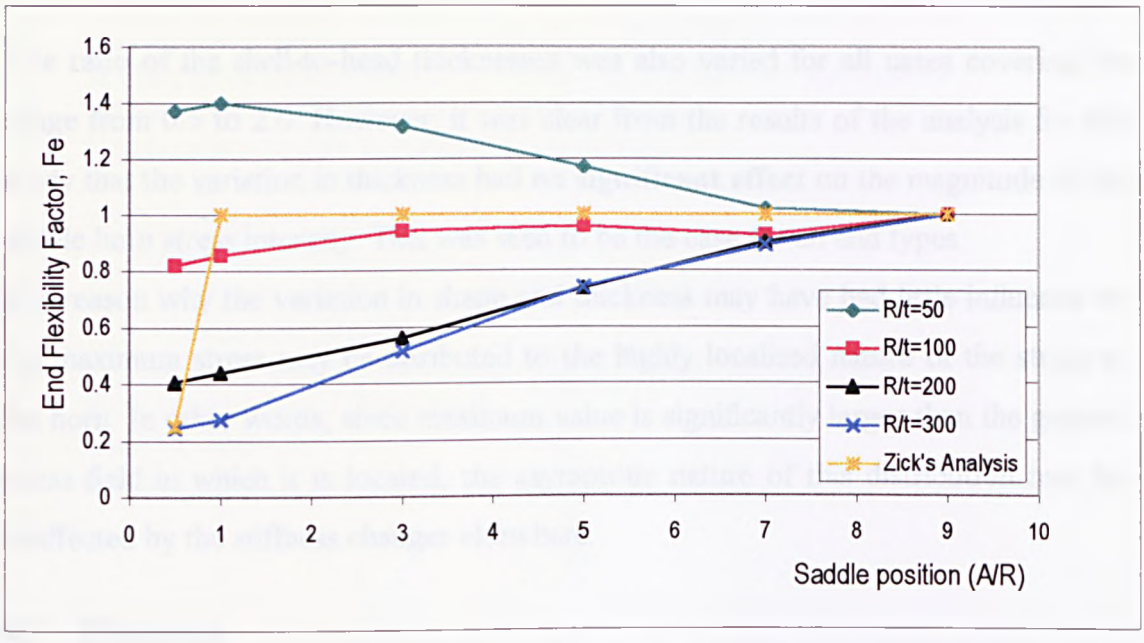

Figure 8.4 Graph of end flexibility factor, F_e

The end flexibility factor is derived by producing a multiplication factor for the basic stress for the saddle position at A/R=9, i.e. the distance at which the saddle horn stress is free from the influence of the end. This factor can now be incorporated into Equation 6.2 and the rigorous shell analysis detailed earlier to represent the influence of the vessel end.

The behaviour at each R/t ratio can be clearly seen and, on comparing the reduction in stress with that predicted by Zick, it is clear that **Zick's approximation is only valid for larger *R/t* ratios.** These large R/t ratio vessels are inherently more flexible and the influence of the end can be effective at distances greater than the A/R=1.0 proposed by Zick.

The analysis procedure was carried out for the three head types detailed earlier. In addition, a rigid head was modelled using constraint equations which simulated a head representing the Fourier series constraints. This end type had the same effect on the saddle horn stress as the three configurations.

The ratio of the shell-to-head thicknesses was also varied for all cases covering the range from 0.5 to 2.0. However, it was clear from the results of the analysis for this study that the variation in thickness had **no significant effect** on the magnitude of the saddle horn stress intensity. This was seen to be the case for all end types.
The reason why the variation in shape and thickness may have had little influence on the maximum stress may be attributed to the highly localised nature of the stress at the horn. In other words, since maximum value is significantly larger than the general stress field in which it is located, the asymptotic nature of this distribution may be unaffected by the stiffness changes elsewhere.

8.7 Discussion

The flexibility of a variety of pressure vessel end closure types has been examined using finite element analysis. A flexibility factor has been identified and presented in a useful form for inclusion to a design method presented previous by the author. This method has particular relevance to those designs where good stress data is required for fatigue assessments. Additional comments have been made with regard to the conventional design procedure of Zick and some guidance is provided on areas where that method is inadequate.

This work is published by the author as Reference [61].

9 THE INFLUENCE OF THE SADDLE FLEXIBILITY ON THE STRESSES AT THE HORN OF THE SADDLE SUPPORT

9.1 Introduction

The twin saddle supported cylindrical vessel is subject to a range of externally applied forces (internal pressure, liquid loading and self-weight) and reactive interface forces are generated at the saddle supports. The key to understanding the behaviour of the support problem lies in deriving these interface forces. Their magnitude and distribution depends upon the vessel flexibility and the rigidity, or otherwise, of the support. In earlier analytical and experimental work by Tooth, the configuration of the support was found to have a crucial effect on the stress in the vessel, primarily in the horn region of the saddle. From earlier experience, it is known that the vessel stresses can be reduced by up to 50 per cent when a flexible saddle is employed.

As a supplement to the previous work of Chapter 6, it is the aim of this chapter to expand on theoretical treatment shown earlier and to show how the flexibility of the saddle may be incorporated into the Fourier series analysis. The generation and important factors in successfully determining the flexibilities of a variety of saddle configurations are examined in detail using the ANSYS finite element program and some simple indication of the benefit of employing a flexible saddle is outlined.

9.2 The Interface System for Flexible Saddles

In order to determine the interface pressures between the saddle and the vessel, the saddle contact area is divided into a number of discrete areas, each of which is subject to ***unknown*** uniformly distributed pressures in both the radial and tangential directions. To reduce the complexity of the computation, the interface forces in the longitudinal direction have been ignored. It is considered that these forces will be small compared with the radial and tangential effects. However, in those cases where thermal effects may be important, the longitudinal interface forces will become more

dominant. In practice, when such effects are envisaged, one support is normally fixed and the other is free to slide, in order to allow for thermal expansion effects.

As mentioned earlier, Tooth and co-workers, in the first instance, assumed that these interface pressures were of constant magnitude across the saddle width. This assumption implied that the saddle had some flexibility across the width, thus avoiding the occurrence of high pressures at the edge profile of the saddle. However, when the saddles are of rigid construction in comparison to the vessel stiffness, for example in the case of concrete saddles, the above assumption is invalid. In order to investigate the effects of saddle flexibility, the saddle/vessel contact surface is divided up as shown in Figure 9.1in a manner previously used by Motashar[16]:

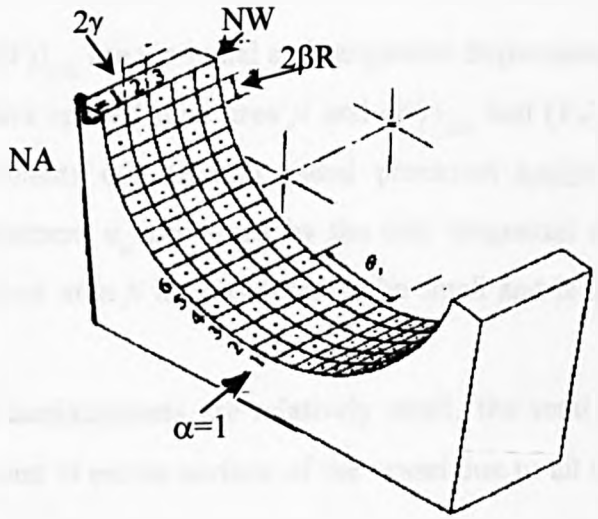

Figure 9.1. Flexible Saddle Interface Contact Areas

The discrete areas shown were made of equal size, $2\beta R \times 2\gamma$, as used in the SADDLE programs (and represented by *2.ALPHA.RADIUS×CC* in the ANSYS listings). The discrete areas in the axial direction are identified as ***i*** in the radial direction with a total number of divisions across the width equal to *NW*, in the ANSYS listings and represented by ***j*** and *NC* in the SADDLE program. In the circumferential direction, they are defined as ***j*** with a total number of angular discrete areas *NA* in the ANSYS

listings from the bottom to the saddle top and represented by i and NA in the SADDLE programs. As indicated, this approach was based on the earlier work of Motashar and Tooth for the analysis of metallic vessels supported on welded saddles which allowed the inclusion of the effects of the variation of the interface pressure across the width.

Each discrete area can be loaded with a uniform radial pressure and tangential shear (or surface traction). For example, on area *ji*, a radial pressure of p_{ji} and tangential traction of t_{ji} is assumed to act. The radial and tangential displacements of the vessel at a general point *kl* due to p_{ji} and t_{ji} is given by:

$$w_{kl} = t_{ji}(W_t)_{ji,kl} + p_{ji}(W_r)_{ji,kl}$$
$$v_{kl} = t_{ji}(V_t)_{ji,kl} + p_{ji}(V_r)_{ji,kl}$$

(9. 1a,b)

where $(W_t)_{ji,kl}$ and $(V_t)_{ji,kl}$ are the radial and tangential displacements of point *kl* due to unit tangential shears applied over area *ji* and $(W_r)_{ji,kl}$ and $(V_r)_{ji,kl}$ are the radial and tangential displacements due to unit radial pressures applied over area *ji*. The longitudinal displacement u_{kl} produced by the unit tangential shears and unit radial pressures applied over area *ji* is considered to be small and is ignored in the present analysis.

Assuming that all displacements are relatively small, the total radial and tangential displacements of point *kl* on the surface of the vessel due to all the interface loads are then given by:

$$W_{kl} = \sum_{j=1}^{NA}\sum_{i=1}^{NW} t_{ij}(w_t)_{ij,kl} + \sum_{j=1}^{NA}\sum_{i=1}^{NW} p_{ij}(w_r)_{ij,kl}$$
$$V_{kl} = \sum_{j=1}^{NA}\sum_{i=1}^{NW} t_{ij}(v_t)_{ij,kl} + \sum_{j=1}^{NA}\sum_{i=1}^{NW} p_{ij}(v_r)_{ij,kl}$$

(9. 2a,b)

These expressions are valid for *NW* discrete areas along the saddle width and the *NA* areas around each half saddle about $\theta = 0°$.

They can be rewritten in matrix form:

$$[W] = [WT][T] + [WR][P]$$
$$[V] = [VT][T] + [VR][P]$$

(9. 3a,b)

The elements of the flexibility matrices $[WR]$, $[VR]$, $[WT]$ and $[VT]$ are given by the series form of the displacements W and V in terms of the loading functions. The matrices $[T]$ and $[P]$ are the interface pressure values in the tangential and radial directions respectively.

These loading coefficients can be found by multiplying both sides of the loading terms contained in Fourier series by suitable orthogonal functions such that integration over the surface of the cylinder eliminates all but one of the terms in each Fourier expansion. In addition to the reactive interface forces, the vessel is subjected to various applied loading which maybe a combination of hydraulic pressure, internal pressure surcharge and the self-weight of the vessel. The loading coefficients for these can also be derived and used to obtain the radial and tangential displacements at the centre of the discrete areas of the support. These are written in matrix form as $[WHSW]$ and $[VHSW]$ respectively.

9.3 The Compatibility Equations

The unknown interfacial forces p_{ji} and t_{ji} which act at the various discrete areas will in general cause radial and tangential displacements of the saddle. The form of these displacements is similar to those for the vessel given in previous equations:

$$[WS] = -[WTS][T] - [WRS][P]$$
$$[VS] = -[VTS][T] - [VRS][P]$$

(9. 4a,b)

where $[WTS]$, $[WRS]$, $[VTS]$ and $[VRS]$ are the flexibility matrices of the saddle. The elements of these matrices can be obtained using a suitable mathematical model.

To enforce compatibility, the vessel displacements at the centres of the discrete area, due to the interface forces $[T]$ and $[P]$, that is $[W]$ and $[V]$, and the applied loading $[WHSW]$ and $[VHSW]$, are equated to the displacements of the corresponding points on the support, that is $[WS]$ and $[VS]$, given in equations (9.4) to give the following,

$$[VHSW] - \Delta[SN] + ([VT] + [VTS])[T] + ([VR] + [VRS])[P] = 0$$
$$[WHSW] - \Delta[CN] + ([WT] + [WTS])[T] + ([WR] + [WRS])[P] = 0$$

(9. 5a,b)

where Δ is a rigid body movement in the vertical direction of the saddles with reference to the vessel end profiles. $[CS]$ is the vector of elements $CS_j = \cos \theta_j$, $[SN]$ is the vector of elements $SN_j = \sin \theta_j$ is the angle to the centre of area j. When the saddle is rigid, its displacements are neglected and so the saddle flexibility matrices are equal to zero. The compatibility equations then become,

$$[VHSW] - \Delta[SN] + [VT][T] + [VR][P] = 0$$
$$[WHSW] - \Delta[CN] + [WT][T] + [WR][P] = 0$$

(9. 6a,b)

Finally, when considering vertical equilibrium, it is possible to write the following equation in the saddle region

$$[SN]^T[T] = S + [CS]^T[P]$$

(9. 7)

where S = (total of vessel weight + contents)/$(16\beta R\gamma)$.

9.4 Values of Strain and Stress in the Vessel Shell

Once the unknown interface forces $[T]$ and $[P]$ are obtained, they can then be combined with the vessel self-weight, fluid contents weight and pressure loading to obtain the total loading coefficients P_{rmn} and $P_{\theta mn}$. These may be used to determine

the displacements u_{mn}, v_{mn} and w_{mn}. Then using Fourier series equations U, V and W can be found, allowing the strain quantities and and stress resultants to be evaluated.

9.5 A Mathematical Model to evaluate the Saddle Flexibility

From the previous derivation, it is theoretically feasible to take the flexibility of the saddles into account by introducing four different matrices *(WRS, WTS, VRS, VTS)*, which represent the saddle displacements, into the two compatibility equations of a circular cylindrical vessel normally supported by rigid saddles. In fact, from a theoretical basis, the method of solving the problem is exactly the same, whether the saddle is considered flexible or not. However, it is quite difficult to obtain the four displacement matrices of the saddle and therefore, solving the flexible case becomes much more involved.

Several other researchers have attempted to solve this problem using finite elements to model the saddle. Motashar, with the help of the present author, solved this problem for two different geometries of welded saddle. However, he was applying **point unit** loads in radial and tangential directions at the centre of the discrete areas instead of applying pressure unit loads in radial or tangential directions on the all discrete areas, the results may not be wholly accurate. More recently, Tolson, also with the help of the present author, solved this problem for a GRP composite material vessel supported on twin rigid saddles with a piece of rubber located at the interface between vessel and saddle. The contact between the rubber and the vessel can be either, loose, frictional or frictionless. Pressure unit loads in the radial direction were applied on the discrete areas. Tolson neglected the displacements due to tangential loads and so this cannot be used to solve the welded case which requires both radial and tangential components of interface reaction.

The present work incorporates the application of radial and tangential pressure loads, in order to analyse and quantify the flexibility of the saddle and therefore obtain the required four flexibility matrices. For this work, the ANSYS finite element program was employed.

Finite Element Models using Shell Elements only

In order to obtain suitable flexibility matrices, a number of finite element models are generated. Previous workers have employed a crude solid saddle, however in order to reflect actual industrial designs, saddles with explicitly defined webs and wrapper plates are developed and progressively refined.

Simpler models can be created in the following manner. The saddle possesses two planes of symmetry and therefore it is only necessary to model one quarter of the geometry. Thereafter, the flexibility matrices can be reflected and populated accordingly as required. The method of construction is as follows. Firstly, the base and the three stiffeners stiffeners are constructed. Thereafter, by rotating a line between the top of each stiffener, the cylindrical portion of the saddle is created. This is designated as the saddle plate. To complete the saddle geometry construction, the central web was added and the geometry part of the model is thus complete. If required, reflecting the quarter model about two symmetry planes can generate a complete saddle as shown in Figure 9.2

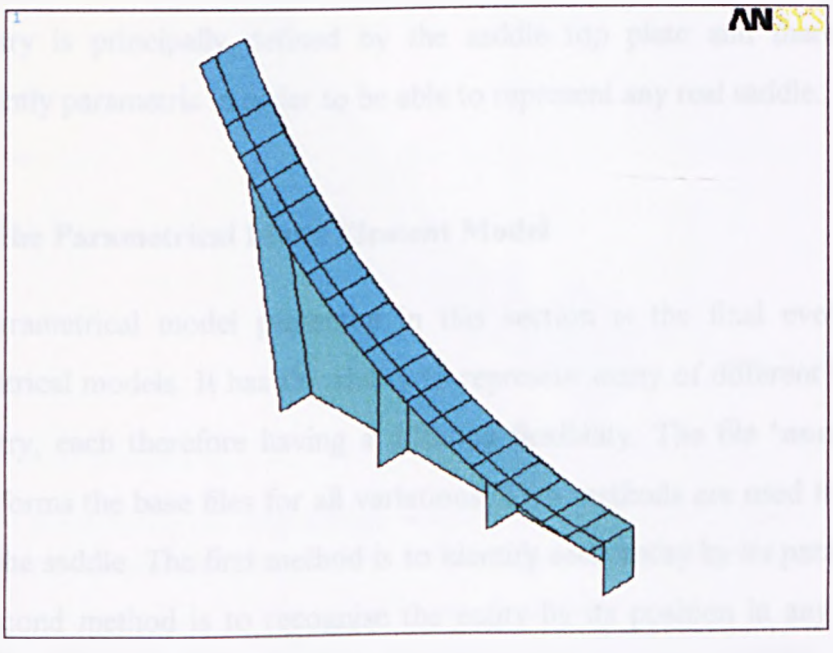

Figure 9.2 ANSYS quarter saddle geometry model

It is necessary to specify the number and the mathematical characteristics of the elements that are used in the finite element analysis for each geometrical part. Higher order quadratic displacement shell elements (ANSYS STIF 93) with 8 nodes, each with 6 degrees of freedom, were used throughout the entire geometric model of the saddle. Thicknesses were initially assumed to be 6mm in each plate. The material properties of steel were assigned as real constants for all elements, therefore Young's Modulus, $E=210\times10^3$ N/mm^2 and Poisson's ratio was taken to be, $\nu=0.3$. Automatic meshing cannot be used for this type of problem. If the standard meshing tool is used, then the element of the cylindrical portion of the saddle plate do not have the same dimensions. This in turn makes it very difficult to have a matching number of this element type on each cylindrical part. In fact, the cylindrical part of the saddle is considered to be the most important part of the finite element model, since the pressure loads will be applied on this region and it is the displacements of this part of the model which are required to generate the required flexibility matrices. In order to solve this problem, it is necessary to commence the finite element modelling of the saddle by the predefining the shaping of the cylindrical part. Thereafter the additional parts, webs, back plate and base would be defined in relation to the already defined saddle plate. Thus a new, completely parametric model was defined, one in which the geometry is principally defined by the saddle top plate and thereafter could be sufficiently parametric in order to be able to represent any real saddle.

9.6 The Parametrical Finite Element Model

The parametrical model presented in this section is the final evolution of many parametrical models. It has the ability to represent many of different styles of saddle geometry, each therefore having a differing flexibility. The file **'normal'** is created which forms the base files for all variations. Two methods are used to parametrically shape the saddle. The first method is to identify each entity by its parametric number. The second method is to recognise the entity by its position in any predefined co-ordinate system as specified in the finite element program, ANSYS. Both methods

have been employed in order to generate the parametric model. Each component of the saddle is described and the method of construction reviewed.

Cylindrical Plate Parameters

The geometry of the cylindrical plate (or saddle top plate) is defined by the radius of the saddle: *RADIUS*, the half saddle angle: *THETA*, and the half saddle width: *C*. It is important that the number of discrete areas also needs to be defined. The number of divisions across the total saddle width: *NW* and the number of divisions across the half saddle angle: *NA*. These divisions must correlate to inputs specified later in the SADDLE program. The flexible regions of the saddle are shown in the cutaway view of Figure 9.3. The width of the cylindrical part which can flex is defined as *T*. In order to have a good junction defined between the mesh of the stiffeners and the cylindrical part, the value of *T* is chosen as follows:

$$T = i*C/NW \text{ with } i=0 \text{ to } NW-1 \ (i \in \mathrm{N})$$

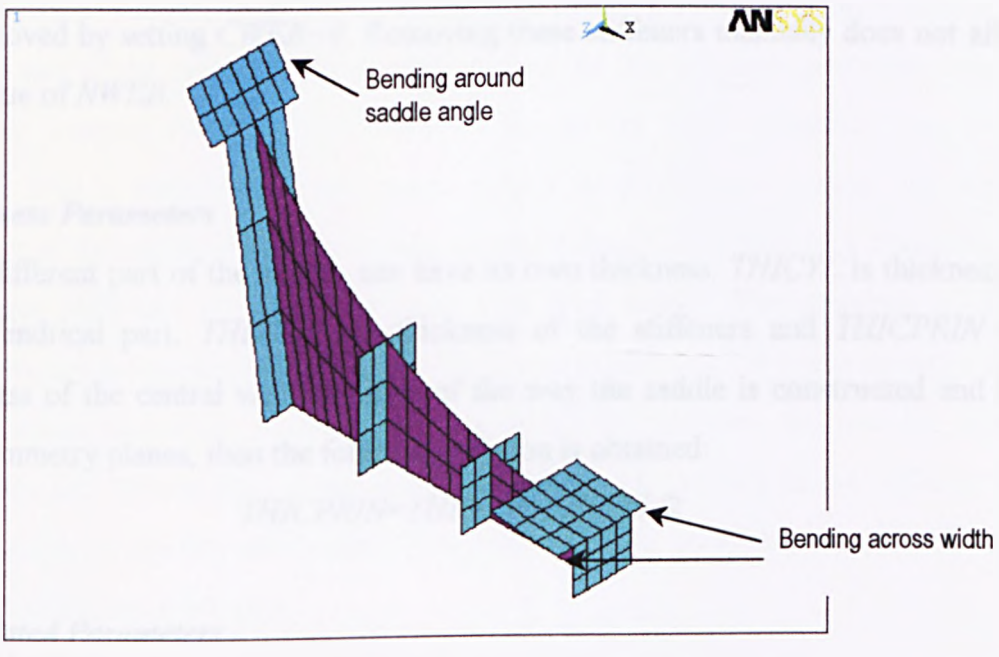

Figure 9.3 ANSYS cut half saddle model showing bending parts: across the width and around the saddle angle (cut for visualisation purposes)

If no extended bending portion is required then *i* is set equal to 0. Obviously, the higher the value of *NW* , the more precise is the value of *T*. Finally, the extended

saddle angle of the cylindrical part which can freely bend is described by: *THETA2*. In order to have a good juncture connection between the mesh of the largest stiffener and the cylindrical portion, the value of *THETA2* is chosen as follows:

$$THETA2=J*THETA/2/NA \text{ with } J=0 \text{ to } 2\times NA-NWEB-1 \ (j\in \mathrm{N})$$

If no extended bending part is required then j is set equal to 0. Obviously, the higher the value of *NA* is the more precise is the value of *THETA2*.

Stiffener Parameters

The basic parameters of the stiffener are defined as the height at the centre of the saddle (at *THETA*=0): *B*, the angle with the vertical axis of the largest stiffener: *BETA*, and the total number of stiffeners excluding counting the stiffener located at the centre of the saddle: *NWEB*. The largest stiffener at the saddle extremity may be removed when *EXTWEB=0*, and the central stiffener at the middle of the saddle can be removed by setting *CWEB=0*. Removing these stiffeners manually does not affect the value of *NWEB*.

Thickness Parameters

Each different part of the saddle, can have its own thickness. *THICYL* is thickness of the cylindrical part, *THIWEB* the thickness of the stiffeners and *THICPRIN* the thickness of the central web. Because of the way the saddle is constructed and has two symmetry planes, then the following relation is obtained:

$$THICPRIN=THIWEB=THICYL/2$$

Calculated Parameters

Various parameters are calculated using the values defined above and these are thereafter are used throughout the program.

The '**normal**' program is divided into four different parts: parametric definition, saddle geometry construction, loading and solution and lastly, results interpretation.

Parametric Definition

The different parameters used by the program are defined into three sub-parts as shown before. Users of the program are only required to modify the first geometrical parameters and the material properties. As this program performs a static analysis with an isotropic material only, the Young's Modulus and the Poisson's ratio are necessary at this stage.

Saddle Geometry Construction

This corresponds with the pre-processing stage (/PREP7) of the ANSYS program. Firstly, the element type and the material properties are defined. In order to have a good representation of the curved cylindrical part, quadratic shell elements with 8 nodes (STIF 93) are used for the mesh. Only one type of material is used and its material properties are defined with the *MP* command. Four different thicknesses, corresponding to the various parts of the model are defined with the *R* command to include the real constants of each saddle component.

Construction is briefly described as follows: by creating a line, rotating it around the central axis of the cylinder with an angle of *ALPHA*, the program generates a curved area. By copying this area *NDIV* times, it shapes the 'rigid' cylindrical part of the saddle. This is performed in the global cylindrical co-ordinate system. The largest stiffener at the saddle extremity is then created (even if *EXTWEB=0.*) Thereafter all the other stiffeners are created in turn (*NWEB-1* times). The positions of these stiffeners are automatically calculated. The layout is such that the space between them is the equal. However, in order to have continuity between the meshing of the stiffeners and the meshing of the cylindrical part, each top line of the stiffener area corresponds to one line which also belongs to one of the areas that are defined within the cylindrical top plate part.

Thereafter, the program generates the central stiffener. This is produced regardless of whether it is required or not (*CWEB=0*) If *CWEB=0*, this stiffener is deleted later. The base is created by generating areas between the bottom lines of the stiffeners. The central web is produced by creating areas between the vertical lines of two

stiffeners. If there is an extended bending part across the width, the program creates this part in a similar manner to the cylindrical part at the beginning. If there is an extended bending part arising from the saddle angle, the program creates one or two curved areas depending on the angle, whether this is required or not. It is deleted later as required.

At this point, one quarter of the model is generated and the number of divisions on each line of the design is defined to prepare for automatic meshing. Firstly, all the lines of the cylindrical part of the model are divided in order to have *NW* elements across the half saddle width and $2\times NA$ elements across the saddle angle. Thereafter, all the other lines from the stiffeners and central web are subdivided according to their reference number. In order to ensure good continuity between the meshing of the rigid cylindrical part and the meshing of the stiffeners, the number of divisions across the horizontal lines of these two parts must be the same: *ELNUM1*. Finally all areas of the model are meshed with their respective thicknesses and the finite element model is created.

If no stiffener at the saddle extremity or no middle stiffener is desired (*EXTWEB* or *CWEB* equal to 0) the respective areas are deleted. The areas that represent the base are deleted since the support fixture can be ensured by constraining all of the nodes on the base of the individual stiffeners and central web.

Finally the program creates the total half saddle by operating a symmetry reflection. All the nodes of the cylindrical part have their local co-ordinate systems rotated into the correct cylindrical co-ordinate system.

Solution Phase

This part is executed using the /SOLU part of the ANSYS program. The boundary conditions for the base of the saddle are applied by locating the nodes at the base of each stiffener bottoms and of the central web and setting their 6 degrees of freedom to zero i.e. fully fixed base. The nodes of the middle stiffener must have their degrees of freedom reduced accordingly because of the symmetry of the saddle in this plane. The load is sequentially applied using two loops. The two loops are created to run

NW×*NA* cases where a uniform pressure is applied on a discrete area. A file is opened to save the results directly for input to the SADDLE programs.

The uniform pressure is applied on four elements that correspond to one discrete area using the *SFE* command. Finally, the ANSYS solution routine is used to repeatedly solve the analysis.

Results

Postprocessing is undertaken to establish the required flexibility matrices using the /POST1 part of the ANSYS program. In this, the radial displacement of the central node of each discrete area is selected and written to the file opened previously. The two loops finally complete, the open file results file is closed, and the program stopped. By this time, ANSYS has solved the stress displacement solution: *NA*×*NW* times. This can take some considerable time to execute.

Output

The results of the '**normal**' program are written in a file called **disp*.***. The size of this file depends on the number of discrete areas chosen to run the ANSYS program. When the number of division across the saddle angle is chosen to be NA and the number of division across the saddle width is NW, the number of discrete areas will be NN=NW×NA. Therefore the **normal** program will **solve NN cases** and the size of the resulting program will be $27 \times NN^2$ bytes which correspond to *NN^2 displacements values*. This is a good method of verifying that all results are available.

This file contains a column of numbers which are the displacements of the central node of each discrete area for each case of applied unit load of pressure. Each block of NW×NA numbers corresponds to one applied load pressure case. Each block contains the displacements of the discrete areas from the bottom to the top across the saddle angle (NA values) and from the left to the right across the saddle width.

In the file **disp*.*** the displacements are saved load case by load case. Each load case generates NN×2 displacement values corresponding to the displacement in radial (first column) and tangential (second column) direction of the central node of each discrete area (NN areas) of the model in the following order: From the bottom to the top (j=1 to NA) across the saddle angle and so on across the saddle width (i=1 to NW).

9.7 Variations of the Parametrical Model

Three other ANSYS programs have been generated to represent structurally different styles of saddle. They are essentially developments or evolutions of the '**normal**' program. These differences are now described for each model.

9.7.1 Two Different Thicknesses In The Cylindrical Part

Under normal industrial circumstances, saddles are generally made with the same metal plate as that used in the cylindrical shell. However, BS 5276 shows saddles with extended wrapper plates and therefore it is possible that two different thicknesses may occur in the cylindrical part of the saddle plate as shown in Figure 9.4. These are often formed by metal plates welded together with the extremity only having one thickness.

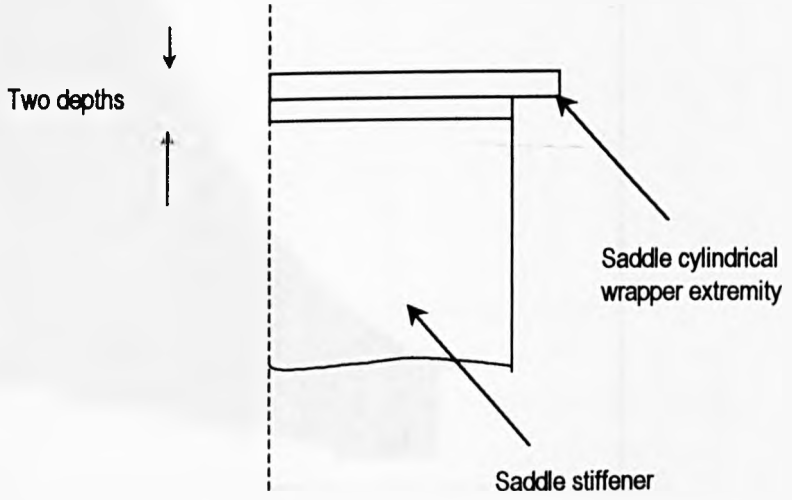

Figure 9.4 Schematic of saddle top plate and wrapper with two thicknesses

In this case, the extremity is able to bend more easily. This flexibility is introduced because it can significantly reduce the stresses in the saddle region. The method of construction is to build a normal saddle first, and thereafter to make a central cylindrical part of two thicknesses and finally another cylindrical part of one thickness around the first one with an offset of : *depth/2*. The nodes that correspond to the discontinuity between the two cylindrical parts have to be coupled with the CPINTF command, in order that they will have the same displacements acting as if there were only one node. This model, named '**twothick**' performs in exactly the same manner as the **normal** model, however has an improved flexibility in the extremity of the cylindrical part.

9.7.2 The Semi-Rigid Model

The '**semi-rigid saddle**' is the intermediate support style between the rigid (for example, a support made of concrete) and the fully flexible saddle. It has extra stiffening at the extreme outer edge and can only flex in certain parts. As with the **normal** flexible saddle, this model is flexible principally in the longitudinal direction.

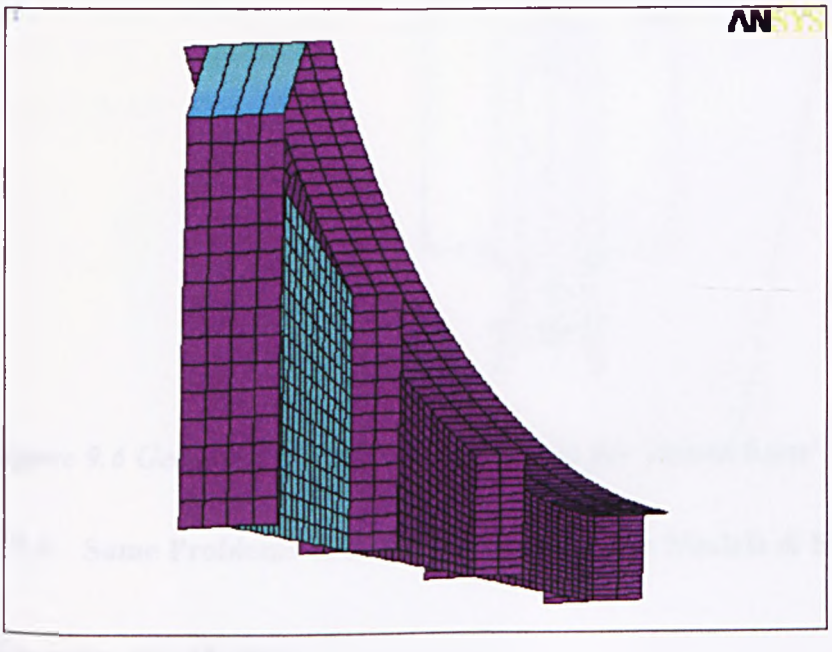

Figure 9.5 Semi rigid saddle model

The '**semi-rig**' model is basically the same as the '**normal**' flexible one but only the last stiffener has a significantly different shape. This stiffener is made of two parts:

one part is vertical and the other one is curved and locates normal to the cylindrical part, as shown in Figure 9.5.

9.7.3 The Round-Horn Model

When a saddle is made with welded metal plate, normally the horns are sometimes cut or formed with an angle grinder to obtain a rounded corner in order to minimise stress concentrations. This allows a reduction of the stresses in this critical part of the cylinder. The method of creation for such this geometry is to make an intersection between the cylindrical part of the saddle and 'virtual' geometric quarter of a cylinder. This model was not made fully parametric and was created just to demonstrate that it is possible to construct such a configuration, see Figure 9.6.

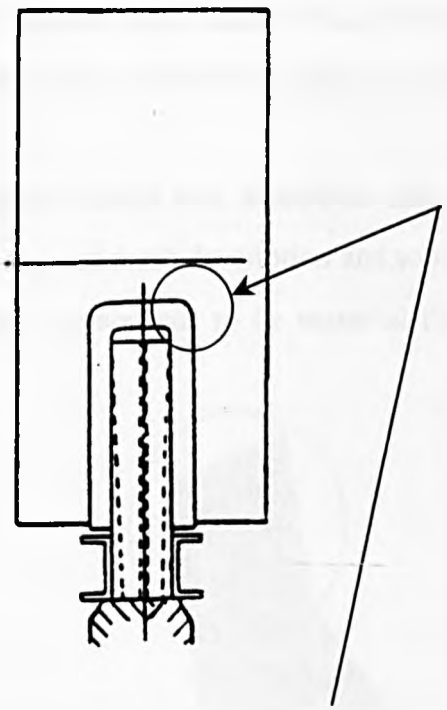

Figure 9.6 Geometry of curved construction for 'round-horn'

9.7.4 Some Problems & Restrictions with such Models & Solutions

Geometry and Meshing

Firstly, in the **normal** and the **twothick** parametric models, because of the sequence of geometry construction, the β angle cannot rise to a value of 90°-θ, as can be seen in Figure 9.7.

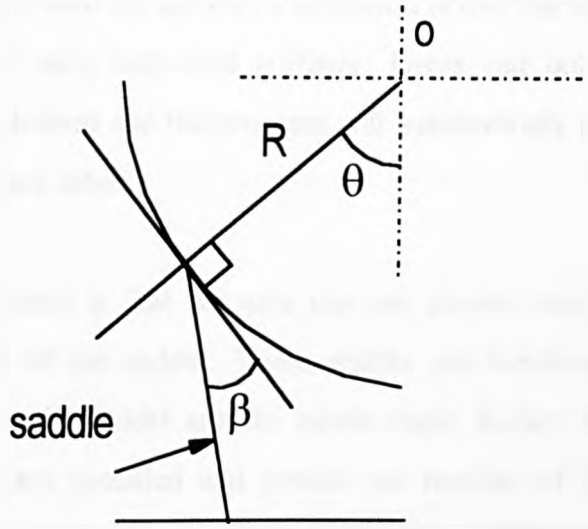

Figure 9.7 Geometry of curved construction

When the central web is meshed, it is impossible to have an element with a zero angle at the horn even when triangular elements are used. In fact, the case where the last stiffener is tangent to the cylindrical part ($\beta=90°-\theta$) cannot be represented by finite elements.

When shell elements are used, if the central web is meshed only with quadrilaterals (*ESHAPE,2*) then in order to have good mesh description and topology, β has to be: $\beta<90°-\theta-10°$. If quadrilaterals are deemed not to be essential then β can have the value of $\beta<90°-\theta-5°$.

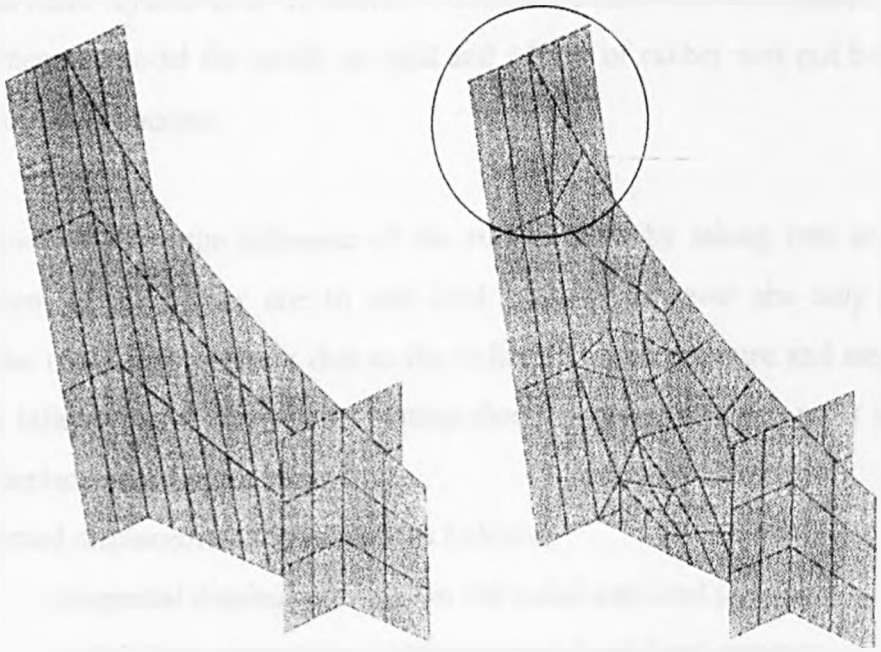

Figure 9.8 Quadrilaterals and triangular meshes showing extreme distortion

One major restriction with the geometry definition is that the user cannot choose the specific location of each individual stiffener. Users can only choose how many stiffeners are to be defined and the program will automatically position them at equal distance one from each other.

Finally, the last problem is that the user can not choose exactly the widths of the bending extremities of the saddle. These widths are functions of the number of divisions across the saddle width and the saddle angle. In fact, the more subdivisions of geometry which are specified and greater are number of discrete areas on the cylindrical part, the more the model is parametrical. However, this results in a significantly longer solution time.

Applied Unit Pressure Loads and Results

In the solution phase of the programs, a uniform unit pressure in the radial direction is applied sequentially, on all the discrete areas of the cylindrical portion of the saddle. Initially only the radial displacements of the central node of each discrete area were saved. This was done initially as the SADDLE solution employed at that stage was of the form generated by Tolson in 1991. In her thesis, she studied the behaviour of horizontal multi-layered GRP cylindrical vessels supported on twin saddles. She used finite element to model the saddle as rigid and a layer of rubber was put between the cylinder and the concrete.

Tolson tried to show the influence of the rubber layer by taking into account the displacement of the rubber due to unit load pressure however she only took into account the radial displacement due to the radial unit load pressure and neglected all the other influencing displacements stating that the radial was the most significant form of displacement for her case.

The neglected displacement forms were as follows:

- tangential displacement due to the radial unit load pressure
- radial displacement due to the tangential unit load pressure
- tangential displacement due to the tangential unit load pressure

In her case, the contact between the saddle and the cylinder was defined as loose frictional contact, which implies that for the interface pressure the following relation holds: $[T] = -\mu[P]$.

As shown previously, the compatibility equations for a circular cylindrical vessel supported by flexible saddles are:

$$(1) \quad [VHSW] - \Delta[SN] + ([VT] + [VTS]) [T] + ([VR] + [VRS]) [P] = 0$$

$$(2) \quad [WHSW] - \Delta[CN] + ([WT] + [WTS]) [T] + ([WR] + [WRS]) [P] = 0$$

(9. 8)

In Tolson's case this becomes:

$$(3) \quad [VHSW] - \Delta[SN] + ([VR] + [VRS] - \mu[VT] - \mu[VTS]) [P] = 0$$

$$(4) \quad [WHSW] - \Delta[CN] + ([WR] + [WRS] - \mu[WT] - \mu[WTS]) [P] = 0$$

(9. 9)

Therefore, in order to evaluate the interface pressure in her case, it is necessary to solve only one compatibility equation. Tolson elected the second one (4) and neglected the radial displacement due to the tangential unit pressure. In her case, it may have been valid because of the rubber. However for the present case, it is felt that this would not represent the interaction between the saddle and shell correctly.

In addition, since the saddle is welded to the cylinder and we do not have the relation: $[T] = -\mu[P]$. Thus Tolson's programs are not valid for the present case. Therefore equations (1) and (2) of (9.8) must be solved to find the interface pressures.

9.7.5 A Possible Solution

In order to establish the correct, complete flexibility matrices, a new finite element approach must be established. The essence of this is that the tangential load, by definition a surface traction, must be applied to the top surface of the saddle plate.

This proved to be a major stumbling block for much of this work since with ANSYS, tangential pressure loads cannot be applied directly onto shell elements. In fact, when the loading algorithm within the ANSYS program has to put a uniform pressure on elements or on surfaces, the logic is such that it applies a fraction of the total load as a series point forces on each node of the selected elements. One possible means of solving this problem would be to find the fraction and to apply these loads on each

node of the selected discrete area. However, the ratio of load application is not easily obtainable and it would be only valid for that one type of finite element (STIF 93 with 8 nodes for example). Different element implementations may have differing ratios. Although ANSYS does not allow the application of tangential pressure on shell elements, it does provide functionality to apply such a load on a brick-type element. This is achieved by the use of a special '**surface effect element'** called SURF22. This element is overlaid onto an area of any 3D-element, and can be thought of as a form of 'skin'. This can be used for various load effect applications. It can be defined to have no structural stiffness and does not contribute to the behaviour of the saddle in any way other than to apply the load at the correct position.

This element was tested using a number of simpler beam models. The first employed only shell element, the second, solid elements with rotations and finally one with both solid and SURF22 elements. A unit load pressure was applied on the top area of the last element of the beam. Using an analytical solution, the displacement at the extremity of the beam is δ_{max}= –0.0196mm. Using a shell element model, this value becomes –0.0302mm and by using a model based on solid elements only, the tip displacement is –0.00191 m. and finally, using the SURF22 model in combination with shells and solids, the results is –0.00191 mm, thus validating and confirming the use of the surface effect element. In order to use the SURF22 element in a structural analysis, all of its material properties must be set zero (Young modulus, Poisson ratio, thickness). Using this approach, it is thus possible to apply tangential pressure with this element as it is shown on Figure 9.9

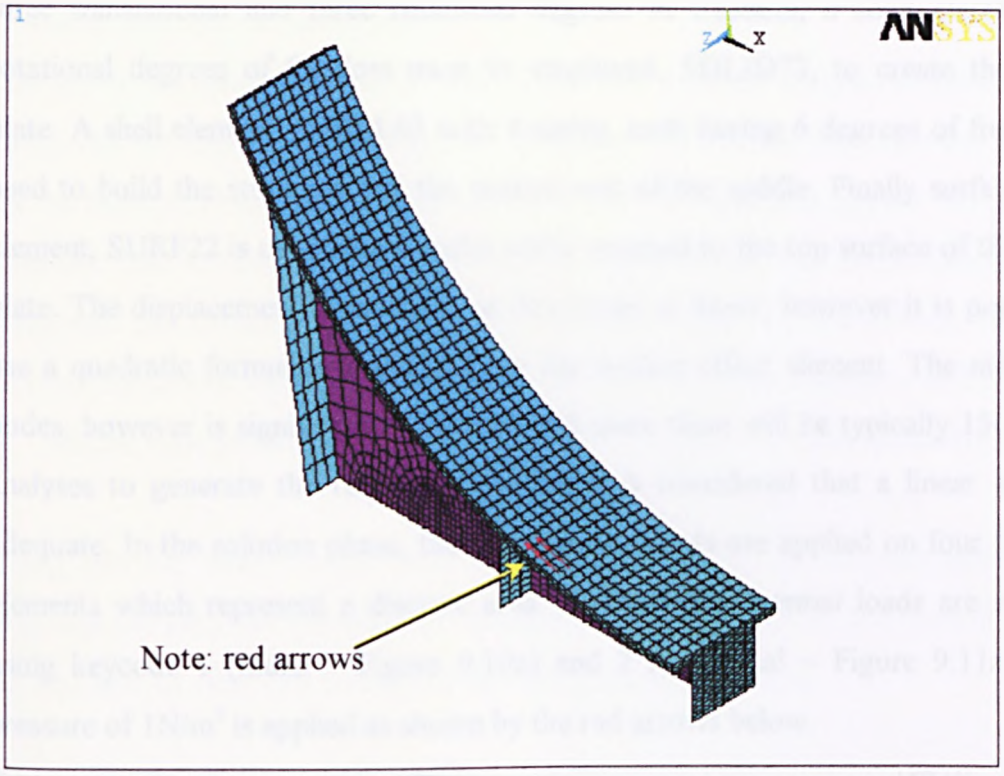

Figure 9.9 Saddle with tangential traction load (shown as red arrows)

Therefore, surface effect elements can be applied to the existing series of models to allow the displacements to be obtained for a radial and tangential unit pressure load.

It is noted however, that the programme constructed by Tolson will not allow the inclusion of the additional flexibility matrices generated by this method. Motashar created FORTRAN programs with a variable pressure loading across the width of the saddle. Therefore, these FORTRAN programmes were modified to solve the case of saddles welded to the vessel and incorporating the case of flexible saddles.

9.7.6 A Saddle Model using Shell, Solid & Surface Elements

Geometry creation and element selection

The final iteration of saddle construction, entitled **'solid'**, employs shells, solids and surface elements and is an extension of the **'normal'** ANSYS model described earlier. The main parameters remain and an extrusion in the local cylindrical co-ordinate system is performed on the top plate only. This operation, in turn, creates the upper surface of the saddle which is directly in contact with the vessel exterior and to which is mapped the surface effect elements. However, since the shell element possesses

three translational and three rotational degrees of freedom, a solid element with rotational degrees of freedom must be employed, SOLID73, to create the saddle plate. A shell element, SHELL63 with 4 nodes, each having 6 degrees of freedom is used to build the stiffeners and the central web of the saddle. Finally surface effect element, SURF22 is used with 4 nodes and is mapped to the top surface of the saddle plate. The displacement formulation of this model in linear, however it is possible to use a quadratic formulation and still use the surface effect element. The number of nodes, however is significantly increased and since there will be typically 150 (30x5) analyses to generate the required matrices, it is considered that a linear model is adequate. In the solution phase, the unit pressure loads are applied on four SURF22 elements which represent a discrete area. Radial and tangential loads are switched using keycode 1 (radial ~ Figure 9.10a) and 2 (tangential ~ Figure 9.11a) and a pressure of $1N/m^2$ is applied as shown by the red arrows below.

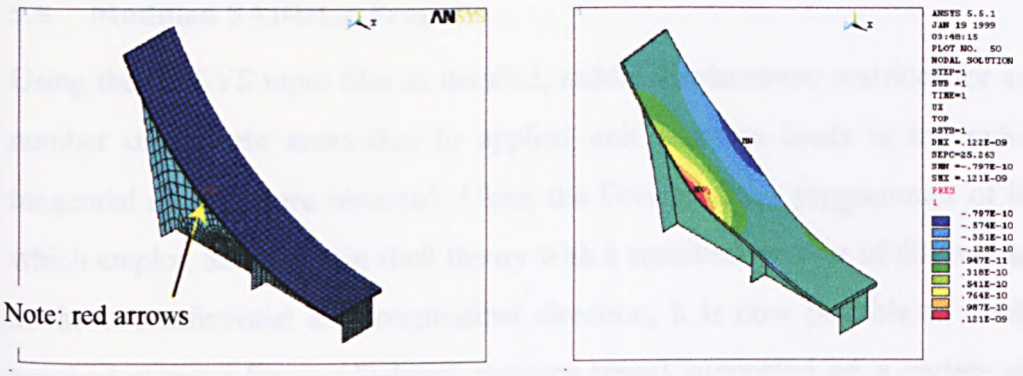

Figure 9.10a,b Complex saddle with shells, solids and surface effect elements - unit pressure applied in radial direction (red arrows)

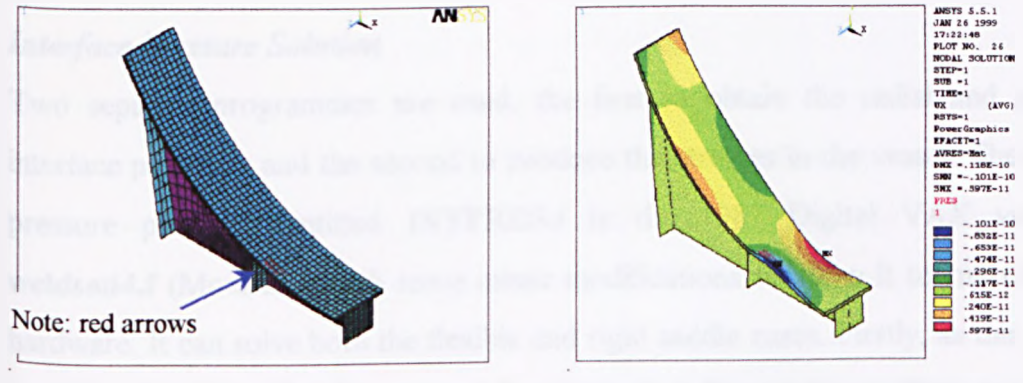

Figure 9.11a,b Complex saddle with shells, solids and surface effect elements - unit pressure applied in tangential direction (red arrows)

Solution and matrix generation

The results sequence is similar to that used in the '**normal**' analysis however both the radial and the tangential displacements are saved into a file in two columns. To obtain all the required results the program is run twice. The first pass applies the radial unit pressure load to obtain the **[WRS]** and **[WTS]** matrices. The second pass uses the tangential unit pressure load to generate the **[VRS]** and **[VTS]** matrices. The results of these sequential runs are two files each with two columns populated as follows:

Radial unit pressure load		**Tangential unit pressure load**	
U_r	U_θ	U_r	U_θ

Using this file, which is generated automatically using ANSYS parametric design language (APDL) and undertaking the sequence of runs required, the flexibility matrix file can now be read into the appropriate SADDLE programme.

9.8 Modified SADDLE Program

Using the ANSYS input files as detailed, saddle displacement matrices for a specified number of discrete areas due to applied unit pressure loads in the radial or the tangential direction are obtained. Using the Fourier series programmes of Motashar, which employ Sanders' thin shell theory with a specified number of discrete areas both in the circumferential and longitudinal direction, it is now possible to obtain all the required stresses for a cylindrical pressure vessel supported on a variety of flexible saddles.

Interface Pressure Solution

Two separate programmes are used, the first to obtain the radial and tangential interface pressures and the second to produce the stresses in the vessel. The interface pressure program, entitled **INTPRES.f** is the 1987 Digital VAX version of **weldsad4.f** (Motashar) with some minor modifications to allow it to run on current hardware. It can solve both the flexible and rigid saddle cases. Firstly, as this program previously ran on a VAX system, a few redundant functions have been removed, to allow this program to compile and run on Unix workstations. In addition, to include the displacements of the saddle it is necessary to modify the compatibility equations

and therefore a few FORTRAN instructions have been added at the end of the program. Other modifications have been included in the input data to make the program quicker to use.

Two types of data are used by this program to run a flexible case: the vessel characteristics and the saddle displacement matrix. The vessel characteristics are input via data file: **fort.52**. This file contains 16 values separated between each other by a space, and with a space in the end. Data is entered in the following sequence: radius of the vessel (*RADIUS* in the ANSYS programs), the thickness of the vessel (normally equal to *THICYL/2* from the ANSYS programs), the length of the vessel, the breadth (distance from the vessel end to the saddle centre), the saddle **total** width (*C×2* from the ANSYS programs), the saddle **total** angle (*THETA×2* from the ANSYS programs), the liquid specific weight, the angle of fill, the vessel material specific weight (=0 if the vessel weight is not to be considered), the end weight, the magnitude of internal pressure, the Modulus of Elasticity and Poisson's ratio of the vessel material (*EX* and *NU* in the ANSYS programs), the number of discrete areas into which the half saddle angle is to be divided (*NA* in the ANSYS programs), the number of discrete areas into which the total saddle width is to be divided (*NW* in the ANSYS programs),the value 2 to run a rigid case and 1 to run the flexible case, and finally, a space.

The four saddle displacement matrices are introduced into the program by copying the displacements due to radial unit pressure load (file called: disp*NWNA*.rad in the ANSYS program) into file **fort.90** and by copying the displacements due to tangential unit pressure load (file called: disp*NWNA*.tan in the ANSYS program) in a file called: **fort.91**. When the program is running, the number of Fourier terms required to solve the analysis is requested. Three types of output data are produced as a result of this analysis. The different displacement matrices are saved into some files for purposes of verification. The interface pressure results are saved into two files and can be examined directly. A third file is created with the vessel characteristic and the interface

pressure results ready for use by the second FORTRAN program which generates the stress solution.

Firstly, the vessel displacement matrices are saved in:	**fort.10** for [WT]
	fort.11 for [VT]
	fort.12 for [WR]
	fort.13 for [VR]
then the saddle displacement matrices are saved in:	**fort.20** for [WTS]
	fort.21 for [VTS]
	fort.22 for [WRS]
	fort.23 for [VRS]
and finally, the global displacement matrices are saved in:	**fort.30** for [WT]+[WTS]
	fort.31 for [VT]+[VTS]
	fort.32for [WR]+[WRS]
	fort.33 for [VR]+[VRS]

In the files, **intpres.rad** and **intpres.tan**, there are $NA \times NW$ values of interface pressure saved. This data can be used to graph the interface pressure system of the studied model directly. Finally, all the vessel characteristics and all the interface pressures are saved in **fort.73**

Stress Solution

The program **STRESS.f** is modified version of **stress4.f** of Motashar with only the input and output statements being altered to allow easier interpretation of the results. The results provided by this program include:

- axial, tangential and radial displacements of vessel : **u, v** and **w**
- axial, circumferential and shear stress resultants in the vessel: $\mathbf{N_x}$, $\mathbf{N_\theta}$, and $\mathbf{N_{x\theta}}$
- axial, circumferential and shear moments resultants in the vessel: $\mathbf{M_x}$, $\mathbf{M_\theta}$, and $\mathbf{M_{x\theta}}$
- axial, circumferential and shear stresses in the vessel: σ_x, σ_θ, and $\sigma_{x\theta}$ on the inside and outside surface of the shell.
- axial, tangential and radial strains in the vessel: ε_x, ε_θ, and γ on the inside and the outside surface of the shell.

Data is read from file **fort.73** (from the **INTPRES.f** program) however two lines of output points on the vessel, at which the solution will be given, must be specified in the **fort.51** file. The input information has the following sequence separated by spaces: Constant x value, first θ value, last θ value, interval between points in the circumferential direction, constant θ value, first x value, last x value, interval between points in the longitudinal direction, 2 and a space at the end. As previous, the required number of Fourier terms is input from the keyboard when the program is running.

The output data of the program can be written to the screen and to datafiles **fort.81** and **fort.82**. In addition, for the purposes of creating three dimensional graphics plots of the variation in solution data, the output is also saved into 14 files without any text strings, to allow the data to be used directly in for example, Excel.

The output files are denoted:

- GRAPHTT.CIR for σ_θ on the outside surface of the vessel around the circumferential line.
- GRAPHXX.CIR for σ_x on the outside surface of the vessel around the circumferential line.
- GRAPHXT.CIR for $\sigma_{x\theta}$ on the outside surface of the vessel around the circumferential line.
- GRAPHTTI.CIR for σ_θ on the inside surface of the vessel around the circumferential line.
- W.CIR for w, the displacement of the vessel around the circumferential line.

The same series of 7 files are also generated for results in the longitudinal direction with *filename*.LON extension.

9.9 Sample Results

The results detailed herein are only shown as an example of the type of information, which can be generated by employing such a system. As an example, a long vessel, with a mean diameter of 1000mm, tangent length of 36000mm, thickness of 6mm, with 200mm wide, 120° wrapround saddles located at 9000mm from each end. The cylindrical part of the vessel was divided into a number of discrete areas. A non-uniform pressure across the width was considered and one case was run with 5×30 discrete areas (NW=5 and NA=30).

Two saddle types were analysed for purposes of comparison. Firstly, a rigid saddle was assumed to be in contact with the shell and the analysis undertaken. The second case considered a flexible saddle of the **'solid'** model type described earlier.

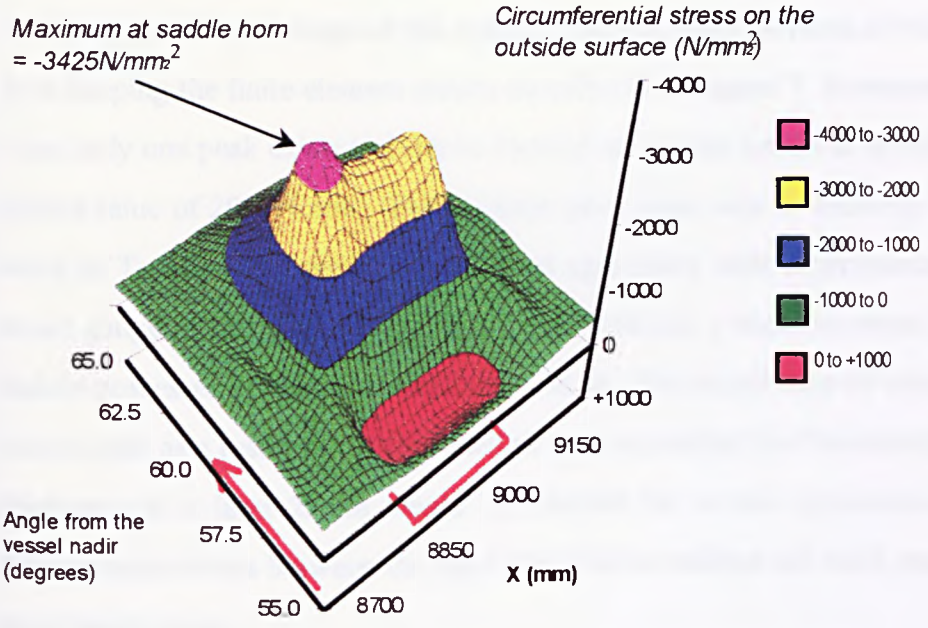

Figure 9.12 Saddle region stress surface plot for the rigid case

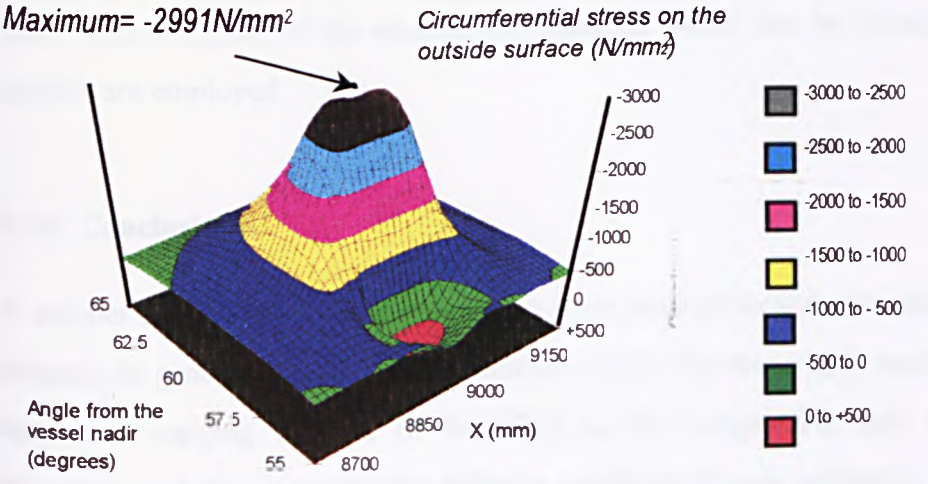

Figure 9.13 Saddle region stress surface plot for the flexible case

Comparison between the rigid and the flexible cases

There are two main differences that arise when rigid and flexible saddles are run through the Fourier series analysis. These differences are shown in the Excel surface plots detailed in Figures 9.12 and 9.13. Firstly, for the rigid case there are two peaks which appear at each edge of the saddle. The maximum of these is 3425N/mm^2. This is in keeping the finite element results described in Chapter 7. However in the flexible case, only one peak exists and this is situated across the centre of profile of the saddle with a value of 2991N/mm^2. This perhaps goes some way to showing why the earlier work of Tooth *et al* proved to be in good agreement with experimentally determined strain gauge results. In addition, this points towards a uniform stress field when the saddle possesses a degree of flexibility. As for the magnitudes of stress, these large values arise as a result of the thin shell thickness selected for the example. Normally a thickness of at least 22mm would be selected for a real application, however the differences in stress between the rigid and flexible saddles are valid, and illustrate the point being made.

In the present case, it can be seen that there is a reduction of 13 % in the magnitudes of the maximum outside circumferential stress between the rigid case and the flexible case. This is typical of the measure of reduction which can be found when flexible saddles are employed.

9.10 Conclusions

A number of variations in the parametric finite element model have been created and detailed in general. These include saddles which are near rigid, semi-rigid, flexible each with varying degrees of flexibility in the longitudinal and circumferential directions and the potential for differing numbers of web stiffeners. Some detailed guidance is provided which shows users of this technique the most appropriate method of geometry creation for complex three-dimensional saddles. In addition, the element selection is justified on the basis of accuracy and efficiency of solution time

especially when considering the significant number of runs required to generate a single set of matrices for one saddle configuration.

The Fortran programs of Tolson and Motashar have been examined and brought up to date to run on modern computers. Some minor modifications have been required and some additional lines of code have been inserted to allow the required flexibility matrices to be employed.

One sample case of a flexible saddle has been successfully run and a new method of graphical representation has been demonstrated. The various files and procedures for execution have been explicitly detailed.

It is clear to the present author that the process of finite element analysis and subsequent SADDLE analysis is extremely complex and time-consuming. The generation of tables of saddle flexibility or the provision of the required flexibility factor, F_f, which includes for variations for all the leading saddle parameters would be a considerable undertaking and is beyond the remit of the current work. However, with the illustrative example used, it has been shown that there is much benefit to be had by the use of a well designed flexible saddle.

10 CONCLUSIONS AND FURTHER WORK

Analysis and design methods for local loading and saddle-supported cylinders have been advanced within this thesis. In particular, the Fourier series loading method and elastic thin shell analysis have been employed to examine the interface pressure distributions for local load patch problems and saddle-supported cylinders.

In the case of the local load patch problems, standalone programs have been developed which allow designers to calculate the important stress quantities on each surface of the cylinder for a given load application. Solutions for a radial load, moment loads in the circumferential and longitudinal directions and steady state thermal loads have been derived and implemented for a variety of prescribed patch forms. Rectangular, circular and elliptical contact regions have been studied and results are made available over a range of discrete points selected by the user. The program can also scan for maximum stresses, which occur at the centre of the loaded area for the radial load and bell-shaped thermal case and at the major axis edges for moment loadings.

To date, this work has direct relevance and application to current designers. Both the BS5500 and ASME pressure vessel codes rely on methods which simplify the contact area and interface loading conditions. Whilst these approaches have been shown in the present work to produce similar maximum results for some cases, the conventional methods do not always produce the highest value. In addition, the new European Standard for Unfired Pressure Vessels, (to be released in draft form in 1999), relies on limit load approaches for design. This form of design may well be adequate if a maximum design load is required. Thereafter, designers can ensure that the largest application of load is below the values generated by the limit load method. However, these approaches do not assist designers where failure by fatigue is a problem. Using the present approach will ensure that maximum stresses are obtained which in turn, provides reliable data for use in fatigue assessments.

Twin saddle supported cylinders have been addressed by developing a robust shell theory and employing a Fourier series approach for the solution of the equations and the representation of the loading systems. A line and patch load model has been used to generate data for a wide range of vessel configurations used in industry. A new design methodology has been considered whereby a basic stress equation has been presented which is progressively adjusted by the use of factors. These factors adjust the basic stress to represent the geometric effect of a number of variables including contents weight, saddle width, saddle angle and position from the end. Separate finite element studies of the influences of the flexibility of the vessel end closure and flexibility of the saddle support have been undertaken, and factors have been identified and quantified, where possible. This new design method is easily programmed into spreadsheets and mathematical scratchpads and an example is provided in the Appendices.

Although finite element analysis is increasingly used in pressure vessel design, there is still some way to go before the method is wholly adopted. The present work has discussed some of the main issues pertaining to the application of FEA to local load and saddle support problems. Whilst these problems can be tacked using FEA, this requires great skill and expertise in both the use of FEA, to model and analyse the components, and interpret the results, in the light of pressure vessel code allowables for specific stress categories. The need for a fine mesh and careful consideration of boundary conditions is essential. One suspects the total component should be handled ~ vessel plus saddle. Furthermore, an examination of the nature of the stress obtained at the horn shows that it may have a mixed response rather than being described as purely secondary.

Because of the governing assumptions of the Fourier series approach, the influence of the flexibility of the end closure was examined using the finite element method. Four end closure styles were analysed and the effects of radius to thickness and shell to end thickness ratios were studied. In conclusion, it was found that the basic shape and the

thickness ratios had little or no effect on the magnitude of the maximum stresses obtained at the horn. An end flexibility factor was developed from this work.

Saddle flexibility was examined by generating flexibility matrices by finite element analysis and importing them into the SADDLE analysis. A modified form of the SADDLE analysis by Tolson was used to show that there is a considerable reduction in maximum stress when a flexible saddle is employed. Guidance has been given to show how a variety of saddle styles may be created, however an improved finite element model has been developed which incorporates shell, solid and surface traction elements. This allows the generation of more realistic flexibility data. An example of the use of this new model is presented and surface plots of stress results for a rigid and flexible saddle are given.

Further Work

Further development of the head flexibility method is required to produce intermediate points on the graph.

A full investigation of the influences of the flexibilities of the saddle should be undertaken as an MSc. Project - this to cover the entire range of saddle geometries as specified by BS5276. The present author is currently completing work on such a study for the case of heated twin saddle supported cylinders subject to high axial expansion.

Having published a number of papers on work arising from this thesis, the author is convinced that the adoption of these methods will only arise by making access to these results more widely available. With this in mind, web based analytical tools should be developed whereby engineers can enter their data and submit an analysis online. With current technology, results will be available immediately if the new design method is employed, or within minutes if a complete analysis using the SADDLE or patch programs is preferred.

11 REFERENCES

[1] **British Standard BS 5500:1997,** 'Specification for unfired fusion welded pressure vessels', BSI, London

[2] **Zick, L P,** 'Stresses in large horizontal cylindrical pressure vessels on two saddle supports', Welding Research Journal Supplement, Sept 1951

[3] **Duthie, G, White, G C and Tooth, A S,** 'An analysis for cylindrical vessels under local loading - application to saddle supported vessel problems', Journal of Strain Analysis, Vol 17 No.3 1982 pp157-167

[4] **Tooth, A S, Duthie G, White, G C and Carmichael, J,** 'Stresses in horizontal storage vessels - a comparison of theory and experiment', Journal of Strain Analysis, Vol 17 No.3 1982 pp 169-176

[5] **Ong, L S and Tooth A S,** 'The effect of high internal pressure on pipes and cylindrical vessels which are subject to external constraint and initial geometric imperfections' Applied Solid Mechanics 1, Elsevier Applied Science ed. Tooth and Spence 1986 pp305-329

[6] **Kendrick, S B and Tooth, A S,** 'The behaviour of a horizontal vessel on loose saddles - a buckling assessment of the support region', Journal of Strain Analysis, Vol.21 No.1 1986, pp45-50

[7] **British Standards Institution PD6493** 'Stresses in horizontal cylindrical pressure vessels supported on twin saddles: a derivation of the basic equations and constants used in G.3.3 of BS 5500:1982', Panel Document, BSI, London, 1982

[8] **Duthie, G** 'An analysis of cylindrical pressure vessels under local and saddle loading using fourier series expansion technique', Ph.D. Thesis, Dept. of Mechanics of Materials, Univ. of Strathclyde, 1976

[9] **Duthie, G, White, G C and Tooth, A S,** 'An analysis for cylindrical vessels under local loading - Application to saddle supported vessel problems', Journal of Strain Analysis, Vol 17, No.3, pp.157-167, Sept. 1982.

[10] **Flügge, W,** 'Stresses in Shells', 2nd Ed., Springer-Verlag, Berlin 1973

[11] **Ong, L S,** 'The effect of high internal pressure on cylindrical vessels with initial geometric imperfections', Ph.D Thesis, The University of Strathclyde, 1985

[12] **Sanders, J L Jr.,** 'An improved first approximation theory for thin shells', NASA TR-R24, 1959

[13] **Leissa, A W,** 'Fundamental equations of thin shell theory', Chapter 1 of 'Vibrations of Shells', NASA SP-288, 1973

[14] **Bushnell, D,** 'Computerised analysis of shells governing equations', Computers and Structures, Vol. 18, No. 3, pp 471-536, 1984.

[15] **ANSYS®,** 'General purpose finite element program', Swanson Analysis Systems Inc. (now ANSYS Inc.), Houston, PA.

[16] **Motashar, F A,** 'The analysis of horizontal cylindrical vessels - supports, local attachments and diaphragms', Ph.D Thesis, The University of Strathclyde, 1988

[17] **Krivy, J and Filho, A S de S,** 'Programas de computador para calculo de tenssem cascas cilindri; cas derido supportamento por sela', 4th Simpio Brasileiro sober Tubules e vasos de press (SIBRAT 4), Salvador BA, Brasil, 1986

[18] **Widera, G E O, Zang, Z F & Natarajan, R,** 'On the design of horizontal pressure vessels', Journal of Pressure Vessel Technology, Trans. of the ASME, Vol 110, pp393-402, Nov 1988

[19] **Widera, G E O, Natarajan, R and Zang, Z F,** 'Three dimensional analysis of horizontal pressure vessels', Proceedings of the 6th International Conference on Pressure Vessel Technology, Beijing, People's Republic of China, 1988

[20] **Křupka, V,** 'The background to a new design proposal for saddle supported vessels', Int. J. Pres. Ves. & Piping, Vol 46, pp51-65, 1991

[21] **Ong, L S,** 'Parametric study of peak circumferential stress at the saddle support', Int. J. Pres. Ves. & Piping, Vol 48, pp183-207, 1991

[22] **Ong, L S,** 'Effectiveness of wear plate at the saddle support', Trans. of the ASME, Vol 114, February 1992

[23] **Ong, L S,** 'Seismic loading on saddle supported cylindrical vessel', Int. J. Pres. Ves. & Piping, Vol 51, pp307-317, 1991

[24] **Timoshenko, S P** 'Theory of plates and shells', MacGrawhill-Kogakusha, 2nd, ed., Tokyo, 1959

[25] **Křupka, V** 'An analysis of lug or saddle supported cylindrical pressure vessels', First Int. Conference on Pressure Vessel Technology, ASME, in Delft, 1969, Part 1, pp.491-500

[26] **European Recommendations for Steel Construction,** Section 4.6, Buckling of Shells

[27] **Kendrick, S & Tooth, A S** 'The behaviour of a horizontal vessel on loose saddles; a buckling assessment of the support region', Journal of Strain Analysis, 21 (1) (1986) 45-49

[28] **Ong, L S** 'A computer program for cylindrical shell analysis', Int. J. Pres. Ves. & Piping, Vol. 30 (1987) 131-149.

[29] **Ong, L S** 'Analysis of twin-saddle-supported vessel subjected to non-symmetric loadings', Int. J. Pres. Ves. & Piping, Vol. 35 (1988) 423-437.

[30] **Leckie, F A and Penny, R K,** 'Shakedown loads for radial nozzles in spherical pressure vessels', Inst. J. Solids and Structures, 1967:3,734

[31] **Wichman, K R, Hopper, A G and Mershon, J L,** 'Local stresses in spherical and cylindrical shells due to external loadings', 1965, Weld. Res. Coun. Bull., No.107

[32] **Bijlaard, P P,** 'Local stresses in spherical shells from radial or moment loadings', Weld. J (Research Supplement). May, 1957.

[33] **Bijlaard, P P,** 'On the stresses from local loads on spherical pressure vessels and pressure vessel heads', 1957. Weld. Res. Coun. Bull., No.34

[34] **Bijlaard, P P,** 'Stresses from radial loads in cylindrical pressure vessels', Weld. J., 1954:33, 615S-623S.

[35] **Bijlaard, P P,** 'Stresses from radial loads and external moments in cylindrical pressure vessels', Weld. J., December, 1955, 608S-617S.

[36] **Bijlaard, P P and Cranch, E T,** 'Stresses and deflections due to local loadings on cylindrical shells', Weld. J.(Research Supplement), July 1960.

[37] **Bijlaard, P P,** 'Stresses in spherical pressure vessels from radial loads and external moments acting on a pipe', 1959, Weld. Res. Coun. Bull. No.49

[38] **Bijlaard, P P** 'Stresses in spherical pressure vessels from local loads transferred by a pipe', 1960, Weld. Res. Coun. Bull. No.50

[39] **Donnell, L H,** 'Stability of thin walled tubes under torsion', NACA, Report No. 479, 1933

[40] **Kempner, J, Sheng, J and Pohle, F V,** 'Tables and curves for deformation and stresses in circular cylindrical shells under localised loadings', Journal of Aeronautical Sciences, 1957, Feb, pp 119-129

[41] **Hoff, N J, Sheng, J and Pohle, F V,** 'Line load applied along generators of thin-walled circular cylindrical shells of finite length', Quarterly Applied Mathematics, 1954, X1(4), pp 411-425

[42] **Bedri, R, McLeish, R D and Gill S S,** 'Some observations on the calculation of stresses due to local loads on cylindrical shells using BS 5500, Appendix G', Int. J. Pres. Ves. & Piping, 13, 1983, pp227-251

[43] **Teixeira, M A, McLeish, R D and Gill, S S,** 'A simplified approach to calculating stresses due to radial loads and moments applied to branches on cylindrical pressure vessels', Journal of Strain Analysis, Vol 16, 4, 1981, pp217-226

[44] **Duthie, G and Tooth A S,** 'Local loads on cylindrical pressure vessels: a Fourier series solution', Behaviour of Thin-walled Structures edited by Rhodes and Spence, Elsevier Applied Science, 1984, pp235-272

[45] **Tooth, A S and Nash, D H,** 'The use of the microcomputer in the design of cylindrical pressure vessels', Int. J. Pres. Vess. & Piping, Vol 24,pp1-12, 1986

[46] **Hueilin, C and Santung, T,** 'The contact stress analysis of plate and shell structures in pressure vessels', Int. J. of Pres. Ves. & Piping, 27 (1987), pp335-352

[47] **Hueilin, C, and Santung, T,** 'The contact stress analysis of pad-reinforced structures', presented at ASME Pres. Ves. & Piping Conf. San Diego, California, 1987. Recent Advances in Structural Dynamics, PVP, 124, pp33-8

[48] **Motashar, F A and Tooth, A S,** 'Radial loading of a cylindrical vessel through a rectangular rigid attachment', Int. J. Pres. Ves. & Piping, 37, 1989, pp345-363

[49] **Thomopoulos, K and Bisbos, C D,** 'Unilateral contact stresses at steel pipes' Thin-Walled Structures, Vol.15, No.4, 1993, pp305-319

[50] **Bisbos, C D, Thomopoulos, K and Tzaferopoulos, M,** 'Computing the frictional contact loads of horizontal steel pipes, loosely resting on saddles' Int. J. Pres. Ves. & Piping, 58, 1994, pp75-85

[51] **Al-Abed, M R, Bisbos, C D, and Panagiotopoulos, P D,** 'The debonding effect in saddles: comparison of the performance of Flugge's and Sanders' shell theories', Int. J. Pres. Ves. & Piping, 65, 1996, pp53-74

[52] **Al-Abed, M R, Banoitopoulos, C C, and Bisbos, C D,** 'Effect of liquid filling in saddle supported pipelines', Int. J. Pres. Ves. & Piping, 68, 1996, pp219-228

[53] **Al-Abed, M R, Banoitopoulos, C C, Bisbos, C D, & Panagiotopoulos, P D,** 'Saddle-supported pipelines: computation of the pressure distribution on the pipe-saddle interface', Journal of Constructional Steel Research, 44, 1997, pp159-178

[54] **Nadarajah, C,** 'A design study of nozzles and attachments in pressure vessels', Ph.D. Thesis, University of Strathclyde, 1993

[55] **Naijie, S, Jitao, Z, and Wenge, L,** 'Stress state in the saddle zone of pressure vessels and piping', Int. J. Pres. Vess. & Piping, 63 (1995), pp155-164

[56] **Nash, D H,** 'An investigation into the suitability of microcomputers in the analysis of cylindrical shells', M.Sc. Thesis, University of Strathclyde, 1985

[57] **Warrender, A J,** 'The support of horizontal cylindrical glass reinforced plastic storage vessels', Ph.D. Thesis, University of Strathclyde, 1986

[58] **Tolson, B A,** 'The support of horizontal multi-layered GRP cylindrical vessels', Ph.D. Thesis, University of Strathclyde, 1991

[59] **Thomson, G, Tooth , A S and Nash, D H,** 'A fourier series solution for a cylindrical shell subject to a radial loading acting over a circular patch', 6th ICPVT, Beijing, China, Vol.1 Design and Analysis, pp53-64, September 1988

[60] **Nash, D H and Tooth, A S,** 'Stress analysis and fatigue assessment of twin saddle supported pressure vessels', ASME Pres. Ves. & Piping Conf, PVP-Vol 217, pp41-48, San Diego, California, 1991

[61] **Nash, D H and Tooth, A S,** 'The influence of the flexibility of the dished end on twin saddle supported pressure vessels', ASME/ICPVT-8, 1996, Montreal, Canada

[62] **Wilson, J D,** 'Thermal stresses in thin cylindrical shells', reprinted from the 2nd International Conference Structural Mechanics in Reactor Technology, Berlin, Germany, 1973, Vol 3, Paper G 1/10, pp 1-12

[63] **BS 5276:Part 2:1983** 'Pressure vessel details (dimensions). Specification for saddle supports for horizontal cylindrical pressure vessels', BSI, London

[64] **Ford, S,** 'The stress analysis of a horizontal cylindrical pressure vessel by the finite element method', M.Sc. Thesis, University of Strathclyde, 1985

[65] **Shoessow, G J and Kooistra, L F,** 'Stresses in a cylindrical shell due to nozzle or pipe connection', The Welding Journal, Vol. 33, pp 615s-623s, 1954

[66] **Tooth, A S and Nash, D H,** 'The derivation of thermal stress in a cylindrical vessel under steady state loading: a Fourier series solution', ASME Pres. Ves. & Piping Conf. 87-NE-3, San Diego, California, 1987

[67] **Nash, D H, Tooth, A S, and Dauda, T,** 'The local loading of circular and elliptical attachements on cylindrical pressure vessels', ASME Pres. Ves. & Piping Conf, PVP-Vol 217, pp41-48, San Diego, California, 1991

[68] **Mershon, J L, Mokhtarian, K, Ranjan, G V and Rodabaugh, E C,** 'Local stresses in cylindrical shells due to external loadings on nozzles - supplement to WRC Bulletin No 107', 1984, Weld. Res. Coun. Bull., No.297

[69] **Dhalla, A K,** 'Verification of an elastic procedure to estimate follow-up', In Design of Elevated Temperature Piping, editied by R H Mallett & R M Mello, ASME, New York, 1984, pp81-96

[70] **Dhalla, A K and Jones, G L,** 'ASME Code classification for pipe stresses: a simplified elastic procedure', Int. J. Pres. Ves. and Piping, Vol. 26, 1986, pp145-166

[71] **Roche, R L,** 'Estimation of piping elastic follow up by using conventional computations', Int. J. Pres. Ves. and Piping, Vol. 26, 1986, pp53-78

[72] **Marriot, D L,** 'Evaluation of deformation or load control of stresses under inelastic conditions using elastic finite element analysis', Proc. ASME-PVP Conf., Vol. 136, Pittsburg, 1988

[73] **Seshadri, R, and Kizhatil, R K,** 'Inelastic analysis of pressure components using the GLOSS diagram', Proc. ASME-PVP, Vol. 186, 1990, Nashville

[74] **Seshadri, R,** 'The generalised local stress strain (GLOSS) analysis-theory and applications', 25th Anniversary Vol., ASME J. Pres. Ves. Tech., 1991, pp219-227

[75] **Mackenzie, D and Boyle, J T,** 'A method of estimating limit loads by iterative elastic analysis: I Simple examples', Int. J. Pres. Ves. and Piping, Vol. 53, 1993, pp77-96

[76] **Boyle, J T,** 'Elastic follow-up and the categorisation of secondary stress', Proc. ASME-PVP, Vol. 161, 1989, Honolulu, pp47-53

[77] **Boyle, J T, and Mackenzie, D,** 'An investigation of a simple procedure for stress categorisation', Proc. ASME-PVP, Vol. 210-2, 1991, San Diego, pp161-165

[78] **Mackenzie, D and Boyle, J T,** 'Assessment of classification procedures for finite element stresses', Proc. Int. Conf. Pres. Ves. Tech., Vol. 1, 1992, Dusseldorf, pp346-358

[79] **Mackenzie, D and Boyle, J T,** 'Computational procedure for calculating primary stress for the ASME B&PV code', ASME J. Pres. Ves. Tech., Vol. 115, 1993, pp27-31

[80] **Chan Geok Chai, M,** 'A design study of the collapse of saddle supported vessels', Ph.D. Thesis, University of Strathclyde, 1995

[81] **Chan, G C M, Tooth A, S and Spence, J,** 'A study of the buckling behaviour of horizontal saddle supported vessels', Thin Walled Structures, Vol. 30, Nos 1-4, pp3-22, 1998

[82] **Tooth, A S, Spence, J, and Chan, G C M,** 'The buckling behaviour of horizontal storage vessels - experiments and codes', 2nd Int. Conf. of Thin Walled Structures 2-4 Dec 1998, Convention City, Singapore, published in 'Thin Walled Structures Research and Developments' editied by N E Shanmugan, J Y Richard Leiw and V Thevendran, pp 597-604, Elsevier, 1998

[83] **Tooth, A S, Panayotti, A and Owen, R,** 'The thermal behaviour of thin cylindrical shells -I. Heat transfer and harmonic analysis', Int. J. Mech. Sci. Vol. 31, No.9, pp 693-706, 1989

[84] **Tooth, A S, Panayotti, A and Owen, R,** 'The thermal behaviour of thin cylindrical shells -II. Elastic thermal stress analysis', Int. J. Mech. Sci. Vol. 31, No.9, pp 707-716, 1989

[85] **Forbes, P D,** 'The behaviour of unstiffened twin saddle supported containment vessels under gravity loading and internal surcharge of pressure', PhD Thesis, Dept. of Mech. of Mat'ls, University of Strathclyde, 1967

[86] **Forbes, P D and Tooth, A S,** 'An analysis for twin supported unstiffened cylindrical vessels', Conf. On recent Advances in Stress Analysis, Royal Aero. Soc., London, Mar. 1968, pp. 47-58

[87] **Stoneking, J K and Sheth, K,** 'Analysis of a large saddle supported horizontal pressure vessel', ASME, Pres. Ves. and Piping Div., 77-PVP-18, 1977

[88] **Wilson, J D and Tooth, A S,** 'The support of unstiffened cylindrical vessels', 2nd. Int. Conf. On Pres. Ves. Tech., San Antonio, 1973, pp. 67-83

[89] **Tooth, A S, Banks, W M, Seah, C P and Tolson, B A,** 'The twin saddle support of horizontal multi-layered GRP vessels - theoretical analysis, experimental work and a design approach', Journal of Proc. Mech. Eng. Part E, Proc Instn Mech Engrs, Vol 208, pp59-74, 1994

[90] **Nadarajah, C, Tooth, A S and Spence, J,** 'The radial loading of cylindrical vessels - influence of attachment rigidity', Int. J. Press. Ves. & Piping 67 (1996) pp65-79

[91] **Nadarajah, C, Tooth, A S and Spence, J,** 'The radial loading of cylindrical vessels - influence of large displacements', Int. J. Press. Ves. & Piping 67 (1996), pp81-94

12 COLLECTED PAPERS

The following list notes the publications written by the author arising from work developed in this thesis.

Tooth, A S and Nash, D H, 'The use of the microcomputer in the design of cylindrical pressure vessels', Int. J. Pres. Vess. & Piping, Vol 24,pp1-12, 1986

Tooth, A S and Nash, D H, 'The derivation of thermal stress in a cylindrical vessel under steady state loading: a Fourier series solution', ASME Pres. Ves. & Piping Conf. 87-NE-3, San Diego, California, 1987

Thomson, G, Tooth , A S and Nash, D H, 'A fourier series solution for a cylindrical shell subject to a radial loading acting over a circular patch', 6th ICPVT, Beijing, China, Vol.1 Design and Analysis, pp53-64, September 1988

Nash, D H and Tooth, A S, 'Stress analysis and fatigue assessment of twin saddle supported pressure vessels', ASME Pres. Ves. & Piping Conf, PVP-Vol 217, pp41-48, San Diego, California, 1991

Nash, D H, Tooth, A S, and Dauda, T, 'The local loading of circular and elliptical attachements on cylindrical pressure vessels', ASME Pres. Ves. & Piping Conf, PVP-Vol 217, pp41-48, San Diego, California, 1991

Nash, D H and Tooth, A S, 'The influence of the flexibility of the dished end on twin saddle supported pressure vessels', ASME/ICPVT-8, 1996, Montreal, Canada

The following has been excluded at the request of the university

Pages 244-290

APPENDIX 1

Program - cyl1pc.f

```
C       HORIZONTALLY END SIMPLY-SUPPORTED CYLINDER
C       PROGRAM MODIFIED TO BE 1ST PASS ONLY - D H NASH
        IMPLICIT REAL*8 (A-H,O-Z)
        CHARACTER*20 NAME*60,TITLE*60,DATA1(5),FILNM,FNAME
        DIMENSION Z(6),ZO(6),PO(3),P(3),P02(3),P2(3),S(3)
        DIMENSION LOAD(3),CL(60),XIMP(3),ES(10),EO(10)
        DIMENSION AN(3,60),BN(3,60),RAD(120),DISP(9,120)
        DIMENSION DELTA(3),PQ(120),KCODE(120),RES(9,120)
        COMMON/BLK2/T3,T4,PI,RADIAN,T,R,XLEN,NCSYM
        COMMON/BLK3/P,PO,P2,P02
        COMMON/BLK4/SDIV,WIDTH,NTYPE,NK,NSIZE,XSAD
        IJOB=1
        LOOP=9
        IF(IJOB.EQ.1.OR.IJOB.GE.3) LOOP=3
        OPEN(2,FILE='PCINPUT',STATUS='UNKNOWN')
        READ(2,103) NAME
103     FORMAT(A60)
        READ (2,*) MTERM,NTERM
        READ (2,*) NSYS,NSYM,NCSYM,IMP
        READ (2,*) R,E,VV,T,XLEN
        IF (IMP.GT.0) READ (2,102) (XIMP(I),DATA1(I),I=1,IMP)
102     FORMAT(E12.5,5X,A)
        READ (2,*) NLOAD
        READ (2,*) (CL(I),I=1,NLOAD*6)
        READ (2,*) CP1,CP2,CP3,CP4,STEP
          NP=1
         IF(CP2.EQ.CP4) NP=2
C-----------SADDLE SUPPORT PROBLEM----------
        IF(IJOB.EQ.1.OR.IJOB.EQ.2) THEN
        READ(2,*) XSAD,SBETA,OFFSET,WIDTH,NTYPE
        READ(2,*) NDIV,NK,NT
        NSIZE=NK+NT
        I1=NDIV+NTYPE
        IF (NTYPE.EQ.2) I1=NDIV
         DO 34 I=1,NK
34         KCODE(I)=I
         DO 35 I=1,NT
35       KCODE(NK+I)=I
        IF (NK.LT.I1) READ(2,*) (KCODE(I),I=1,NK)
        IF (NT.GT.0.AND.NT.LT.I1) READ(2,*)
(KCODE(I),I=NK+1,NSIZE)
        IF (NCSYM.EQ.2) THEN
         NTS=NT/2
         NKS=(NK+1)/2
         DO 33 I=1,NTS
33       KCODE(NKS+I)=KCODE(NK+I)
         NT=NTS
         NK=NKS
         NSIZE=NK+NT
         END IF
          NS1=NSIZE+1
          NS2=NSIZE+2
         IF(IJOB.EQ.1) THEN
         SDIV=SBETA/NDIV
         A1=(SBETA-SDIV)/2.0
         IF(NTYPE.EQ.1) A1=SBETA/2.0
         NP=1
         CP1=XSAD
         CP2=OFFSET-A1
         IC=MAX0(NK,NT)
         CP4=OFFSET+(KCODE(IC)-1)*SDIV-A1
         STEP=SDIV
        END IF
          END IF
        CLOSE (UNIT=2)
C-----------------------------
C       AXIAL SYMMETRY  NSYM=2, KM=1
C       NON AXIAL SYMMETRY  NSYM=1, KM=0
        KM=1
        IF (NSYM.EQ.1) KM=0
C-----------------------------
C       GLOBAL CONSTANTS
        PI=ASIN(1.0)*2.0
        RADIAN=PI/180.0
```

```
      PI2=PI*PI
      T1=1.0-VV
      T2=T*T
      A=E*T/(1.0-VV*VV)
      T3=PI*R/XLEN
      T4=PI/XLEN
      T5=R*R/A
      T6=T2/12.0
C-----------------------------
C     LOOPING FOR LOADS
      DO 40 I=1,3
40    LOAD(I)=0
      DO 41 I=1,NLOAD
       K=(I-1)*6+1
       IF(CL(K).EQ.1.0.OR.CL(K).GE.4.0) LOAD(1)=1
       IF(CL(K).EQ.2.0) LOAD(2)=1
41     IF(CL(K).EQ.3.0) LOAD(3)=1
C-----------------------------
      IF(IJOB.EQ.2) THEN
        IC=1
        IF(NCSYM.EQ.1) IC=2
        N=NSIZE
       IF(NTYPE.EQ.2) N=NSIZE+IC
      OPEN(16,FILE='PQ.DAT',STATUS='OLD')
      READ(16,*) (PQ(I),I=1,N)
      READ(16,*) (DELTA(I),I=1,3)
      CLOSE (16)
      IF (NT.GT.0) LOAD(3)=1
      END IF
C-----------------------------
      C1=T6/(R*R)
      C2=0.0
      PRESS=0.0
C     CL(2)=SWV, CL(3)=PRESS, CL(4)=SW, CL(5)=ALPHA
      IF (CL(1).EQ.0.0) THEN
       LOAD(1)=1
       IF(CL(2).NE.0.0) LOAD(3)=1
      ALPHA=CL(5)*RADIAN
      PRESS=CL(3)
      C11=SIN(ALPHA)
      C12=COS(ALPHA)
      PBAR=CL(3)+CL(4)*R*(C11-ALPHA*C12)/PI
      C2=PBAR*R/A
      END IF
      IF (NSYS.EQ.1) C2=0.0
      C3=0.5*T1*C1
      C4=0.5*(3.0-VV)*C1
      C5=0.125*T1*(4.0+C1)
      C6=0.125*(4.0*(1.0+VV)-3.0*C1*T1)
      C7=0.125*T1*(4.0+9.0*C1)
C
      IF (IJOB.EQ.1) GOTO 111
C-------------PRINT INPUT DATA--------------
      OPEN(6,FILE='OUTPUT',STATUS='NEW')
      WRITE (6,780) NAME
780   FORMAT(//5X,A/)
      IF (NSYS.EQ.2) WRITE (6,360)
360   FORMAT(5X,'STIFFENING EFFECT OF PRESSURE HAS BEEN
CONSIDERED')
      IF (IMP.GT.0) THEN
       WRITE (6,*) 'CROSS SECTIONAL PROFILES'
       WRITE (6,102) (XIMP(I),DATA1(I),I=1,IMP)
      END IF
C
      WRITE (6,782) MTERM,NTERM
782   FORMAT(/5X,'MTERM =',I4/5X,'NTERM =',I4)
      WRITE (6,330)
330   FORMAT(//5X,'CYLINDRICAL SHELL')
      WRITE (6,300) XLEN,R,T,E,VV
300   FORMAT(/10X,'LENGTH =',E12.5,2X,'UNIT'/
     &        10X,'RADIUS =',E12.5,2X,'UNIT'/
     &        10X,'THICKNESS =',E12.5,2X,'UNIT'/
     &        10X,'YOUNGS MODULUS =',E12.5,2X,'UNIT'/
     &        10X,'POISSON RATIO =',F7.3)
C
      WRITE (6,306)
```

```
306    FORMAT(//5X,'*LOADING*')
305    FORMAT(/5X,'SP. WT.=',E12.5,2X,'PRESSURE =',E12.5/
     & 5X,'SP. WT. OF FLUID =',E12.5,2X,'LEVEL OF
FILL=',F7.2,'DEG')
343    FORMAT(/5X,'TYPE = RADIAL PATCH (1)     AXIAL SHEAR PATCH
(2)'/
     &         5X,'   HOOP SHEAR PATCH (3)     AXIAL TRIANGULAR
(4)'/
     &         5X,'   HOOP TRIANGULAR  (5)'//

&5X,'TYPE',4X,'MAGNITUDE',9X,'X',11X,'PHY',8X,'2C',8X,'2BETA')
344    FORMAT(7X,I2,2(2X,E12.5),2X,F7.2,2X,E12.5,2X,F7.2)
       IF (CL(1).EQ.0.0) WRITE (6,305) (CL(I),I=2,5)
       IF (CL(1).NE.0.0) WRITE (6,343)
       DO 333 I=1,NLOAD
        J=(I-1)*6+1
        IC=CL(J)
        IF(IC.EQ.0) GOTO 333
        WRITE(6,344) IC,(CL(K),K=J+1,J+5)
333    CONTINUE
C------------IMPERFECTION-------------------
       KC=0
111    IF (IMP.EQ.0) GOTO 404
       DO 400 I=1,IMP
       OPEN(1,FILE=DATA1(I),STATUS='OLD')
       READ(1,103) TITLE
       READ(1,*) NDRAD,CONVT,DRIFT
       READ(1,*) (RAD(J),J=1,NDRAD)
       READ(1,*) DATUM
       CLOSE(1)
       DO 401 J=1,NDRAD
401    RAD(J)=(RAD(J)-DRIFT)*CONVT+DATUM
       KC=NDRAD/2
       IF(KC.GE.NTERM) KC=NTERM
       A2=2.0/NDRAD
       A1=PI*A2
       DO 402 N=2,KC
        SSUM=0.0
       CSUM=0.0
       A3=A1*N
       DO 403 J=1,NDRAD
        PHY=(J-1)*A3
       SSUM=SSUM+RAD(J)*SIN(PHY)
       CSUM=CSUM+RAD(J)*COS(PHY)
403    CONTINUE
       AN(I,N)=CSUM*A2
402    BN(I,N)=SSUM*A2
400    CONTINUE
       IF(NSYM.EQ.1) GOTO 404
        IF(XIMP(IMP).GT.XLEN/2.0) XIMP(IMP)=XLEN/2.0
404    CONTINUE
C-----------------------------------------
C      ANGULAR POSITIONS OF CONTACT NODES
       IF (IJOB.EQ.2) THEN
       SBETA=SBETA*RADIAN
       SDIV=SBETA/NDIV
       A1=(SBETA-SDIV)/2.0
       IF(NTYPE.EQ.1) A1=SBETA/2.0
       A2=OFFSET*RADIAN-A1
       DO 80 I=1,NSIZE
80     RAD(I)=(KCODE(I)-1)*SDIV+A2
       IF(NTYPE.EQ.2) THEN
        RAD(NS1)=A1+A2-SBETA/2.0
        RAD(NS2)=RAD(NS1)+SBETA
       END IF
       END IF
C-----------------------------------------
        IF (STEP.EQ.0.0) ITOL=1
       IF (STEP.NE.0.0) THEN
          A1=(CP4-CP2)/STEP
          IF (NP.EQ.2) A1=(CP3-CP1)/STEP
          ITOL=1.1+A1
       END IF
       DO 990 J=1,LOOP
        E0(J)=0.0
       DO 990 I=1,ITOL+NTYPE
```

```
990    RES(J,I)=0.0
       Z0(3)=0.0
       Z0(4)=0.0
       P02(1)=0.0
       P02(2)=0.0
C
       X=CP1
       PHY=CP2*RADIAN
       STEP1=STEP*RADIAN
C-----------------------------------------
c***       WRITE(*,*) '1st PASS - CALCULATIONS IN PROGRESS'
c***       write(*,*) ' '
       DO 3001 M=1,MTERM
c***        WRITE(6,2313) M
c***2313    FORMAT(1h+,'TERM NUMBER = ',I4)
         K=M*NSYM-KM
         C8=T3*K
         C9=C8*C8
         A1=1.0+C1*C9*C9
         A4=-VV*C8
         A5=A1*C9-A4*A4
         Z0(1)=C9/A5
         Z0(2)=-A4/A5
         Z0(5)=1.0/(C7*C9)
         Z0(6)=A1/A5
         DO 3004 I=1,3
3004     P0(I)=0.0
         P02(3)=0.0
         CALL PJMN(K,0,NLOAD,CL)
          IF(IJOB.EQ.2) CALL PQP(K,0,PQ,RAD)
         IF (NP.EQ.1) CALL ENO(X,K,E0,Z0,P0,P02,LOAD,LOOP)
        DO 3001 N=1,NTERM
         N2=N*N
        A11=1.0+C1*(N2+C9)**2+C2*((N2-1)+0.5*C9)
        A12=C8*(C3*N2-VV)
        A13=N*(1.0+N2*C1)+C4*N*C9
        A22=C9+C5*N2
        A23=-C6*N*C8
        A33=N2*(1.0+C1)+C7*C9
        DEN=A11*A22*A33+2.0*A12*A23*A13-A11*A23*A23
     &-A22*A13*A13-A33*A12*A12
        Z(1)=(A22*A33-A23*A23)/DEN
        Z(2)=(A13*A23-A12*A33)/DEN
        Z(3)=(A12*A23-A13*A22)/DEN
        Z(4)=(A12*A13-A11*A23)/DEN
        Z(5)=(A11*A22-A12*A12)/DEN
        Z(6)=(A11*A33-A13*A13)/DEN
         DO 3003 I=1,3
         P(I)=0.0
3003     P2(I)=0.0
         CALL PJMN(K,N,NLOAD,CL)
         IF (IJOB.EQ.2) CALL PQP(K,N,PQ,RAD)
         IF(KC.GE.N.AND.N.GT.1)
     &  CALL FIMP(NSYM,IMP,XIMP,PBAR,P,P2,AN,BN,K,N)
        L=1
        I1=-1
100     IF (I1.EQ.ITOL) GOTO 555
        IF (NP.EQ.1) THEN
        PHI=(L-1)*STEP1+PHY
        CALL ENN(X,PHI,K,N,ES,Z,P,P2,LOAD,LOOP)
        ELSE
        X=(L-1)*STEP+CP1
        CALL ENN(X,PHY,K,N,ES,Z,P,P2,LOAD,LOOP)
        CALL ENO(X,K,ES,Z0,P0,P02,LOAD,LOOP)
        STEP1=T4*K*STEP/N
        END IF
        DO 900 JC=1,LOOP
900     DISP(JC,L)=ES(JC)
        I1=L*2-1
        IF (I1.GE.ITOL) I1=ITOL
        DO 500 I=L+1,I1
        A1=COS(N*(I-L)*STEP1)*2.0
        IC=2*L-I
        DO 30 JC=1,LOOP
30      DISP(JC,I)=A1*ES(JC)-DISP(JC,IC)
500     CONTINUE
```

```
      L=L*2
      GOTO 100
555   DO 910 J=1,LOOP
      DO 910 I=1,ITOL
910   RES(J,I)=RES(J,I)+DISP(J,I)
      IF(NTYPE.NE.2.AND.IJOB.NE.1) GOTO 3001
       A1=2.0*COS(N*STEP1/2.0)
      RES(1,NS1)=RES(1,NS1)+A1*DISP(1,1)-
(DISP(1,1)+DISP(1,2))/A1
      RES(1,NS2)=RES(1,NS2)+A1*DISP(1,ITOL)-(DISP(1,ITOL-1)
     & +DISP(1,ITOL))/A1
3001   CONTINUE
C-----------------------------------------
      IF (NP.EQ.1) THEN
       DO 930 I=1,LOOP
       DO 930 J=1,ITOL
930    RES(I,J)=RES(I,J)+E0(I)
      END IF
C
C     STORE [WVL],[S]
      IF(IJOB.EQ.1) THEN
      DO 948 I=1,3
948    S(I)=0.0
        IF(NTYPE.EQ.2) THEN
         RAD(NS1)=(RES(1,NS1)+E0(1))*T5
         RAD(NS2)=(RES(1,NS2)+E0(1))*T5
          IC=1
           IF(NCSYM.EQ.1) IC=2
           NSIZE=NSIZE+IC
         END IF
       I1=0
       IF(NCSYM.EQ.1) I1=1
       IF(CL(1).EQ.0.0) S(1)=2.0*PI*R*T*XLEN*CL(2)+CL(4)
      &*XLEN*R*R*(ALPHA-SIN(2.0*ALPHA)/2.0)+CL(6)
       DO 949 I=1,NLOAD
        J=(I-1)*6+1
        IC=CL(J)
        IF(IC.EQ.0.OR.IC.EQ.2) GOTO 949
        A1=CL(J+4)
        A2=CL(J+5)*R*RADIAN
       IF(A1.EQ.0.0) A1=1.0
       IF(A2.EQ.0.0) A2=1.0
       A3=A1*A2*CL(J+1)
       A4=CL(J+3)*RADIAN
      IF(IC.EQ.1) THEN
       S(1)=S(1)+A3*COS(A4)
       S(2)=S(2)+I1*A3*SIN(A4)
      END IF
      IF(IC.EQ.3) THEN
       S(1)=S(1)-A3*SIN(A4)
       S(2)=S(2)+I1*A3*COS(A4)
       S(3)=S(3)+I1*A3*R
      END IF
949   CONTINUE
      DO 947 J=1,NK
947    RAD(J)=RES(1,KCODE(J))*T5
      DO 946 J=NK+1,NK+NT
946   RAD(J)=RES(3,KCODE(J))*T5
      OPEN(3,FILE='PCSAD',STATUS='UNKNOWN')
       WRITE(3,*) (RAD(J),J=1,NSIZE)
       WRITE(3,*) (S(I),I=1,3)
       GOTO 999
      END IF
      A3=1.0E6/A
      A4=PRESS*0.5/(1.0-VV*VV)
C***      WRITE(*,*) 'WRITE TO OUTPUT FILE'
      DO 940 J=1,ITOL
       IF (NP.EQ.1) THEN
        ANG=CP2+(J-1)*STEP
       ELSE
        X=CP1+(J-1)*STEP
       END IF
      RES(1,J)=RES(1,J)*T5
      RES(2,J)=RES(2,J)*T5
      RES(3,J)=RES(3,J)*T5
      IF(IJOB.EQ.2) THEN
```

```
      PHI=ANG*RADIAN
      SNT=SIN(PHI)
      CNT=COS(PHI)
      RES(1,J)=RES(1,J)+DELTA(1)*CNT+DELTA(2)*SNT
      RES(3,J)=RES(3,J)-DELTA(1)*SNT+DELTA(2)*CNT+R*DELTA(3)
     END IF
     WRITE (6,310) X,ANG
     WRITE (6,311) (RES(K,J),K=1,3)
     IF(LOOP.EQ.3) GOTO 940
     RES(4,J)=RES(4,J)+A4
     RES(5,J)=RES(5,J)-A4*VV
     ES(1)=R*(RES(4,J)+VV*RES(5,J))
     ES(2)=R*(RES(5,J)+VV*RES(4,J))
     ES(3)=R*T1*RES(6,J)/2.0
     ES(4)=T6*(RES(7,J)+VV*RES(8,J))
     ES(5)=T6*(RES(8,J)+VV*RES(7,J))
     ES(6)=T6*T1*RES(9,J)
     A1=ES(1)/T
     A2=ES(2)/T
     E0(1)=A1-6.0*ES(4)/T2
     E0(2)=A1+6.0*ES(4)/T2
     E0(3)=A2-6.0*ES(5)/T2
     E0(4)=A2+6.0*ES(5)/T2
     E0(5)=(R*RES(4,J)+T*0.5*RES(7,J))*A3
     E0(6)=(R*RES(4,J)-T*0.5*RES(7,J))*A3
     E0(7)=(R*RES(5,J)+T*0.5*RES(8,J))*A3
     E0(8)=(R*RES(5,J)-T*0.5*RES(8,J))*A3
C
     WRITE (6,312) (ES(K),K=1,6)
     WRITE (6,313) (E0(K),K=1,4)
     WRITE (6,314) (E0(K),K=5,8)
940  CONTINUE
C
310  FORMAT(//5X,'X =',E12.5,3X,'ANGLE =',F7.2,'DEG')
311  FORMAT(5X,'W =',E12.5,3X,'U =',E12.5,3X,'V =',E12.5)
312  FORMAT(4X,'NX=',E12.5,3X,'NPY=',E12.5,3X,'NXPY=',E12.5/
    &       4X,'MX=',E12.5,3X,'MPY=',E12.5,3X,'MXPY=',E12.5)
313  FORMAT(4X,'SXI=',E12.5,1X,'SXO=',E12.5,1X,'SPYI=',E12.5,
    & 1X,'SPYO=',E12.5)
314  FORMAT(4X,'EXO=',F8.2,3X,'EXI=',F8.2,3X,'EPYO=',F8.2,
    & 3X,'EPYI=',F8.2)
999  STOP
     END
C
     SUBROUTINE EN0(X,M,E0,Z0,P0,P02,LOAD,LOOP)
     IMPLICIT REAL*8 (A-H,O-Z)
     DIMENSION E0(10),Z0(6),P0(3),P02(3),LOAD(3)
     COMMON/BLK2/T3,T4,PI,RADIAN,T,R,XLEN,NCSYM
     C2=M*T4
     C3=C2*R
     C1=C3*C3
     C4=SIN(C2*X)
     C5=COS(C2*X)
     C45=C4/C5
     DO 10 J=1,3
     IF(LOAD(J).EQ.0) GOTO 10
     JU=J+1
     IF(J.EQ.2) JU=6
     JV=J+2
     C8=P0(J)*C4
     C9=-P02(J)*C5
     E0(1)=E0(1)+Z0(J)*C8
     E0(2)=E0(2)+Z0(JU)*C8/C45
     E0(3)=E0(3)+Z0(JV)*C9*C45
     IF(LOOP.EQ.3) GOTO 10
     E0(4)=E0(4)-C8*C3*Z0(JU)
     E0(5)=E0(5)+C8*Z0(J)
     E0(6)=E0(6)+C9*C3*Z0(JV)
     E0(7)=E0(7)+C8*C1*Z0(J)
     E0(9)=E0(9)+C9*0.75*C3*Z0(JV)
10   CONTINUE
     RETURN
     END
C
     SUBROUTINE ENN(X,PHI,M,N,ES,Z,P,P2,LOAD,LOOP)
     IMPLICIT REAL*8 (A-H,O-Z)
```

```
      DIMENSION ES(10),Z(6),P(3),P2(3),LOAD(3)
      COMMON/BLK2/T3,T4,PI,RADIAN,T,R,XLEN,NCSYM
      DO 5 I=1,9
5     ES(I)=0.0
      CNT=COS(N*PHI)
      SNT=SIN(N*PHI)
      A2=M*T4
      A3=A2*R
      A1=A3*A3
      A4=SIN(A2*X)
      A5=COS(A2*X)
      A45=A4/A5
      DO 10 J=1,3
      IF(LOAD(J).EQ.0) GOTO 10
      JU=J+1
      IF(J.EQ.2) JU=6
      JV=J+2
      A6=(P(J)*CNT+P2(J)*SNT)*A4
      A7=(P(J)*SNT-P2(J)*CNT)*A5
      ES(1)=ES(1)+Z(J)*A6
      ES(2)=ES(2)+Z(JU)*A6/A45
      ES(3)=ES(3)+Z(JV)*A7*A45
      IF(LOOP.EQ.3) GOTO 10
      ES(4)=ES(4)-A6*A3*Z(JU)
      ES(5)=ES(5)+A6*(N*Z(JV)+Z(J))
      ES(6)=ES(6)+A7*(A3*Z(JV)-N*Z(JU))
      ES(7)=ES(7)+A6*Z(J)*A1
      ES(8)=ES(8)+A6*(Z(J)*N*N+N*Z(JV))
      ES(9)=ES(9)+A7*(0.75*A3*Z(JV)+N*A3*Z(J)
     &+0.25*N*Z(JU))
10    CONTINUE
      RETURN
      END
C
      SUBROUTINE PJMN(M,N,NLOAD,CL)
      IMPLICIT REAL*8 (A-H,O-Z)
      DIMENSION P(3),P0(3),P2(3),P02(3),CL(60)
      COMMON/BLK2/T3,T4,PI,RADIAN,T,R,XLEN,NCSYM
      COMMON/BLK3/P,P0,P2,P02
      I1=(M+1)/2
      IF(M.LT.2*I1) I1=0
      DO 20 I=1,NLOAD
      J=(I-1)*6+1
      IC=CL(J)
      A1=CL(J+1)
      A2=CL(J+2)
      A3=CL(J+3)
      A4=CL(J+4)
      A5=CL(J+5)
      IF (IC.EQ.0.AND.I1.EQ.0) CALL SWP(P,P0,M,N,A1,A2,A3,A4)
      IF (IC.NE.0) CALL PATCH(IC,A1,A2,A3,A4,A5,M,N)
20    CONTINUE
      RETURN
      END
C
      SUBROUTINE SWP(P,P0,M,N,SWV,PRESS,SW,ALPHA)
      IMPLICIT REAL*8 (A-H,O-Z)
      DIMENSION P(3),P0(3)
      COMMON/BLK2/T3,T4,PI,RADIAN,T,R,XLEN,NCSYM
      ALPHA=ALPHA*RADIAN
      A1=SIN(ALPHA)
      A2=COS(ALPHA)
      A3=SW*R/(M*PI*PI)
      IF(N.GT.1) GOTO 20
      IF(N.EQ.1) GOTO 10
      P0(1)=4.0*PRESS/(M*PI)+4.0*A3*(A1-ALPHA*A2)
      RETURN
10    A5=4.0*T*SWV/(PI*M)
      P(1)=A5+4.0*A3*(ALPHA-A1*A2)
      P(3)=-A5
      RETURN
20    AN=8.0*(SIN(N*ALPHA)*A2-N*COS(N*ALPHA)*A1)/(N*(N*N-1))
      P(1)=AN*A3
      RETURN
      END
C
```

```
      P(1)=P(1)+A2*AM*AN(I,N)
      P2(1)=P2(1)+A2*AM*BN(I,N)
10    CONTINUE
      RETURN
      END
C
      SUBROUTINE PQP(M,N,PQ,RAD)
      IMPLICIT REAL*8 (A-H,O-Z)
      DIMENSION PQ(120),RAD(120),P(3),P2(3),P0(3),P02(3)
      COMMON/BLK2/T3,T4,PI,RADIAN,T,R,XLEN,NCSYM
      COMMON/BLK3/P,P0,P2,P02
      COMMON/BLK4/SDIV,WIDTH,NTYPE,NK,NSIZE,XSAD
      CC=WIDTH/2.0
      BETA=SDIV/2.0
      IC=0
      IF(NCSYM.EQ.1) IC=1
      A1=M*T4
      AM=4.0*SIN(A1*XSAD)*SIN(A1*CC)/(M*PI)
      IF(N.NE.0) GOTO 4
      A2=2.0*BETA*NCSYM/PI
      IF(NTYPE.EQ.1) A2=NCSYM/(R*PI)
      AN0=0.0
      DO 1 I=1,NK
1     AN0=AN0-PQ(I)*A2
      IF(NTYPE.EQ.2) AN0=AN0-(PQ(NSIZE+1)+
     & IC*PQ(NSIZE+2))*NCSYM/(R*PI)
      P0(1)=P0(1)+AN0*AM
      IF (NK.EQ.NSIZE) RETURN
      AN0=0.0
      DO 2 I=NK+1,NSIZE
2     AN0=AN0-PQ(I)
      P02(3)=P02(3)-IC*AN0*A2*AM
      RETURN
4     AN=0.0
      BN=0.0
      A1=-4.0*NCSYM*SIN(N*BETA)/(N*PI)
      IF(NTYPE.EQ.1) A1=-2.0*NCSYM/(R*PI)
      DO 10 I=1,NK
      PHI=RAD(I)*N
      A4=PQ(I)*A1
      AN=AN+A4*COS(PHI)
10    BN=BN+A4*SIN(PHI)
      IF(NTYPE.EQ.2) THEN
       A2=-2.0*NCSYM/(R*PI)
       DO 5 II=1,1+IC
        I=II+NSIZE
        PHI=RAD(I)*N
        A4=PQ(I)*A2
       AN=AN+A4*COS(PHI)
5      BN=BN+A4*SIN(PHI)
      END IF
      P(1)=P(1)+AM*AN
      P2(1)=P2(1)+IC*AM*BN
      IF(NK.EQ.NSIZE) RETURN
      AN=0.0
      BN=0.0
      DO 40 I=NK+1,NSIZE
      PHI=RAD(I)*N
      A4=PQ(I)*A1
      AN=AN+A4*COS(PHI)
40    BN=BN+A4*SIN(PHI)
      P(3)=P(3)+AM*BN
      P2(3)=P2(3)-IC*AM*AN
      RETURN
      END
```

```
      SUBROUTINE PATCH(KTYPE,Q,B,AFA,CC,BETA1,M,N)
      IMPLICIT REAL*8 (A-H,O-Z)
      DIMENSION P(3),P0(3),P2(3),P02(3)
      COMMON/BLK2/T3,T4,PI,RADIAN,T,R,XLEN,NCSYM
      COMMON/BLK3/P,P0,P2,P02
      AFA=AFA*RADIAN
      BETA1=BETA1*RADIAN
      C=CC/2.0
      BETA=BETA1/2.0
      IC=0
      IF (NCSYM.EQ.1) IC=1
      A1=M*T4
      A2=A1*B
      A3=A1*C
      A4=M*PI
      GOTO (1,2,1,4,1) KTYPE
1     IF (CC.EQ.0.0) AM=2.0*SIN(A2)/XLEN
      IF (CC.GT.0.0) AM=4.0*SIN(A2)*SIN(A3)/A4
      GOTO 30
2      IF (CC.EQ.0.0) AM=2.0*COS(A2)/XLEN
      IF (CC.GT.0.0) AM=4.0*COS(A2)*SIN(A3)/A4
      GOTO 30
4     AM=(COS(A2)*(SIN(A3)/(A1*C)-
COS(A3))+SIN(A2)*SIN(A3))*2.0/A4
30    IF (N.EQ.0) GOTO 60
      A4=N*AFA
      IF (BETA1.EQ.0.0) THEN
      A5=Q/(R*PI)
      GOTO 50
      END IF
      A1=2.0*Q/(N*PI)
      A2=N*BETA
      A5=A1*SIN(A2)
      IF(KTYPE.EQ.5) A5=A5/2.0+A1*(COS(A2)-SIN(A2)/A2)
50    AN=A5*COS(A4)
      BN=A5*SIN(A4)
      GOTO(500,600,700,500,500),KTYPE
500   P(1)=P(1)+AM*AN
      P2(1)=P2(1)+IC*AM*BN
      RETURN
600   P(2)=P(2)+AM*AN
      P2(2)=P2(2)+IC*AM*BN
      RETURN
700   P(3)=P(3)+AM*BN
      P2(3)=P2(3)-IC*AM*AN
      RETURN
60    IF (BETA1.EQ.0.0) AN0=Q/(2.0*R*PI)
      IF (BETA1.GT.0.0) AN0=BETA*Q/PI
      IF(KTYPE.EQ.5) AN0=AN0/2.0
      GOTO(501,601,701,501,501),KTYPE
501   P0(1)=P0(1)+AM*AN0
      RETURN
601   P0(2)=P0(2)+AM*AN0
      RETURN
701   P02(3)=P02(3)-IC*AN0*AM
      RETURN
      END
C----------IMPERFECTIONS----------
C*****ONLY FOR SHAPE SYMMETRIC ABOUT CENTRE,(AXIAL SYMMETRY)
      SUBROUTINE FIMP(NSYM,IMP,XIMP,PBAR,P,P2,AN,BN,M,N)
      IMPLICIT REAL*8 (A-H,O-Z)
      DIMENSION XIMP(3),P(3),P2(3),AN(3,60),BN(3,60)
      COMMON/BLK2/T3,T4,PI,RADIAN,T,R,XLEN,NCSYM
      A1=2.0*NSYM/XLEN
      A2=M*T4
      DO 10 I=1,IMP
      A3=XIMP(I)
      IF(I.EQ.1) XC=A3/2.0
      IF(IMP.GT.1) XC=(A3-XIMP(I-1))/3.0
      IF(I.LT.IMP) XD=(XIMP(I+1)-A3)/3.0
      IF(I.EQ.IMP) XD=(XLEN-A3*NSYM)/(1.0+NSYM)
      AM=(SIN(A2*(A3-XC))-SIN(A2*(A3-2.0*XC)))/XC
      IF(XD.GT.0.0) AM=AM-(SIN(A2*(A3+2.0*XD))
     &-SIN(A2*(A3+XD)))/XD
      AM=AM*A1/(A2*A2)
      A2=-PBAR*((N*N-1)+(M*T3)**2/2.0)/R
```

APPENDIX 2

Program - saddlepc f

```
C     SOLUTION FOR INTERFACE PRESSURE
      IMPLICIT REAL*8 (A-H,O-Z)
      DIMENSION C(110,3),CF(3,110),B(3,3),PQ(110),BB(3,3)
      DIMENSION DELTA(3),S(3),ES(3),WKS1(110,110),WVL(110)
      DIMENSION F(110,110),F1(60),F2(120),F4(60),KCODE(110)
      DIMENSION F5(110),F6(110),F7(110),F8(110)
      CHARACTER*10 NAME*60,GAPP,FLEX,FLNAM
C
      OPEN(2,FILE='PCINPUT',STATUS='UNKNOWN')
      READ(2,103) NAME
103   FORMAT(A60)
      READ(2,*) MTERM,NTERM
      READ(2,*) NSYS,NSYM,NCSYM,IMP
      READ(2,*) R,E,VV,T,XLEN
      IF(IMP.NE.0) THEN
      DO 5 I=1,IMP
5     READ(2,*) DUMMY
      END IF
      READ(2,*) NLOAD
      READ(2,*) A1,A2,A3,A4,A5,A6
      DO 6 I=2,NLOAD+1
6     READ(2,*) DUMMY
      READ(2,*) XSAD,SBETA,OFFSET,WIDTH,NTYPE
      READ(2,*) NDIV,NK,NT
      NSIZE=NK+NT
      I1=NDIV+NTYPE
      IF(NTYPE.EQ.2) I1=NDIV
      DO 33 I=1,NK
33      KCODE(I)=I
      DO 35 I=1,NT
35    KCODE(NK+I)=I
      IF (NK.LT.I1) READ(2,*) (KCODE(I),I=1,NK)
      IF              (NT.GT.0.AND.NT.LT.I1)              READ(2,*)
(KCODE(I),I=NK+1,NSIZE)
      READ(2,*) IGAP,IFLEX
      IF(IGAP.EQ.1) READ(2,104) GAPP
      IF(IFLEX.EQ.1) READ(2,104) FLEX
104   FORMAT(A10)
      CLOSE (2)
C
C     GLOBAL CONSTANTS
      PI=ASIN(1.0)*2.0
      PI2=PI*PI
      T1=1.0-VV
      T2=T*T
      T3=PI*R/XLEN
      T4=PI/XLEN
      A=E*T/(1.0-VV*VV)
      T5=R*R/A
      T6=T2/12.0
C
       C2=0.0
      IF(A1.EQ.0.0) THEN
       A5=A5*PI/180.0
       C11=SIN(A5)
       C12=COS(A5)
       PBAR=A3+A4*R*(C11-A5*C12)/PI
       C2=PBAR*R/A
      END IF
      C1=T6/(R*R)
      C2=PBAR*R/A
      IF(NSYS.EQ.1) C2=0.0
      C3=T1*C1/2.0
      C4=(3.0-VV)*C1/2.0
      C5=T1*(4.0+C1)/8.0
      C6=(4.0*(1.0+VV)-3.0*C1*T1)/8.0
      C7=T1*(4.0+9.0*C1)/8.0
C
      ITOL=NDIV+NTYPE
      SBETA=SBETA*PI/180.0
      SDIV=SBETA/NDIV
      DIV=SDIV
      IF(NTYPE.EQ.2) THEN
       ITOL=2*NDIV+1
       DIV=SDIV/2.0
      END IF
```

```
C
c***      WRITE(*,*) 'SADDLE PASS - CALCULATIONS IN PROGRESS'
c***      write(*,*) ' '
C         VECTORS F1,F2,F4,F5,F6,F7,F8
      W0=0.0
      V0=0.0
      WL2=0.0
      WL=0.0
      IEND=NTYPE+NDIV
      ISYM=1
      IK=0
      IF (NTYPE.EQ.2) THEN
         IEND=NDIV
         ISYM=2
         IK=1
      END IF
C
      DO 820 I=1,IEND
      F5(I)=0.0
      F6(I)=0.0
      F7(I)=0.0
      F8(I)=0.0
      F1(I)=0.0
      F2(I)=0.0
820   F4(I)=0.0
C
       A9=8.0/PI2
       BETA=SDIV/2.0
      IF (NTYPE.EQ.1) THEN
       A9=A9/(2.0*R)
       BETA=1.0
      END IF
      A2=T4*WIDTH/2.0
      A3=T4*XSAD
      A8=2.0
C
      DO 3001 M=1,MTERM
c***      write(6,2313) M

c***2313  FORMAT(1h+,'TERM NUMBER = ',I4)
      K=M*2-1
      C8=T3*K
      C9=C8*C8
      A1=1.0+C1*C9*C9
      A4=-VV*C8
      Z01=C9/(A1*C9-A4*A4)
      Z05=1.0/(C7*C9)
      A5=SIN(K*A3)
      A6=A9*SIN(K*A2)*A5*A5/K
      A7=A6*BETA
      W0=W0+A7*Z01
      V0=V0+A7*Z05
      DO 3001 N=1,NTERM
      N2=N*N
      A11=1.0+C1*(N2+C9)**2+C2*((N2-1)+0.5*C9)
      A12=C8*(C3*N2-VV)
      A13=N*(1.0+N2*C1)+C4*N*C9
      A22=C9+C5*N2
      A23=-C6*N*C8
      A33=N2*(1.0+C1)+C7*C9
      DEN=A11*A22*A33+2.0*A12*A23*A13-A11*A23*A23
     &-A22*A13*A13-A33*A12*A12
       Z1=(A22*A33-A23*A23)/DEN
       Z3=(A12*A23-A13*A22)/DEN
       Z5=(A11*A22-A12*A12)/DEN
       IF(NTYPE.EQ.0.OR.NTYPE.EQ.2) A8=2.0*SIN(N*BETA)/N
       CON=R*A8
       L=1
       I1=-1
100    IF(I1.EQ.ITOL) GOTO 555
       PHI=(L-1)*DIV
       CNT=A8*COS(N*PHI)
       ES(1)=CNT*A6*Z1
       ES(2)=-A6*Z3*A8*SIN(N*PHI)
       ES(3)=CNT*A6*Z5
       DO 900 JC=1,3
900    CF(JC,L)=ES(JC)
```

```
      I1=L*2-1
      IF(I1.GE.ITOL) I1=ITOL
      DO 500 I=L+1,I1
      A1=COS(N*(I-L)*DIV)*2.0
      IC=2*L-I
      DO 30 JC=1,3
30    CF(JC,I)=A1*ES(JC)-CF(JC,IC)
500   CONTINUE
      L=L*2
      GOTO 100
555   DO 910 I=1,IEND
       II=I*ISYM-IK
      F1(I)=F1(I)+CF(1,II)
      F2(I)=F2(I)+CF(2,II)
910   F4(I)=F4(I)+CF(3,II)
      IF(NTYPE.NE.2) GOTO 3001
      WL=WL+CF(1,1)/CON
      WL2=WL2+CF(1,ITOL)/CON
      DO 909 I=1,IEND
       II=I*ISYM
      F7(I)=F7(I)+CF(1,II)
      F8(I)=F8(I)+CF(2,II)
      F5(I)=F5(I)+CF(1,II)/CON
909   F6(I)=F6(I)+CF(2,II)/CON
3001   CONTINUE
C
       W0A=W0/(2.0*BETA*R)
      DO 930 J=1,IEND
      F1(J)=(F1(J)+W0)*T5
      F2(J)=F2(J)*T5
      F4(J)=(F4(J)+V0)*T5
       IF (NTYPE.NE.2) GOTO 930
      F5(J)=(F5(J)+W0A)*T5
      F6(J)=F6(J)*T5
      F7(J)=(F7(J)+W0)*T5
      F8(J)=F8(J)*T5
930   CONTINUE
      WL=(WL+W0A)*T5
      WL2=(WL2+W0A)*T5
C---------------------------------
c****       WRITE(*,*) 'FORMING FLEXIBILITY MATRIX [F]'
      GOTO(3020,3030),NCSYM
3020  DO 200 I=1,NK
      IC=KCODE(I)
       DO 200 J=I,NK
        I1=KCODE(J)-IC+1
200     F(I,J)=F1(I1)
      IF(NTYPE.EQ.2) THEN
      K1=NSIZE+1
      K2=NSIZE+2
      KCODE(K1)=0
      KCODE(K2)=99
      K3=NDIV+1
      DO 813 I=1,NK
       IC=KCODE(I)
       F(I,K1)=F5(IC)
       F(I,K2)=F5(K3-IC)
       F(K1,I)=F7(IC)
813    F(K2,I)=F7(K3-IC)
       F(K1,K1)=WL
       F(K2,K2)=WL
       F(K1,K2)=WL2
       F(K2,K1)=WL2
       NSIZE=NSIZE+2
      END IF
      IF(NT.EQ.0) GOTO 3005
      DO 802 I=1,NK
       IC=KCODE(I)
       DO 802 K=1,NT
        I1=NK+K
        I2=KCODE(I1)-IC
        IF(I2.GT.0) F(I,I1)=-F2(I2+1)
        IF(I2.LE.0) F(I,I1)=F2(1-I2)
802   CONTINUE
      DO 812 I=NK+1,NSIZE
       IC=KCODE(I)
```

```
        DO 812 J=I,NSIZE
          F(I,J)=F4(KCODE(J)-IC+1)
812    CONTINUE
       IF(NTYPE.EQ.2) THEN
       DO 811 I=NK+1,NK+NT
        IC=KCODE(I)
        F(I,K1)=F6(IC)
        F(I,K2)=-F6(K3-IC)
        F(K1,I)=-F8(IC)
811     F(K2,I)=F8(K3-IC)
       END IF
       GOTO 3005
C
C------DEFORMATIONS  SYMMETRIC ABOUT VERTICAL AXIS----
3030   NKS=(NK+1)/2
       NTS=NT/2
       DO 300 I=1,NKS
       K1=KCODE(I)
       DO 300 J=I,NKS
        I1=KCODE(J)-K1+1
        I2=KCODE(NK-J+1)-K1+1
        F(I,J)=F1(I1)+F1(I2)
300    CONTINUE
       IF(NT.EQ.0) GOTO 3333
       DO 301 I=1,NKS
       K1=KCODE(I)
       DO 301 J=1,NTS
        I1=KCODE(NK+J)-K1
        I2=KCODE(NSIZE-J+1)-K1
        IF(I1.GT.0) C1=-F2(I1+1)
        IF(I1.LE.0) C1=F2(1-I1)
        IF(I2.GT.0) C2=-F2(I2+1)
        IF(I2.LE.0) C2=F2(1-I2)
        F(I,NKS+J)=C1-C2
301    CONTINUE
       DO 302 I=1,NTS
        K1=KCODE(NK+I)
        DO 302 J=I,NTS
        I1=KCODE(NK+J)-K1+1
        I2=KCODE(NSIZE-J+1)-K1+1
302     F(I+NKS,J+NKS)=F4(I1)-F4(I2)
C
3333   IF (NTYPE.NE.2) GOTO 53
       I1=NKS+NTS+1
       K1=NDIV+1
       DO 51 I=1,NKS
        IC=KCODE(I)
        F(I,I1)=F5(IC)+F5(K1-IC)
51      F(I1,I)=F7(IC)+F7(K1-IC)
        F(I1,I1)=WL+WL2
        IF(NT.EQ.0) GOTO 53
       DO 52 I=1,NT
        IC=KCODE(I)
        F(I+NKS,I1)=F6(K1-IC)-F6(IC)
52      F(I1,I+NKS)=F8(K1-IC)-F8(IC)
C      RESET KCODE
53      DO 345 I=1,NTS
345     KCODE(NKS+I)=KCODE(NK+I)
       NK=NKS
       NT=NTS
       NSIZE=NK+NT
       KCODE(NSIZE+1)=0
       IF (NTYPE.EQ.2) NSIZE=NSIZE+1
3005   CONTINUE
       NKT=NK+NT
       DO 303 I=2,NKT
       DO 303 J=1,I-1
303    F(I,J)=F(J,I)
C
C--------INVERT [F]----------
       DO 123 I=1,NSIZE
       DO 123 J=1,NSIZE
123    WKS1(I,J)=F(I,J)
c****       WRITE(*,*) 'INVERT [F]'
       CALL MIV(WKS1,NSIZE)
C----------------------------
```

```
      OPEN(3,FILE='PCSAD',STATUS='UNKNOWN')
      READ(3,*) (WVL(I),I=1,NSIZE)
      READ(3,*) (S(I),I=1,3)
      CLOSE (3)
       NKT=NK+NT
       RSDIV=R*SDIV
      DO 815 I=1,3
      IF(NTYPE.EQ.0.OR.NTYPE.EQ.2) S(I)=S(I)/RSDIV
815   S(I)=S(I)/(2.0*NCSYM*WIDTH)
      IF(NTYPE.EQ.2) THEN
       DO 818 I=NKT+1,NSIZE
        DO 818 J=1,NSIZE
818       WKS1(I,J)=WKS1(I,J)/RSDIV
       END IF
C     GAP VECTOR [GAP]
      IF (IGAP.EQ.1) THEN
      OPEN (55,FILE=GAPP,STATUS='OLD')
      READ (55,*) K
      READ (55,*) (F1(I),I=1,K)
      CLOSE (55)
      DO 890 I=1,K
890   WVL(I)=WVL(I)-F1(I)
      END IF
C
      A11=(SBETA-SDIV)/2.0
      IF (NTYPE.EQ.1) A11=SBETA/2.0
      C1=OFFSET*PI/180.0-A11
      DO 800 I=1,NK
       PHI=(KCODE(I)-1)*SDIV+C1
       C(I,1)=COS(PHI)
       C(I,2)=SIN(PHI)
800    C(I,3)=0.0
C
      IF (NTYPE.EQ.2) THEN
         A1=C1+A11-SBETA/2.0
         A2=A1+SBETA
         C(NKT+1,1)=COS(A1)
         C(NKT+1,2)=SIN(A1)
         C(NKT+1,3)=0.0
         C(NKT+2,1)=COS(A2)
         C(NKT+2,2)=SIN(A2)
         C(NKT+2,3)=0.0
      END IF
      IF (NT.EQ.0) GOTO 814
      L=NK+1
      DO 747 I=L,NKT
      PHI=(KCODE(I)-1)*SDIV+C1
      C(I,1)=-SIN(PHI)
      C(I,2)=COS(PHI)
747   C(I,3)=R
814   CONTINUE
C      [C]T*[F](-1)
       NDEL=3
       IF (NT.EQ.0) NDEL=2
       IF (NCSYM.EQ.2) NDEL=1
       ITER=0
       DO 776 I=1,3
        DO 775 J=1,3
775       B(I,J)=0.0
776       B(I,I)=1.0
896    DO 777 I=1,NDEL
        DO 777 J=1,NSIZE
         CF(I,J)=0.0
          DO 777 K=1,NSIZE
777    CF(I,J)=CF(I,J)+C(K,I)*WKS1(K,J)
C
C---------[B] MATRIX--------
       DO 902 I=1,NDEL
        DO 902 J=1,NDEL
         B(I,J)=0.0
          DO 902 K=1,NSIZE
902    B(I,J)=B(I,J)+CF(I,K)*C(K,J)
C
C-------COMPUTE THE INVERSE OF [B] MATRIX----------
     C1=B(1,1)*B(2,2)*B(3,3)+B(1,2)*B(2,3)*B(3,1)
    1  +B(1,3)*B(2,1)*B(3,2)-B(1,3)*B(3,1)*B(2,2)
```

```
     2  -B(1,1)*B(2,3)*B(3,2)-B(1,2)*B(2,1)*B(3,3)
        BB(1,1)=(B(2,2)*B(3,3)-B(2,3)*B(3,2))/C1
        BB(1,2)=(B(1,3)*B(3,2)-B(1,2)*B(3,3))/C1
        BB(1,3)=(B(1,2)*B(2,3)-B(1,3)*B(2,2))/C1
        BB(2,1)=(B(2,3)*B(3,1)-B(2,1)*B(3,3))/C1
        BB(2,2)=(B(1,1)*B(3,3)-B(1,3)*B(3,1))/C1
        BB(2,3)=(B(1,3)*B(2,1)-B(1,1)*B(2,3))/C1
        BB(3,1)=(B(2,1)*B(3,2)-B(2,2)*B(3,1))/C1
        BB(3,2)=(B(1,2)*B(3,1)-B(1,1)*B(3,2))/C1
        BB(3,3)=(B(1,1)*B(2,2)-B(1,2)*B(2,1))/C1
C
C-------[DELTA]---------
888     DO 904 I=1,NDEL
        F2(I)=0.0
        DO 904 J=1,NSIZE
904     F2(I)=F2(I)+CF(I,J)*WVL(J)
        DO 906 I=1,NDEL
906     F2(I)=S(I)-F2(I)
        DO 907 I=1,3
907     DELTA(I)=0.0
        DO 908 I=1,NDEL
        DO 908 J=1,NDEL
908     DELTA(I)=DELTA(I)+BB(I,J)*F2(J)
C
C-------[PQ]------------
        DO 666 I=1,NSIZE
          F2(I)=0.0
          DO 666 J=1,NDEL
        F2(I)=F2(I)+C(I,J)*DELTA(J)
666     CONTINUE
        DO 911 I=1,NSIZE
        F2(I)=F2(I)+WVL(I)
911     CONTINUE
        DO 912 I=1,NSIZE
          PQ(I)=0.0
          DO 912 J=1,NSIZE
912     PQ(I)=PQ(I)+WKS1(I,J)*F2(J)
        IF(NTYPE.EQ.2) THEN
          PQ(NKT+1)=PQ(NKT+1)*RSDIV
          PQ(NKT+2)=PQ(NKT+2)*RSDIV
        END IF
C
        IF (NT.GT.0) GOTO 960
        ITER=ITER+1
        WRITE(*,*) 'NO. OF ITERACTION = ',ITER
         NEP=0
        DO 950 I=1,NSIZE
          IF (PQ(I).GE.0.0) GOTO 950
        DO 951 J=1,NSIZE
          F(I,J)=0.0
951       F(J,I)=0.0
          F(I,I)=1.0
          C(I,1)=0.0
          C(I,2)=0.0
          WVL(I)=0.0
          NEP=NEP+1
950       CONTINUE
        IF(NEP.EQ.0) GOTO 960
        DO 124 I=1,NSIZE
        DO 124 J=1,NSIZE
124     WKS1(I,J)=F(I,J)
         CALL MIV(WKS1,NSIZE)
         IF(NTYPE.NE.2) GOTO 896
          DO 128 I=NKT+1,NSIZE
            DO 128 J=1,NSIZE
128           WKS1(I,J)=WKS1(I,J)/RSDIV
         GOTO 896
960     CONTINUE
C
C---------OUTPUT RESULTS---------
        OPEN(6,FILE='PCSADRES',STATUS='UNKNOWN')
        WRITE(6,780) NAME
780     FORMAT(5X,A/)
        WRITE(6,782) MTERM,NTERM
782     FORMAT(/5X,'MTERM =',I4/5X,'NTERM =',I4/)
        SBETA=INT(SBETA*180000.0/PI)/1000.0
```

```
      WRITE(6,784) XSAD,WIDTH,SBETA,OFFSET
784   FORMAT(10X,'DISTANCE OF SUPPORT FROM END =',E12.5/
     1       10X,'SADDLE WIDTH =',E12.5,' UNIT'/
     2       10X,'FULL SADDLE ARC ANGLE =',F7.2,' DEG'/
     3       10X,'SADDLE OFFSET BY ',F7.2,' DEG'/)
      WRITE(6,*) '** SUPPORT INTERFACE REACTIONS **'
      IF(NTYPE.EQ.0) WRITE(6,*) 'PATCH LOAD MODEL'
      IF(NTYPE.EQ.1) WRITE(6,*) 'LINE LOAD MODEL'
      IF(NTYPE.EQ.2) WRITE(6,*) 'PATCH + LINE AT HORN'
      WRITE (6,785)
785   FORMAT(/,4X,'NO.  CODE.NO      PQ(I)')
      DO 788 I=1,NSIZE
788   WRITE(6,790) I,KCODE(I),PQ(I)
790   FORMAT(3X,I3,2X,I3,6X,E15.8)
      WRITE(6,*) ' '
      WRITE(6,*) '   RIGID BODY DISPLACEMENT'
      WRITE(6,791) (DELTA(I),I=1,3)
791   FORMAT(10X,'VERTICAL     : ',E12.5,2X,'UNIT'/
     1       10X,'HORIZONTAL   : ',E12.5,2X,'UNIT'/
     2       10X,'ROTATIONAL   : ',E12.5,2X,'UNIT')
C     STORE [PQ],[DELTA] IN FILE PQ.DAT
      OPEN(16,FILE='PCPQ',STATUS='UNKNOWN')
      WRITE (16,*) (PQ(I),I=1,NSIZE)
      WRITE (16,*) (DELTA(I),I=1,3)
      CLOSE (16)
      STOP
      END
C---------INVERSION ROUTINE------------
      SUBROUTINE MIV(A,N)
      IMPLICIT REAL*8 (A-H,O-Z)
      DIMENSION A(110,110),B(110,110),NROW(110)
      DO 20 I=1,N
       DO 10 J=1,N
10    B(I,J)=0.0
20    B(I,I)=1.0
      DO 40 I=1,N
40    NROW(I)=I
      DO 130 KK=2,N
      K=N-KK+2
      XT=0.0
      DO 50 J=1,K
       DO 50 I=1,J
        IF(XT.GE.ABS(A(I,J))) GOTO 50
       XT=ABS(A(I,J))
       JMAX=J
       IMAX=I
50    CONTINUE
      IF(XT.EQ.0.0) RETURN
      IF(JMAX.EQ.K) GOTO 70
      DO 60 I=1,N
       HOLD=A(I,JMAX)
       A(I,JMAX)=A(I,K)
60    A(I,K)=HOLD
      HOLD=NROW(JMAX)
      NROW(JMAX)=NROW(K)
      NROW(K)=HOLD
70    IF(IMAX.EQ.K) GOTO 100
      DO 80 J=1,N
      HOLD=A(IMAX,J)
      A(IMAX,J)=A(K,J)
80    A(K,J)=HOLD
      DO 90 J=1,N
       HOLD=B(IMAX,J)
       B(IMAX,J)=B(K,J)
90    B(K,J)=HOLD
100   KM1=K-1
      DO 120 I=1,KM1
       FACTOR=A(I,K)/A(K,K)
       DO 110 J=1,N
110    A(I,J)=A(I,J)-FACTOR*A(K,J)
      DO 120 J=1,N
120    B(I,J)=B(I,J)-FACTOR*B(K,J)
130   CONTINUE
      DO 150 J=1,N
      IF (A(1,1).EQ.0.0) RETURN
      B(1,J)=B(1,J)/A(1,1)
```

```
      DO 150 I=2,N
       IF(A(I,I).EQ.0.0) RETURN
       IM1=I-1
       DO 140 K=1,IM1
140   B(I,J)=B(I,J)-A(I,K)*B(K,J)
150   B(I,J)=B(I,J)/A(I,I)
      DO 160 K=1,N
      I=NROW(K)
      DO 160 J=1,N
160   A(I,J)=B(K,J)
      RETURN
      END
```

APPENDIX 3

Program - cyl2pc.f

```
C      SOLUTION FOR INTERFACE PRESSURE
C      HORIZONTALLY END SIMPLY-SUPPORTED CYLINDER
C      PROGRAM CONVERTED FOR 2ND PASS - D H NASH
C
       IMPLICIT REAL*8 (A-H,O-Z)
       CHARACTER*20 NAME*60,TITLE*60,DATA1(5),FILNM,FNAME
       DIMENSION Z(6),Z0(6),P0(3),P(3),P02(3),P2(3),S(3)
       DIMENSION LOAD(3),CL(60),XIMP(3),ES(10),E0(10)
       DIMENSION AN(3,60),BN(3,60),RAD(120),DISP(9,120)
       DIMENSION DELTA(3),PQ(120),KCODE(120),RES(9,120)
       COMMON/BLK2/T3,T4,PI,RADIAN,T,R,XLEN,NCSYM
       COMMON/BLK3/P,P0,P2,P02
       COMMON/BLK4/SDIV,WIDTH,NTYPE,NK,NSIZE,XSAD
       IJOB=2
       LOOP=9
       IF(IJOB.EQ.1.OR.IJOB.GE.3) LOOP=3
       OPEN(2,FILE='PCINPUT',STATUS='UNKNOWN')
       READ(2,103) NAME
103    FORMAT(A60)
       READ (2,*) MTERM,NTERM
       READ (2,*) NSYS,NSYM,NCSYM,IMP
       READ (2,*) R,E,VV,T,XLEN
       IF (IMP.GT.0) READ (2,102) (XIMP(I),DATA1(I),I=1,IMP)
102    FORMAT(E12.5,5X,A)
       READ (2,*) NLOAD
       READ (2,*) (CL(I),I=1,NLOAD*6)
       READ (2,*) CP1,CP2,CP3,CP4,STEP
         NP=1
        IF(CP2.EQ.CP4) NP=2
C-----------SADDLE SUPPORT PROBLEM----------
       IF(IJOB.EQ.1.OR.IJOB.EQ.2) THEN
       READ(2,*) XSAD,SBETA,OFFSET,WIDTH,NTYPE
       READ(2,*) NDIV,NK,NT
       NSIZE=NK+NT
       I1=NDIV+NTYPE
       IF (NTYPE.EQ.2) I1=NDIV
        DO 34 I=1,NK
34        KCODE(I)=I
        DO 35 I=1,NT
35      KCODE(NK+I)=I
       IF (NK.LT.I1) READ(2,*) (KCODE(I),I=1,NK)
       IF              (NT.GT.0.AND.NT.LT.I1)              READ(2,*)
(KCODE(I),I=NK+1,NSIZE)
       IF (NCSYM.EQ.2) THEN
        NTS=NT/2
        NKS=(NK+1)/2
        DO 33 I=1,NTS
33      KCODE(NKS+I)=KCODE(NK+I)
        NT=NTS
        NK=NKS
        NSIZE=NK+NT
        END IF
         NS1=NSIZE+1
         NS2=NSIZE+2
        IF(IJOB.EQ.1) THEN
        SDIV=SBETA/NDIV
        A1=(SBETA-SDIV)/2.0
        IF(NTYPE.EQ.1) A1=SBETA/2.0
        NP=1
        CP1=XSAD
        CP2=OFFSET-A1
        IC=MAX0(NK,NT)
        CP4=OFFSET+(KCODE(IC)-1)*SDIV-A1
        STEP=SDIV
       END IF
         END IF
       CLOSE (UNIT=2)
C-----------------------------
C      AXIAL SYMMETRY  NSYM=2, KM=1
C      NON AXIAL SYMMETRY  NSYM=1, KM=0
       KM=1
       IF (NSYM.EQ.1) KM=0
C-----------------------------
C      GLOBAL CONSTANTS
       PI=ASIN(1.0)*2.0
       RADIAN=PI/180.0
```

```
      PI2=PI*PI
      T1=1.0-VV
      T2=T*T
      A=E*T/(1.0-VV*VV)
      T3=PI*R/XLEN
      T4=PI/XLEN
      T5=R*R/A
      T6=T2/12.0
C-----------------------------
C     LOOPING FOR LOADS
      DO 40 I=1,3
40    LOAD(I)=0
      DO 41 I=1,NLOAD
       K=(I-1)*6+1
       IF(CL(K).EQ.1.0.OR.CL(K).GE.4.0) LOAD(1)=1
       IF(CL(K).EQ.2.0) LOAD(2)=1
41     IF(CL(K).EQ.3.0) LOAD(3)=1
C-----------------------------
      IF(IJOB.EQ.2) THEN
        IC=1
        IF(NCSYM.EQ.1) IC=2
        N=NSIZE
       IF(NTYPE.EQ.2) N=NSIZE+IC
      OPEN(16,FILE='PCPQ',STATUS='UNKNOWN')
      READ(16,*) (PQ(I),I=1,N)
      READ(16,*) (DELTA(I),I=1,3)
      CLOSE (16)
      IF (NT.GT.0) LOAD(3)=1
      END IF
C-----------------------------
      C1=T6/(R*R)
      C2=0.0
      PRESS=0.0
C     CL(2)=SWV, CL(3)=PRESS, CL(4)=SW, CL(5)=ALPHA
      IF (CL(1).EQ.0.0) THEN
       LOAD(1)=1
       IF(CL(2).NE.0.0) LOAD(3)=1
      ALPHA=CL(5)*RADIAN
      PRESS=CL(3)
      C11=SIN(ALPHA)
      C12=COS(ALPHA)
      PBAR=CL(3)+CL(4)*R*(C11-ALPHA*C12)/PI
      C2=PBAR*R/A
      END IF
      IF (NSYS.EQ.1) C2=0.0
      C3=0.5*T1*C1
      C4=0.5*(3.0-VV)*C1
      C5=0.125*T1*(4.0+C1)
      C6=0.125*(4.0*(1.0+VV)-3.0*C1*T1)
      C7=0.125*T1*(4.0+9.0*C1)
C
      IF (IJOB.EQ.1) GOTO 111
C-------------PRINT INPUT DATA--------------
      OPEN(7,FILE='PCOUT',STATUS='UNKNOWN')
      WRITE (7,780) NAME
780   FORMAT(//5X,A/)
      IF (NSYS.EQ.2) WRITE (7,360)
360       FORMAT(5X,'STIFFENING EFFECT OF PRESSURE HAS BEEN
CONSIDERED')
      IF (IMP.GT.0) THEN
       WRITE (7,*) 'CROSS SECTIONAL PROFILES'
       WRITE (7,102) (XIMP(I),DATA1(I),I=1,IMP)
      END IF
C
      WRITE (7,782) MTERM,NTERM
782   FORMAT(/5X,'MTERM =',I4/5X,'NTERM =',I4)
      WRITE (7,330)
330   FORMAT(//5X,'CYLINDRICAL SHELL')
      WRITE (7,300) XLEN,R,T,E,VV
300   FORMAT(/10X,'LENGTH =',E12.5,2X,'UNIT'/
     &        10X,'RADIUS =',E12.5,2X,'UNIT'/
     &        10X,'THICKNESS =',E12.5,2X,'UNIT'/
     &        10X,'YOUNGS MODULUS =',E12.5,2X,'UNIT'/
     &        10X,'POISSON RATIO =',F7.3)
C
      WRITE (7,306)
```

```
306   FORMAT(//5X,'*LOADING*')
305   FORMAT(/5X,'SP. WT.=',E12.5,2X,'PRESSURE =',E12.5/
     &    5X,'SP.    WT.    OF    FLUID    =',E12.5,2X,'LEVEL    OF
FILL=',F7.2,'DEG')
343   FORMAT(/5X,'TYPE = RADIAL PATCH (1)      AXIAL SHEAR PATCH
(2)'/
     &          5X,'    HOOP SHEAR PATCH (3)      AXIAL TRIANGULAR
(4)'/
     &        5X,'    HOOP TRIANGULAR  (5)'//

&5X,'TYPE',4X,'MAGNITUDE',9X,'X',11X,'PHY',8X,'2C',8X,'2BETA')
344   FORMAT(7X,I2,2(2X,E12.5),2X,F7.2,2X,E12.5,2X,F7.2)
      IF (CL(1).EQ.0.0) WRITE (7,305) (CL(I),I=2,5)
      IF (CL(1).NE.0.0) WRITE (7,343)
      DO 333 I=1,NLOAD
       J=(I-1)*6+1
       IC=CL(J)
       IF(IC.EQ.0) GOTO 333
       WRITE(6,344) IC,(CL(K),K=J+1,J+5)
333   CONTINUE
C------------IMPERFECTION-------------------
      KC=0
111   IF (IMP.EQ.0) GOTO 404
      DO 400 I=1,IMP
      OPEN(1,FILE=DATA1(I),STATUS='OLD')
      READ(1,103) TITLE
      READ(1,*) NDRAD,CONVT,DRIFT
      READ(1,*) (RAD(J),J=1,NDRAD)
      READ(1,*) DATUM
      CLOSE(1)
      DO 401 J=1,NDRAD
401   RAD(J)=(RAD(J)-DRIFT)*CONVT+DATUM
      KC=NDRAD/2
      IF(KC.GE.NTERM) KC=NTERM
      A2=2.0/NDRAD
      A1=PI*A2
      DO 402 N=2,KC
       SSUM=0.0
       CSUM=0.0
       A3=A1*N
       DO 403 J=1,NDRAD
        PHY=(J-1)*A3
       SSUM=SSUM+RAD(J)*SIN(PHY)
       CSUM=CSUM+RAD(J)*COS(PHY)
403   CONTINUE
      AN(I,N)=CSUM*A2
402   BN(I,N)=SSUM*A2
400   CONTINUE
       IF(NSYM.EQ.1) GOTO 404
        IF(XIMP(IMP).GT.XLEN/2.0) XIMP(IMP)=XLEN/2.0
404   CONTINUE
C-----------------------------------------
C     ANGULAR POSITIONS OF CONTACT NODES
      IF (IJOB.EQ.2) THEN
      SBETA=SBETA*RADIAN
      SDIV=SBETA/NDIV
      A1=(SBETA-SDIV)/2.0
      IF(NTYPE.EQ.1) A1=SBETA/2.0
      A2=OFFSET*RADIAN-A1
      DO 80 I=1,NSIZE
80    RAD(I)=(KCODE(I)-1)*SDIV+A2
      IF(NTYPE.EQ.2) THEN
       RAD(NS1)=A1+A2-SBETA/2.0
       RAD(NS2)=RAD(NS1)+SBETA
      END IF
      END IF
C-----------------------------------------
       IF (STEP.EQ.0.0) ITOL=1
      IF (STEP.NE.0.0) THEN
         A1=(CP4-CP2)/STEP
         IF (NP.EQ.2) A1=(CP3-CP1)/STEP
         ITOL=1.1+A1
      END IF
      DO 990 J=1,LOOP
       E0(J)=0.0
      DO 990 I=1,ITOL+NTYPE
```

```
990    RES(J,I)=0.0
       Z0(3)=0.0
       Z0(4)=0.0
       P02(1)=0.0
       P02(2)=0.0
C
       X=CP1
       PHY=CP2*RADIAN
       STEP1=STEP*RADIAN
c****       PRINT *, '2nd PASS - CALCULATIONS IN PROGESS'
c****       WRITE(6,*) ' '
C-----------------------------------------
       DO 3001 M=1,MTERM
c***        WRITE(6,2313) M
c***2313    FORMAT(1h+,'TERM NUMBER = ',I4)
        K=M*NSYM-KM
        C8=T3*K
        C9=C8*C8
        A1=1.0+C1*C9*C9
        A4=-VV*C8
        A5=A1*C9-A4*A4
        Z0(1)=C9/A5
        Z0(2)=-A4/A5
        Z0(5)=1.0/(C7*C9)
        Z0(6)=A1/A5
        DO 3004 I=1,3
3004    P0(I)=0.0
        P02(3)=0.0
        CALL PJMN(K,0,NLOAD,CL)
         IF(IJOB.EQ.2) CALL PQP(K,0,PQ,RAD)
        IF (NP.EQ.1) CALL EN0(X,K,E0,Z0,P0,P02,LOAD,LOOP)
       DO 3001 N=1,NTERM
       N2=N*N
       A11=1.0+C1*(N2+C9)**2+C2*((N2-1)+0.5*C9)
       A12=C8*(C3*N2-VV)
       A13=N*(1.0+N2*C1)+C4*N*C9
       A22=C9+C5*N2
       A23=-C6*N*C8
       A33=N2*(1.0+C1)+C7*C9
       DEN=A11*A22*A33+2.0*A12*A23*A13-A11*A23*A23
     &-A22*A13*A13-A33*A12*A12
       Z(1)=(A22*A33-A23*A23)/DEN
       Z(2)=(A13*A23-A12*A33)/DEN
       Z(3)=(A12*A23-A13*A22)/DEN
       Z(4)=(A12*A13-A11*A23)/DEN
       Z(5)=(A11*A22-A12*A12)/DEN
       Z(6)=(A11*A33-A13*A13)/DEN
        DO 3003 I=1,3
        P(I)=0.0
3003    P2(I)=0.0
        CALL PJMN(K,N,NLOAD,CL)
        IF (IJOB.EQ.2) CALL PQP(K,N,PQ,RAD)
        IF(KC.GE.N.AND.N.GT.1)
     &  CALL FIMP(NSYM,IMP,XIMP,PBAR,P,P2,AN,BN,K,N)
        L=1
        I1=-1
100     IF (I1.EQ.ITOL) GOTO 555
        IF (NP.EQ.1) THEN
        PHI=(L-1)*STEP1+PHY
        CALL ENN(X,PHI,K,N,ES,Z,P,P2,LOAD,LOOP)
        ELSE
        X=(L-1)*STEP+CP1
        CALL ENN(X,PHY,K,N,ES,Z,P,P2,LOAD,LOOP)
        CALL EN0(X,K,ES,Z0,P0,P02,LOAD,LOOP)
        STEP1=T4*K*STEP/N
        END IF
        DO 900 JC=1,LOOP
900     DISP(JC,L)=ES(JC)
        I1=L*2-1
        IF (I1.GE.ITOL) I1=ITOL
        DO 500 I=L+1,I1
        A1=COS(N*(I-L)*STEP1)*2.0
        IC=2*L-I
        DO 30 JC=1,LOOP
30      DISP(JC,I)=A1*ES(JC)-DISP(JC,IC)
500     CONTINUE
```

```
      L=L*2
      GOTO 100
555   DO 910 J=1,LOOP
      DO 910 I=1,ITOL
910   RES(J,I)=RES(J,I)+DISP(J,I)
      IF(NTYPE.NE.2.AND.IJOB.NE.1) GOTO 3001
       A1=2.0*COS(N*STEP1/2.0)
      RES(1,NS1)=RES(1,NS1)+A1*DISP(1,1)-
(DISP(1,1)+DISP(1,2))/A1
      RES(1,NS2)=RES(1,NS2)+A1*DISP(1,ITOL)-(DISP(1,ITOL-1)
     & +DISP(1,ITOL))/A1
3001   CONTINUE
C-----------------------------------------
      IF (NP.EQ.1) THEN
       DO 930 I=1,LOOP
       DO 930 J=1,ITOL
930    RES(I,J)=RES(I,J)+E0(I)
      END IF
C
C     STORE [WVL],[S]
      IF(IJOB.EQ.1) THEN
      DO 948 I=1,3
948   S(I)=0.0
       IF(NTYPE.EQ.2) THEN
        RAD(NS1)=(RES(1,NS1)+E0(1))*T5
        RAD(NS2)=(RES(1,NS2)+E0(1))*T5
         IC=1
          IF(NCSYM.EQ.1) IC=2
          NSIZE=NSIZE+IC
         END IF
       I1=0
       IF(NCSYM.EQ.1) I1=1
       IF(CL(1).EQ.0.0) S(1)=2.0*PI*R*T*XLEN*CL(2)+CL(4)
      &*XLEN*R*R*(ALPHA-SIN(2.0*ALPHA)/2.0)+CL(6)
       DO 949 I=1,NLOAD
        J=(I-1)*6+1
        IC=CL(J)
        IF(IC.EQ.0.OR.IC.EQ.2) GOTO 949
        A1=CL(J+4)
        A2=CL(J+5)*R*RADIAN
       IF(A1.EQ.0.0) A1=1.0
       IF(A2.EQ.0.0) A2=1.0
       A3=A1*A2*CL(J+1)
       A4=CL(J+3)*RADIAN
      IF(IC.EQ.1) THEN
       S(1)=S(1)+A3*COS(A4)
       S(2)=S(2)+I1*A3*SIN(A4)
      END IF
      IF(IC.EQ.3) THEN
       S(1)=S(1)-A3*SIN(A4)
       S(2)=S(2)+I1*A3*COS(A4)
       S(3)=S(3)+I1*A3*R
      END IF
949   CONTINUE
      DO 947 J=1,NK
947    RAD(J)=RES(1,KCODE(J))*T5
      DO 946 J=NK+1,NK+NT
946   RAD(J)=RES(3,KCODE(J))*T5
      OPEN(3,FILE='PCSAD',STATUS='UNKNOWN')
       WRITE(3,*) (RAD(J),J=1,NSIZE)
       WRITE(3,*) (S(I),I=1,3)
       GOTO 999
      END IF
      A3=1.0E6/A
      A4=PRESS*0.5/(1.0-VV*VV)
C***      WRITE(*,*) 'WRITE TO OUTPUT FILE'
      DO 940 J=1,ITOL
       IF (NP.EQ.1) THEN
        ANG=CP2+(J-1)*STEP
       ELSE
        X=CP1+(J-1)*STEP
       END IF
      RES(1,J)=RES(1,J)*T5
      RES(2,J)=RES(2,J)*T5
      RES(3,J)=RES(3,J)*T5
      IF(IJOB.EQ.2) THEN
```

```
      PHI=ANG*RADIAN
      SNT=SIN(PHI)
      CNT=COS(PHI)
      RES(1,J)=RES(1,J)+DELTA(1)*CNT+DELTA(2)*SNT
      RES(3,J)=RES(3,J)-DELTA(1)*SNT+DELTA(2)*CNT+R*DELTA(3)
     END IF
     WRITE (7,310) X,ANG
     WRITE (7,311) (RES(K,J),K=1,3)
     IF(LOOP.EQ.3) GOTO 940
     RES(4,J)=RES(4,J)+A4
     RES(5,J)=RES(5,J)-A4*VV
     ES(1)=R*(RES(4,J)+VV*RES(5,J))
     ES(2)=R*(RES(5,J)+VV*RES(4,J))
     ES(3)=R*T1*RES(6,J)/2.0
     ES(4)=T6*(RES(7,J)+VV*RES(8,J))
     ES(5)=T6*(RES(8,J)+VV*RES(7,J))
     ES(6)=T6*T1*RES(9,J)
     A1=ES(1)/T
     A2=ES(2)/T
     E0(1)=A1-6.0*ES(4)/T2
     E0(2)=A1+6.0*ES(4)/T2
     E0(3)=A2-6.0*ES(5)/T2
     E0(4)=A2+6.0*ES(5)/T2
     E0(5)=(R*RES(4,J)+T*0.5*RES(7,J))*A3
     E0(6)=(R*RES(4,J)-T*0.5*RES(7,J))*A3
     E0(7)=(R*RES(5,J)+T*0.5*RES(8,J))*A3
     E0(8)=(R*RES(5,J)-T*0.5*RES(8,J))*A3
C
     WRITE (7,312) (ES(K),K=1,6)
     WRITE (7,313) (E0(K),K=1,4)
     WRITE (7,314) (E0(K),K=5,8)
940  CONTINUE
C
310  FORMAT(//5X,'X =',E12.5,3X,'ANGLE =',F7.2,'DEG')
311  FORMAT(5X,'W =',E12.5,3X,'U =',E12.5,3X,'V =',E12.5)
312  FORMAT(4X,'NX=',E12.5,3X,'NPY=',E12.5,3X,'NXPY=',E12.5/
    &       4X,'MX=',E12.5,3X,'MPY=',E12.5,3X,'MXPY=',E12.5)
313  FORMAT(4X,'SXI=',E12.5,1X,'SXO=',E12.5,1X,'SPYI=',E12.5,
    & 1X,'SPYO=',E12.5)
314  FORMAT(4X,'EXO=',F8.2,3X,'EXI=',F8.2,3X,'EPYO=',F8.2,
    & 3X,'EPYI=',F8.2)
999  STOP
     END
C
     SUBROUTINE EN0(X,M,E0,Z0,P0,P02,LOAD,LOOP)
     IMPLICIT REAL*8 (A-H,O-Z)
     DIMENSION E0(10),Z0(6),P0(3),P02(3),LOAD(3)
     COMMON/BLK2/T3,T4,PI,RADIAN,T,R,XLEN,NCSYM
     C2=M*T4
     C3=C2*R
     C1=C3*C3
     C4=SIN(C2*X)
     C5=COS(C2*X)
     C45=C4/C5
     DO 10 J=1,3
     IF(LOAD(J).EQ.0) GOTO 10
     JU=J+1
     IF(J.EQ.2) JU=6
     JV=J+2
     C8=P0(J)*C4
     C9=-P02(J)*C5
     E0(1)=E0(1)+Z0(J)*C8
     E0(2)=E0(2)+Z0(JU)*C8/C45
     E0(3)=E0(3)+Z0(JV)*C9*C45
     IF(LOOP.EQ.3) GOTO 10
     E0(4)=E0(4)-C8*C3*Z0(JU)
     E0(5)=E0(5)+C8*Z0(J)
     E0(6)=E0(6)+C9*C3*Z0(JV)
     E0(7)=E0(7)+C8*C1*Z0(J)
     E0(9)=E0(9)+C9*0.75*C3*Z0(JV)
10   CONTINUE
     RETURN
     END
C
     SUBROUTINE ENN(X,PHI,M,N,ES,Z,P,P2,LOAD,LOOP)
     IMPLICIT REAL*8 (A-H,O-Z)
```

```
      DIMENSION ES(10),Z(6),P(3),P2(3),LOAD(3)
      COMMON/BLK2/T3,T4,PI,RADIAN,T,R,XLEN,NCSYM
      DO 5 I=1,9
5     ES(I)=0.0
      CNT=COS(N*PHI)
      SNT=SIN(N*PHI)
      A2=M*T4
      A3=A2*R
      A1=A3*A3
      A4=SIN(A2*X)
      A5=COS(A2*X)
      A45=A4/A5
      DO 10 J=1,3
      IF(LOAD(J).EQ.0) GOTO 10
      JU=J+1
      IF(J.EQ.2) JU=6
      JV=J+2
      A6=(P(J)*CNT+P2(J)*SNT)*A4
      A7=(P(J)*SNT-P2(J)*CNT)*A5
      ES(1)=ES(1)+Z(J)*A6
      ES(2)=ES(2)+Z(JU)*A6/A45
      ES(3)=ES(3)+Z(JV)*A7*A45
      IF(LOOP.EQ.3) GOTO 10
      ES(4)=ES(4)-A6*A3*Z(JU)
      ES(5)=ES(5)+A6*(N*Z(JV)+Z(J))
      ES(6)=ES(6)+A7*(A3*Z(JV)-N*Z(JU))
      ES(7)=ES(7)+A6*Z(J)*A1
      ES(8)=ES(8)+A6*(Z(J)*N*N+N*Z(JV))
      ES(9)=ES(9)+A7*(0.75*A3*Z(JV)+N*A3*Z(J)
     &+0.25*N*Z(JU))
10    CONTINUE
      RETURN
      END
C
      SUBROUTINE PJMN(M,N,NLOAD,CL)
      IMPLICIT REAL*8 (A-H,O-Z)
      DIMENSION P(3),P0(3),P2(3),P02(3),CL(60)
      COMMON/BLK2/T3,T4,PI,RADIAN,T,R,XLEN,NCSYM
      COMMON/BLK3/P,P0,P2,P02
      I1=(M+1)/2
      IF(M.LT.2*I1) I1=0
      DO 20 I=1,NLOAD
      J=(I-1)*6+1
      IC=CL(J)
      A1=CL(J+1)
      A2=CL(J+2)
      A3=CL(J+3)
      A4=CL(J+4)
      A5=CL(J+5)
      IF (IC.EQ.0.AND.I1.EQ.0) CALL SWP(P,P0,M,N,A1,A2,A3,A4)
      IF (IC.NE.0) CALL PATCH(IC,A1,A2,A3,A4,A5,M,N)
20    CONTINUE
      RETURN
      END
C
      SUBROUTINE SWP(P,P0,M,N,SWV,PRESS,SW,ALPHA)
      IMPLICIT REAL*8 (A-H,O-Z)
      DIMENSION P(3),P0(3)
      COMMON/BLK2/T3,T4,PI,RADIAN,T,R,XLEN,NCSYM
      ALPHA=ALPHA*RADIAN
      A1=SIN(ALPHA)
      A2=COS(ALPHA)
      A3=SW*R/(M*PI*PI)
      IF(N.GT.1) GOTO 20
      IF(N.EQ.1) GOTO 10
      P0(1)=4.0*PRESS/(M*PI)+4.0*A3*(A1-ALPHA*A2)
      RETURN
10    A5=4.0*T*SWV/(PI*M)
      P(1)=A5+4.0*A3*(ALPHA-A1*A2)
      P(3)=-A5
      RETURN
20    AN=8.0*(SIN(N*ALPHA)*A2-N*COS(N*ALPHA)*A1)/(N*(N*N-1))
      P(1)=AN*A3
      RETURN
      END
C
```

```
      SUBROUTINE PATCH(KTYPE,Q,B,AFA,CC,BETA1,M,N)
      IMPLICIT REAL*8 (A-H,O-Z)
      DIMENSION P(3),P0(3),P2(3),P02(3)
      COMMON/BLK2/T3,T4,PI,RADIAN,T,R,XLEN,NCSYM
      COMMON/BLK3/P,P0,P2,P02
      AFA=AFA*RADIAN
      BETA1=BETA1*RADIAN
      C=CC/2.0
      BETA=BETA1/2.0
      IC=0
      IF (NCSYM.EQ.1) IC=1
      A1=M*T4
      A2=A1*B
      A3=A1*C
      A4=M*PI
      GOTO (1,2,1,4,1) KTYPE
1     IF (CC.EQ.0.0) AM=2.0*SIN(A2)/XLEN
      IF (CC.GT.0.0) AM=4.0*SIN(A2)*SIN(A3)/A4
      GOTO 30
2      IF (CC.EQ.0.0) AM=2.0*COS(A2)/XLEN
      IF (CC.GT.0.0) AM=4.0*COS(A2)*SIN(A3)/A4
      GOTO 30
4                                    AM=(COS(A2)*(SIN(A3)/(A1*C)-
COS(A3))+SIN(A2)*SIN(A3))*2.0/A4
30    IF (N.EQ.0) GOTO 60
      A4=N*AFA
      IF (BETA1.EQ.0.0) THEN
      A5=Q/(R*PI)
      GOTO 50
      END IF
      A1=2.0*Q/(N*PI)
      A2=N*BETA
      A5=A1*SIN(A2)
      IF(KTYPE.EQ.5) A5=A5/2.0+A1*(COS(A2)-SIN(A2)/A2)
50    AN=A5*COS(A4)
      BN=A5*SIN(A4)
      GOTO(500,600,700,500,500),KTYPE
500   P(1)=P(1)+AM*AN
      P2(1)=P2(1)+IC*AM*BN
      RETURN
600   P(2)=P(2)+AM*AN
      P2(2)=P2(2)+IC*AM*BN
      RETURN
700   P(3)=P(3)+AM*BN
      P2(3)=P2(3)-IC*AM*AN
      RETURN
60    IF (BETA1.EQ.0.0) AN0=Q/(2.0*R*PI)
      IF (BETA1.GT.0.0) AN0=BETA*Q/PI
      IF(KTYPE.EQ.5) AN0=AN0/2.0
      GOTO(501,601,701,501,501),KTYPE
501   P0(1)=P0(1)+AM*AN0
      RETURN
601   P0(2)=P0(2)+AM*AN0
      RETURN
701   P02(3)=P02(3)-IC*AN0*AM
      RETURN
      END
C
C----------IMPERFECTIONS----------
C*****ONLY FOR SHAPE SYMMETRIC ABOUT CENTRE,(AXIAL SYMMETRY)
      SUBROUTINE FIMP(NSYM,IMP,XIMP,PBAR,P,P2,AN,BN,M,N)
      IMPLICIT REAL*8 (A-H,O-Z)
      DIMENSION XIMP(3),P(3),P2(3),AN(3,60),BN(3,60)
      COMMON/BLK2/T3,T4,PI,RADIAN,T,R,XLEN,NCSYM
      A1=2.0*NSYM/XLEN
      A2=M*T4
      DO 10 I=1,IMP
      A3=XIMP(I)
      IF(I.EQ.1) XC=A3/2.0
      IF(IMP.GT.1) XC=(A3-XIMP(I-1))/3.0
      IF(I.LT.IMP) XD=(XIMP(I+1)-A3)/3.0
      IF(I.EQ.IMP) XD=(XLEN-A3*NSYM)/(1.0+NSYM)
      AM=(SIN(A2*(A3-XC))-SIN(A2*(A3-2.0*XC)))/XC
      IF(XD.GT.0.0) AM=AM-(SIN(A2*(A3+2.0*XD))
     &-SIN(A2*(A3+XD)))/XD
      AM=AM*A1/(A2*A2)
```

```
      A2=-PBAR*((N*N-1)+(M*T3)**2/2.0)/R
      P(1)=P(1)+A2*AM*AN(I,N)
      P2(1)=P2(1)+A2*AM*BN(I,N)
10    CONTINUE
      RETURN
      END
C
      SUBROUTINE PQP(M,N,PQ,RAD)
      IMPLICIT REAL*8 (A-H,O-Z)
      DIMENSION PQ(120),RAD(120),P(3),P2(3),P0(3),P02(3)
      COMMON/BLK2/T3,T4,PI,RADIAN,T,R,XLEN,NCSYM
      COMMON/BLK3/P,P0,P2,P02
      COMMON/BLK4/SDIV,WIDTH,NTYPE,NK,NSIZE,XSAD
      CC=WIDTH/2.0
      BETA=SDIV/2.0
      IC=0
      IF(NCSYM.EQ.1) IC=1
      A1=M*T4
      AM=4.0*SIN(A1*XSAD)*SIN(A1*CC)/(M*PI)
      IF(N.NE.0) GOTO 4
      A2=2.0*BETA*NCSYM/PI
      IF(NTYPE.EQ.1) A2=NCSYM/(R*PI)
      AN0=0.0
      DO 1 I=1,NK
1     AN0=AN0-PQ(I)*A2
      IF(NTYPE.EQ.2) AN0=AN0-(PQ(NSIZE+1)+
     & IC*PQ(NSIZE+2))*NCSYM/(R*PI)
      P0(1)=P0(1)+AN0*AM
      IF (NK.EQ.NSIZE) RETURN
      AN0=0.0
      DO 2 I=NK+1,NSIZE
2     AN0=AN0-PQ(I)
      P02(3)=P02(3)-IC*AN0*A2*AM
      RETURN
4     AN=0.0
      BN=0.0
      A1=-4.0*NCSYM*SIN(N*BETA)/(N*PI)
      IF(NTYPE.EQ.1) A1=-2.0*NCSYM/(R*PI)
      DO 10 I=1,NK
      PHI=RAD(I)*N
      A4=PQ(I)*A1
      AN=AN+A4*COS(PHI)
10    BN=BN+A4*SIN(PHI)
      IF(NTYPE.EQ.2) THEN
       A2=-2.0*NCSYM/(R*PI)
       DO 5 II=1,1+IC
        I=II+NSIZE
        PHI=RAD(I)*N
        A4=PQ(I)*A2
       AN=AN+A4*COS(PHI)
5      BN=BN+A4*SIN(PHI)
      END IF
      P(1)=P(1)+AM*AN
      P2(1)=P2(1)+IC*AM*BN
      IF(NK.EQ.NSIZE) RETURN
      AN=0.0
      BN=0.0
      DO 40 I=NK+1,NSIZE
      PHI=RAD(I)*N
      A4=PQ(I)*A1
      AN=AN+A4*COS(PHI)
40    BN=BN+A4*SIN(PHI)
      P(3)=P(3)+AM*BN
      P2(3)=P2(3)-IC*AM*AN
      RETURN
      END
```

APPENDIX 4

Finite Element Listing - rigida.inp

1

```
C*** Modified file : Rigid Head
C*** - Change in postprocessing strip size
C*** - Head thickness (real,2) included
C*** - Change in mesh above saddle portion (nicer looking !?) -
MDV1 & MDV2
C***
C*** - (a) designator means valid A>0.4R
C***
/prep7
/nopr
C***
C*** 31/10/94      :::::
/TITLE,TWIN SADDLE VESSEL - Rigid Constrained Head using CERIG
C*** Fixed saddle angle of 60 degrees
C*** Length factor      LFAC
C*** Saddle position    AFAC
C*** Saddle Width       BFAC
c*** Thickness - shell   TKS
C*** Thickness - head    TKH
C*** DEFINE PARAMETERS
TKS=10
TKH=10
R=1000
ANG=60
LFAC=36
L=LFAC*R
AFAC=9
A=AFAC*R
BFAC=0.2
B=BFAC*R
B2=B/2
L2=L/2
L2A=L2-A
C*** Setup values
/show,3d,,1
/view,1
C*** MATERIAL VALUES and THICKNESSES 1) SHELL 2) HEAD
EX,1,210000
NUXY,1,0.3
R,1,TKS
R,2,TKH
C*** DEFINE KEYPOINTS
k,1,A                    ! kpoint 1 is at saddle centreline (sadcl)
k,2,(A-B2)               ! kpoint 2 is at (sadcl) minus half saddle
width
k,3,(A-(1.5*B2))         ! kpoint 3 is at (sadcl) minus 1.5*half
saddle width
k,4,(A-B)                ! kpoint 4 is at (sadcl) minus saddle
width
k,5,(A-(3*B2))           ! kpoint 5 is at (sadcl) minus 3*half
saddle width
C*** Note if A is less than 0.4*R this file will not work
C*** if A has to be less than 0.4R then modify positions of k3,4
and 5
C*** if 2nd set is used...watch out for line shift half way down
file
c*** at negative Z coord of K,5
c***
C***
C*** To find the right line , do a search on Watch
C***
c*** k,3,(A-(1.2*B2))
c*** k,4,(A-(1.5*B2))
c*** k,5,(A-(1.75*B2))
C*** Using co-ord system :
local,11,1,,R,,,90
csys,11
dsys,11
kgen,2,1,2,1,,2
a,1,2,7,6
C*** Generate areas 1t14 of saddle:
agen,14,1,1,1,,2
kmerge
C*** Continue with saddle.  Transitional area of saddle:
kgen,2,59,,,,2,(0.5*B2)
kgen,2,58,59,1,,2
```

```
a,58,8,59,59
a,58,9,8,8
a,59,8,12,12
C***  a15t17 form trans'n in saddle (= patch 15)
kgen,2,8,9,1,,2
kgen,2,12,,,,2
a,8,9,16,13
a,12,8,13,17
C***  a18+19 = PATCH 16 of saddle
agen,15,18,19,1,,2
kmerge
C***  a1t47 form saddle
C***  Start on 1st trans'n band :
kgen,2,3,,,,4
a,2,3,20,7
a,7,20,10,10
C***  a48+49 = Trans'n of Patch 1+2 of saddle
agen,15,48,49,1,,4
kmerge
C***  a48t77 form  1st trans'l band from saddle
C***  Start 2nd trans'l band
kgen,2,4,,,,8
a,3,4,21,20
a,20,21,32,32
C***  a78+79 start of sequence
agen,7,78,79,1,,8
kmerge
kgen,2,112,,,,4
a,118,112,32,150
C***  a92 regular in 2nd trans'l band , a78t92 form 2nd TB
C***  Start on 3rd TB
kgen,2,5,,,,16
a,4,5,33,21
a,21,33,40,40
C***  a93+94 start sequence of 3rd TB
agen,3,93,94,1,,16
kmerge
kgen,2,82,,,,12
a,86,82,52,112
a,112,52,32,32
C***  a99+100 irregular from others in 3rd TB , a93t100 form 3rd
TB
C***   END OF SADDLE + TRANSITION BANDS
C***  Up to 90 deg. ( including another saddle transition)
kgen,2,123,150,27,,20
kgen,2,120,121,1,,20
kgen,2,32,52,20,,20
a,123,121,74,56
a,121,120,71,74
a,120,150,65,71
a,150,32,76,65
a,32,52,88,76
kgen,2,56,71,15,,10
kgen,2,65,76,11,,10
kgen,2,88,,,,10
C***  Transition
a,56,74,94,94
a,74,95,94,94
a,74,71,95,95
a,71,65,98,95
a,65,76,100,98
a,76,88,106,100
C***  a101t111 form upto 90 deg.
C***  change that
adel,109,111
ldel,224,229
a,71,65,95,95
a,65,76,100,95
a,76,88,106,100
kdel,98
C***  upper 90 deg segment ( above saddle+TB's)
kgen,2,94,95,1,,30
kgen,2,100,106,6,,30
a,94,95,107,98
a,95,100,110,107
a,100,106,116,110
```

```
agen,3,112,114,1,,30
kmerge
C***  Refine region above saddle horn grid
MDV1=4
MDV2=2
ldvs,219,,MDV1
ldvs,220,,MDV1
ldvs,221,,MDV1
ldvs,223,,MDV1
ldvs,224,,MDV1
ldvs,225,,MDV1
ldvs,227,,MDV2
C***  Upper 90 deg complete
C***  a1t120 form 180 deg segment (saddle + TB + remainer)
local,12,0,A,0,0
arsym,0,1,120
kmerge
C***  Generate areas to head
csys,11
C***
C*** Select negative Z coord of K,5          ! Here for -ve Z of
K,5
C***
C***  Watch
C***
C***
kprsel,z,-(A-(3*B2))
lskp,1
kgen,2,5,5,1,,,(A-(3*B2))
1,5,119
adrag,143,168,192,162,217,227,246
adrag,234,244,254,,,,246
kmerge
kpall
lsall
C*** Areas to centre of vessel from saddle portion:
kprsel,z,0
lskp,1
lgen,2,all,,,,,-L2
kpas,,234
1,128,234
adrag,256,298,333,338,343,348,368
adrag,353,358,363,,,,368
kpall
lsall
kmerge
dsys,0
C***     Start meshing
et,1,43
real,1
C***     Start at saddle
ldvs,1,,2
elsi,,1,2
amesh,1,14
elsi,,2,2
amesh,18,19
elsi,,1,1
amesh,15,17
elsi,,2,2
amesh,20,47,1
C***    1st Trans'n band from saddle
REF1=4
ldvs,49,,REF1/2
ldvs,69,,REF1/2
ldvs,169,,REF1/2
elsiz,,REF1/2
amesh,48,63,1
elsize,,REF1,2
amesh,64,76,2
elsiz,,REF1
amesh,65,77,2
C***     2nd Trans'n band
REF2=4
ldvs,170,,REF2
elsiz,,REF2/2
amesh,79,85,2
```

```
elsiz,,REF2/2,2
amesh,78,84,2
elsi,,REF2
amesh,87,91,2
elsi,,REF2,2
amesh,86,92,2
C***    3rd Trans'n band
C*** WREF is the transition region at areas 93t100 width
refinement
WREF=4
elsi,,WREF,2
amesh,93,95,2
elsi,,WREF
amesh,94,96,2
amesh,98,100,2
elsi,,WREF,2
amesh,97,99,2
C***    Mesh remainder up to head :: Angle refinement AREF must
be divisible by 4
AREF=20
ldvs,207,,AREF,0.2
ldvs,186,,AREF,5
ldvs,210,,AREF,5
ldvs,213,,AREF,5
ldvs,215,,AREF,5
ldvs,226,,2
ldvs,222,,2
ldvs,217,,(AREF/4)
elsi,,2,2
amesh,101,104
elsiz,,2
amesh,105
elsi,,1
amesh,106,111,1
elsi,,2,2
amesh,112,120,1
lsrs,,246
lsas,,259,274,3
lsas,,303,313,5
ldvs,all,,((4*AFAC)+2),2.5
elsi,,2,2
amesh,241,249,1
kpall
lsall
arall
nall
eall
ncompre
ecompre
merge
local,12,0,A,0,0
adel,121,240,1,all
arsym,0,1,120
merge
kmerge
csys,11
lsrs,,368
lsas,,459,469,10
lsas,,480,494,7
lsas,,499
lsas,,507,509
ldvs,all,,(40-(2*AFAC)),0.1
elsize,,2,2
amesh,250,258,1
kpall
lsall
arall
merge
ncompr
ecompr
C***
c*** Rigid End Constraints for Comparsion with Fourier Model
csys,0
c*** Define Mass Element at Centre of Disc
n,10000,,R
et,2,21
```

```
r,3,1
type,2
real,3
e,10000
nrsel,x,0
c*** Define Rigid Surface Constraints
cerig,10000,all,0
nall
C*** Loads & BC's from loadline.f18
C*** Add in bits to complete run
csys,0
nusel,x,0
csys,11
nrotat,all
symbc,11,3,-L2
symbc,11,2,90
symbc,11,2,-90
csys,0
nall
C*** Displacement constraints - Please select
C*** Select edges only
C*** Left Hand Edge
lsrsel,,2,54,4
lsasel,,13,29,16
lsasel,,53,63,10
lsasel,,70,147,7
C*** Add in Top Edge
lsasel,,148,151,3
lsasel,,370,372,2
C*** Add in Right Hand Edge
lsasel,,240,250,10
lsasel,,257,290,3
lsasel,,295,299,4
lsasel,,304,369,5
C*** Optional Centreline
c*** lsasel,,4,56,4
c*** lsasel,,25,45,20
c*** lsasel,,61,152,7
```

```
C*** Now get nodes from lines
nline,1
d,all,all,0
nall
lsall
C*** Add in load option
apsf,all,,,0,2,R*2,9.81E-6
wsort,x
AFWRIT
FINI
/INPUT,27
FINI
```

APPENDIX 5

Finite Element Listing - rigidb.inp

1

```
C*** Modified file : Rigid Head
C*** - Change in postprocessing strip size
C*** - Head thickness (real,2) included
C*** - Change in mesh above saddle portion (nicer looking !?) -
MDV1 & MDV2
C***
C*** - (b) designator means valid A<0.4R
C***
/PREP7
/nopr
C***
C*** 31/10/94     :::::
/TITLE,TWIN SADDLE VESSEL - Rigid Constrained Head using CERIG
C*** Fixed saddle angle of 60 degrees
C*** Length factor      LFAC
C*** Saddle position    AFAC
C*** Saddle Width       BFAC
C*** Thickness - shell  TKS
C*** Thickness - head   TKH
C*** DEFINE PARAMETERS
TKS=10
TKH=10
R=1000
ANG=60
LFAC=36
L=LFAC*R
AFAC=9
A=AFAC*R
BFAC=0.2
B=BFAC*R
B2=B/2
L2=L/2
L2A=L2-A
C*** Setup values
/show,3d,,1
/view,1
C*** MATERIAL VALUES and THICKNESSES 1) SHELL 2) HEAD
EX,1,210000
NUXY,1,0.3
R,1,TKS
R,2,TKH
C*** DEFINE KEYPOINTS
k,1,A                    ! kpoint 1 is at saddle centreline (sadcl)
k,2,(A-B2)               ! kpoint 2 is at (sadcl) minus half saddle
width
c***k,3,(A-(1.5*B2))          ! kpoint 3 is at (sadcl) minus
1.5*half saddle width
c***k,4,(A-B)                 ! kpoint 4 is at (sadcl) minus saddle
width
C***k,5,(A-(3*B2))            ! kpoint 5 is at (sadcl) minus 3*half
saddle width
C*** Note if A is less than 0.4*R this file will not work
C*** if A has to be less than 0.4R then modify positions of k3,4
and 5
C*** if 2nd set is used...watch out for line shift half way down
file
c*** at negative Z coord of K,5
C***
C*** Do a search on Watch
C***
k,3,(A-(1.2*B2))
k,4,(A-(1.5*B2))
k,5,(A-(1.75*B2))
C*** Using co-ord system :
local,11,1,,R,,,90
csys,11
dsys,11
kgen,2,1,2,1,,2
a,1,2,7,6
C*** Generate areas 1t14 of saddle:
agen,14,1,1,1,,2
kmerge
C*** Continue with saddle.  Transitional area of saddle:
kgen,2,59,,,,2,(0.5*B2)
kgen,2,58,59,1,,2
a,58,8,59,59
```

```
a,58,9,8,8
a,59,8,12,12
C***  a15t17 form trans'n in saddle (= patch 15)
kgen,2,8,9,1,,2
kgen,2,12,,,,2
a,8,9,16,13
a,12,8,13,17
C***  a18+19 = PATCH 16 of saddle
agen,15,18,19,1,,2
kmerge
C***  a1t47 form saddle
C***  Start on 1st trans'n band :
kgen,2,3,,,,4
a,2,3,20,7
a,7,20,10,10
C***  a48+49 = Trans'n of Patch 1+2 of saddle
agen,15,48,49,1,,4
kmerge
C***  a48t77 form  1st trans'l band from saddle
C***  Start 2nd trans'l band
kgen,2,4,,,,8
a,3,4,21,20
a,20,21,32,32
C***  a78+79 start of sequence
agen,7,78,79,1,,8
kmerge
kgen,2,112,,,,4
a,118,112,32,150
C***  a92 regular in 2nd trans'l band , a78t92 form 2nd TB
C***  Start on 3rd TB
kgen,2,5,,,,16
a,4,5,33,21
a,21,33,40,40
C***  a93+94 start sequence of 3rd TB
agen,3,93,94,1,,16
kmerge
kgen,2,82,,,,12
a,86,82,52,112
a,112,52,32,32
C***  a99+100 irregular from others in 3rd TB , a93t100 form 3rd
TB
C***   END OF SADDLE + TRANSITION BANDS
C***  Up to 90 deg. ( including another saddle transition)
kgen,2,123,150,27,,20
kgen,2,120,121,1,,20
kgen,2,32,52,20,,20
a,123,121,74,56
a,121,120,71,74
a,120,150,65,71
a,150,32,76,65
a,32,52,88,76
kgen,2,56,71,15,,10
kgen,2,65,76,11,,10
kgen,2,88,,,,10
C***  Transition
a,56,74,94,94
a,74,95,94,94
a,74,71,95,95
a,71,65,98,95
a,65,76,100,98
a,76,88,106,100
C***  a101t111 form upto 90 deg.
C***  change that
adel,109,111
ldel,224,229
a,71,65,95,95
a,65,76,100,95
a,76,88,106,100
kdel,98
C***  upper 90 deg segment ( above saddle+TB's)
kgen,2,94,95,1,,30
kgen,2,100,106,6,,30
a,94,95,107,98
a,95,100,110,107
a,100,106,116,110
agen,3,112,114,1,,30
```

```
kmerge
C***  Refine region above saddle horn grid
MDV1=4
MDV2=2
ldvs,219,,MDV1
ldvs,220,,MDV1
ldvs,221,,MDV1
ldvs,223,,MDV1
ldvs,224,,MDV1
ldvs,225,,MDV1
ldvs,227,,MDV2
C***  Upper 90 deg complete
C***  alt120 form 180 deg segment (saddle + TB + remainer)
local,12,0,A,0,0
arsym,0,1,120
kmerge
C***  Generate areas to head
csys,11
C***
C*** Select negative Z coord of K,5          ! Here for -ve Z of
K,5
C***
C***  Watch
C***
C***
kprsel,z,-(A-(3*B2))
lskp,1
kgen,2,5,5,1,,,(A-(3*B2))
l,5,119
adrag,143,168,192,162,217,227,246
adrag,234,244,254,,,,246
kmerge
kpall
lsall
C*** Areas to centre of vessel from saddle portion:
kprsel,z,0
lskp,1
lgen,2,all,,,,,-L2
kpas,,234
l,128,234
adrag,256,298,333,338,343,348,368
adrag,353,358,363,,,,368
kpall
lsall
kmerge
dsys,0
C***      Start meshing
et,1,43
real,1
C***      Start at saddle
ldvs,1,,2
elsi,,1,2
amesh,1,14
elsi,,2,2
amesh,18,19
elsi,,1,1
amesh,15,17
elsi,,2,2
amesh,20,47,1
C***    1st Trans'n band from saddle
REF1=4
ldvs,49,,REF1/2
ldvs,69,,REF1/2
ldvs,169,,REF1/2
elsiz,,REF1/2
amesh,48,63,1
elsize,,REF1,2
amesh,64,76,2
elsiz,,REF1
amesh,65,77,2
C***      2nd Trans'n band
REF2=4
ldvs,170,,REF2
elsiz,,REF2/2
amesh,79,85,2
elsiz,,REF2/2,2
```

```
amesh,78,84,2
elsi,,REF2
amesh,87,91,2
elsi,,REF2,2
amesh,86,92,2
C***    3rd Trans'n band
C***  WREF  is  the  transition  region  at  areas  93t100  width
refinement
WREF=4
elsi,,WREF,2
amesh,93,95,2
elsi,,WREF
amesh,94,96,2
amesh,98,100,2
elsi,,WREF,2
amesh,97,99,2
C***    Mesh remainder up to head :: Angle refinement AREF must
be divisible by 4
AREF=20
ldvs,207,,AREF,0.2
ldvs,186,,AREF,5
ldvs,210,,AREF,5
ldvs,213,,AREF,5
ldvs,215,,AREF,5
ldvs,226,,2
ldvs,222,,2
ldvs,217,,(AREF/4)
elsi,,2,2
amesh,101,104
elsiz,,2
amesh,105
elsi,,1
amesh,106,111,1
elsi,,2,2
amesh,112,120,1
lsrs,,246
lsas,,259,274,3
lsas,,303,313,5
ldvs,all,,((4*AFAC)+2),2.5
elsi,,2,2
amesh,241,249,1
kpall
lsall
arall
nall
eall
ncompre
ecompre
merge
local,12,0,A,0,0
adel,121,240,1,all
arsym,0,1,120
merge
kmerge
csys,11
lsrs,,368
lsas,,459,469,10
lsas,,480,494,7
lsas,,499
lsas,,507,509
ldvs,all,,(40-(2*AFAC)),0.1
elsize,,2,2
amesh,250,258,1
kpall
lsall
arall
merge
ncompr
ecompr
C***
c*** Rigid End Constraints for Comparsion with Fourier Model
csys,0
c*** Define Mass Element at Centre of Disc
n,10000,,R
et,2,21
r,3,1
```

```
type,2
real,3
e,10000
nrsel,x,0
c*** Define Rigid Surface Constraints
cerig,10000,all,0
nall
C*** Loads & BC's from loadline.f18
C*** Add in bits to complete run
csys,0
nusel,x,0
csys,11
nrotat,all
symbc,11,3,-L2
symbc,11,2,90
symbc,11,2,-90
csys,0
nall
C*** Displacement constraints - Please select
C*** Select edges only
C*** Left Hand Edge
lsrsel,,2,54,4
lsasel,,13,29,16
lsasel,,53,63,10
lsasel,,70,147,7
C*** Add in Top Edge
lsasel,,148,151,3
lsasel,,370,372,2
C*** Add in Right Hand Edge
lsasel,,240,250,10
lsasel,,257,290,3
lsasel,,295,299,4
lsasel,,304,369,5
C*** Optional Centreline
c*** lsasel,,4,56,4
c*** lsasel,,25,45,20
c*** lsasel,,61,152,7
C*** Now get nodes from lines
nline,1
d,all,all,0
nall
lsall
C*** Add in load option
apsf,all,,,0,2,R*2,9.81E-6
wsort,x
AFWRIT
FINI
/INPUT,27
FINI
```

APPENDIX 6

File - Various End Types - ***capell.f18; capsph.f18; capflat.f18***

File - capell.f18

```
C*** - C*** ellipsoidal head 2:1
C*** This file must follow cyl.f18
FAC=0.5
csys,11
k,500
csys,0
local,21,1,,R,,,,,2
csys,11
k,501,,,R*FAC
csys,21
l,154,501
ldiv,373,0.85
ldvs,373,,12
ldvs,500,,4
csys,0
arot,373,500,,,,,500,501,-30
arot,503,504,,,,,500,501,-30
arot,510,511,,,,,500,501,-30
arot,514,515,,,,,500,501,-10
arot,518,519,,,,,500,501,-20
arot,522,523,,,,,500,501,-12
arot,526,527,,,,,500,501,-16
arot,530,531,,,,,500,501,-16
arot,534,535,,,,,500,501,-16
kmerge
elsiz,,2
amesh,259,264
elsiz,,2,2
amesh,265,275,2
elsiz,,2
amesh,266,276,2
```

File - capsph.f18

```
C*** spherical head
C*** This file must follow cyl.f18
FAC=1
csys,11
k,500
csys,0
local,21,1,,R
csys,11
k,501,,,R*FAC
csys,21
l,154,501
ldiv,373,0.85
ldvs,373,,12
ldvs,500,,4
csys,0
arot,373,500,,,,,500,501,-30
arot,503,504,,,,,500,501,-30
arot,510,511,,,,,500,501,-30
arot,514,515,,,,,500,501,-10
arot,518,519,,,,,500,501,-20
arot,522,523,,,,,500,501,-12
arot,526,527,,,,,500,501,-16
arot,530,531,,,,,500,501,-16
arot,534,535,,,,,500,501,-16
kmerge
elsiz,,2
amesh,259,264
elsiz,,2,2
amesh,265,275,2
elsiz,,2
amesh,266,276,2
```

File - capflat.f18

```
C***  flat head
csys,11
k,500,,,-1
k,501
l,154,501
ldiv,373,0.85
ldvs,373,,12
ldvs,500,,4
csys,0
arot,373,500,,,,,500,501,-30
arot,503,504,,,,,500,501,-30
arot,510,511,,,,,500,501,-30
arot,514,515,,,,,500,501,-10
arot,518,519,,,,,500,501,-20
arot,522,523,,,,,500,501,-12
arot,526,527,,,,,500,501,-16
arot,530,531,,,,,500,501,-16
arot,534,535,,,,,500,501,-16
kmerge
C*** Element thickness is real 2
real,2
elsiz,,2
amesh,259,264
elsiz,,2,2
amesh,265,275,2
elsiz,,2
amesh,266,276,2
```

APPENDIX 7

File - pcinput

```
 600 200
 1 2 2 0

  0.18290E+04  0.20700E+06     0.300  2.66300E+01  0.54858E+05
  1
0  0.00000E+00  0.00000E+00  0.98100E-05  180.000  0.00000E+00
 0.68580E+04  79.00000E+00  0.68580E+04  81.000E+0  0.100E+00
 0.68580E+04  162.000     0.000  0.76200E+03  2

70 70 70
  0   0
```

Bourne shell control file - run

```
#!/bin/sh

 echo "R/t ratio 25 to 300, Position 18R to 2R " > Resultsfile
 for j in `cat Thickness`
  do
  for i in `cat Middle`
   do
   echo " test " > PCINPUT
   echo " 600 200 " >> PCINPUT
   echo " 1 2 2 0 " >> PCINPUT
   echo " " >> PCINPUT
   echo "  0.10000E+04  0.20700E+06     0.300  $j   $i" >> PCINPUT
   echo "  1 ">> PCINPUT
   echo " 0  0.00000E+00  0.00000E+00  0.98100E-05  180.000  0.00000E+00 " >> PCINPUT
   echo "  9000.0  59.0000 9000.0  61.0000  0.100E+00 " >> PCINPUT
   echo "  9000.0  120     0.000  200.00  2 " >> PCINPUT
   echo " " >> PCINPUT
   echo " 50 50 50 " >> PCINPUT
   echo "   0   0 " >> PCINPUT

   cp PCINPUT INPUTend$j$i

   cyl1
   sad
   cyl2
   small
   cp PCOUT OUTPUTend$j$i
   cp PCSORT SORTend$j$i
    for k in `cat PCSMALL`
     do
      echo " $k " >> Resultsfile
     done
  done
done
```

Program - small.f

```
program small to find the minimum value for the horn outside circ. stress
      open(20,file='PCSORT',status='old')
      smallest=1000000
10    read(20,*,end=90) value
      if (value.lt.smallest) smallest=value
goto 10
90    close(20)
      open(21,file='PCSMALL',status='unknown')
      write(21,*) smallest
      close(21)
      end
```

APPENDIX 8

File - VariousFlexible Saddle Types: normal, semi_rig, stwothick, semi_rig.sol, solid.rig

File - normal

```
/COM,*****************************
/COM,******THE PARAMETERS********
/COM,*****************************
/UNITS,SI
*AFUN,DEG

/COM,***GEOMETRICAL PARAMETERS TO BE MODIFIED***
*AFUN,DEG

NW=3                        ! Number of divisions across the saddle
width !
NA=10                         ! Number of divisions across the half
saddle angle !
C=0.1                       ! Half saddle width !
B=0.1                             ! Height at center of the saddle
(theta=0) !
THETA=60                    ! Half saddle angle !
RADIUS=1                    ! Radius of the saddle !
BETA=10                           ! Incline angle of the first web
(external web) !
CWEB=1                      ! Do you want to put a web in the middle
(y=1 or n=0) !
EXTWEB=1                       ! Do you want to put an external web
(y=1 or n=0) !
NWEB=3                           ! Total number of webs without the
middle web !
T=1*C/NW                    ! Width of the cylindrical part which is
not webed !
                            ! T=i*C/NW with i=0 to NW-1 !
THETA2=2*THETA/2/NA         ! Saddle angle of not webed part !
                            !  THETA2=i*THETA/2/NA  with  i=0  to  NA-
NWEB-1 !
ELNUM3=NA/3
THICYL=0.012
THIWEB=0.006
THICPRIN=0.006

/COM,***CALCULATED PARAMETERS***

THETA1=THETA-THETA2
CC=2*C/NW
ELNUM1=NW-T*NW/C
ELNUM4=T*NW/C
ELNUM5=THETA2/THETA*2*NA
TOLY=THETA/8/NA
TOLZ=CC/8
X=C-T
NDIV=2*NA-THETA2*2*NA/THETA
ALPHA=THETA/NA/2
L=RADIUS*SIN(THETA1)
H1=B-RADIUS*(SIN(90-THETA1)-1)
LBASE=L-H1*TAN(BETA)

/COM,***MATERIAL PROPERTIES TO BE MODIFIED***

EXX=210E9
NU=.3

/COM,*************************
/COM,***THE SADDLE BUILDING***
/COM,*************************

/COM,***ELEMENT TYPE AND MATERIAL PROPERTIES DEFINITION***

/PREP7
/VIEW,,1,1,1
ET,1,93
MP,EX,1,EXX
MP,NUXY,1,NU
R,1,THICYL
R,2,THIWEB
R,3,THICPRIN
```

```
R,4,THIWEB/2

/COM,***CYLINDRICAL PART MODELING***

CSYS,1
K,1
K,2,,,C
K,3,RADIUS,-90,0
K,6,RADIUS,-90,X
L,3,6
AROTAT,1,,,,,,1,2,-ALPHA
AGEN,NDIV,1,,,,-ALPHA

/COM,***SADDLE ETREMITY STIFFENER***

CSYS,0
K,1001,-LBASE,-(RADIUS+B),X
K,1002,-LBASE,-(RADIUS+B),0
A,4*NDIV,4*NDIV+1,1001,1002

/COM,***OTHER STIFFENERS***

*DO,I,1,NWEB-1,1
DIST=(NWEB-I)*LBASE/NWEB
AS=ASIN(DIST/RADIUS)
NI=NINT(AS/ALPHA)
KI=4*NI+3
*GET,XK,KP,KI,LOC,X
*GET,YK,KP,KI,LOC,Y
K,1001+10*I,XK,-(RADIUS+B),X
K,1002+10*I,XK,-(RADIUS+B),0
A,KI,KI+3,1001+10*I,1002+10*I
*ENDDO

/COM,***MIDDLE STIFFENER***

K,1001+NWEB*10,0,-(RADIUS+B),X
K,1002+NWEB*10,0,-(RADIUS+B),0
A,3,6,1001+NWEB*10,1002+NWEB*10

/COM,***BASE***

*DO,I,0,NWEB-1,1
A,1002+I*10,1001+I*10,1011+I*10,1012+I*10
*ENDDO

/COM,***CENTRAL WEB***

KJ=4*NDIV
*DO,I,1,NWEB,1
DIST=(NWEB-I)*LBASE/NWEB
AS=ASIN(DIST/RADIUS)
NI=NINT(AS/ALPHA)
KI=4*NI+3
LARC,KJ,KI,1,RADIUS
AL,4*NDIV+3*(NWEB+1)+2*NWEB+I,4*NDIV+3*I,4*NDIV+3*NWEB+3+2*I,4*N
DIV+3*(I+1)
KJ=KI
*ENDDO

/COM,***BENDING PART ACROSS THE WIDTH***

*IF,C,GT,X,THEN
CSYS,1
K,2000,RADIUS,-90,C
L,6,2000
AROTAT,4*(NDIV+1)+6*NWEB,,,,,,1,2,-ALPHA
AGEN,NDIV,NDIV+3*NWEB+2,,,,-ALPHA
*ENDIF

/COM,***BENDING PART ACROSS THE SADDLE ANGLE***

*IF,THETA2,GT,0,THEN
AROTAT,4*NDIV-2,,,,,,1,2,-THETA2
*IF,C,GT,X,THEN
AROTAT,8*NDIV+6*NWEB+1,,,,,,1,2,-THETA2
```

```
*ENDIF
*ENDIF
NUMMRG,KP

/COM,***NUMBER OF DIVISIONS ON THE CYLIDRICAL PART LINES***

CSYS,1
LSEL,S,LOC,X,RADIUS
LSEL,R,LOC,Z,0,X
LSEL,U,LOC,Z,0
LSEL,U,LOC,Z,X
LESIZE,ALL,,,ELNUM1

LSEL,S,LOC,Z,C
LSEL,A,LOC,Z,X
LSEL,A,LOC,Z,0
LSEL,R,LOC,X,RADIUS
LSEL,U,LOC,Y,-(90+THETA1),-(90+THETA)
LESIZE,ALL,,,1

LSEL,S,LOC,X,RADIUS
LSEL,R,LOC,Z,X,C
LSEL,U,LOC,Z,C
LSEL,U,LOC,Z,X
LESIZE,ALL,,,ELNUM4

LSEL,S,LOC,Z,C
LSEL,A,LOC,Z,X
LSEL,A,LOC,Z,0
LSEL,R,LOC,X,RADIUS
LSEL,R,LOC,Y,-(90+THETA1),-(90+THETA)
LESIZE,ALL,,,ELNUM5

/COM,***NUMBER OF DIVISIONS ON STIFFENERS AND CENTRAL WEB
LINES***

ALLSEL
*DO,I,0,NWEB,1
LESIZE,4*NDIV+3*I+3,,,ELNUM3
*ENDDO

*IF,CWEB,EQ,0,THEN
K=NWEB-1
*ELSEIF,CWEB,EQ,1
K=NWEB
*ENDIF

*DO,I,0,K,1
LESIZE,4*NDIV+3*I+1,,,ELNUM3
LESIZE,4*NDIV+3*I+2,,,ELNUM1
*ENDDO

NIPREC=NDIV
*DO,I,1,NWEB,1
DIST=(NWEB-I)*LBASE/NWEB
AS=ASIN(DIST/RADIUS)
NI=NINT(AS/ALPHA)
NII=NIPREC-NI
LESIZE,4*NDIV+5*NWEB+3+I,,,NII
LESIZE,4*NDIV+3*(NWEB+1)+2*I-1,,,NII
LESIZE,4*NDIV+3*(NWEB+1)+2*I,,,NII
NIPREC=NI
ENDDO
ALLSEL

/COM,*****************
/COM,***THE MESHING***
/COM,*****************

TYPE,1
REAL,1
*DO,I,1,NDIV,1
AMESH,I
*IF,C,GT,X,THEN
AMESH,NDIV+3*NWEB+1+I
*ENDIF
```

```
*ENDDO
*IF,C,GT,X,THEN
AMESH,2*NDIV+3*NWEB+2
AMESH,2*NDIV+3*NWEB+3
*ELSE
AMESH,NDIV+3*NWEB+2
*ENDIF

ESHAPE,2
REAL,2
*IF,EXTWEB,EQ,1,THEN
AMESH,NDIV+1
*ENDIF
*IF,NWEB,GT,1,THEN
AMESH,NDIV+2,NDIV+NWEB,1
*ENDIF

*IF,CWEB,EQ,1,THEN
REAL,4
AMESH,NDIV+NWEB+1
*ENDIF

REAL,3
AMESH,NDIV+2*NWEB+2,NDIV+3*NWEB+1,1

NUMMRG,ELEM

ADELE,NDIV+NWEB+2,NDIV+2*NWEB+1,1
*DO,I,1,NWEB,1
LDELE,4*NDIV+3*NWEB+2+2*I
*ENDDO

*IF,CWEB,EQ,0,THEN
ADELE,NDIV+NWEB+1
LDELE,4*NDIV+3*NWEB+1,4*NDIV+3*NWEB+2,1
*ENDIF

*IF,EXTWEB,EQ,0,THEN
ADELE,NDIV+1
LDELE,4*NDIV+1,4*NDIV+2,1
*ENDIF

NUMMRG,NODE

ASEL,S,LOC,Z,0,0
ASEL,INVE
CSYS,0
ARSYM,Z,ALL,,,,0,0

NUMMRG,NODE

CSYS,1
NSEL,S,LOC,X,RADIUS
NROTAT,ALL
ALLSEL

FINISH

/COM,******************
/COM,***THE SOLUTION***
/COM,******************

/SOLU
ANTYPE,STAT

CSYS,0
NSEL,S,LOC,Y,-(RADIUS+B)
D,ALL,ALL

CSYS,0
NSEL,S,LOC,X,0
DSYM,SYMM,X,0

*CFOPEN,disp110,nor
*DO,I,1,NW,1
*DO,JJ,0,NA-1,1
```

```
J=NA-1-JJ

/SOLU
ANTYPE,STAT

CSYS,1
SFEDELE,ALL,,PRES
NSEL,S,LOC,X,RADIUS
NSEL,R,LOC,Z,C-(I-1)*CC+TOLZ,C-I*CC-TOLZ
NSEL,R,LOC,Y,-(90+THETA)+J*2*ALPHA-TOLY,-
(90+THETA)+(J+1)*2*ALPHA+TOLY
ESLN,R,1
SFE,ALL,,PRES,,-1
ALLSEL

!SOLVE
FINISH

/POST1
SET,LAST
RSYS,1
*DO,II,1,NW,1
*DO,KK,1,2*NA-1,2
K=2*NA-KK
NSEL,S,LOC,X,RADIUS
NSEL,R,LOC,Z,C-(2*II-1)*CC/2,C-(2*II-1)*CC/2
NSEL,R,LOC,Y,-(90+THETA)+K*ALPHA,-(90+THETA)+K*ALPHA
NSORT,UY
*GET,DISP,MAX
*VWRITE,DISP
(E13.6)
NSEL,ALL
*ENDDO
*ENDDO
ALLSEL

FINISH
*ENDDO
*ENDDO
*CFCLOSE
/EXIT
```

File - semi_rig

```
/BATCH
/UNITS,SI

/COM,***GEOMETRICAL PARAMETERS***
*AFUN,DEG

NW=3                          ! Number of divisions across the saddle
width !
NA=10                           ! Number of divisions across the half
saddle angle !
C=0.1                         ! Half saddle width !
B=0.1                               ! Height at center of the saddle
(theta=0) !
THETA=60                      ! Half saddle angle !
RADIUS=1                      ! Radius of the saddle !
CWEB=0                        ! Do you want to put a web in the middle
(y=1 or n=0) !
LEXTWEB=0.05
EXTWEB=1                         ! Do you want to put an external web
(y=1 or n=0) !
NWEB=3                             ! Total number of webs without the
middle web !
T=1*C/NW                      ! Width of the cylindrical part which is
not webed !
                              ! T=i*C/NW with i=0 to NW-1 !
THETA2=2*THETA/2/NA           ! Saddle angle of not webed part !
                              !  THETA2=i*THETA/2/NA with  i=0  to  NA-
NWEB-1 !
ELNUM2=1
ELNUM3=4
THICYL=0.012
```

```
THIWEB=0.006
THICPRIN=0.006


THETA1=THETA-THETA2
CC=2*C/NW
ELNUM1=NW-T*NW/C
ELNUM4=T*NW/C
ELNUM5=THETA2/THETA*2*NA
TOLY=THETA/8/NA
TOLZ=CC/8
X=C-T
NDIV=2*NA-THETA2*2*NA/THETA
ALPHA=THETA/NA/2
L=RADIUS*SIN(THETA1)
LBASE=L+LEXTWEB
R=LEXTWEB/(1-COS(THETA1))
XO=-(L-R*COS(THETA1))
YO=-(RADIUS*COS(THETA1)+R*SIN(THETA1))


S=2*ASIN((C-X)/(2*RADIUS))
SYL=THETA2-S


/COM,***MATERIAL PARAMETERS***
EXX=210E9
NU=.3


/COM,***BUILD THE MODEL***

/VIEW,,1,1,1
/PREP7
/SHOW,X11
ET,1,93
MP,EX,1,EXX
MP,NUXY,1,NU
```

```
R,1,THICYL
R,2,THIWEB
R,3,THICPRIN/2
R,4,THIWEB/2

CSYS,1
K,1
K,2,,,C
K,3,RADIUS,-90,0
K,6,RADIUS,-90,X
L,3,6
AROTAT,1,,,,,,1,2,-ALPHA
AGEN,NDIV,1,,,,-ALPHA

CSYS,0
K,999,XO,YO,0
K,1000,XO,YO,X
AROTAT,4*NDIV-2,,,,,,999,1000,THETA1
K,1001,-(L+LEXTWEB),-(RADIUS+B),X
K,1002,-(L+LEXTWEB),-(RADIUS+B),0
A,4*NDIV+3,4*NDIV+4,1001,1002

*DO,I,1,NWEB-1,1
DIST=(NWEB-I)*LBASE/NWEB
AS=ASIN(DIST/RADIUS)
NI=NINT(AS/ALPHA)
KI=4*NI+3
*GET,XK,KP,KI,LOC,X
*GET,YK,KP,KI,LOC,Y
*IF,I,EQ,1,THEN
KK=KI
*ENDIF
K,1001+10*I,XK,-(RADIUS+B),X
K,1002+10*I,XK,-(RADIUS+B),0
A,KI,KI+3,1001+10*I,1002+10*I
*ENDDO

K,1001+NWEB*10,0,-(RADIUS+B),X
```

```
K,1002+NWEB*10,0,-(RADIUS+B),0
A,3,6,1001+NWEB*10,1002+NWEB*10

*DO,I,0,NWEB-1,1
A,1002+I*10,1001+I*10,1011+I*10,1012+I*10
*ENDDO

*IF,NWEB,EQ,1,THEN
KK=3
*ENDIF
L,KK,4*NDIV+3

KJ=4*NDIV
*DO,I,1,NWEB,1
DIST=(NWEB-I)*LBASE/NWEB
AS=ASIN(DIST/RADIUS)
NI=NINT(AS/ALPHA)
KI=4*NI+3
LARC,KJ,KI,1,RADIUS
*IF,I,EQ,1,THEN
AL,4*NDIV+5*NWEB+8,4*NDIV+2,4*NDIV+5*NWEB+7
AL,4*NDIV+5*NWEB+7,4*NDIV+6,4*NDIV+3*NWEB+8,4*NDIV+9
*ELSE
AL,4*NDIV+5*NWEB+7+I,4*NDIV+3+3*I,4*NDIV+3*NWEB+6+2*I,4*NDIV+6+3
*I
*ENDIF
KJ=KI
*ENDDO

*IF,C,GT,X,THEN
CSYS,1
K,2000,RADIUS,-90,C
L,6,2000
AROTAT,4*NDIV+6*NWEB+8,,,,,,1,2,-ALPHA
AGEN,NDIV,NDIV+3*NWEB+4,,,,-ALPHA
*ENDIF

AROTAT,4*NDIV-2,,,,,,1,2,-GAMA

AROTAT,8*NDIV+6*NWEB+5,,,,,,1,2,-GAMA

NUMMRG,KP

LSEL,S,LINE,,6,4*NDIV,2
LSEL,A,LINE,,1,2,1
LSEL,A,LINE,,8*NDIV+6*NWEB+8
LESIZE,ALL,,,ELNUM1

ALLSEL
LSEL,S,LINE,,5,4*NDIV-1,2
LSEL,A,LINE,,3,4,1
LSEL,A,LINE,,8*NDIV+6*NWEB+9
LSEL,A,LINE,,8*NDIV+6*NWEB+11
LESIZE,ALL,,,ELNUM2

ALLSEL
ASEL,S,AREA,,NDIV+3*NWEB+4,2*NDIV+3*NWEB+3,1
ASEL,A,AREA,,2*NDIV+3*NWEB+5
LSLA,S
LESIZE,ALL,,,1

ALLSEL
*DO,I,0,NWEB,1
LESIZE,4*NDIV+3*I+6,,,ELNUM3
LESIZE,4*NDIV+3*I+4,,,ELNUM3
LESIZE,4*NDIV+3*I+5,,,ELNUM1
*ENDDO

LESIZE,4*NDIV+1,,,ELNUM1
LESIZE,4*NDIV+2,,,ELNUM4
LESIZE,4*NDIV+3,,,ELNUM4

NIPREC=NDIV
*DO,I,1,NWEB,1
DIST=(NWEB-I)*LBASE/NWEB
AS=ASIN(DIST/RADIUS)
NI=NINT(AS/ALPHA)
```

```
NII=NIPREC-NI
*IF,I,EQ,1,THEN
LESIZE,4*NDIV+5*NWEB+7,,,NII
LESIZE,4*NDIV+5*NWEB+8,,,NII
LESIZE,4*NDIV+3*NWEB+8,,,NII
LESIZE,4*NDIV+3*NWEB+7,,,NII
*ELSE
LESIZE,4*NDIV+5*NWEB+7+I,,,NII
LESIZE,4*NDIV+3*NWEB+5+2*I,,,NII
LESIZE,4*NDIV+3*NWEB+6+2*I,,,NII
*ENDIF
NIPREC=NI
*ENDDO
ALLSEL


TYPE,1
MAT,1

REAL,1
*DO,I,1,NDIV,1
AMESH,I
AMESH,NDIV+3*NWEB+3+I
*ENDDO
AMESH,2*NDIV+3*NWEB+4
AMESH,2*NDIV+3*NWEB+5

REAL,2
*IF,EXTWEB,EQ,1,THEN
AMESH,NDIV+1
*ENDIF
REAL,3
AMESH,NDIV+2*NWEB+3

ESHAPE,2
REAL,2
*IF,EXTWEB,EQ,1,THEN
AMESH,NDIV+2
*ENDIF
AMESH,NDIV+3,NDIV+NWEB+1,1

*IF,CWEB,EQ,1,THEN
REAL,4
AMESH,NDIV+NWEB+2
*ENDIF

REAL,3
AMESH,NDIV+2*NWEB+4,NDIV+3*NWEB+4,1


ADELE,NDIV+NWEB+3,NDIV+2*NWEB+2,1
*DO,I,1,NWEB,1
LDELE,4*NDIV+3*NWEB+5+2*I
*ENDDO

*IF,CWEB,EQ,0,THEN
ADELE,NDIV+NWEB+2
LDELE,4*NDIV+3*NWEB+4,4*NDIV+3*NWEB+5,1
*ENDIF

*IF,EXTWEB,EQ,0,THEN
ADELE,NDIV+1
ADELE,NDIV+2
LDELE,4*NDIV+1
LDELE,4*NDIV+3,4*NDIV+5,1
*ENDIF

NUMMRG,NODE

ASEL,S,LOC,Z,0,0
ASEL,INVE
CSYS,0
ARSYM,Z,ALL,,,,0,0

NUMMRG,NODE
```

```
CSYS,1
NSEL,S,LOC,X,RADIUS
NROTAT,ALL
ALLSEL

FINISH

c*** SOLUTION PHASE STARTS HERE.....

/SOLU
ANTYPE,STAT

CSYS,0
NSEL,S,LOC,Y,-(RADIUS+B)
D,ALL,ALL
ALLSEL

CSYS,0
NSEL,S,LOC,X,0
DSYM,SYMM,X,0
ALLSEL


*CFOPEN,displx,rig
*DO,I,1,NA,1
*DO,J,0,NC-1,1

/SOLU
ANTYPE,STAT

CSYS,1
SFEDELE,ALL,,PRES
NSEL,S,LOC,X,RADIUS
NSEL,R,LOC,Z,C-(I-1)*CC+TOLZ,C-I*CC-TOLZ
NSEL,R,LOC,Y,-(90+THETA+ALPHA)+J*2*ALPHA-TOLY,-
(93+THETA)+(J+1)*2*ALPHA+TOLY
ESLN,R,1
SFE,ALL,,PRES,,-1

ALLSEL

SOLVE
FINISH

/POST1
SET,LAST
RSYS,1
*DO,II,1,NA,1
*DO,K,1,2*NC-1,2
NSEL,S,LOC,X,RADIUS
NSEL,R,LOC,Z,C-(2*II-1)*CC/2,C-(2*II-1)*CC/2
NSEL,R,LOC,Y,-(90+THETA+ALPHA)+K*ALPHA,-(90+THETA+ALPHA)+K*ALPHA
!NSORT,UX
*GET,DISP,MAX
*VWRITE,DISP
(E13.6)
NSEL,ALL
*ENDDO
*ENDDO
ALLSEL

FINISH
*ENDDO
*ENDDO

*CFCLOSE
/EXIT
```

File - stwothick

```
/UNITS,SI
/COM,***GEOMETRICAL PARAMETERS***
*AFUN,DEG
```

```
NW=3                        ! Number of divisions across the saddle
width !
NA=10                         ! Number of divisions across the half
saddle angle !
C=0.1                       ! Half saddle width !
B=0.1                            ! Height at center of the saddle
(theta=0) !
THETA=60                    ! Half saddle angle !
RADIUS=1                    ! Radius of the saddle !
BETA=10                          ! Incline angle of the first web
(external web) !
CWEB=1                      ! Do you want to put a web in the middle
(y=1 or n=0) !
EXTWEB=1                       ! Do you want to put an external web
(y=1 or n=0) !
NWEB=3                           ! Total number of webs without the
middle web !
T=1*C/NW                    ! Width of the cylindrical part which is
not webed !
                            ! T=i*C/NW with i=0 to NW-1 !
THETA2=2*THETA/2/NA         ! Saddle angle of not webed part !
                            !  THETA2=i*THETA/2/NA with i=0 to NA-
NWEB-1 !
ELNUM2=1
ELNUM3=4
THICYL1=0.012
THICYL2=0.006
THIWEB=0.006
THICPRIN=0.006

RADIUS2=RADIUS-(THICYL1-THICYL2)/2
THETA1=THETA-THETA2
CC=2*C/NW
ELNUM1=NW-T*NW/C
ELNUM4=T*NW/C
ELNUM5=THETA2/THETA*2*NA
TOLY=THETA/8/NA
TOLZ=CC/8

X=C-T
NDIV=2*NA-THETA2*2*NA/THETA
ALPHA=THETA/NA/2
L=RADIUS*SIN(THETA1)
H1=B-RADIUS*(SIN(90-THETA1)-1)
LBASE=L-H1*TAN(BETA)
S=2*ASIN((C-X)/(2*RADIUS))
SYL=GAMA-S


/COM,***MATERIAL PARAMETERS***
EXX=210E9
NU=.3


/COM,***BUILD THE MODEL***
/VIEW,,1,1,1
/PREP7
ET,1,93
MP,EX,1,EXX
MP,NUXY,1,NU
R,1,THICYL1
R,2,THICYL2
R,3,THIWEB
R,4,THICPRIN
R,5,THIWEB/2

CSYS,1
K,1
K,2,,,C
K,3,RADIUS,-90,0
K,6,RADIUS,-90,X
L,3,6
AROTAT,1,,,,,,1,2,-ALPHA
AGEN,NDIV,1,,,,-ALPHA

CSYS,0
K,1001,-LBASE,-(RADIUS+B),X
```

```
K,1002,-LBASE,-(RADIUS+B),0
A,4*NDIV,4*NDIV+1,1001,1002

*DO,I,1,NWEB-1,1
DIST=(NWEB-I)*LBASE/NWEB
AS=ASIN(DIST/RADIUS)
NI=NINT(AS/ALPHA)
KI=4*NI+3
*GET,XK,KP,KI,LOC,X
*GET,YK,KP,KI,LOC,Y
K,1001+10*I,XK,-(RADIUS+B),X
K,1002+10*I,XK,-(RADIUS+B),0
A,KI,KI+3,1001+10*I,1002+10*I
*ENDDO

K,1001+NWEB*10,0,-(RADIUS+B),X
K,1002+NWEB*10,0,-(RADIUS+B),0
A,3,6,1001+NWEB*10,1002+NWEB*10

*DO,I,0,NWEB-1,1
A,1002+I*10,1001+I*10,1011+I*10,1012+I*10
*ENDDO

KJ=4*NDIV
*DO,I,1,NWEB,1
DIST=(NWEB-I)*LBASE/NWEB
AS=ASIN(DIST/RADIUS)
NI=NINT(AS/ALPHA)
KI=4*NI+3
LARC,KJ,KI,1,RADIUS
AL,4*NDIV+3*(NWEB+1)+2*NWEB+I,4*NDIV+3*I,4*NDIV+3*NWEB+3+2*I,4*N
DIV+3*(I+1)
KJ=KI
*ENDDO

*IF,C,GT,X,THEN
CSYS,1
K,2000,RADIUS2,-90,C
K,1999,RADIUS2,-90,X
L,1999,2000
AROTAT,4*(NDIV+1)+6*NWEB,,,,,,1,2,-ALPHA
AGEN,NDIV,NDIV+3*NWEB+2,,,,-ALPHA
*ENDIF

K,2001,RADIUS2,-(90+THETA1),0
K,2002,RADIUS2,-(90+THETA1),X
L,2001,2002

AROTAT,8*NDIV+6*NWEB+4,,,,,,1,2,-THETA2
*IF,C,GT,X,THEN
AROTAT,8*NDIV+6*NWEB+1,,,,,,1,2,-THETA2
*ENDIF

ALLSEL

NUMMRG,KP

CSYS,1
LSEL,S,LOC,X,RADIUS
LSEL,R,LOC,Z,0,X
LSEL,U,LOC,Z,0
LSEL,U,LOC,Z,X
LESIZE,ALL,,,ELNUM1

LSEL,S,LOC,Z,C
LSEL,A,LOC,Z,X
LSEL,A,LOC,Z,0
LSEL,R,LOC,X,RADIUS
LSEL,U,LOC,Y,-(90+THETA1),-(90+THETA)
LESIZE,ALL,,,1

LSEL,S,LOC,X,RADIUS
LSEL,R,LOC,Z,X,C
LSEL,U,LOC,Z,C
LSEL,U,LOC,Z,X
LESIZE,ALL,,,ELNUM4
```

```
LSEL,S,LOC,Z,C
LSEL,A,LOC,Z,X
LSEL,A,LOC,Z,0
LSEL,R,LOC,X,RADIUS
LSEL,R,LOC,Y,-(90+THETA1),-(90+THETA)
LESIZE,ALL,,,ELNUM5

ALLSEL
*DO,I,0,NWEB,1
LESIZE,4*NDIV+3*I+3,,,ELNUM3
*ENDDO

*IF,CWEB,EQ,0,THEN
ADELE,NDIV+NWEB+1
K=NWEB-1
*ELSEIF,CWEB,EQ,1
K=NWEB
*ENDIF

*DO,I,0,K,1
LESIZE,4*NDIV+3*I+1,,,ELNUM3
LESIZE,4*NDIV+3*I+2,,,ELNUM1
*ENDDO

NIPREC=NDIV
*DO,I,1,NWEB,1
DIST=(NWEB-I)*LBASE/NWEB
AS=ASIN(DIST/RADIUS)
NI=NINT(AS/ALPHA)
NII=NIPREC-NI
LESIZE,4*NDIV+5*NWEB+3+I,,,NII
LESIZE,4*NDIV+3*(NWEB+1)+2*I-1,,,NII
LESIZE,4*NDIV+3*(NWEB+1)+2*I,,,NII
NIPREC=NI
*ENDDO
ALLSEL
```

```
TYPE,1
*DO,I,1,NDIV,1
REAL,1
AMESH,I
*IF,C,GT,X,THEN
REAL,2
AMESH,NDIV+3*NWEB+1+I
*ENDIF
*ENDDO
*IF,C,GT,X,THEN
REAL,2
AMESH,2*NDIV+3*NWEB+2
*IF,THETA,GT,THETA1,THEN
AMESH,2*NDIV+3*NWEB+3
*ENDIF
*ENDIF

REAL,3
ESHAPE,2
*IF,EXTWEB,EQ,1,THEN
AMESH,NDIV+1
*ENDIF
*IF,NWEB,GT,1,THEN
AMESH,NDIV+2,NDIV+NWEB,1
*ENDIF

*IF,CWEB,EQ,1,THEN
REAL,5
AMESH,NDIV+NWEB+1
*ENDIF

REAL,4
AMESH,NDIV+2*NWEB+2,NDIV+3*NWEB+1,1

NUMMRG,ELEM

ADELE,NDIV+NWEB+2,NDIV+2*NWEB+1,1
```

```
*DO,I,1,NWEB,1
LDELE,4*NDIV+3*NWEB+2+2*I
*ENDDO

*IF,CWEB,EQ,0,THEN
ADELE,NDIV+NWEB+1
LDELE,4*NDIV+3*NWEB+1,4*NDIV+3*NWEB+2,1
*ENDIF

*IF,EXTWEB,EQ,0,THEN
ADELE,NDIV+1
LDELE,4*NDIV+1,4*NDIV+2,1
*ENDIF

NUMMRG,NODE

ASEL,S,LOC,Z,0,0
ASEL,INVE
CSYS,0
ARSYM,Z,ALL,,,,0,0

NUMMRG,NODE

CSYS,1
NSEL,S,LOC,X,RADIUS
NSEL,A,LOC,X,RADIUS2
NSEL,R,LOC,Y,-(90+THETA1)
CPINTF,ALL,.005
ALLSEL

NSEL,S,LOC,X,RADIUS
NSEL,A,LOC,X,RADIUS2
NSEL,U,LOC,Y,-90
NSEL,U,LOC,Y,-(90+THETA1),-(90+THETA)
NSEL,R,LOC,Z,X
CPINTF,ALL,.025
ALLSEL
```

```
NSEL,S,LOC,X,RADIUS
NSEL,A,LOC,X,RADIUS2
NSEL,U,LOC,Y,-90
NSEL,U,LOC,Y,-(90+THETA1),-(90+THETA)
NSEL,R,LOC,Z,-X
CPINTF,ALL,.025
ALLSEL

CSYS,1
NSEL,S,LOC,X,RADIUS
NSEL,A,LOC,X,RADIUS2
NROTAT,ALL
ALLSEL

FINISH

c*** SOLUTION PHASE STARTS HERE.....

/SOLU
ANTYPE,STAT

CSYS,0
NSEL,S,LOC,Y,-(RADIUS+B)
D,ALL,ALL

CSYS,0
NSEL,S,LOC,X,0
DSYM,SYMM,X,0

*CFOPEN,disp,nor
*DO,I,1,NW,1
*DO,J,0,NA-1,1

/SOLU
ANTYPE,STAT

CSYS,1
SFEDELE,ALL,,PRES
```

```
NSEL,S,LOC,X,RADIUS
NSEL,R,LOC,Z,C-(I-1)*CC+TOLZ,C-I*CC-TOLZ
NSEL,R,LOC,Y,-(90+THETA)+J*2*ALPHA-TOLY,-
(90+THETA)+(J+1)*2*ALPHA+TOLY
ESLN,R,1
SFE,ALL,,PRES,,-1
ALLSEL

!SOLVE
FINISH

/POST1
SET,LAST
RSYS,1
*DO,II,1,NW,1
*DO,K,1,2*NA-1,2
NSEL,S,LOC,X,RADIUS
NSEL,R,LOC,Z,C-(2*II-1)*CC/2,C-(2*II-1)*CC/2
NSEL,R,LOC,Y,-(90+THETA)+K*ALPHA,-(90+THETA)+K*ALPHA
NSORT,UX
*GET,DISP,MAX
*VWRITE,DISP
(E13.6)
NSEL,ALL
!*ENDDO
!*ENDDO
ALLSEL

FINISH
!*ENDDO
!*ENDDO

*CFCLOSE
/EXIT
```


File - semi_rig.sol

```
/BATCH
/UNITS,SI

/COM,***GEOMETRICAL PARAMETERS***
*AFUN,DEG

NW=3                        ! Number of divisions across the saddle
width !
NA=30                       ! Number of divisions across the half
saddle angle !
C=0.1                       ! Half saddle width !
B=0.1                       ! Height at center of the saddle
(theta=0) !
THETA=60                    ! Half saddle angle !
RADIUS=1                    ! Radius of the saddle !
CWEB=1                      ! Do you want to put a web in the middle
(y=1 or n=0) !
LEXTWEB=0.05
EXTWEB=1                    ! Do you want to put an external web
(y=1 or n=0) !
NWEB=3                      ! Total number of webs without the
middle web !
T=1*C/NW                    ! Width of the cylindrical part which is
not webed !
                            ! T=i*C/NW with i=0 to NW-1 !
THETA2=2*THETA/2/NA         ! Saddle angle of not webed part !
                            ! THETA2=i*THETA/2/NA with i=0 to NA-

NWEB-1 !
ELNUM2=1
ELNUM6=5
ELNUM3=NINT(NA/2)
THICYL=0.012
THIWEB=0.006
THICPRIN=0.006
RADIUS=RADIUS+THICYL/2
```

```
THETA1=THETA-THETA2
CC=2*C/NW
ELNUM1=NW-T*NW/C
ELNUM4=T*NW/C
ELNUM5=THETA2/THETA*2*NA
TOLX=0.00001
TOLY=THETA/8/NA
TOLZ=CC/8
X=C-T
NDIV=2*NA-THETA2*2*NA/THETA
ALPHA=THETA/NA/2
L=RADIUS*SIN(THETA1)
LBASE=L+LEXTWEB
RAD=RADIUS-THICYL
R=LEXTWEB/(1-COS(THETA1))
XO=-(L-R*COS(THETA1))
YO=-(RADIUS*COS(THETA1)+R*SIN(THETA1))
S=2*ASIN((C-X)/(2*RADIUS))
SYL=THETA2-S


/COM,***MATERIAL PARAMETERS***
EXX=210E9
NU=.3
/COM,***BUILD THE MODEL***

/VIEW,,1,1,1
/PREP7
/SHOW,X11
ET,1,63
ET,10,73
ET,11,22
MP,EX,1,EXX
MP,EX,10,EXX
MP,EX,11,0
MP,NUXY,1,NU
MP,NUXY,10,NU
MP,NUXY,11,0
R,1,THICYL
R,2,THIWEB
R,3,THICPRIN
R,4,THIWEB/2

CSYS,1
K,1
K,2,,,C
K,3,RADIUS,-90,0
K,6,RADIUS,-90,X
L,3,6
AROTAT,1,,,,,,1,2,-ALPHA
AGEN,NDIV,1,,,,-ALPHA

CSYS,0
K,999,XO,YO,0
K,1000,XO,YO,X
AROTAT,4*NDIV-2,,,,,,999,1000,THETA1
K,1001,-(L+LEXTWEB),-(RADIUS+B),X
K,1002,-(L+LEXTWEB),-(RADIUS+B),0
A,4*NDIV+3,4*NDIV+4,1001,1002

*DO,I,1,NWEB-1,1
DIST=(NWEB-I)*LBASE/NWEB
AS=ASIN(DIST/RADIUS)
NI=NINT(AS/ALPHA)
KI=4*NI+3
*GET,XK,KP,KI,LOC,X
*GET,YK,KP,KI,LOC,Y
*IF,I,EQ,1,THEN
KK=KI
*ENDIF
K,1001+10*I,XK,-(RADIUS+B),X
K,1002+10*I,XK,-(RADIUS+B),0
A,KI,KI+3,1001+10*I,1002+10*I
*ENDDO
```

```
K,1001+NWEB*10,0,-(RADIUS+B),X
K,1002+NWEB*10,0,-(RADIUS+B),0
A,3,6,1001+NWEB*10,1002+NWEB*10

*DO,I,0,NWEB-1,1
A,1002+I*10,1001+I*10,1011+I*10,1012+I*10
*ENDDO

*IF,NWEB,EQ,1,THEN
KK=3
*ENDIF
L,KK,4*NDIV+3

KJ=4*NDIV
*DO,I,1,NWEB,1
DIST=(NWEB-I)*LBASE/NWEB
AS=ASIN(DIST/RADIUS)
NI=NINT(AS/ALPHA)
KI=4*NI+3
LARC,KJ,KI,1,RADIUS
*IF,I,EQ,1,THEN
AL,4*NDIV+5*NWEB+8,4*NDIV+2,4*NDIV+5*NWEB+7
AL,4*NDIV+5*NWEB+7,4*NDIV+6,4*NDIV+3*NWEB+8,4*NDIV+9
*ELSE
AL,4*NDIV+5*NWEB+7+I,4*NDIV+3+3*I,4*NDIV+3*NWEB+6+2*I,4*NDIV+6+3
*I
*ENDIF
KJ=KI
*ENDDO

*IF,C,GT,X,THEN
CSYS,1
K,2000,RADIUS,-90,C
L,6,2000
AROTAT,4*NDIV+6*NWEB+8,,,,,,1,2,-ALPHA
AGEN,NDIV,NDIV+3*NWEB+4,,,,-ALPHA
*ENDIF

*IF,THETA2,GT,0,THEN
AROTAT,4*NDIV-2,,,,,,1,2,-THETA2
*IF,C,GT,X,THEN
AROTAT,8*NDIV+6*NWEB+5,,,,,,1,2,-THETA2
*ENDIF
*ENDIF
NUMMRG,KP

CSYS,1
LSEL,S,LOC,X,RADIUS
ASLL,S,1
VEXT,ALL,,,-THICYL
ALLSEL

NUMMRG,KP
CSYS,1

ASLV,S
LSLA,S
LSEL,R,LOC,X,RAD+0.0001,RADIUS-0.0001
LESIZE,ALL,,,ELNUM2

ASLV,S
LSLA,S
LSEL,R,LOC,Z,0,X
LSEL,U,LOC,Z,0
LSEL,U,LOC,Z,X
LESIZE,ALL,,,ELNUM1

LSEL,S,LOC,Z,C
LSEL,A,LOC,Z,X
LSEL,A,LOC,Z,0
LSEL,R,LOC,X,RAD,RADIUS
LSEL,U,LOC,Y,-(90+THETA1),-(90+THETA)
LESIZE,ALL,,,1

ASLV,S
LSLA,S
```

```
LSEL,R,LOC,Z,X,C
LSEL,U,LOC,Z,C
LSEL,U,LOC,Z,X
LSEL,U,LOC,Y,-(90+THETA1),-(90+THETA)
LESIZE,ALL,,,ELNUM4

LSEL,S,LOC,Z,C
LSEL,A,LOC,Z,X
LSEL,A,LOC,Z,0
LSEL,R,LOC,X,RAD,RADIUS
LSEL,R,LOC,Y,-(90.1+THETA1),-(89.9+THETA)
LESIZE,ALL,,,ELNUM5

ALLSEL
*DO,I,0,NWEB,1
LESIZE,4*NDIV+3*I+6,,,ELNUM3
LESIZE,4*NDIV+3*I+4,,,ELNUM3
LESIZE,4*NDIV+3*I+5,,,ELNUM1
*ENDDO

LESIZE,4*NDIV+1,,,ELNUM1
LESIZE,4*NDIV+2,,,ELNUM6
LESIZE,4*NDIV+3,,,ELNUM6


NIPREC=NDIV
*DO,I,1,NWEB,1
DIST=(NWEB-I)*LBASE/NWEB
AS=ASIN(DIST/RADIUS)
NI=NINT(AS/ALPHA)
NII=NIPREC-NI
*IF,I,EQ,1,THEN
LESIZE,4*NDIV+5*NWEB+7,,,NII
LESIZE,4*NDIV+5*NWEB+8,,,NII
LESIZE,4*NDIV+3*NWEB+8,,,NII
LESIZE,4*NDIV+3*NWEB+7,,,NII
*ELSE
LESIZE,4*NDIV+5*NWEB+7+I,,,NII
LESIZE,4*NDIV+3*NWEB+5+2*I,,,NII
LESIZE,4*NDIV+3*NWEB+6+2*I,,,NII
*ENDIF
NIPREC=NI
*ENDDO
ALLSEL

TYPE,10
MAT,10
VMESH,ALL

TYPE,1
MAT,1

REAL,2
*IF,EXTWEB,EQ,1,THEN
AMESH,NDIV+1
*ENDIF
REAL,3
AMESH,NDIV+2*NWEB+3
ESHAPE,2
REAL,2
*IF,EXTWEB,EQ,1,THEN
AMESH,NDIV+2
*ENDIF
AMESH,NDIV+3,NDIV+NWEB+1,1

*IF,CWEB,EQ,1,THEN
REAL,4
AMESH,NDIV+NWEB+2
*ENDIF
REAL,3
AMESH,NDIV+2*NWEB+4,NDIV+3*NWEB+4,1


ADELE,NDIV+NWEB+3,NDIV+2*NWEB+2,1
*DO,I,1,NWEB,1
LDELE,4*NDIV+3*NWEB+5+2*I
```

```
*ENDDO

*IF,CWEB,EQ,0,THEN
ADELE,NDIV+NWEB+2
LDELE,4*NDIV+3*NWEB+4,4*NDIV+3*NWEB+5,1
*ENDIF

*IF,EXTWEB,EQ,0,THEN
ADELE,NDIV+1
ADELE,NDIV+2
LDELE,4*NDIV+1
LDELE,4*NDIV+3,4*NDIV+5,1
*ENDIF

NUMMRG,NODE

ASEL,S,LOC,Z,0,0
ASEL,INVE
CSYS,0
ARSYM,Z,ALL,,,,0,0
VSEL,ALL
VSYMM,Z,ALL,,,,0,0

NUMMRG,NODE
CSYS,1
NSEL,S,LOC,X,RAD-TOLX,RAD+TOLX
TYPE,11
MAT,11
REAL,5
ESURF
ALLSEL

CSYS,1
NSEL,S,LOC,X,RADIUS
NROTAT,ALL
ALLSEL
WAVES
FINISH
```

```
c*** SOLUTION PHASE STARTS HERE.....
/SOLU
ANTYPE,STAT

CSYS,0
NSEL,S,LOC,Y,-(RADIUS+B)
D,ALL,ALL
ALLSEL

CSYS,0
NSEL,S,LOC,X,0
DSYM,SYMM,X,0
ALLSEL

*CFOPEN,rig330,rad
*DO,I,1,NW,1
*DO,JJ,0,NA-1,1
J=NA-1-JJ
/SOLU
ANTYPE,STAT
CSYS,1
SFEDELE,ALL,1,PRES
ESEL,S,TYPE,,11
NSLE,ALL
NSEL,R,LOC,Z,C,0
NSEL,R,LOC,Z,C-(I-1)*CC+TOLZ,C-I*CC-TOLZ
NSEL,R,LOC,Y,-(90+THETA)+J*2*ALPHA-TOLY,-
(90+THETA)+(J+1)*2*ALPHA+TOLY
ESLN,R,1
SFE,ALL,1,PRES,,1
ESEL,S,TYPE,,11
NSLE,ALL
NSEL,R,LOC,Z,0,-C
NSEL,R,LOC,Z,C-(I-1)*CC+TOLZ,C-I*CC-TOLZ
NSEL,R,LOC,Y,-(90+THETA)+J*2*ALPHA-TOLY,-
(90+THETA)+(J+1)*2*ALPHA+TOLY
ESLN,R,1
SFE,ALL,1,PRES,,1
```

```
ALLSEL
SOLVE
FINISH

/POST1
SET,LAST
RSYS,1
!/show,x11
!/psf,pres,2
!plnsol,u,x
*DO,II,1,NW,1
*DO,KK,1,2*NA-1,2
K=2*NA-KK
ESEL,S,TYPE,,11
NSLE,ALL
NSEL,R,LOC,Z,C-(2*II-1)*CC/2,C-(2*II-1)*CC/2
NSEL,R,LOC,Y,-(90+THETA)+K*ALPHA,-(90+THETA)+K*ALPHA
NSORT,U,X
*GET,DISPX,MAX
NSORT,U,Y
*GET,DISPY,MAX
*VWRITE,DISPX,DISPY
(E13.6,E13.6)
NSEL,ALL
!*ENDDO
!*ENDDO
ALLSEL
FINISH
!*ENDDO
!*ENDDO
!*CFCLOSE
/EXIT
```

File - solid.rig

```
/UNITS,SI
/COM,***GEOMETRICAL PARAMETERS***
*AFUN,DEG
NW=5                          ! Number of divisions across the saddle
width !
NA=30                          ! Number of divisions across the half
saddle angle !
C=0.1                         ! Half saddle width !
B=0.1                              ! Height at center of the saddle
(theta=0) !
THETA=60                      ! Half saddle angle !
RADIUS=1                      ! Radius of the saddle !
BETA=10                            ! Incline angle of the first web
(external web) !
CWEB=1                         ! Do you want to put a stiffener in the
middle (y=1 or n=0) !
EXTWEB=1                         ! Do you want to put an external web
(y=1 or n=0) !
NWEB=2                             ! Total number of webs without the
middle web !
T=2*C/NW                       ! Width of the cylindrical part which is
not webed !
                               ! T=i*C/NW with i=0 to NW-1 !
THETA2=2*THETA/2/NA            ! Saddle angle of not webed part !
                               !  THETA2=i*THETA/2/NA  with  i=0  to  NA-
NWEB-1 !
ELNUM2=2
ELNUM3=NA/2
THICYL=0.012
THIWEB=0.006
THICPRIN=0.006
RADIUS=RADIUS+THICYL/2

THETA1=THETA-THETA2
CC=2*C/NW
ELNUM1=NW-T*NW/C
ELNUM4=T*NW/C
ELNUM5=THETA2/THETA*2*NA
TOLX=0.00001
TOLY=THETA/8/NA
```

```
TOLZ=CC/8
X=C-T
NDIV=2*NA-THETA2*2*NA/THETA
ALPHA=THETA/NA/2
L=RADIUS*SIN(THETA1)
H1=B-RADIUS*(SIN(90-THETA1)-1)
LBASE=L-H1*TAN(BETA)
RAD=RADIUS-THICYL

/COM,***MATERIAL PARAMETERS***
EXX=210E9
NU=.3
/COM,***BUILD THE MODEL***

/VIEW,,1,1,1
/PREP7
ET,1,63
ET,10,73
ET,11,22
MP,EX,1,EXX
MP,EX,10,EXX
MP,EX,11,0
MP,NUXY,1,NU
MP,NUXY,10,NU
MP,NUXY,11,0
R,1,THICYL
R,2,THIWEB
R,3,THICPRIN
R,4,THIWEB/2

CSYS,1
K,1
K,2,,,C
K,3,RADIUS,-90,0
K,6,RADIUS,-90,X
L,3,6
AROTAT,1,,,,,,1,2,-ALPHA
AGEN,NDIV,1,,,,-ALPHA

CSYS,0
K,1001,-LBASE,-(RADIUS+B),X
K,1002,-LBASE,-(RADIUS+B),0
A,4*NDIV,4*NDIV+1,1001,1002

*DO,I,1,NWEB-1,1
DIST=(NWEB-I)*LBASE/NWEB
AS=ASIN(DIST/RADIUS)
NI=NINT(AS/ALPHA)
KI=4*NI+3
*GET,XK,KP,KI,LOC,X
*GET,YK,KP,KI,LOC,Y
K,1001+10*I,XK,-(RADIUS+B),X
K,1002+10*I,XK,-(RADIUS+B),0
A,KI,KI+3,1001+10*I,1002+10*I
*ENDDO

K,1001+NWEB*10,0,-(RADIUS+B),X
K,1002+NWEB*10,0,-(RADIUS+B),0
A,3,6,1001+NWEB*10,1002+NWEB*10

*DO,I,0,NWEB-1,1
A,1002+I*10,1001+I*10,1011+I*10,1012+I*10
*ENDDO

KJ=4*NDIV
*DO,I,1,NWEB,1
DIST=(NWEB-I)*LBASE/NWEB
AS=ASIN(DIST/RADIUS)
NI=NINT(AS/ALPHA)
KI=4*NI+3
LARC,KJ,KI,1,RADIUS
AL,4*NDIV+3*(NWEB+1)+2*NWEB+I,4*NDIV+3*I,4*NDIV+3*NWEB+3+2*I,4*N
DIV+3*(I+1)
KJ=KI
*ENDDO
```

```
*IF,C,GT,X,THEN
CSYS,1
K,2000,RADIUS,-90,C
L,6,2000
AROTAT,4*(NDIV+1)+6*NWEB,,,,,,1,2,-ALPHA
AGEN,NDIV,NDIV+3*NWEB+2,,,,-ALPHA
*ENDIF

*IF,THETA2,GT,0,THEN
AROTAT,4*NDIV-2,,,,,,1,2,-THETA2
*IF,C,GT,X,THEN
AROTAT,8*NDIV+6*NWEB+1,,,,,,1,2,-THETA2
*ENDIF
*ENDIF
NUMMRG,KP

CSYS,1
LSEL,S,LOC,X,RADIUS
ASLL,S,1
VEXT,ALL,,,-THICYL
ALLSEL
NUMMRG,KP

CSYS,1
ASLV,S
LSLA,S
LSEL,R,LOC,X,RAD+0.0001,RADIUS-0.0001
LESIZE,ALL,,,ELNUM2

ASLV,S
LSLA,S
LSEL,R,LOC,Z,0,X
LSEL,U,LOC,Z,0
LSEL,U,LOC,Z,X
LESIZE,ALL,,,ELNUM1

LSEL,S,LOC,Z,C
LSEL,A,LOC,Z,X
LSEL,A,LOC,Z,0
LSEL,R,LOC,X,RAD,RADIUS
LSEL,U,LOC,Y,-(90+THETA1),-(90+THETA)
LESIZE,ALL,,,1

ASLV,S
LSLA,S
LSEL,R,LOC,Z,X,C
LSEL,U,LOC,Z,C
LSEL,U,LOC,Z,X
LSEL,U,LOC,Y,-(90+THETA1),-(90+THETA)
LESIZE,ALL,,,ELNUM4

LSEL,S,LOC,Z,C
LSEL,A,LOC,Z,X
LSEL,A,LOC,Z,0
LSEL,R,LOC,X,RAD,RADIUS
LSEL,R,LOC,Y,-(90.1+THETA1),-(89.9+THETA)
LESIZE,ALL,,,ELNUM5

ALLSEL
*DO,I,0,NWEB,1
LESIZE,4*NDIV+3*I+3,,,ELNUM3
*ENDDO

*IF,CWEB,EQ,0,THEN
ADELE,NDIV+NWEB+1
K=NWEB-1
*ELSEIF,CWEB,EQ,1
K=NWEB
*ENDIF

*DO,I,0,K,1
LESIZE,4*NDIV+3*I+1,,,ELNUM3
LESIZE,4*NDIV+3*I+2,,,ELNUM1
*ENDDO
NIPREC=NDIV
*DO,I,1,NWEB,1
```

```
DIST=(NWEB-I)*LBASE/NWEB
AS=ASIN(DIST/RADIUS)
NI=NINT(AS/ALPHA)
NII=NIPREC-NI
LESIZE,4*NDIV+5*NWEB+3+I,,,NII
LESIZE,4*NDIV+3*(NWEB+1)+2*I-1,,,NII
LESIZE,4*NDIV+3*(NWEB+1)+2*I,,,NII
NIPREC=NI
*ENDDO
ALLSEL

TYPE,10
MAT,10
VMESH,ALL

TYPE,1
MAT,1

!ESHAPE,2
REAL,2
*IF,EXTWEB,EQ,1,THEN
AMESH,NDIV+1
*ENDIF
*IF,NWEB,GT,1,THEN
AMESH,NDIV+2,NDIV+NWEB,1
*ENDIF

*IF,CWEB,EQ,1,THEN
REAL,4
AMESH,NDIV+NWEB+1
*ENDIF

REAL,3
AMESH,NDIV+2*NWEB+2,NDIV+3*NWEB+1,1
NUMMRG,ELEM

ADELE,NDIV+NWEB+2,NDIV+2*NWEB+1,1
*DO,I,1,NWEB,1
LDELE,4*NDIV+3*NWEB+2+2*I
*ENDDO

*IF,CWEB,EQ,0,THEN
ADELE,NDIV+NWEB+1
LDELE,4*NDIV+3*NWEB+1,4*NDIV+3*NWEB+2,1
*ENDIF

*IF,EXTWEB,EQ,0,THEN
ADELE,NDIV+1
LDELE,4*NDIV+1,4*NDIV+2,1
*ENDIF

NUMMRG,NODE

ASEL,S,LOC,Z,0,0
ASEL,INVE
CSYS,0
ARSYM,Z,ALL,,,,0,0
VSEL,ALL
VSYMM,Z,ALL,,,,0,0

NUMMRG,NODE

CSYS,1
NSEL,S,LOC,X,RAD-TOLX,RAD+TOLX
TYPE,11
MAT,11
REAL,5
ESURF
ALLSEL

CSYS,1
NSEL,S,LOC,X,RAD-TOLX,RAD+TOLX
NROTAT,ALL
ALLSEL
WAVES
FINISH
```

```
c*** SOLUTION PHASE STARTS HERE.....
/SOLU
ANTYPE,STAT
CSYS,0
NSEL,S,LOC,Y,-(RADIUS+B)
D,ALL,ALL

CSYS,0
NSEL,S,LOC,X,0
DSYM,SYMM,X,0

*CFOPEN,disp530,rad
*DO,I,1,NW,1
*DO,JJ,0,NA-1,1
J=NA-1-JJ
/SOLU
ANTYPE,STAT

CSYS,1
SFEDELE,ALL,1,PRES
ESEL,S,TYPE,,11
NSLE,ALL
NSEL,R,LOC,Z,C,0
NSEL,R,LOC,Z,C-(I-1)*CC+TOLZ,C-I*CC-TOLZ
NSEL,R,LOC,Y,-(90+THETA)+J*2*ALPHA-TOLY,-
(90+THETA)+(J+1)*2*ALPHA+TOLY
ESLN,R,1
SFE,ALL,1,PRES,,1
ESEL,S,TYPE,,11
NSLE,ALL
NSEL,R,LOC,Z,0,-C
NSEL,R,LOC,Z,C-(I-1)*CC+TOLZ,C-I*CC-TOLZ
NSEL,R,LOC,Y,-(90+THETA)+J*2*ALPHA-TOLY,-
(90+THETA)+(J+1)*2*ALPHA+TOLY
ESLN,R,1
SFE,ALL,1,PRES,,1
ALLSEL

SOLVE
FINISH

/POST1
SET,LAST
RSYS,1
!/show,x11
!/psf,pres,2
!plnsol,u,x
*DO,II,1,NW,1
*DO,KK,1,2*NA-1,2
K=2*NA-KK
ESEL,S,TYPE,,11
NSLE,ALL
NSEL,R,LOC,Z,C-(2*II-1)*CC/2,C-(2*II-1)*CC/2
NSEL,R,LOC,Y,-(90+THETA)+K*ALPHA,-(90+THETA)+K*ALPHA
NSORT,U,X
*GET,DISPX,MAX
NSORT,U,Y
*GET,DISPY,MAX
*VWRITE,DISPX,DISPY
(E13.6,E13.6)

NSEL,ALL
*ENDDO
*ENDDO
ALLSEL

FINISH
*ENDDO
*ENDDO
*CFCLOSE
/EXIT
```

APPENDIX 9

PEAK STRESS EVALUATION USING FORMULA METHOD -
- used for ASME PVP 91 Paper by D H Nash

$A := 6858$ $t := 26.6$ $\theta := 162$

$L := 54864$ $R := 1829$ $b := 762$ $D := L - (2 \cdot A)$

$LR := \frac{L}{R}$ $Rt := \frac{R}{t}$ $AR := \frac{A}{R}$ $DR := \frac{D}{R}$

$DR = 22.498$

$AR = 3.75$

$Rt = 68.759$

$LR = 29.997$

Note: if DR>18 then Fd is equal to 1.0 if AR>9 then Fa is equal to 1.0

$DR := if(DR > 18, 18, DR)$ $DR = 18$

Basic Stress $\sigma_b := 0.000625 \cdot R^{2.7} \cdot t^{-1.71}$ $\sigma_b = 1.47 \cdot 10^3$ N/mm2

Weight Factor $F_w := \frac{LR}{36}$ $F_w = 0.833$

****** Now compute the factor Fa based on polynominal coefficients ******
Factor Fa

$$Fa(a_0, a_1, a_2, a_3, a_4) := a_0 + a_1 \cdot AR + a_2 \cdot AR^2 + a_3 \cdot AR^3 + a_4 \cdot AR^4$$

$$C1 := \begin{bmatrix} 0.192 & 0.492 & -0.110 & 0.0108 & -0.00039 \\ 0.0628 & 0.372 & -0.068 & 0.0067 & -0.000272 \\ 0.0435 & 0.3147 & -0.053 & 0.0052 & -0.000206 \\ 0.0329 & 0.2839 & -0.045 & 0.0048 & -0.00018 \\ 0.0217 & 0.2483 & -0.035 & 0.0034 & -0.00014 \end{bmatrix} \quad RT := \begin{bmatrix} 25 \\ 83.3 \\ 125 \\ 166.7 \\ 250 \end{bmatrix} \quad i := 0..4$$

$F_i := Fa(C1_{i,0}, C1_{i,1}, C1_{i,2}, C1_{i,3}, C1_{i,4})$

$F_a := linterp(RT, F, Rt)$ $F_a = 0.846$

F_i	RT_i
0.983	25
0.801	83.3
0.712	125
0.682	166.7
0.612	250

****** Now compute the factor Fd based on polynominal coefficients ******
Factor Fd

$$Fd(a_0, a_1, a_2, a_3, a_4) := a_0 + a_1 \cdot DR + a_2 \cdot DR^2 + a_3 \cdot DR^3 + a_4 \cdot DR^4$$

$$C2 := \begin{bmatrix} 0.768 & 0.0311 & 0.00105 & -0.00027 & 0.0000086 \\ 0.729 & 0.0328 & -0.00272 & 0.00018 & -0.0000045 \\ 0.706 & 0.0413 & -0.00452 & 0.00028 & -0.0000059 \\ 0.710 & 0.0336 & -0.00304 & 0.00016 & -0.0000026 \\ 0.719 & 0.0207 & -0.00072 & 0.000005 & 0.0000009 \end{bmatrix}$$

$F_i := Fd(C2_{i,0}, C2_{i,1}, C2_{i,2}, C2_{i,3}, C2_{i,4})$

$F_d := linterp(RT, F, Rt)$ $F_d = 1.011$

F_i	RT_i
0.996	25
1.015	83.3
0.999	125
0.99	166.7
0.982	250

**Peak stress after factorization $F_w = 0.833$ $F_a = 0.846$ $F_d = 1.011$

$F_a := if(F_a > 1, 1, F_a)$ $F_a = 0.846$

$F_d := if(F_d > 1, 1, F_d)$ $F_d = 1$

$\sigma_f := \sigma_b \cdot F_a \cdot F_d \cdot F_w$ $\sigma_f = 1.037 \cdot 10^3$ N/mm2

**** Now compute the factor Fθ based on polynominal coefficients ****

$rad \equiv 1$ $deg \equiv \frac{\pi}{180}$ $\theta := \theta \cdot deg$ $\theta = 2.827$

$F\theta(a_0, a_1, a_2, a_3, a_4) := a_0 + a_1 \cdot \theta + a_2 \cdot \theta^2 + a_3 \cdot \theta^3 + a_4 \cdot \theta^4$

$$C4 := \begin{bmatrix} 3.0942 & -0.7109 & -0.5451 & 0.2663 & -0.0344 \\ 3.0957 & -0.7541 & -0.4288 & 0.1918 & -0.0207 \\ 4.7471 & -3.2885 & 0.8949 & -0.0646 & -0.0099 \\ 6.1644 & -5.5586 & 2.1783 & -0.3609 & 0.0124 \\ 6.2541 & -5.6086 & 2.1141 & -0.3090 & 0.0031 \end{bmatrix}$$

$F_i := F\theta(C4_{i,0}, C4_{i,1}, C4_{i,2}, C4_{i,3}, C4_{i,4})$

$F_\theta := linterp(RT, F, Rt)$ $F_\theta = 0.548$

F_i	RT_i
0.547	25
0.548	83.3
0.51	125
0.497	166.7
0.511	250

**** Now compute the factor Fb based on polynominal coefficients ****

$B := \frac{b}{R}$ $B = 0.417$

$FB(a_0, a_1, a_2, a_3, a_4) := a_0 + a_1 \cdot B + a_2 \cdot B^2 + a_3 \cdot B^3 + a_4 \cdot B^4$

$$C5 := \begin{bmatrix} 1.6770 & -4.871 & 8.7307 & -6.2936 & 0 \\ 1.7040 & -5.094 & 9.2423 & -6.6604 & 0 \\ 1.7303 & -5.325 & 9.8450 & -7.1439 & 0 \\ 1.7563 & -5.566 & 10.526 & -7.7273 & 0 \\ 1.7746 & -5.738 & 11.011 & -8.1269 & 0 \\ 1.8110 & -6.105 & 12.149 & -9.1860 & 0 \end{bmatrix}$$

$F_i := FB(C5_{i,0}, C5_{i,1}, C5_{i,2}, C5_{i,3}, C5_{i,4})$

$F_b := \text{linterp}(RT, F, Rt)$ $F_b = 0.705$

F_i	RT_i
0.708	25
0.704	83.3
0.704	125
0.706	166.7
0.708	250

****** Now compute the factor FL based on polynominal coefficients ******

$FL(a_0, a_1, a_2, a_3, a_4) := a_0 + a_1 \cdot LR + a_2 \cdot LR^2 + a_3 \cdot LR^3 + a_4 \cdot LR^4$

$$C5 := \begin{bmatrix} 1.8607 & -0.1312 & 0.00681 & -0.000151 & 0.0000012 \\ 0.4414 & 0.161 & -0.01120 & 0.00029 & -0.0000025 \\ 0.295 & 0.172 & -0.01040 & 0.00024 & -0.0000019 \\ 0.8206 & 0.0393 & -0.00007 & -0.000081 & 0.0000015 \\ 1.195 & -0.0533 & 0.00610 & -0.000234 & 0.0000028 \end{bmatrix}$$

$F_i := FL(C5_{i,0}, C5_{i,1}, C5_{i,2}, C5_{i,3}, C5_{i,4})$

$F_L := \text{linterp}(RT, F, Rt)$ $F_L = 0.984$

F_i	RT_i
0.708	25
0.704	83.3
0.704	125
0.706	166.7
0.708	250

******* Hence final results for factors and peak stress is given by: *******

$F_w = 0.833$ $F_\theta = 0.548$ $F_d = 1$

$F_b = 0.705$ $F_a = 0.846$ $F_L = 0.984$

$\sigma_p := \sigma_b \cdot F_w \cdot F_b \cdot F_\theta \cdot F_a \cdot F_d \cdot F_L$ $\sigma_p = 394.239$ N/mm2